The Analysis of Exosomal Tau Release and its Regulation

Aaron Bradshaw

A thesis submitted for the degree of Doctor of Philosophy

Department of Clinical Neuroscience, Institute of Neurology

University College London

2018

Declaration

I, Aaron Bradshaw confirm that the work presented in this thesis is my own. Where information has been derived from other sources, I confirm that this has been indicated in the thesis.

Abstract

The secretion of Tau protein from cells combined with its trans-cellular uptake has been hypothesised as a central component in the progression of Tauopathic neurodegenerative diseases. Exosomes, small (30 – 140 nm) vesicles released from cells, may represent a privileged route for secretion and transmission of neurodegenerative proteins. We hypothesised that *1)* Tau protein may be released from cells in exosomes *2)* that this process may be regulated by the interaction of Tau with the chaperone network and SUMOylation of Tau and *3)* exosomes may transmit Tau to naïve cells.

We established and characterised the exosomal release of Tau from SH-SY5Y cells; all isoforms of Tau studied, including endogenous SH-SY5Y Tau, were detected in exosomal fractions. Exosomal 2N4R-Tau was C-terminally truncated and intra-luminal. We investigated the role of Tau-Hsc70 interaction in its exosomal release and identified the co-chaperone DNAjC5 as a key mediator in this process. SUMOylation of Tau protein was also identified as a key process regulating its exosomal release. We furthermore gathered evidence connecting Tau protein dysfunction (P301L-Tau; oligomerisation) and exosomal release, implicating exosomal Tau release as a potentially disease relevant process. In order to model the transmission of Tau between cells, we studied the uptake of a) Tau recovered from cells and b) Tau secreted from cells. However, naïve SH-SY5Y cells were able to internalise extracellular Tau only to a low extent. When co-cultured, Tau protein transferred efficiently between cells. This process was potentiated by lysosomal compromise and dependent upon cell density. Finally, we determined that exosomes isolated from SH-SY5Y cells with ectopic expression of P301L-Tau were selectively toxic to primary mouse cortical neurons.

Overall the work presented here confirms the exosomal release of Tau protein and links this process to pathological Tau. Our work identifies key cellular mechanisms governing the

exosomal release of Tau that may serve as points of departure for future studies investigating the release and transmission of Tau, and the role of exosomes therein.

Impact statement

The cellular misfolding and aggregation of Tau protein is central pathological feature in a spectrum of neurodegenerative diseases collectively referred to as Tauopathies. Tauopathies include Alzheimer's disease, Pick's disease, progressive supranuclear palsy, corticobasal degeneration and chronic traumatic encephalopathy. The aetiology of Tauopathies in most patients is unknown, although mutations in the *MAPT* gene, which codes for the Tau protein, are causative of some Tauopathies.

Tau pathology in neurodegenerative disease is progressive and this progression occurs through stereotypical stages. Evidence suggests that the progressive nature of Tau pathology is related to the release of pro-aggregating forms of Tau from cells and their uptake by neighbouring cells.

One hypothetical mechanism for the release of Tau protein from cells is in small vesicles termed 'exosomes' which are 30 – 140 nm in size.

Here we have investigated the hypothesis that Tau protein is released from cells in exosomes, and we have examined how these exosomes affect recipient cells. We have also investigated different cell systems to model the spread of Tau protein between cells.

We have demonstrated that Tau protein is released from cells in exosomes. We have characterised this process in detail, demonstrating that different isoforms of Tau are released in exosomes. We have also identified factors affecting the exosomal release of Tau, including Tau SUMOylation and interaction with chaperones. In addition we have developed systems to analyse the spread of Tau proteins between cells in culture.

Most directly these findings have impact for researchers working within the field of the cell biology of Tau protein. The demonstration of exosomal Tau release contributes to a growing body of literature that is concerned with uncovering the mechanisms contributing

to the release of Tau from cells. The findings presented here serve to solidify the base of data upon which future research in this area may build.

In this work we have examined how a mutation in Tau associated with frontotemporal dementia-Tau (P301L) affected its exosomal release. The exosomal release of pathogenic P301L-Tau was increased relative to wild type Tau. Moreover, these exosomes were toxic to cortical neurons. These findings link our research to disease relevant processes and may therefore help to open understanding toward how release of Tau in exosomes links with neurodegeneration. The initial stages of this impact will be felt in the research community, with the goal of opening understanding toward mechanistic targets for therapeutic intervention. The benefit in the longer term therefore would be to individuals affected, in one way or another, by dementia.

Impact of this research has also been felt in academic – non-academic dialogue. During the undertaking of this research we have disseminated our key hypotheses and findings to members of the Alzheimer's Society Research Network. Members of this network are generally individuals affected directly or indirectly by dementia and, as such, the people situated most closely to the tangible benefits posited on the ultimate horizon of our research. However, dissemination through these channels has beneficial impact regardless of these tangible benefits, as communication itself operates to strengthen connections, in this case between academic and non-academic institutions.

List of abbreviations

3R – Three repeat Tau

4R – Four repeat Tau

A260 – Absorbance at 260 nm

A280 – Absorbance at 280 nm

AA – Amino acid

AD – Alzheimer's disease

AMPA - α-amino-3-hydroxy-5-methyl-4-isoxazolepropionic acid

ATCC – American type culture collection

ARF6 – ADP-ribosylation factor 6

BAG-1 – BAG family molecular chaperone regulator 1

BCA - Bicinchoninic acid

BSA – Bovine serum albumin

CA1 – Cornu ammonis 1

CBD – Corticobasal degeneration

CD – cluster of differentiation

Cdk5 – Cyclin dependent kinase 5

cDNA – Complementary DNA

CHIP – Carboxyl terminus of the Hsc70 interacting protein

CIP – Calf intestinal phosphatase

CM – conditioned medium

CMA – Chaperone mediated autophagy

CMO – Cell mask orange

CNS – Central nervous system

CSF – Cerebral spinal fluid

CTE – Chronic traumatic encephalopathy

DAPI - 4', 6-diamidino-2-phenylindole

DG – Dentate gyrus

DMEM – Dulbecco's modified eagle media

DMSO – Dimethyl sulfoxide

DNA – Deoxyribonucleic acid

DNAjC5 – DnaJ homolog subfamily C member 5

dNTP – deoxyribonucleotide triphosphate

ECL – Electro-chemi-luminescence

EDTA - Ethylenediaminetetraacetic acid

ELISA – Enzyme linked immunosorbent assay

EM – Electron microscopy

ESCRT – Endosomal complex required for sorting

EtOH – Ethanol

EVs – Extracellular vesicles

FBS – Foetal bovine serum

FTD – Frontotemporal dementia

GABA - γ-aminobutyric acid

GAPDH - Glyceraldehyde 3-phosphate dehydrogenase

GFAP – Glial fibrillary acid protein

GFP – Green fluorescent protein

GSK-3 – Glycogen synthase kinase 3

HA – Heamagglutinin

HCl – Hydrochloric acid

HEK293 – Human embryonic kidney cells

HMW – High molecular weight

HPLC – High performance liquid chromatography

Hsc70 – Heat shock cognate protein 71 kDa protein

ICC – Immunocytochemistry

IgG – Immunoglobulin G

iHCN – Induced human cortical neurons

ILV – Intraluminal vesicle

IP – Immunoprecipitation

IP'd – Immunoprecipitated

iPSC – Induced pluripotent stem cells

Kb – Kilobase

KEGG – Kyoto encyclopaedia of genes and genomes

KCl – Potassium chloride

kDa – Kilodalton

LAMP2A – Lysosomal membrane associated protein 2A

LB – Lysogeny broth

LDS – Lithium dodecyl sulphate

LED – Light emitting diode

LTP – Long term potentiation

M1 – Muscarinic acetylcholine receptor M1

M3 – Muscarinic acetylcholine receptor M3

MAP – Microtubule Associated Protein

MAPK – Mitogen-activated protein kinase

MAPS – Misfolded associated protein secretion

MAPT – Microtubule Associated Protein Tau

MeOH – Methanol

MES - 2-(N-morpholino)ethanesulfonic acid

mM – Millimolar

MMSE – Mini mental state examination

ms – Milliseconds

MTBR – Microtubule binding region

MTT - 3-(4,5-dimethylthiazol-2-yl)-2,5-diphenyltetrazolium bromide

MVB – Multivesicular body

NADH – Nicotinamide adenine dinucleotide

NEAA – non-essential amino acids

NFT – Neurofibrillary tangle

NGS – Normal goat serum

nM – Nanomolar

NP – Neuropil threads

NSMase – Neutral sphingomyelinase

NTA – Nanoparticle tracking analysis

PBS – Phosphate buffered saline

PCR – Polymerase chain reaction

PHF – Paired helical filament

PiD – Pick's disease

PKA – Protein kinase A

PKC – Protein kinase C

pmol – Picomoles

PNS – Peripheral nervous system

Pro – proline

PrP – Prion protein

PSEN-1 – Presenilin-1

PSD – Particle size distribution

PSP – Progressive supranuclear palsy

PTM – Post translational modification

pX – Phosphorylated amino acid X

RD-Tau – Repeat domain Tau

RIPA - Radioimmunoprecipitation assay (buffer)

RNA – Ribonucleic acid

RPM – Revolutions per minute

SDS-PAGE – Sodium dodecyl sulphate polyacrylamide gel electrophoresis

Ser – Serine

SF – Straight filament

SNAP23 – Synaptosomal-associated protein 23

SOD-1 – Superoxide dismutase 1

SUMO – Small ubiquitin-like modification

TAE - Tris-acetate EDTA buffer

TCA – Trichloroacetic acid

TDP-43 – TAR DNA-binding protein 43

TEM – Transmission electron microscopy

Thr – Threonine

TNAP – Tissue non-specific alkaline phosphatase

TRPS – Tuneable resistive pulse sensing

TSG101 – Tumour susceptibility gene 101

U – Unit

USP19 – Ubiquitin specific peptidase 19

V – Volts

v/v – Volume per volume

w/v – Weight per volume

WT – Wild type

Acknowledgements

It is my pleasure to thank my primary supervisor, Dr J Mark Cooper, for his consistent and insightful supervision during this project. It cannot be understated how much I value the relationship that Mark and I have developed over the course of this work.

Dr Rohan de Silva was the secondary supervisor for this project. His generous donation of Tau cell models and constructs have been central to this work. The expertise provided by Dr Lydia Alvarez-Erviti has proved very important to the initiation and ongoing support of this project.

I would also like to extend my gratitude toward Dr M Di Stefano. His presence as both a mentor and a friend during my PhD (and beyond) has been invaluable.

During my PhD there have been many students come in and out of the lab, some of whom I have worked closely with on projects related to my thesis. I would like to thank Jitesh Chauhan and Saba Manshaei specifically for their contributions.

I must also thank everyone in the Department of Clinical Neurosciences who have contributed toward generating a friendly and supportive research environment.

This work would not have been possible without the funding provided by the Alzheimer's Society.

I cannot express how grateful I am to my girlfriend, Sammi, who has constantly been there for me over the past three and a half years. My mum has also been an unfailing source of support throughout this work, as have been all my family. Thank you.

Table of contents

List of figures

Chapter 1: Introduction

Chapter 2: Methods

List of Tables

1 Introduction

1.1 Overall rationale

The dysfunction of Tau protein is at the centre of numerous neurodegenerative diseases, referred collectively to as 'Tauopathies'.

Tau protein exists in the CNS as six alternatively spliced isoforms and has important cellular functions with a key role in stabilising microtubules and organising the cytoskeleton. It is the abnormal phosphorylation and aggregation of Tau that underlies Tauopathy. The aggregation of Tau can occur under sporadic settings, and can also result from mutations that alter the primary sequence of Tau, its splicing or both.

Tau neuropathology is progressive. In Alzheimer's disease the progression of Tau pathology occurs through stereotypical stages in a well characterised hierarchical neuroanatomical pattern.

In mouse models Tau pathology can be induced in mice not normally developing Tau pathology by intracerebral injection of Tau aggregates extracted from Tauopathic brain material. Thus aggregated Tau may seed the aggregation of normal Tau, a process which is hypothesised to account for the progression of Tau pathology in human disease. Moreover, once Tau aggregation has been induced, it may spread away from the injection site.

Based on these findings, models of the progression of Tau pathology hypothesise a transmission mechanism. This hypothesis proposes that aggregated / pathological Tau is released from cells and taken up by neighbouring cells. Once taken up, pathological Tau seeds the aggregation of non-pathological Tau into an aggregated form in these cells, with a concomitant *transmission* of Tau pathology.

The release of Tau from cells has recently been demonstrated to occur via non-conventional mechanisms, including the release of Tau in small vesicles (40-150 nm) of

endocytic origin termed ‘exosomes’. Because exosomes can serve as vehicles of inter-cellular communication, the release of Tau protein in exosomes represents a hypothetically privileged mechanism for the dissemination of Tau protein between neighbouring neuronal cells.

Mechanistic factors underlying the targeting of protein cargo to exosomes identifies roles for the chaperone network (such as Hsc70 and DNAjC5) and SUMOylation, processes which Tau protein is known to be involved in.

In this work we characterise the release of Tau protein in exosomes and investigate some of the mechanistic factors and processes which govern this process. The role(s) of exosomal Tau release and Tau secretion in general in Tauopathy and neurodegeneration is an important area of work, which may provide clues toward understanding the progression of Tau pathology observed in these conditions.

1.2 Tau gene

Tau protein is encoded from the *MAPT* (Microtubule Associated Protein Tau) gene located at chromosomal position 17q21.3. *MAPT* spans ~150 kb and exhibits a complex genomic architecture, constituted by one non-coding and 14 coding exons. Numerous mutations associated with frontotemporal dementia and Tauopathic neurodegenerative disease are linked to the *MAPT* gene, and *MAPT* itself is situated within a genomic region composing a haplotype that regulates risk for numerous neurodegenerative diseases, including PD, PSP, CBD and AD (Pittman et al. 2006). A schematic representation of the genomic structure of the *MAPT* gene is depicted in **figure 1.1**

1.3 Tau transcripts

Tau mRNA is primarily expressed in the central and peripheral nervous systems, and is also expressed in the testis (Ashman et al. 1992). PNS Tau contains extra sequence compared to

CNS Tau, coded for by exons 4a, 6 and 8. Inclusion of exon 4a gives rise to the PNS form of 'big-Tau' (Pittman et al. 2006; Goedert et al. 1992a). In the CNS the alternative splicing of exons 2, 3 and 10 result in the expression of 6 distinct Tau transcripts. The inclusion pattern of exons 2 and 3 are regulated in an 'augmented combinatorial' manner (i.e. 2 can be present without 3, but 3 is never present without 2) and translate to two 29 amino acid inserts in the N-terminal region of Tau, giving rise to mature proteins with 0, 1, or 2 N-terminal inserts (0N, 1N, 2N). Exon 10 is translated into a repeat region, its inclusion resulting in 4 repeat regions in the carboxy domain of Tau, adding to the three constitutive repeat regions (4R vs 3R; Kolarova et al. 2012). These are the regions through which Tau interacts with and stabilises microtubules. The translation of these transcript combinations gives rise to six distinct isoforms of Tau protein: 0N3R, 0N4R, 1N3R, 1N4R, 2N3R, and 2N4R which are represented in **figure 1.1**. Tau splicing is developmentally and regionally regulated, and alterations in splicing bear pathological relevance (Andreadis. 2005; section **1.6.1.2**). In the foetal brain only the shortest isoform (0N3R) of Tau is expressed, whereas in the adult brain Tau mRNA containing all possible combinations of exon 2 and 3 inclusion / exclusion are detected, as are transcripts lacking and containing exon 10. Expression of these mRNA transcripts varies between brain regions, for instance white matter only contains transcripts without exons 2 and 3, which is likely predominantly contributed to by glial cells (Boutajangout et al. 2004; Lopresti et al. 1995). In adult brain levels of 3R and 4R Tau are roughly equal and 1N isoforms are overrepresented relative to 2N containing isoforms (Hong et al. 1998; Hefti et al. 2018).

The pattern of Tau splicing differs between humans and mice (Andreadis, 2005). Whereas the human brain expresses roughly equimolar ratios of 3R and 4R-Tau, only 4R-Tau is expressed in the adult mouse brain. As in human, mouse Tau isoform expression is developmentally regulated with expression of 0N3R-Tau in a highly phosphorylated state being the major isoform until ~postnatal day 9 (Kosik et al. 1989; Tuerde et al. 2018).

Thereafter expression levels of 3R-Tau reduce with concomitant increases in the expression of 0N4R and 1N4R-Tau. 3R-Tau is only detected at low levels at postnatal day 90.

1.4 Tau structure

1.4.1.1 Primary structure

Physiologically, Tau is a soluble hydrophilic protein with the 2N4R isoform containing 80 total Ser/Thr residues, 56 negatively charged residues and 58 positively charged residues (441 total amino acids). The charged residues are asymmetrically divided in the molecule with the N-terminal region having a net negative charge and the microtubule binding region having a positive charge (Rosenberg et al. 2008), and the distribution of charge is key to mediating the physiological and pathophysiological status of the molecule (Wang & Mandelkow 2016).

The two domains are linked by a proline rich domain, the site of seven Pro-XX-Pro motifs, proline residues in the sixth and seventh of which (Pro213, Pro216, Pro219) are important for the interaction of Tau and the tyrosine kinase Fyn (Lau et al. 2016). Within the C-terminal half of the molecule there is three or four (depending upon exon 10 exclusion or inclusion, respectively) imperfect repeats of 18 amino acids, separated by 13-14 amino acid inter-repeat regions (Lee 1990) and these are the regions that bind to and stabilise microtubules, with 4R Tau doing so more efficiently than 3R Tau (Panda et al. 2003). There is conservation in the primary amino acid sequence of Tau and other microtubule associated proteins (MAPs) and phylogenetic analyses suggest Tau, alongside MAP2, originated from the ancestral duplication of MAP4 (Sündermann et al. 2016). The primary sequence of Tau and its subdivision into domains is displayed in **figure 1.2**.

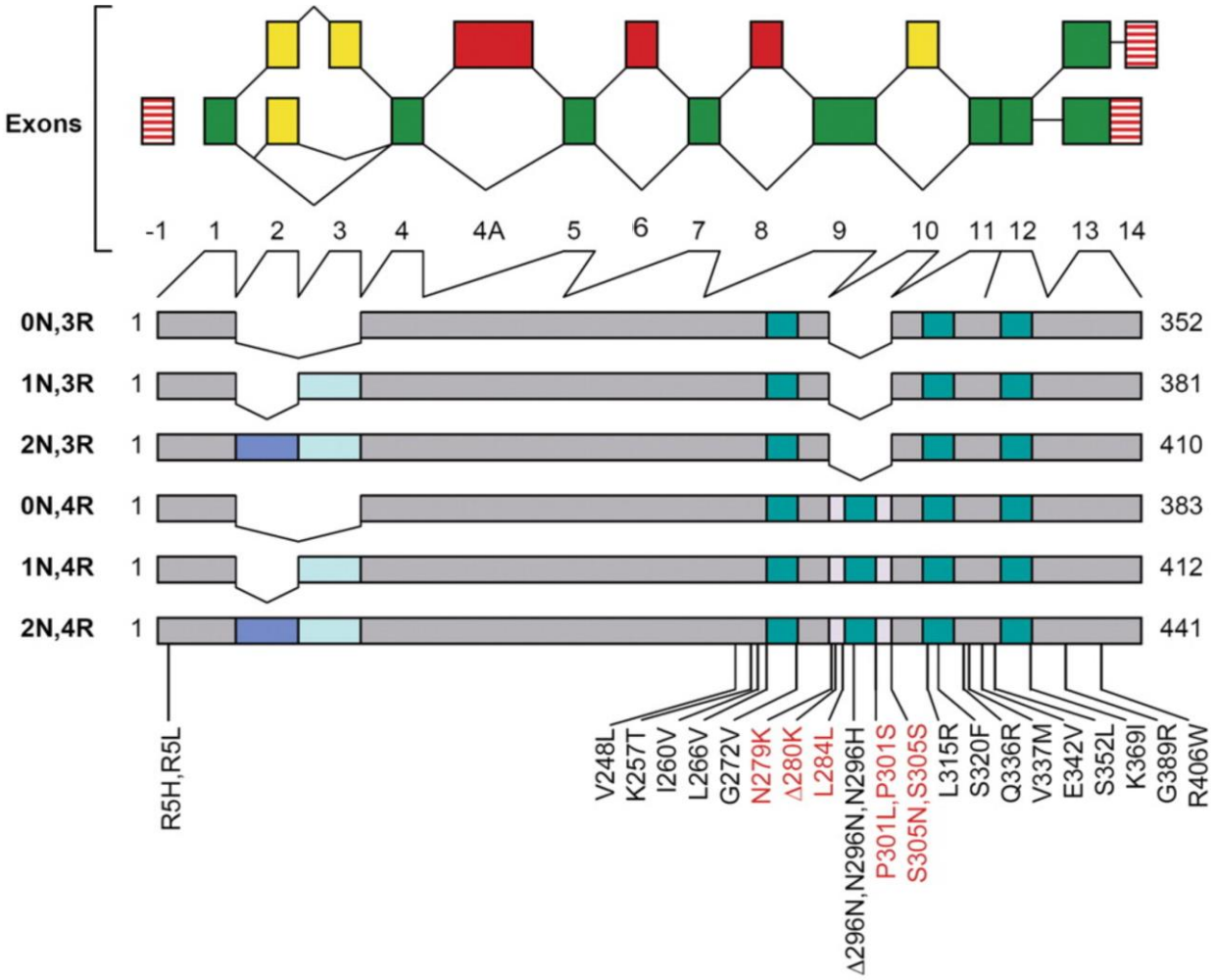

Figure 1.1 MAPT gene and transcripts, displaying effects of alternative splicing in the CNS. The exonic structure of the MAPT gene is displayed at top, with constitutive exons in green and alternatively spliced exons in yellow. Red boxes represent exons not included in CNS Tau. Exon 4a is present in PNS Tau. Below shows the six CNS Tau isoforms generated by alternative splicing, distinguished by their differential exclusion or inclusion of one or two N-terminal inserts and either three or four microtubule binding repeats. The number on the right indicate how many amino acids the mature proteins the corresponding splice variants contain, and at left is indicated the standard nomenclature of Tau isoforms: XNYR, where X = 0,1 or 2, and Y= 3 or 4. On the longest Tau isoform (2N4R) displayed at bottom, are represented the location and identity of the missense mutations arising from specific MAPT mutations and those indicated in red also affect splicing of exon 10. This figure is adapted from Pittman et al. (2006).

1.4.1.2 Secondary structure

Uncovering the secondary structure of Tau protein is of great interest as the aggregation of Tau protein into insoluble filaments is a characteristic feature of numerous neurodegenerative diseases. Under normal conditions, however, biophysical structural characterisation reveals Tau as a natively unfolded or intrinsically disordered protein with minimal and transient secondary structure, such as beta sheets and alpha-helices (Mukrasch et al. 2009; Avila et al. 2016). Regions of Tau which participate in these formations of transient secondary structure are depicted in **figure 1.2**.

Moreover, there is evidence Tau may from a 'paperclip' conformation whereby the N and C-terminal regions come into close proximity (Jeganethan et al. 2006). This structure may protect against the self-aggregation of Tau protein by shielding residues critical for this process. Interaction between Tau and other proteins may also promote the formation of secondary structure in Tau thereby with the effect of diverting Tau away from aggregation (Grüning et al. 2014).

Overall, the evidence suggests that Tau protein exhibits a structural flexibility. Such flexibility is important for the physiological functioning of Tau, but is also implicated the pathophysiological process of Tau aggregation.

1.1.1.1 Structure of Tau aggregates

Efforts to resolve the structure of aggregated Tau using cryo-EM have recently revealed the conformation of Tau aggregates from Alzhimer's disease (Fitzpatrick et al., 2017) and Pick's disease (Falcon et al. 2018). Predominantly two kinds of Tau filaments are extracted from Alzheimer's disease brain: straight filaments and paired helical filaments. These ultrastructural polymorphs are each composed of two C-shaped protofilaments, with residues V^{306}-F^{378} (R3 and R4) forming the core of the filaments upon which successive Tau molecules pack to form a beta-sheet structure (Fitzpatrick et al. 2017). The second microtubule binding repeat (R2) therefore does not form part of the core of the AD Tau

aggregates, consistent with the mixed 3R/4R-Tau composition of these structures and their ability to seed aggregation of 3R and 4R-Tau (Guo et al. 2016).

On the other hand, aggregates from Pick's disease brain reveal a distinct molecular conformation with the filament core being composed of amino acids K^{254}-F^{378} (R1, R3 and R4) exclusively from 3R-Tau (Falcon et al. 2018). Two kinds of filaments are extracted from Pick's disease brain – narrow filaments and wide filaments. The former are composed of a single protofilament, two of which may associate to form the latter (Falcon et al. 2018). The cryo-EM structure of Tau aggregates from Alzheimer's disease and Pick's disease are shown in **figure 1.2**.These findings suggest that specific conformers of aggregated Tau may underlie the heterogeneity of Tauopathies, the precise folding of Tau aggregates may segregate with distinct neurodegenerative diseases and indicate regional vulnerability in addition to seeding mechanisms.

1.4.2 Post-translational and structural modifications of Tau

1.4.2.1 Phosphorylation

1.4.2.1.1 Physiological

Tau protein function is regulated by extensive post translational modifications (PTMs). Physiological phosphorylation and pathophysiological hyperphosphorylation of Tau is well described, and 2N4R Tau contains 80 Ser/Thr and 5 Tyr residues, putative targets for proline directed kinases and non-proline directed kinases (Guo et al. 2017). Phosphorylation of Tau in the microtubule binding domain can impair the association of Tau with tubulin (Correas. 1992) thus modulating its microtubule stabilising function. Specifically, Ser262 is identified as a key residue, the phosphorylation of which dramatically inhibits Tau - microtubule binding (Biernat et al. 1993). Interestingly, there appears to be cross-talk between kinases and 'priming' may occur, whereby phosphorylation of one Tau residue may promote the subsequent phosphorylation of other nearby residues. For

example the pre-phosphorylation of Tau at ser235 primes Tau phosphorylation at Thr231 by GSK-3 (Cho & Johnson 2004). This particular pattern of phosphorylation furthermore strongly inhibits the association of Tau with microtubules.

There is evidence that the phosphorylation of foetal Tau exceeds that of mature Tau and it shares phosphoepitopes with PHF Tau from AD brain (Kanemaru et al. 1992). Foetal brain undergoes extensive synaptogenesis and remodelling, and therefore higher levels of phosphorylation of Tau may serve to prevent excess microtubule binding which would otherwise interfere with this process (Hanger et al. 2009).

Tau protein associated with membranous structures is de-phosphorylated relative to cytosolic Tau fractions, further indicating that the phosphorylation status of Tau correlates with its sub-cellular localisation (Arrasate et al. 2000).

Overall, phosphorylation is a key PTM that regulates the cellular function of Tau protein.

1.4.2.1.2 Pathophysiological

Pathological Tau from AD brains is characterised as hyperphosphorylated, with approximately eight phosphates per molecule, 3-4 fold higher than cytosolic Tau from control brains (Köpke et al. 1993). Furthermore, in AD phosphorylation occurs at abnormal sites including Thr-231 and Ser-235 (Hasegawa et al. 1992). Tau hyperphosphorylation promotes its missorting to somatodendritic compartment (Hoover et al. 2010). Moreover, Tau hyperphosphorylation influences its trafficking and degradation, for example phospho-mimic Tau mutants accumulate to a greater extent than WT-Tau upon inhibition of autophagy (Rodríguez-Martín et al. 2013).

The balance of activity of kinases and phosphatases will ultimately be responsible for the phosphorylation status of Tau within neurons. In pathological conditions there is a shift toward phosphorylation will may be reflective of reduced phosphatase activity, increased kinase activity, or both (Hanger et al. 2009).

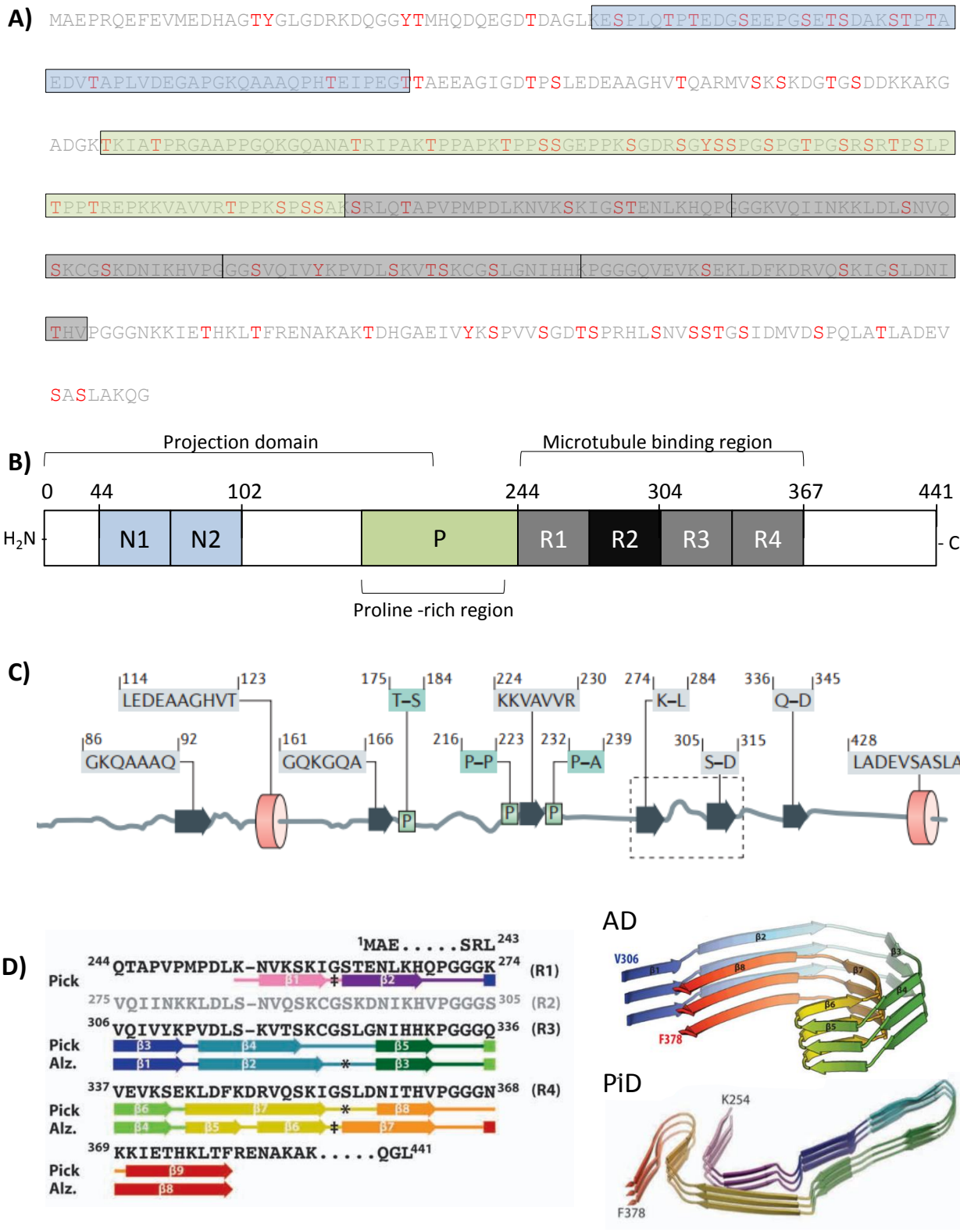

Figure 1.2 Primary and secondary structure of Tau protein. A) Primary amino acid sequence of the human 2N4R Tau isoform. Putative phosphorylation sites are indicated in red text. The coloured boxes identify molecularly and functionally defined regions of Tau: blue = N-terminal inserts, green = proline rich domain, grey = microtubule binding regions**. B)** Schematic representation of the primary structure of WT-2N4R-Tau protein illustrating the two N-terminal insets (N1, N2; blue boxes) proline rich domain (P; green boxes) and constitutive (R1, R3 and R4) and alternatively spliced (R2) microtubule binding regions. **C)** Tau protein is predominantly natively unfolded, represented by grey lines in the image. Regions of beta-sheets (grey arrows) and alpha helices (red cylinders) form transiently, as do secondary structures arising from proline residues (green boxes). The dashed boxed region is the locus of peptide motifs in Tau critical for self-assembly. Figure is adapted from Wang & Mandelkow (2015) . **D)** Primary sequence of Tau indicating regions involved in beta-sheet formation in Alzheimer's disease (Alz) and Pick's disease (Pick) aggregates. Rendered images of the aggregate cores are shown on the right. Adapted from Fitzpatrick et al. (2017) and Falcon et al. (2018).

1.4.2.2 Other PTMs of Tau

Other PTMs of Tau have been observed including *O*-linked *N*-acetylglucosamination, which may hinder aggregation and toxicity (Yuzwa et al. 2012), but aberrant glycosylation may promote hyperphosphorylation in some settings (Liu et al. 2002). Truncation of Tau by caspases has been reported, which may produce pro-aggregating and toxic Tau fragments (De-Calignon et al. 2010). Tau also undergoes SUMOylation (at K340; Luo et al. 2014), nitration (Horiguchi et al. 2003) and acetylation (Cohen et al. 2011) all of which have been linked to pathophysiological effects. The effects of Tau SUMOylation are introduced below, in section **1.9.3** in the context of exosomal Tau sorting.

1.5 Tau function

1.5.1.1 Cytoskeletal functions

Tau is primarily distributed in axons of CNS neurons and through its repeat domain (residues 200 -400) Tau interacts with tubulin (at a ratio of 0.5) promoting tubulin polymerisation and stabilising microtubule dynamics (Hong et al. 1998; Mandelkow & Mandelkow 2012; Feinstein & Wilson 2005). Microtubule function is fundamental to the information processing property of neurons through establishing and maintaining neuronal polarity. Tau protein has been implicated in neurite formation through interaction with microtubules (Caceres & Kosik, 1990) and promotes formation of axon-like processes when expressed in non-neuronal cells (Knops et al. 1991; Baas et al. 1991).

Immunoprecipitation of N-terminally truncated Tau species from the human brain identified Tau species with differing abilities to bind microtubules; Gln124-Tau (i.e. Tau missing the first 124 amino acids) bound microtubules more avidly than WT-Tau, and was able to more strongly protect against nocodazole induced microtubule disassembly (Derisbourg et al. 2015). The presence of such fragments in the brain may have deleterious effects on the dynamicity of the cytoskeletal network, potentially impinging upon synaptic plasticity mechanisms including neurite outgrowth and transportation of cargo required for

local metabolism. Such findings are likely due to the fact that the N-terminus of Tau is negatively charged; therefore its removal promotes interaction with the negatively charged microtubules.

Tau protein also acts to co-organise actin and microtubule formation by cross-linking the adjacent networks. Tau binds to actin, and through the formation of alpha-helices separated by flexible linkers, promotes actin bundling. Binding to actin occurs at microtubule binding regions in Tau (Cabrales Fontela et al. 2017) and bundling activity is attenuated by phosphorylation at KXGS motifs. Because Tau promotes the elongation of F-actin co-aligned with the microtubules, and this function is dependent upon the presence of at least two microtubule binding repeat domains and is independent of the N-terminal region, it is suggested Tau organises the two cytoskeletal networks simultaneously through distributing its MTBR between them (Elie et al. 2015).

These findings have relevance to neuronal function and health, as aberrations in Tau's ability to modulate the actin cytoskeleton may promote abnormal actin bundling and lead to neurodegeneration (Fulga et al. 2007).

It is well appreciated that the ability of Tau protein to bind to and affect the stability and polymerisation of microtubules is modulated by phosphorylation at distinct sites in Tau. Phosphorylation confers local negative charge thereby disrupting electrostatic interactions with microtubules. Indeed, phosphorylation as Ser262, a residue located within the first MTBR of Tau, inhibits the binding of Tau to microtubules (Biernat et al. 1993). Dual phosphorylation of other residues within the MTBRs - Thr231 and Ser235 – maximally inhibit the binding of microtubules by Tau (Sengupta et al. 1998) and phospho-mimics of the proline-rich domain of Tau also inhibit its ability to promote the polymerisation of microtubules (Eidenmu et al. 2001). A schematic model of Tau binding to microtubules and its regulation by phosphorylation is displayed in **figure 1.3**.

These lines of evidence indicate that Tau's ability to organise cytoskeletal components is an important cellular function with a concomitantly rich level of modulation. The role of Tau in stabilising and nucleating the polymerisation of microtubules is conferred upon the molecule predominantly by its MTBR, although adjacent N and C-termini may modulate this function. For example, the N-terminal projection domain of Tau plays a role in determining the spacing between adjacent microtubules (Chen et al. 1992) and interacts with the plasma membrane (Brandt et al. 1995). PNS specific Tau contains an extra exon (4a) coding for an additional N-terminal insert that may be important for the large diameter axons projected in the PNS (Goedert et al. 1992a).

A Recent study contests the widely held conception of Tau protein functioning as a microtubule *stabilising* protein. Qiang et al. (2018) demonstrated that Tau expression was localised to labile domains of microtubules and knockout of Tau in superior cervical ganglia neuron axons resulted in a reduction of tyrosinated Tubulin – a marker of stable microtubules. The authors also noted that post nocodazole recovery of axonal microtubules was associated with the localisation of Tau to labile domains and the rate of nocodazole induced depolymerisation of microtubules was reduced in Tau knockdown axons, suggesting microtubules were more stable in the absence of Tau. MAP6 on the other hand was demonstrated to genuinely stabilise microtubules as MAP6 knockdown increased vulnerability to nocodazole induced depolymerisation. The authors concluded that, contrary to popular belief, Tau protein does not stabilise axonal microtubules but allows the formation of long labile microtubular domains. One drawback of this study was that the expression of Tau in the neuronal cultures was not characterised. These cultures came from rat foetuses / pups of 0-2 days a developmental stage at which there is a predominant expression of 3R-Tau (Kosik et al. 1989). It is therefore important to address whether 4R-Tau affects the microtubule network in the same way.

Tau knockout mice are viable and lack an overt phenotype which may be due to compensation by other microtubule binding proteins (MAPs). However, a recent report identified subtle yet important deficits in Tau knockout mice. Behaviourally, Tau knockout mice exhibited increased locomotor activity, (mild) short term memory deficits, working memory and contextual memory deficits. Whilst electrophysiologically, Tau knockout mice had significantly impaired LTP at the CA1-CA3 synapse (Biundo et al. 2018). Furthermore, there have been reports of muscle weakness with increasing age in Tau knockout mice, although elsewhere opposing effects on synaptic plasticity have been noted (For reviews see: Ke et al. 2012; Wang & Mandelkow. 2016).

1.5.1.2 Non-cytoskeletal functions of Tau

The microtubule binding and stabilisation function of Tau is perhaps the most important role of Tau, and clearly the most well studied. The developmental regulation of isoform expression (i.e. 3R vs 4R) and phosphorylation of Tau is consistent with this function. However, there may be differential subcellular localisation of different Tau isoforms as a function of selective blockade of Tau transport by the axon initial segment (Zempel et al. 2017) and sub-cellular localisation may be the key to understanding non-microtubule based functions of Tau. For instance, Tau protein is also detected in the nucleus and at the plasma membrane. The functional role of nuclear Tau is unknown, as is its molecular identity, but the interaction of Tau with DNA, and the ability of Tau to increase the melting temperature of DNA suggests Tau may have a role in the stabilisation of chromosomes (Bukar Maina et al. 2016). Moreover, Tau protein has recently been implicated in insulin signalling; Tau knockout reduces the sensitivity of hippocampal neurons to insulin, demonstrated by reductions in the phosphorylation of downstream signalling components (Marciniak et al. 2017). Other atypical functions of Tau are still being discovered and characterised, and involve functions related to myelination and effects on neuroplasticity (review (Sotiropoulos et al. 2017)). Tau may also exert effects as an extracellular signalling

molecule. Tau promotes calcium influx via M1 and M3 receptors, an effect which is localised to the C-terminal part of the molecule and may promote calcium dys-homeostasis in hippocampal neurons. The physiological / pathophysiological role of extracellular Tau as a signalling molecule is therefore an important question (Gómez-Ramos et al. 2008). Overall there is clear evidence that Tau protein participates in cellular and extracellular functions beyond its chief role in the stabilisation of microtubules.

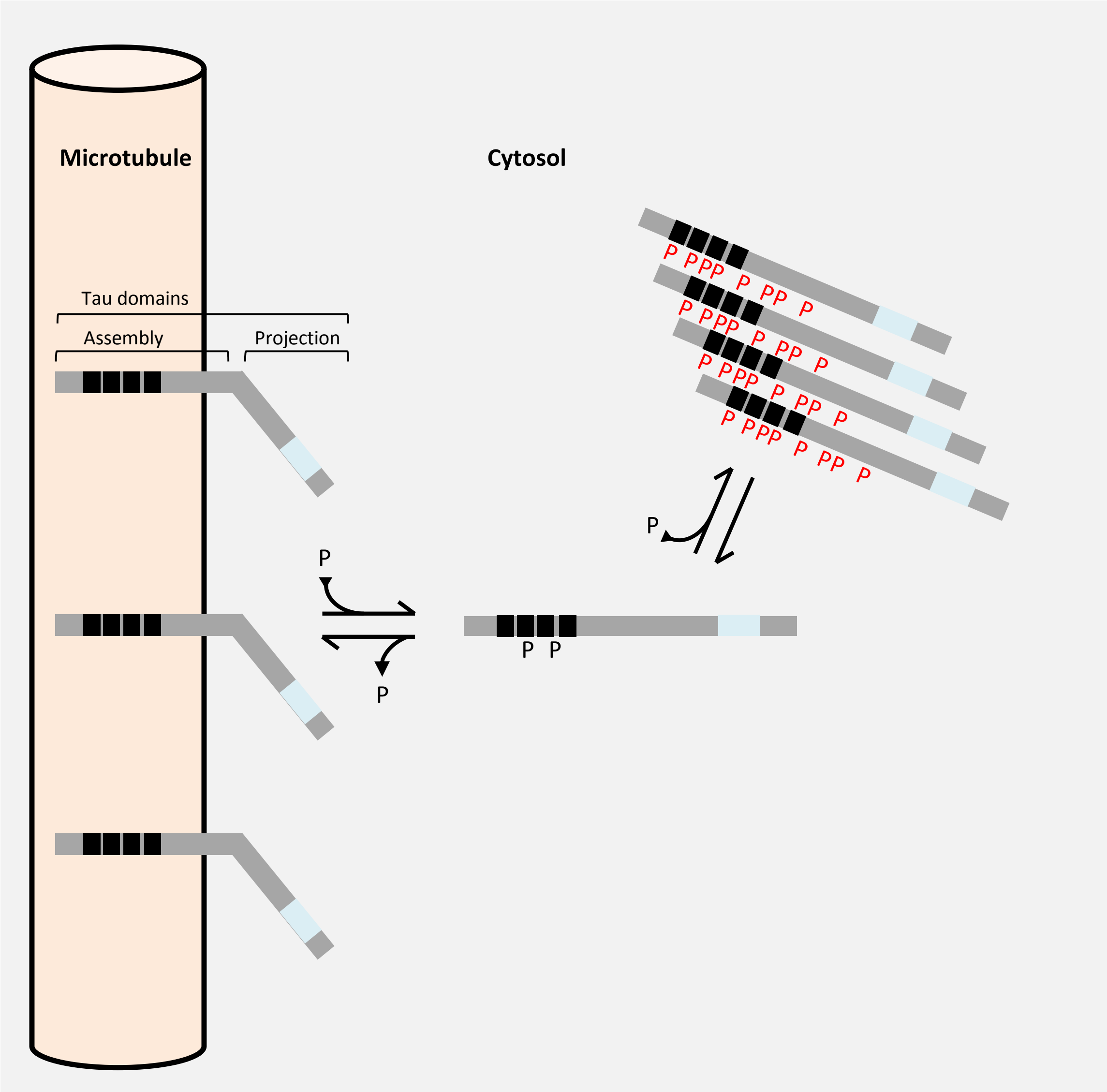

Figure 1.3 Model of the regulation of Tau – microtubule interaction. In the axonal compartments of neurons, Tau (grey box with blue and black colouring) binds to microtubules (orange cylinder) thus stabilising them. The ‘assembly’ domain of Tau, containing 3 or 4 repeats (4R only displayed, black boxes), is the region of Tau that directly interacts with microtubules. The ‘projection’ domain, containing the prole rich region and N-terminal inserts (blue box) projects away from the microtubules. The equilibration of Tau between cytosolic ‘free’ forms and microtubule ‘bound’ forms is regulated by phosphorylation (black ‘P’) of Tau, which favours the detachment of Tau from microtubules. Hyperphosphorylation of Tau (rep ‘P’) is associated with the aggregation of Tau molecules (upper right).

1.6 Tau and neurodegeneration

1.6.1 Tau mutations

1.6.1.1 Missense mutations

Mutations in *MAPT* have been linked to Tauopathies resembling Pick's disease, CBD and PSP, and identify aberrations in Tau as sufficient for the genesis of neurodegenerative disease (D'Souza et al. 1999). Over 80 missense mutations in *MAPT* have been described, some of which are displayed in **figure 1.4** (Wang & Mandelkow. 2016). Pathological Tau mutations tend to coalesce around the microtubule binding regions of the Tau protein such as P301L and R406W (Hutton et al. 1999). This is the most highly conserved region of Tau; alterations in the physio-chemical properties of this region are therefore associated with dramatic functional and pathophysiological effects. For instance there is evidence that such mutations affect the ability of Tau to bind to and stabilise microtubules (Dayanandan et al. 1999). Such a situation favours the equilibration of Tau into the free cytosolic form, thereby increasing the accessibility of the molecule to kinases such as GSK-3 and leading to increased phosphorylation associated with pathological Tau conformations. Mutations such as P301L and ΔK280 may directly alter the local structural properties of Tau independent from their effects on microtubule binding, thereby directly favouring inter-molecular beta-sheet formation with neighbouring Tau molecules (Fischer et al. 2007). In living cells, however, detachment from microtubules, hyperphosphorylation and aggregation are likely interlinked events contributed to more or less by distinct mutations.

Interestingly, mutations that lie at the extreme N-terminal of Tau have also been described (R5H, R5L) that are linked to neurodegenerative disease (FTD and PSP respectively, Alzforum, Poorkaj et al. 2002). This is a highly conserved residue in Tau and whilst lying outside the microtubule binding regions, the R5L mutation has been shown to have

reduced ability to promote microtubule assembly (Poorkaj et al. 2002) activity implicating the N-terminus in the microtubule stabilising function of Tau. Furthermore, according to the cryo-EM structure of SFs and PHFs from AD brain, the extreme N-terminus participates in cross beta-structure with the core of the aggregates (Fitzpatrick et al. 2017). The N and C-termini of Tau may furthermore come into close proximity in a paperclip formation that stabilises the molecule and may prevent aggregation (Jeganathan et al. 2006). It is therefore conceivable that mutations in the N-terminus of Tau could contribute to the molecules intrinsic ability to self-aggregate, potentially by destabilising intramolecular interactions and promoting inter-molecular Tau – Tau self-association.

1.6.1.2 Splicing mutations

There are also 'silent' mutations in Tau that are associated with neurodegenerative disease. Such mutations alter the splicing of Tau, favouring exon Tau inclusion, potentially through destabilisation of a stem-loop structure located at the exon-10-intron boundary (Wolfe 2009). The location of such mutations, including missense mutations with the same effect, and the stem loop structure in Tau RNA is shown in **figure 1.4**. Such mutations therefore result in changes to the ratio of 4R:3R Tau expression. How this leads to neurodegeneration is unclear, but is potentially mediated through effects on the cytoskeleton, as 3R and 4R Tau differentially promote microtubule stabilisation. Most splicing mutations favour the inclusion of exon 10 resulting in increased 4R:3R Tau. Excessive levels of 4R Tau may decrease the dynamic function of microtubules (Panda et al. 2003). Moreover, aggregation of 4R Tau is inhibited by 3R Tau, therefore increasing the ratio of 4R:3R Tau is likely to favour 4R Tau aggregation (Adams et al. 2010). On the other hand, some splicing mutations such as L266V and G272V are primarily associated with 3R containing Tau Pick bodies (Bronner et al. 2005; Hogg et al. 2003) and this may be associated with decreased exon 10 inclusion and a decreased 4R:3R Tau ratio (Liu & Gong 2008).

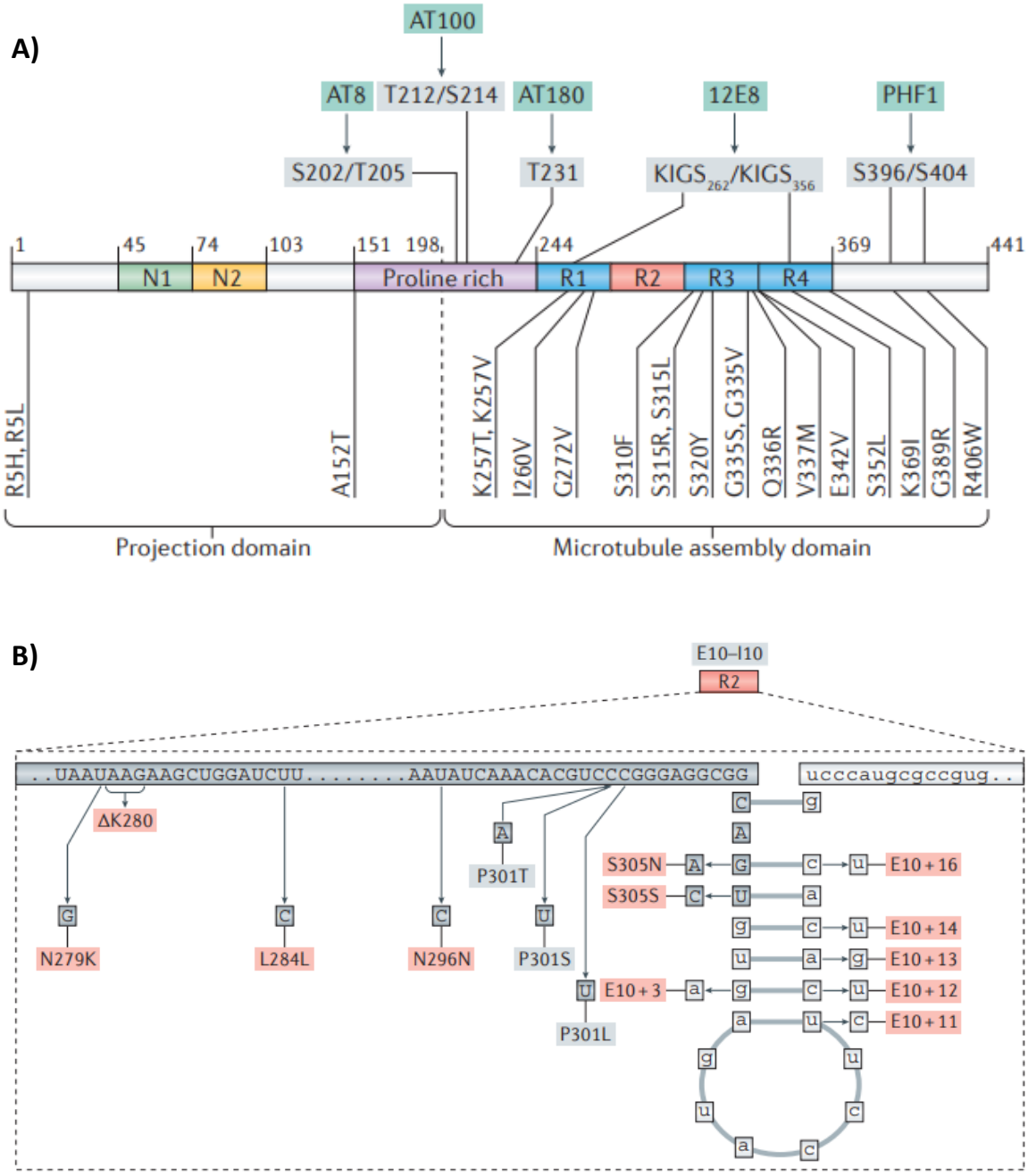

Figure 1.4 Pathological changes in Tau. A) Schematic diagram of 2N4R-Tau and its subdivision into the projection and assembly domains. Pathological hyperphosphorylation is associated with Tau pathology and can be characterised by specific phosphoepitopes including PHF-1, AT8, AT100, AT80 and 12E8 which are displayed. The locations of various pathological mutations, which tend to coalesce around the microtubule binding regions are indicated below. **B)** mRNA sequence of Tau at the exon 10 – intron 10 boundary. Exonic sequence is shown in uppercase and intronic sequence in lowercase. Mutations that occur near the exon-10 intron-10 boundary may affect the splicing of Tau through destabilisation the stem-loop structure. These mutations are shown in red boxes. This figure is adapted from Wang & Mandelkow. (2016).

These lines of evidence collectively demonstrate that the precise control of the expression ratios of distinct Tau isoforms is important in Tau pathophysiology.

Overall, Mutations in Tau that cause or increase the risk of neurodegeneration may be reflective of the causes and mechanisms of apparently sporadic Tauopathy. Mutations unmask the ability of Tau to self-associate and implicate loss of Tau's microtubule stabilising function in neurodegeneration.

1.6.2 Tau pathology

Dys-homeostasis of Tau protein is at the centre of numerous neurodegenerative diseases termed 'Tauopathies'. Alzheimer's disease (AD) is the most common neurodegenerative Tauopathy and is also associated with a co-pathology of amyloid beta plaques (Murphy et al. 2010). Alzheimer's disease is therefore referred to as a 'secondary Tauopathy'. Primary Tauopathies include, among others (see **table 1.1**) Frontotemporal dementia-Tau (FTD-Tau) and its subtypes Pick's disease, (PiD), corticobasal degeneration (CBD) and progressive supranuclear palsy (PSP) all of which are characterised by the intracellular accumulation and aggregation of hyperphosphorylated Tau protein into a filamentous form (Spillantini & Goedert. 2013). The topographic distribution of Tau pathology segregates distinct Tauopathies and correlates with clinical presentation (e.g. memory loss in AD, Tau pathology and neurodegeneration in hippocampus, behavioural changes in frontotemporal dementia) and severity (Bierer et al. 1995). The composition of the Tau isoforms (3R vs 4R) found in the hallmark pathological inclusions also varies between the diseases, as discussed below.

1.6.2.1 Alzheimer's disease

The aggregates typifying different Tauopathies are composed of distinct Tau isoforms. Alzheimer's disease which is the most common Tauopathy is characterised by the accumulation of Tau into neurofibrillary tangles (NFTs) and neuropil threads (NPs). NFTs are

deposited in the limbic cortices of Alzheimer disease brain and the entorhinal cortex is the most strongly affected region (Arnold et al. 1991). Paired helical filament (PHF) Tau refers to the filamentous forms of Tau that are extracted from AD brains by ultracentrifugation. PHF Tau is composed of all six Tau isoforms in a heavily phosphorylated state (Goedert et al. 1992b). Moreover, pathological Tau in AD brain exhibits phosphorylation at abnormal sites and is immunoreactive with the AT8 antibody which detects Tau triply phosphorylated at S202, T205 and S208 (Malia et al. 2016). Furthermore, Tau in AD brains is selectively detected by the Alz50 antibody which recognises a discontinuous epitope in Tau, comprising regions from the N-terminal and microtubule binding regions (Carmel et al. 1996). This suggests that AD Tau forms intramolecular interactions distinguishing it from normal Tau. ThioS birefringence of AD hippocampi demonstrates the presence of beta-sheet rich structures, arising from aggregated Tau proteins, the presence of which is confirmed by cryo-EM structural analysis of PHF and SF Tau extracted from AD brains (Fitzpatrick et al. 2017). Hippocampal Tau pathology detected in an AD brain is shown in **figure 1.5**.

1.6.2.2 Frontotemporal dementia

The frontotemporal dementias represent a set of heterogeneous neurodegenerative diseases involving degeneration of the frontal lobes. The precise relationship between the FTDs difficult to decipher, however, ~40% of FTD cases are associated with Tau pathology (Young et al. 2018), termed FTD-Tau. FTD-Tau can be further sub-divided into Pick's disease (PiD), corticobasal degeneration (CBD) and progressive supranuclear palsy (PSP), each of which can be characterised by distinct neuropathological changes in Tau related to Tau isoforms involvement and morphologies of glial inclusions (Finger 2016; Dickson 1999).

1.6.2.2.1 Pick's disease

PiD is associated with Tau pathology in neuronal and glial cells. The distinctive neuropathological feature of PiD is large spherical neuronal cytoplasmic inclusions termed 'Pick bodies'. Intra-neuronal Pick bodies are primarily composed of 3R-Tau (Mackenzie & Neumann 2016) which are found in the limbic and neocortical regions as well as the granule cells of the dentate gyrus and hippocampal neurons. Typical Pick bodies are shown in **figure 1.5**. Tau positive glial inclusions, on the other hand, contain predominantly 4R-Tau isoforms (Mackenzie & Neumann 2016; Hogg et al. 2003). Some sporadic cases, however, were associated with 3R positive 4R negative astrocytic inclusions (Irwin et al. 2016). Although Pick bodies are not co-stained with 3R and 4R Tau antibodies, consistent with a preferential homo-isoform aggregation mechanism (Adams et al. 2010), NFTs composed of mixed 3R/4R Tau isoforms may also be detected in PiD (Zhukareva et al. 2002). Collectively, these observations highlight heterogeneity in the Tau neuropathological makeup of PiD.

1.6.2.2.2 PSP and CBD

There is considerable clinical and neuropathological overlap between PSP and CBD although they are distinct entities, classifiable as such on the basis of distinct Tau pathology in glial cells (Scaravilli et al. 2005; Dickson 1999).

Typical clinical features of PSP include rigidity and bradykinesia that are unresponsive to levodopa, falls and vertical supranuclear gaze palsy (Josephs 2015). PSP displays frontal lobe degeneration and is neuropathologically characterised by the presence of Tau aggregates composed of 4R Tau isoforms. However, the specific neuropathological feature of PSP is 'tufted astrocytes' which display Tau filaments that localise to nuclear regions and are immunoreactive with the AT8 antibody. Tufted astrocytes display a redistribution of GFAP immunoreactivity to nuclear locations (Mackenzie & Neumann 2016; Ferrer et al. 2014). Tufted astrocytes typical of PSP are shown in **figure 1.5**.

CBD presents clinically as a movement disorder, with rigidity and dystonia that are unresponsive to levodopa. Cortical symptoms are also present such as ideomotor apraxia (Wenning et al. 1998) as both cortical and subcortical regions are affected by Tau pathology. Specifically, degeneration is observed in the frontal and parietal cortices, and the basal ganglia. CBD neuropathology is distinguished from other FTD-Tau subtypes by the presence of Tau positive astrocytic plaques (Mackenzie & Neumann 2016). Astrocytic plaques seen in CBD are shown in **figure 1.5**. CBD Tau inclusions are formed predominantly of 4R-Tau (Buée et al. 2000) although 3R-Tau inclusions are also observed in some brain regions in CBD cases such as the basal ganglia. These observations suggest that certain brain regions may be differentially susceptible to the aggregation of specific Tau isoforms.

1.6.2.3 Chronic traumatic encephalopathy

Chronic traumatic encephalopathy (CTE) is a neurodegenerative disease associated with repetitive brain trauma leading to progressive dementia. CTE is characterised neuropathologically by the presence of neurofibrillary tangles composed of phosphorylated Tau species. Tau deposits in CTE are distinguished from those present in other Tauopathies by their presence in the cortical sulci. Tau aggregates in CTE are mixed 3R and 4R and all six Tau isoforms are present. CTE also presents with astrocytic tangles in periventricular and subpial regions, both of which distinguish CTE from AD (McKee et al. 2013; McKee et al. 2015). Detection of Tau aggregates and abnormal Tau phosphorylation in the hippocampi of post-mortem CTE brains is shown in **figure 1.5**.

There are a number of primary Tauopathies that have not been directly mentioned here. A more complete list of primary Tauopathies (and the secondary Tauopathy, Alzheimer's disease) along with their aggregate isoform specificity are displayed in **table 1.1**.

Table 1.1 Summary of Tau isoform pathology in different Tauopathies. This table is modified from (Josephs 2017)

Current pathological diagnosis	Type of Tauopathy
Alzheimer's disease	3R+4R
Pick disease	3R
Progressive supranuclear palsy	4R
Corticobasal degeneration	4R
Argyrophilic grain disease	4R
Globular glial Tauopathies	4R
Aging-related tau astrogliopathy	4R
Chronic traumatic encephalopathy	3R+4R
Tangle dominant dementia /Primary age-related Tauopathy	3R+4R
Parkinsonism-dementia complex of Guam	3R+4R
Postencephalitic parkinsonism	3R+4R
Atypical parkinsonism of Guadeloupe	3R+4R
Diffuse neurofilament tangles with calcification	3R+4R
Frontotemporal dementia and parkinsonism linked to chromosome 17	3R, 4R, or 3R+4R

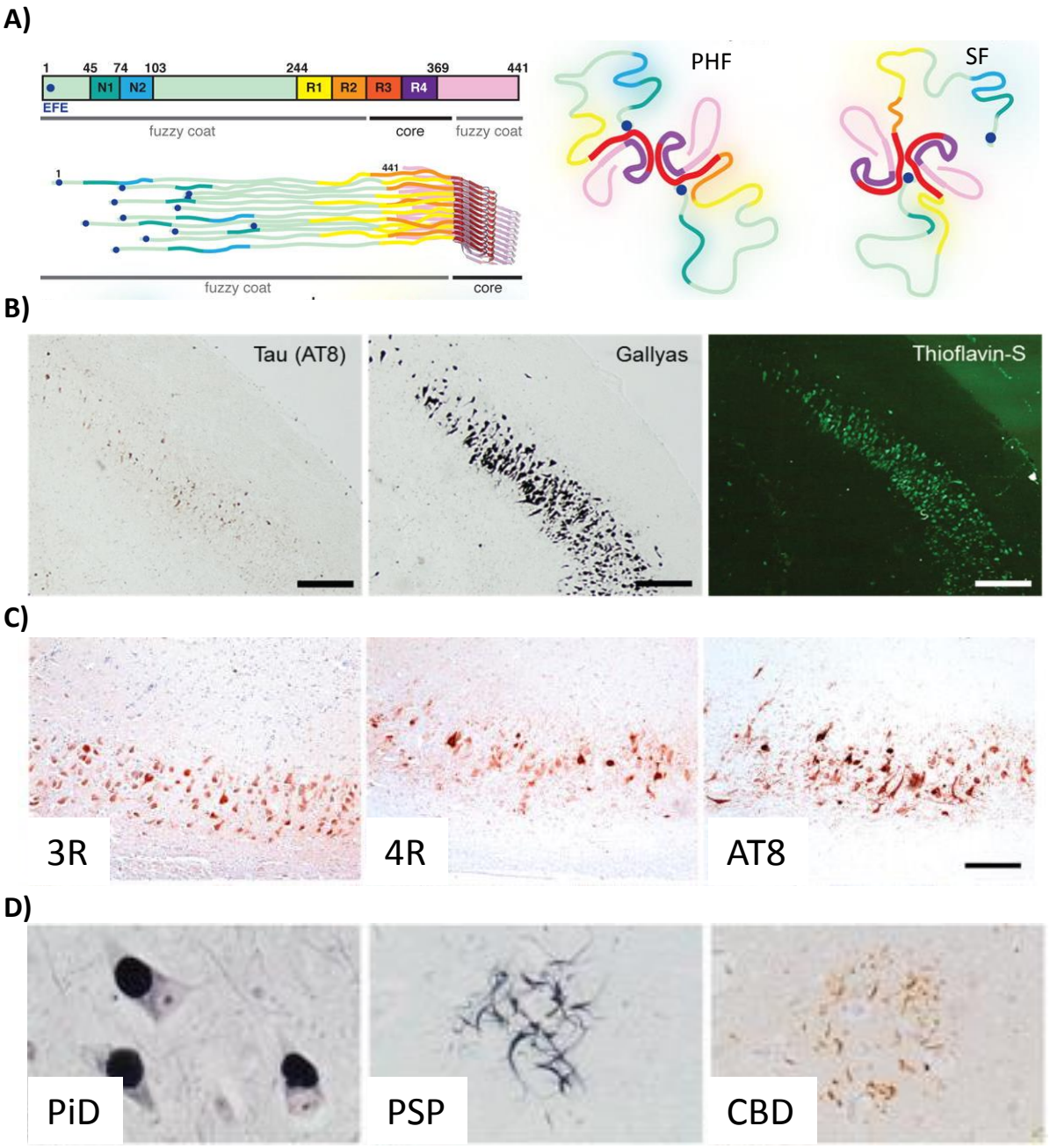

Figure 1.5 Tau neuropathology in distinct neurodegenerative diseases A) Cryo-EM defined structure of Tau filaments isolated from AD brain. Left side displays primary structure of Tau aligned with side view of a Tau filament, Tau filaments stack on the helical axis of the filament, independently of N-terminal inserts. Right side shows cross sectional views of paired helical filaments (PHF; left) and straight filaments (SF; right). Figure is adapted from Fitzpatrick et al. (2017). **B)** Tau pathology in the hippocampus of an Alzheimer's disease brain, stained with, from left to right, AT8 demonstrating phosphorylated Tau, Gallyas stain and Thioflvain-S demonstrating cross-beta sheet structure of the Tau aggregates. Figure is adapted from Harada et al. (2016). **C)** Hippocampal Tau pathology in CTE characterised by (from left to right) 3R and 4R-Tau pathology, and AT8 staining identifying the presence of pathologically phosphorylated Tau. Scale bar 50 µm. Figure is adapted from Mckee et al. (2015). **D)** Distinct tau pathology in the FTD-Tau variants, from left to right: Pick bodies in PiD, tufted astrocytes in PSP and astrocytic plaques in CBD. Figure is adapted from Mackenzie and Neumann (2016).

1.6.3 Relationship between *MAPT* mutations and Tau pathology

Distinct Tau mutations may give rise to Tau pathology reminiscent of sporadic forms of Tauopathy. A recent study compared Tau pathology in sporadic and familial cases, and determined that pathology associated with specific mutations segregates into disease types classified by neuropathology. Thus CBD like pathology was associated with the R406W mutation whilst Pick's disease like pathology was associated with the K257T mutation (Forrest et al. 2018). Moreover, the P301S mutation has been associated with both frontotemporal dementia and CBD in different members of the same family (Bugiani et al. 1999) and the S305S Tau mutation (a silent splicing mutation) was associated with PSP and CBD like Tau pathology. These findings suggest that the relationship between primary changes in Tau and clinical presentation and neuropathology are complex and likely regulated by a number of modulatory factors. These findings also suggest that pathogenic mechanisms may be shared between familial forms of Tauopathy and sporadic Tauopathy.

1.6.4 Relationship between Tau aggregation and neurodegeneration

The precise relationship between the aggregation of Tau into NFTs and neurodegeneration is unclear. NFT burden in Alzheimer's disease correlates with disease duration and severity but lags behind the extent of neuronal loss (Gómez-Isla et al. 1997). This suggests that processes prior to the formation of NFTs promote neurodegeneration and cells contain NFTs are somehow resistant to this process because regions of neuronal loss coincide with those bearing NFTs. Moreover, the presence of NFTs may be dissociated from disruptions in neuronal function. For instance, when ectopic P301L expression was suppressed in transgenic mice, NFTs and sarkosyl insoluble Tau continued to accumulate, whereas memory function improved (SantaCruz et al. 2005). However, the ability of Tau to adopt beta-sheet structure is central to Tau mediated motor and behavioural deficits. Proline substitutions that prevent Tau aggregation, also prevent Tau induced motor deficits when

expressed in mouse brain (Lathuilière et al. 2017). Such effects are mediated through enhanced microtubule binding ability of proline-substituted Tau, arguing that Tau mediated neurodegeneration arises from both the loss of normal function (i.e. microtubule binding) and the gain of toxic function (i.e. aggregation). Moreover, expression of the repeat domain of Tau (RD-Tau) in mice results in Tau hyperphosphorylation and co-aggregation with endogenous mouse Tau. This phenotype is associated with neuronal and loss and hippocampal neurogliosis. However, neuronal loss is spared when the ability of RD-Tau to aggregate is curbed through the introduction of proline mutations (I^{277} and I^{308} to P^{277} and P^{308}). These findings tightly couple Tau aggregation to neuronal loss and neurodegeneration in a mouse model (Mocanu et al. 2008).

1.6.5 Mechanisms of aggregation

The aggregation of Tau in sporadic settings is likely due to interplay of the intrinsic properties of the molecule and post-translational modifications of Tau, combining with genetic factors. The adoption of a cross-beta sheet structure characterises the paired helical filaments and straight filaments of aggregated Tau isolated from AD brain. In these structures the third and fourth microtubule binding repeats form the 'core' of the filaments with the rest of the Tau molecule (i.e. the N and C-termini) forming a 'fuzzy coat' which is generally disordered but can fold back around to add additional beta structure via residues ^{7}EFE^{9} (Fitzpatrick et al. 2017) The structure of Tau filaments from AD brain is shown in **figure 1.5**. These structural findings correlate well with biochemical evidence which demonstrates the C-terminal hexapeptide motif ($_{306}$VQIVYK$_{311}$) in Tau is critical for its polymerisation *in vitro* (von Bergen et al. 2000). It is the propensity of this sequence to adopt a beta-sheet structure that underlies Tau self-assembly (von Bergen et al. 2005) as well as aggregation and neurodegeneration *in vivo* (Mocanu et al. 2008).

Tauopathy brain derived Tau is hyperphosphorylated with antibodies distinguishing pathological Tau inclusions through disease specific phosphoepitopes, (for example PHF-1

(pS396 + pS404), AT8 (pS202 + pT205), AT180 (pT231 + pS235), AT270 (pT181) and AT100 (pT212 + pS214) (Mandelkow & Mandelkow 2012). Tau phosphorylation may precede tangle formation in AD (Luna-Munoz et al. 2007) which suggests PTMs of Tau may causally influence aggregation. Additionally, truncation / limited proteolysis of Tau may be a key step to downstream NFT formation. For instance caspase cleaved Tau is detected in vascular dementia (Day et al. 2015) and caspase cleavage at D421 liberates a pro-aggregating Tau fragment that may be an early event in the development of AD tangle pathology (Rissman et al. 2004).

Overall the evidence suggests that in disease settings, aberrant processing of Tau, including PTMs such as phosphorylation may unmask the molecules intrinsic propensity for beta-sheet structure and self-association.

1.7 Progression and spread of tau pathology

1.7.1 Human studies

The topographical pattern of Tau aggregation observed in in the aforementioned diseases is not random. In each disease the neuroanatomical pattern of Tau deposition follows a stereotyped course that correlates with disease severity and is invariant between affected individuals. Neuropathology may therefore be categorised into distinct stages which have been elaborated for these diseases.

1.7.1.1 Alzheimer's disease

Neuropathological analysis of AD brains reveals NFT pathology to be progressive. Braak & Braak (1991) observed that AD associated Tau pathology follows a stereotypical topographic distribution with increasing severity that they classified into six stages; in AD ,Tau pathology originates in the entorhinal and transentorhinal cortices (stage I) with the hippocampus next to be involved (II). Limbic structures (subiculum, hippocampal formation) are affected next (III) followed by the amygdala, thalamus and claustrum (IV).

NFT pathology affects the isocortical regions in stage V, and stage VI is characterised by the involvement of the primary motor, sensory, and visual areas (Braak & Braak. 1991; Serrano-Pozo et al. 2011). This pattern of Tau pathology progression observed in Alzheimer's disease is displayed in **figure 1.6**.

Advances in Tau PET imaging may be able to reveal the precise spatio-temporalities of Tau progression in neurodegenerative diseases such as AD and provides promise as an early biomarker for AD (Saint-Aubert et al. 2017). For instance, live Tau imaging with the PET tracer [18F]THK5317 demonstrate increased Tau load in pre-AD and AD dementia patients over 17 months, and also reveal a complex, non-linear relationship between Tau burden and more stringent biomarker (hypometabolism) and clinical (MMSE) manifestations of dementia (Chiotis et al. 2017).

The application of PET Tau imaging to study the trans-neuronal spread of Tau has recently been adopted. Cope et al. (2018) used Tau imaging with 18F-AV-1451 and observed that more highly connected brain regions exhibited increased Tau radiotracer binding indicative of increased Tau burden and moreover positions Tau anterior to trophic deficits. The concentration of Tau pathology at densely connected brain regions implicates functional connectivity in the likelihood of a brain region developing pathology. This is reflective of models of infectious disease spread through populations and implicates a transmission of Tau between neurons in the progression of Alzheimer's disease.

1.7.1.2 Chronic traumatic encephalopathy

The phospho-Tau pathology characteristic of chronic traumatic encephalopathy (CTE) may also be neuropathologically staged. Pathology is initiated in localised foci on the cerebral cortex (stage I) followed by its invasion into the superficial cortical layers which is associated with astrocytic pathology (stage II). At this stage the substantia nigra and thalamus also display some NFT pathology. Stage III is characterise by a more severe pathology and associated reductions in brain weight. NFTs coalesce in the sulcal depths at

this stage, often localising to small vessels. In the latest stage (stage IV) pathology is characterised by severe and widespread phospho-Tau staining in the cerebral cortex, medial temporal lobes and hippocampal formation. The cerebellum also displays Tau pathology at this stage. This stage is associated with pronounced atrophy, enlargement of the ventricles and septal abnormalities (Stein et al. 2014). The pattern of phospho-Tau pathology in CTE is therefore highly progressive and follows a relatively predictable and stereotyped pattern (McKee et al. 2015). **Figure 1.6** schematically represents the topographic distribution of Tau pathology in the progressive CTE stages.

1.7.1.3 Frontotemporal dementia

Tau pathology in FTD follows a sequential pattern that may be categorised into five stages. Pathology is observed in limbic and frontotemporal neocortical regions in the earliest two stages of the disease – stage I limbic and stage I neocortical. Tau pathology next affects subcortical structures including the thalamus and striatum (stage II). Tau deposition in the primary motor cortex and medullary pre-cerebellar nuclei characterise stage III and widespread severe Tau pathology with encroachment into visual cortex is observed in stage IV (Irwin et al. 2016). The progression of Tau pathology in FTD-Tau is represented in **figure 1.7**. Tau load in CBD increases with disease duration and there is speculation that CBD initiates as an astrogliopathy that is sequentially overtaken by severity of neuronal lesions (Ling et al. 2016).

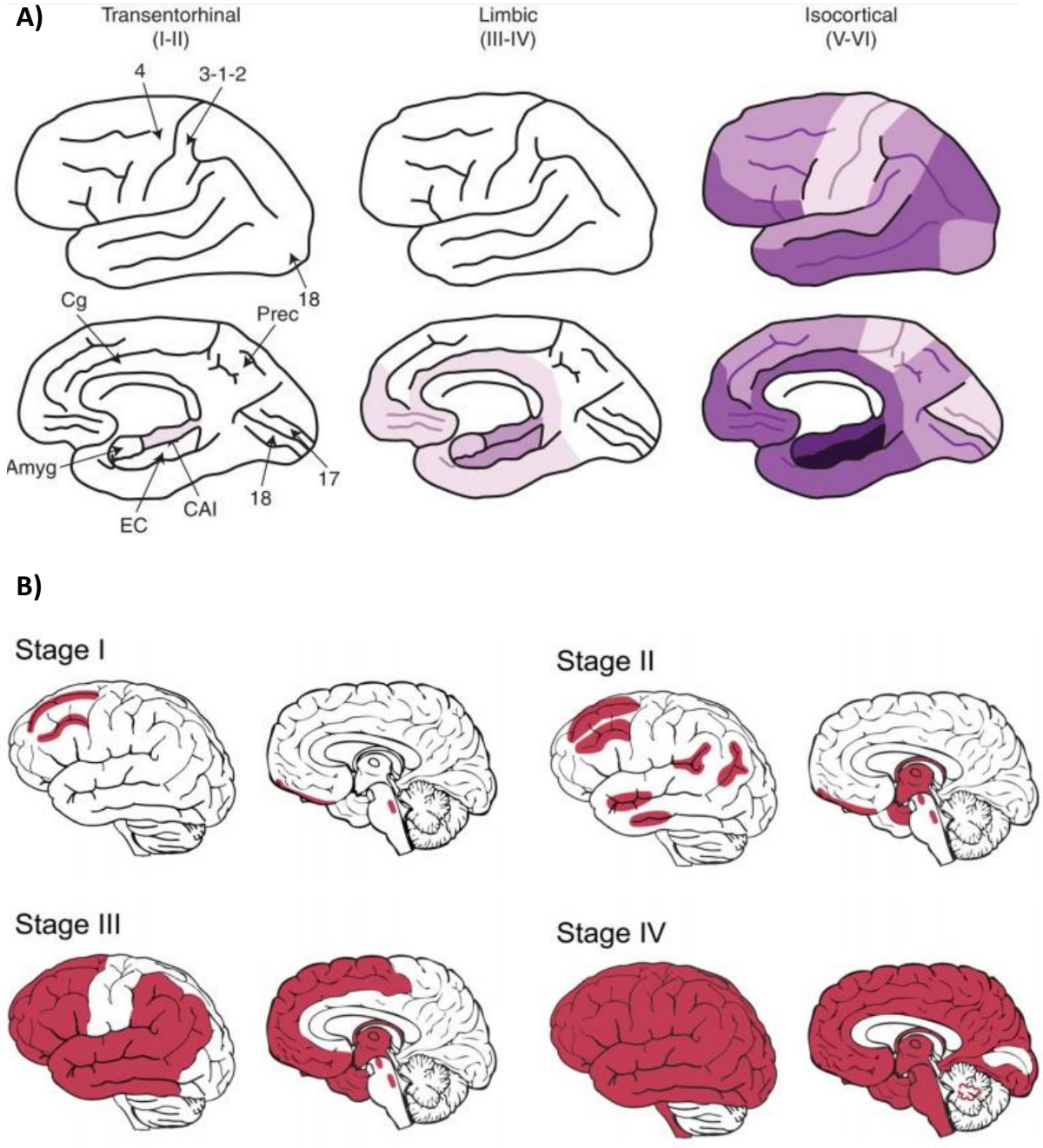

Figure 1.6 Neuropathological staging of Tau pathology in AD and CTE A) in AD Tau pathology follows a stereotypical progression as staged by Braak & Braak (1991). Three topographic stages are displayed (which are subdivided further to give 6 stages, see text), with Tau pathology extent indicated by depth of purple shading. Transentorhinal pathology is followed by limbic involvement and finally isocortical regions are affected. 4 = primary motor cortex, 3-1-2 = primary sensory cortex, 18 = associative visual cortex, 17 = primary visual cortex, Cg = cingulate cortex, Prec = precuneus, EC = entorhinal cortex, CA1= cornus ammonis 1 hippocampal subfield. This figure is adapted from Serrano-Pozo et al. (2011). **B)** CTE is categorised into four stages on the basis of Tau pathology. The stages involve, respectively, focal Tau deposition (I), cortical Tau pathology (II), Tau deposition in the sulcal depths (III) and widespread cortical and hippocampal Tau aggregation (IV). Figure is adapted from Stein et al. (2014).

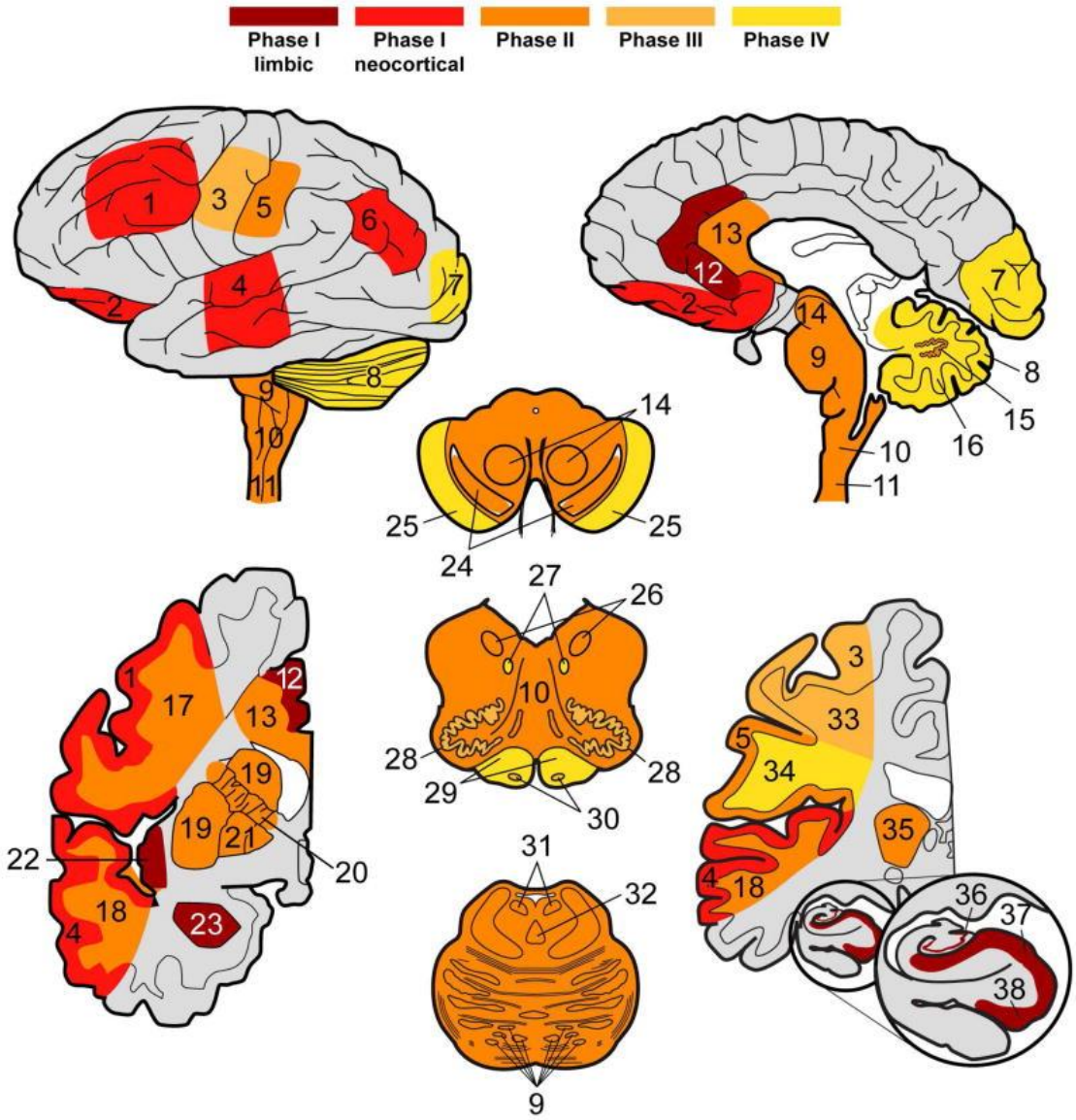

Figure 1.7 Staging of Tau pathology in frontotemporal dementia. In FTD Tau pathology follows a stereotyped progression which may be categorised into four stages. The areas affected in each stage are indicated by the colour code at the top of the diagram. Key: 1= mid frontal cortex , 2= orbitofrontal cortex, 3= motor cortex, 4= superior mid temporal cortex, 5= sensory cortex, 6= angular gyrus, 7= visual cortex, 8= cerebellar granule layer, 9=Pons, 10, reticular formation medulla, 11= cervical spinal cord, 12= anterior cingulate cortex, 13=CC, 14= midbrain red nucleus, 15= cerebellar dentate gyrus, 16= cerebellar white matter, 17= mid frontal cortex white matter, 18= superior mid temporal gyrus white matter, 19= striatum, 20= Internal capsule, 21= globus pallidus, 22= insular cortex, 23= amygdala, 24= midbrain substantia nigra, 25=crus cerebri, 26= dorsal motor nucleus vagus, 27= hypoglossal nucleus, 28= inferior olive, 29=medulla pyramids, 30= arcuate nucleus / pontobulbar body, 31= locus coeruleus, 32= raphe nuclei, 33= motor cortex white matter, 34= sensory cortex white matter, 35= thalamus, 36= hippocampus dentate gyrus, 37= hippocampus cornu ammonis, 38= hippocampus entorhinal cortex. Figure and key is from Irwin et al. 2017.

1.7.2 Tau seeding and Tau transmission in experimental systems

The above lines of evidence demonstrate that in human disease Tau pathology follows progressive and stereotyped topographical patterns of deposition. Furthermore, in Alzheimer's disease, the pattern of Tau pathology progression is suggestive of neuroanatomical connectivity (Cope et al. 2018). These observations have led to suggestions that in human disease, Tau pathology progresses via cell non-autonomous mechanisms i.e. that aggregated and misfolded Tau spreads from affected cells to adjacent healthy neighbouring neurons. This hypothesis is constituted by a number of subsidiary hypotheses which collectively outline the model of progressive Tau pathology.

For instance, evidence demonstrates that pathologically conformed and aggregated Tau promotes the aggregation of monomeric / native Tau into a pathological state (Frost et al. 2009; Kfoury et al. 2012; Holmes et al. 2014). This process is referred to as *seeding* and forms a central component of models regarding the progression of Tau pathology. In *in vivo* settings, aggregated Tau is hypothesised to be released from affected *donor* cells and be taken up / *internalised* by neighbouring *recipient* cells in a process referred to as *transmission*. If transmission induces the aggregation of endogenously expressed Tau in the recipient cell, this process is referred to as *propagation*. There is a wealth of evidence that supports each component of this hypothesis, which is now covered.

1.7.2.1 Tau seeding

A lot of the work investigating Tau seeding has the used the HEK293 FRET biosensor line, which co-expresses CFP and YFP tagged pro-aggregating forms of Tau (Holmes et al. 2014). Exogenous aggregated Tau seeds nucleate the aggregation of these tagged Tau constructs resulting in a FRET signal that can be interpreted as a readout of Tau 'seeding'. The seeding activities of AD brain extract in the HEK293 biosensor line correlated well with disease stage (I – IV) and brain region; transentorhinal/entorhinal cortices induced seeding at all

stages, whereas primary visual cortex only induced seeding at later disease stages. Moreover, the seeding activity of locus coeruleus, superior temporal gyrus and visual cortex regions lagged behind that of the entorhinal cortex but correlated well at later stages. Thus suggesting the species responsible for seeding was present first in the entorhinal cortical region and locus coeruleus later, followed by the superior temporal gyrus and visual cortex – a similar pattern to disease progression. Thus species capable of seeding Tau follow a similar pattern to *bona fide* Tau pathology in AD brain demonstrating a strong correlation and tempting to designate as causal (Kaufman et al. 2018).

These data were corroborated by the finding that brain regions from AD patients that do not display significant NFTs are able to seed aggregation in biosensor cells. Tau seeding was evident from brain regions 1 – 2 stages preceding the formation NFTs, consistent with the hypothesis of specific Tau species propagating downstream aggregation. Moreover, seeding activity was enriched in isolated synaptosomes, regions which also demonstrated increased PHF-1 immunoreactivity. This suggests seeding species concentrate at synaptic sites, a sub-cellular localisation consistent with their transmission to neighbouring regions at synaptic sites (DeVos et al. 2018) .

1.7.2.2 Tau transmission

The first study to demonstrate experimental transmission of Tau pathology in an animal model was published in 2009. The ALZ17 mouse, which expresses the longest isoform of human Tau (2N4R), does not develop Tau pathology under normal conditions. The 0N4R-P301S mouse on the other hand demonstrates abundant Tau inclusions. When brain lysates from P301S mice were inoculated into the brains of ALZ17 mice, the ALZ17 mice developed Tau pathology evidenced by Gallyas Braak silver staining and AT8 immunoreactivity. Induction of Tau pathology in the recipient mice was dependent upon the presence of insoluble Tau in the inoculating material. Moreover, Tau aggregates in the recipient mouse brain were detected by Tau antibodies specific for the N-terminal inserts,

demonstrating that they were composed of Tau isoforms that had been expressed in the ALZ17 mouse and were not remnants of the inoculated material.

The brain homogenate from P301S mouse was injected into the hippocampus and overlying cerebral cortex of the recipient mouse, and pathology was observed in sites as distal as the hypothalamus, thalamus and amygdala. This indicates that following the induction of local Tau pathology, aggregation is able to spread to downstream brain regions (Clavaguera et al. 2009).

In a different animal model of Tau pathology transmission, human Tau expression was restricted to the entorhinal cortex in mice. Following 17 months of expression, ectopic, human Tau protein was detected in dentate gyrus and CA1 neurons in the absence of transgene expression. Therefore human Tau was proposed to have spread to these downstream neurons from neurons in which it was expressed, demonstrating Tau transmission. Moreover, Tau pathology progressed with time and human and mouse Tau co-localised in pathological aggregates demonstrating Tau propagation (Calignon et al. 2012). Other studies have used different sources to induce Tau aggregation in recipient mice (recombinant fibrils, cell extracts and human and mouse brain material; Liu et al. 2012; Boluda et al. 2015; Ahmed et al. 2014; Sanders et al. 2014; Kaufman et al. 2016; Clavaguera et al. 2013) and in all studies there has been the observation of the induction of Tau pathology and its anterograde and retrograde spreading between interconnected neuronal circuitry.

1.8 Mechanisms for the transmission of proteins between cells

The observation of the transmission of experimentally induced Tauopathy raises questions as to which mechanisms underlie the spread of Tau between cells. There are a number of hypothetical mechanisms which result in the dissemination of proteins between cells as displayed in **figure 1.8**. For example, direct connections between cells via tunnelling

nanotubes may play a role in the movement of some proteins between cells, including Tau (Tardivel et al. 2016). Other mechanisms rely upon the release of Tau protein into the extracellular space, whether in free or in vesicle encapsulated forms. The release of Tau protein by cells must be complemented by its uptake by neighbouring cells to form the process of transmission. Thus, the uptake of Tau by cells is covered below, followed by an introduction to the release of Tau from cells. The cell biology of exosomes and their role in the release of proteins from cells is also introduced.

1.8.1 Internalisation and uptake of Tau by recipient cells

The findings discussed above regarding the induction of Tau pathology in mouse brain with exogenous aggregates proposes that Tau can be internalised by neuronal cells. Indeed, studies demonstrate that recombinant and brain derived Tau oligomers and fibrils can be internalized by recipient cells in culture, a phenomenon that may be dependent upon heparin sulphate proteoglycans on recipient cells (Holmes et al. 2013). Certain species of Tau (HMW and LMW oligomers) are internalized with differential efficiency by neurons, with LMW oligomers being taken up more readily. Once internalised, Tau oligomers can be transported in axons anterogradely and retrogradely and co-localise with dextran and Rab5, markers of endocytosis (Wu et al. 2013). Internalization of Tau added to the culture medium can promote the induction of Tau misfolding and aggregation in the recipient cells, supporting the hypothesis of propagation of pathology and template directed misfolding of Tau (Frost et al. 2009; Kfoury et al. 2012; discussed above). Takeda et al. (2015) identified that soluble, phosphorylated, HMW Tau species are preferentially internalized by recipient neurons in culture. Moreover, internalised Tau spread between neurons cultured in microfluidic chambers, suggesting that the same form of Tau which is readily internalised is also readily transmitted between cells (Takeda et al. 2015). Furthermore, endogenously expressed Tau released from iPSCs and overexpressed P301L Tau released from mouse

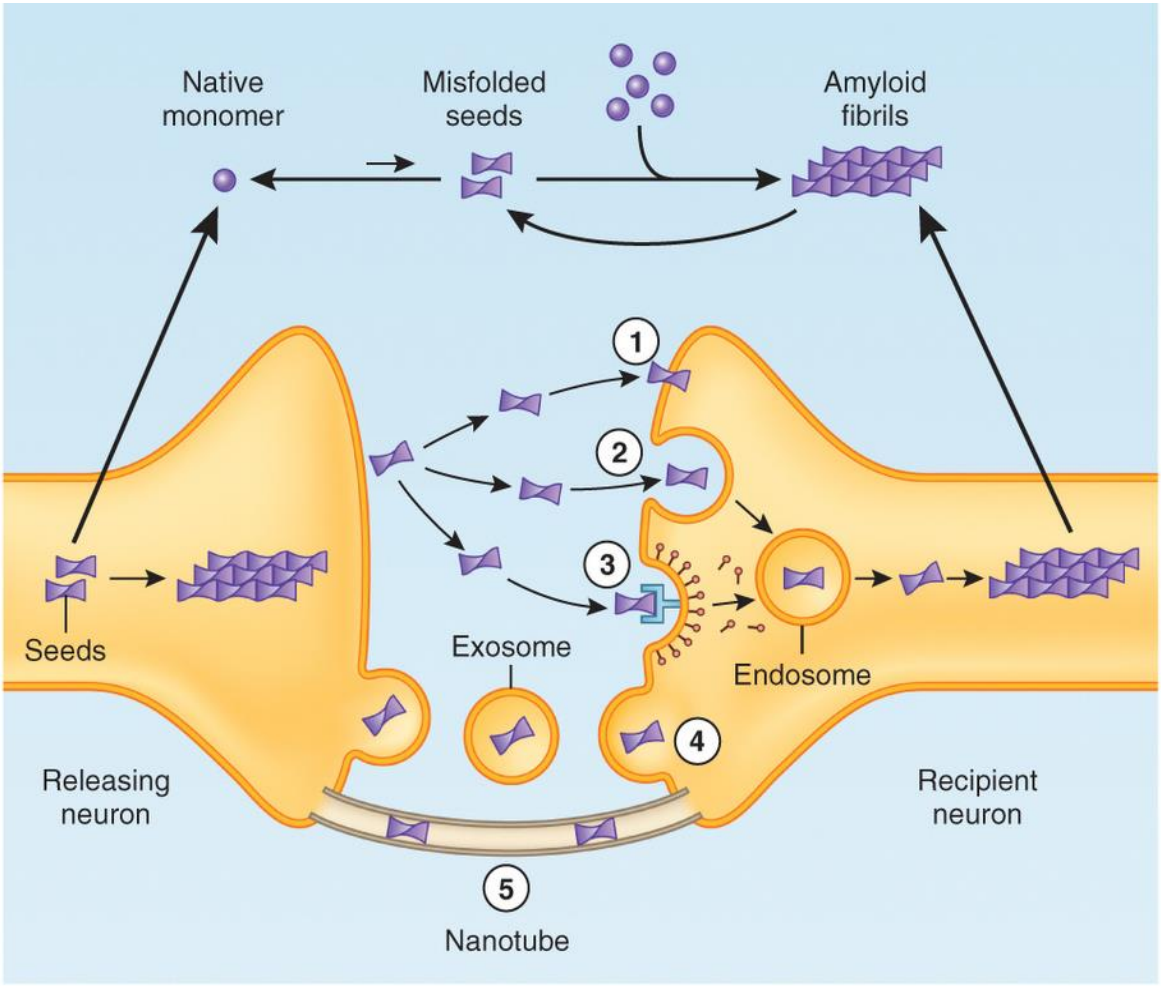

Figure 1.8 Hypothetical mechanisms of trans-neuronal spread of neurodegenerative proteins. Neurons may release monomers or aggregates from cells which may interconvert between monomeric and aggregated forms. Monomeric and aggregated proteins released freely by cells may (1) associate with membranes of recipient cells or be internalised by (2) endocytosis or (3) receptor mediated endocytosis. Alternatively (4) neurons may release aggregated / misfolded proteins in exosomes which may then be taken up by recipient neurons.(5) Direct cell to cell contact in the form of tunnelling nanotubes may provide an efficient pathway for the spread of neurodegenerative proteins between neurons, this mechanism does not require the release of proteins into the extracellular space. Figure is adapted from Guo & Lee (2014).

neurons can be internalized by recipient WT mice neurons (Wu et al. 2016). The release of Tau from cells is covered below (**1.9**)

These observations collectively indicate that recombinant Tau can be internalised by recipient neuronal cells, and moreover that this process can induce pathology in recipient cells.

1.9 Cellular mechanisms of Tau release

The direct release of Tau into the extracellular space is a central component in hypotheses of Tau transmission. The presence of Tau protein in the CSF of AD patients has been known for over 30 years (Wolozin & Davies, 1987; Vandermeeren et al. 1993) and was driven by attempts to identify AD biomarkers. It has been thought that CSF Tau reflects neuronal damage and degeneration, and acute brain trauma leads to transient increases in CSF Tau (Hesse et al. 2000).

However, the relationship between cellular Tau load, ISF Tau and CSF Tau levels are complex. Yamada et al. (2011) used In vivo microdialysis of WT and P301S-Tg mice to demonstrate the presence of Tau in the ISF of awake, freely moving mice. ISF Tau levels were directly related to intracellular soluble Tau levels, being five times higher in P301S Tau transgenic mice than WT mice. Tau was also detected in the CSF of these animals, but at ~10 fold lower levels than in the ISF. Moreover, ISF Tau levels decreased with increasing age of P301S mice, but remained stable in WT mice. This decrease in ISF Tau levels was coterminous with the onset of Tau aggregation in the P301S Tau mice and reductions in soluble intracellular Tau. Consistent with this, injection of Tau aggregates into the brains of P301S mice decreased the levels of ISF Tau.

These findings suggest that ISF Tau is in equilibrium with soluble cellular Tau and represents an active release mechanism. Moreover, the aggregation of Tau reduces ISF Tau levels due to a proportional decrease in soluble Tau levels.

These findings also complicate the interpretation of the detection of Tau in the CSF of Alzheimer's disease patients. Whereas CSF-Tau levels did increase with age in the P301S Tau mice, these levels did not correlate with ISF-Tau levels. The latter is likely reflective of active Tau release from cells which is prone to local fluctuations, whereas the authors argued the former to be reflective of global neuronal damage that increased with age.

1.9.1 Tau Secretion as a physiological process

The debate therefore ensued around whether the release of Tau from cells was an active and regulated process, or represented a passive process, an index of cell damage and death. In 2012 Chai et al. addressed this question with a set of experiments on HEK293 cells with inducible expression of 2N4R-Tau. Tau was detected in the conditioned medium by ELISA and shown to increase over 6 hour's culture time; over the same time period LDH activity in the medium did not increase. Furthermore, lowering the temperature to 25◦C abolished release of Tau from these cells. Similar results were obtained from iCell® neurons (iPS neurons). Karch et al. also in 2012 established the release of endogenous Tau from primary mouse mixed neuronal cultures and substantiated the findings of Tau release from ectopically expressing HEK293 cells. Further to these lines of evidence, Kanmert et al. (2015) published a rigorous investigation into the release of Tau from neuronal cells, studying both the quality and quantity of secreted Tau from a plethora of cell models. Confirming previous lines of evidence, the kinetic of Tau secretion was dissociable from that of LDH, thereby distinguishing it from cell death dependent mechanisms. Endogenous Tau from N2a cells, iHCNs and primary rat hippocampal neurons was studied and using custom built ELISAs, secreted Tau was identified as predominantly 'mid-region' i.e. most of the extracellular Tau lacked the extreme C-terminus (designated by the Tau46 epitope) and the MTBR. Collectively, these observations position Tau secretion from neuronal cells as an active process occurring under physiological conditions and independently from cell death.

1.9.2 Mechanisms of the unconventional secretion of Tau

These findings, identifying Tau secretion as a physiological process dissociable from cell death raised a new set of questions; Tau protein does not contain a consensus secretion motif and therefore does not enter into the conventional secretory pathway. Indeed, Tau secretion was shown to be insensitive to brefeldin A and monensin (Chai et al. 2012; Karch et al. 2012; Katsinelos et al. 2018) confirming its exclusion from this pathway. Tau secretion was henceforth designated as 'unconventional' and a number of studies have begun to interrogate the formative principles of the pathway(s) of Tau secretion. 'Unconventional Protein Secretion' (UPS) designates a set of heterogeneous and overlapping systems that target proteins without leader sequences for secretion (Zhang & Schekman 2013). Unconventional secretion of misfolded proteins has moreover been argued as a supplementary mechanism to alleviate proteotoxic stress (Xu et al. 2018). UPS of Tau protein has been shown to involve the co-chaperone DNAjC5; Fontaine et al. (2017) demonstrated that ectopic expression of DNAjC5 strongly potentiated the secretion of Tau protein from neuronal and non-neuronal cells. This process was also dependent upon the synaptic protein SNAP 23 and Hsc70. The formation of a heterotrimeric complex between Tau – Hsc70 – DNAjC5 was suggested to explain the findings, as blocking Tau – Hsc70 interaction abolished the effects of DNAjC5. Furthermore, the ER associated deubiquitinase USP19 was shown to promote the secretion of Tau protein in an Hsc70 and DNAjC5 dependant manner (Xu et al. 2018). These findings show that Tau protein enters into unconventional secretion pathways formed by chaperone-like molecules and its secretion can be regulated by their activity.

1.9.3 Factors affecting Tau release

The grounding work revealing key molecular pathways and identities in MAPS was principally performed in HEK293 cells using ectopic expression of proteins of interest. Whilst this approach is valid, it removes the proteostasis of Tau from its physiological

context (i.e. the neuron) and therefore is unable to model other aspects which regulate Tau secretion. For instance, Pooler et al. (2013) demonstrated that endogenously expressed Tau was secreted by primary rat neurons in culture. Furthermore, this process was potentiated by KCl induced depolarisation and could be mimicked with glutamate and AMPA treatment. The process was specific to AMPA receptors, as the antagonist NBQX blocked the potentiation. Interestingly, depolarisation induced Tau release was orchestrated through presynaptic mechanisms as it was blocked tetanus toxin. This suggests neuronal Tau release occurs through machinery overlapping with synaptic vesicle release despite not being a member of the synaptic vesicle proteome (Wang & Mandelkow, 2016). It is likely, therefore, that Tau's interaction with the synaptic machinery is transient and in some way forms the process of AMPA mediated Tau secretion. Stimulation of neuronal activity was also demonstrated to promote the release of endogenous mouse (primary culture) and human (iPSC neurons) Tau; blockade of GABA receptors with picrotoxin increased Tau release into the medium. Optogenetic approaches were also used to stimulate mouse neurons, which resulted in the secretion of transiently transfected human Tau from these cells (Wu et al. 2016). In terms of disease relevance, depolarisation of Alzheimer's disease brain synaptosomes (with KCl) promoted the secretion of Tau from these subcellular compartments (Sokolow et al. 2015). These observations collectively demonstrate that the neuronal environment is central to the regulation of Tau secretion.

1.9.4 Form of secreted tau

1.9.4.1 Dephosphorylation

It is important to identify asymmetries between intracellular and extracellular Tau in order to assemble maps of the events regulating release of Tau from cells. Contributing to this understanding is an increasing recognition that Tau protein released from cultured cells is

dephosphorylated relative to cellular tau. For instance, Plouffe et al. (2012) demonstrated that Tau secreted from HeLa cells was dephosphorylated at all residues tested, relative to IC Tau. Such observations may be accounted for by extracellular phosphatases, in fact, tissue non-specific alkaline phosphatase (TNAP) may promote the neurotoxic effects of extracellular Tau (Díaz-Hernández et al. 2010). This positions dephosphorylation as a process occurring exterior to that co-ordinating secretion of Tau protein. However, recent work suggests that dephosphorylated Tau accumulates in membrane fractions of organotypic slice cultures when cells are depolarised (Croft et al. 2017) and depolarisation has been demonstrated to induce Tau release from neuronal cells (Croft et al. 2017; Pooler et al. 2013; Wu et al. 2016). Furthermore, it was demonstrated that starvation promoted the secretion of endogenous Tau from rat neurons (Mohamed et al. 2015). Lysosomal inhibition and starvation induced the dephosphorylation of Tau, and the Tau which was secreted was primarily dephosphorylated. Integrating these findings suggests that the favoured release of dephosphorylated Tau is a function of its accumulation at sites which are proximal to secretion i.e. membranous regions.

1.9.4.2 Truncation

In their recent study, Kanmert et al. (2015) used an array of targeted ELISAs to interrogate the primary structure of Tau secreted from N2a, iPSC neurons and primary rat hippocampal neurons. Interestingly, only a minority of secreted Tau protein was FL and this was potentially arising from cell death dependant mechanisms. The majority of Tau detected contained the middle region of Tau (BT2 and Tau5 capture) but lacked both the extreme C-terminal (Tau46) and the MTBR (DAKO Tau).

Furthermore, Tau secreted from HeLa cells following transient transfection is more mobile than cellular Tau on SDS-PAGE and non cross reactive with the Tau46 antibody, consistent with C-terminal truncation of extracellular Tau (Plouffe et al. 2012). The conditioned medium from iPSC cortical neurons (PSEN1 mutants) contains C-terminally truncated forms

of Tau that were not immunoprecipitated with the Tau46 antibody (Bright et al. 2015). Furthermore, NB2a/d1 cells expressing full-length Tau and full-length Tau with a C-terminal GFP tag secrete a common fragment that is slightly more mobile than intracellular untagged Tau, and detected by Tau12. C-terminal cleavage is the only process, therefore, that could underlie such a commonality (Kim et al. 2010b).

The weight of available evidence therefore suggests that Tau protein secreted from cultured cells is truncated in some way. There is general agreement that secreted Tau lacks the C-terminus, although the exact site(s) of cleavage and resulting fragments generated is unknown. It is not known whether the processes contributing to this truncation are themselves formative of the secretory mechanisms or incidental to it. Interestingly, caspase cleavage of Tau at D421 promotes its secretion when transiently expressed in HEK293 cells (Plouffe et al. 2012). Such misprocessing is emblematic of Tau pathology and these observations thereby pose a putative link between Tau pathology, misprocessing and its secretion from cells.

1.10 Exosomes and extracellular vesicles

The unconventional secretion of Tau protein has been investigated by a number of groups, and some of this work has been summarised above. However, these investigations were predominantly studying 'naked' or 'free' Tau that was secreted directly into the conditioned medium of cultured cells. Unconventional protein secretion incorporates distinct pathways resulting in the release into the extracellular space of either free or vesicular encapsulated protein cargo. These secreted vesicles are referred to collectively as 'extracellular vesicles' (EVs) and consist of heterogeneous populations, defined in terms of their biosynthesis, molecular composition and size range. Given the status of Tau protein as a substrate of unconventional protein secretion, and given that vesicular secretion of

proteins is a sub-system of unconventional protein secretion, there is reason to hypothesise Tau as a substrate of vesicular release.

1.10.1 Kinds of vesicles released by cells

Based on current knowledge, exosomes, microvesicles and apoptotic bodies are identified as constituting the distinct vesicle populations secreted by cells. Microvesicles are generally defined as being in the size range of 50 to 1000 nm and shed directly from the plasma membrane, which, when occurring from apoptotic cells produces 'apoptotic bodies', a distinct subset of microvesicles (van Niel et al. 2018).

1.10.2 Exosome biogenesis and composition

Exosomes are extracellular lipid bilayer bounded vesicles secreted by most (if not all) cell types including neurons (Fauré et al. 2006; Lachenal et al. 2011). Exosomes are heterogeneous in size, having a diameter ranging from 40 – 150 nm, are of endosomal origin, and transmit cargo of bioactive macromolecules (including proteins and RNAs) trans-cellularly, thus serving a communicative function (Thery et al. 2002). Exosomes represent a class of extracellular vesicles generally defined against microvesicles, in that their biosynthesis occurs via endocytic pathways; exosomes are formed within the cell, not at its surface. There are a number of independent machineries involved in the biogenesis of exosomes, and the processes of exosome formation and cargo sorting are not wholly dissociable. Exosomes are formed as the intraluminal vesicles (ILVs) of multivesicular bodies (MVBs) and their biosynthesis involves the clustering, budding and scission of microdomains on the endosomal membrane. Endosomal complex required for sorting (ESCRT) proteins orchestrate, sequentially, these three processes; ESCRT-0 promotes cargo clustering, whilst a 'supercomplex' ESCRT-I and ESCRT-II drives the budding of membranes with ESCRT-III promoting their fission into the lumen of maturing endosomes (Wollert & Hurley 2010). Despite the sufficiency of ESCRT mediated processes for ILV and thereby

exosome formation, there exists independent pathways with the same endpoint; ILVs are still formed when the ESCRT machinery is knocked out (Stuffers et al. 2009). One potential mechanism guiding the formation of ILVs in the absence of ESCRT is the local generation of ceramide. Neutral sphingomyelinase II (NSmase II) catalyses the hydrolysis of sphingomyelin to produce ceramide, ceramide subdomains on endosomal membranes then, owing to their negative curvature, promote inward budding of the membrane to form ILVs (Trajkovic et al. 2008). Tetraspanins including CD81, CD63 and CD9 are also involved in exosomes biogenesis. The formation of tetraspanin microdomains on endosomal membranes concentrate to form local clusters that bud off as intraluminal vesicles. This pathways may be associated with the ceramide pathway and it has been demonstrated that ceramide may associate with an intramembrane pocket formed by CD81 (Zimmerman et al. 2016; van Niel & Raposo 2018). These pathways of exosomes biogenesis are represented in **figure 1.9**.

Exosomes are characterised by the presence of specific protein markers that are reflective of their biogenesis. Thus exosomes are enriched in ESCRT associated proteins such as Alix (Baietti et al. 2012) as well as tetraspanins (such as CD81 and CD63) (Andreu & Yáñez-Mó 2014). Exosomes also contain chaperones including Hsc70, which may co-sort cytosolic proteins to exosomes (van Niel & Raposo 2018; Géminard et al. 2001; Géminard et al. 2004) and the lipid raft associated protein Flotilin-1 (van Niel & Raposo 2018)..

It is likely that distinct biogenesis mechanisms promote the formation of biochemically (lipidomic, proteomic, etc) distinct sub-populations of exosomes. Cells release exosomes that differ in key physio-chemical properties such as their density, which is itself an indicator of distinct transcriptomic and proteomic identities, as well as communicational effects on recipient cells (Willms et al. 2016). The separation of distinct sub-populations by purely physical means is challenging. The ‘gold standard’ enrichment protocol for exosomes is differential ultracentrifugation of conditioned medium / biofluids, such an approach

however is likely to co-purify vesicles from different cellular origins (Angelique Bobrie et al. 2012).

1.10.3 Functions of exosomes

Exosomes may serve dual functions of disposal and communication. Exosomal pathways are therefore intimately involved in homeostasis and their dysregulation or 'hijack' may be involved in the generation of toxic microenvironments. The homeostatic function of exosomes is exemplified by findings that heat shock proteins secreted in exosomes can inhibit huntingtin inclusion formation in recipient cells (Takeuchi et al. 2015).

On the other hand, exosomes secreted by tumours have pro-cancerous and metastatic effects in the local and systemic environments, including promotion of angiogenesis, activation of fibroblasts, formation of pre-metastatic niches and immunosuppression (Kahlert & Kalluri 2013). These findings are consistent with exosomal cargo gaining entry to and having functional effects upon recipient cells.

1.10.4 Role of exosomes in trans-cellular spread of neurodegeneration associated proteins

Exosomes may represent a favourable environment for the aggregation of neurodegenerative associated proteins; high local protein concentration, pH, and the presence of various lipid co-factors may promote misfolding and aggregation (Schneider & Simons. 2013). Exosomes are released by primary neurons (Faure et al. 2006) and there is evidence that exosomal mechanisms may be involved in the spreading of certain neurodegenerative disease associated proteins.

The pathological conformer of prion protein (PrP^{sc}) is released in exosomes from infected cells. These exosomes induced the formation of protease K resistant PrP in recipient cells, indicating that exosomal PrP^{sc} was sufficient to template endogenous PrP to a pathological form. Moreover, these exosomes induced prion disease in mice demonstrating their

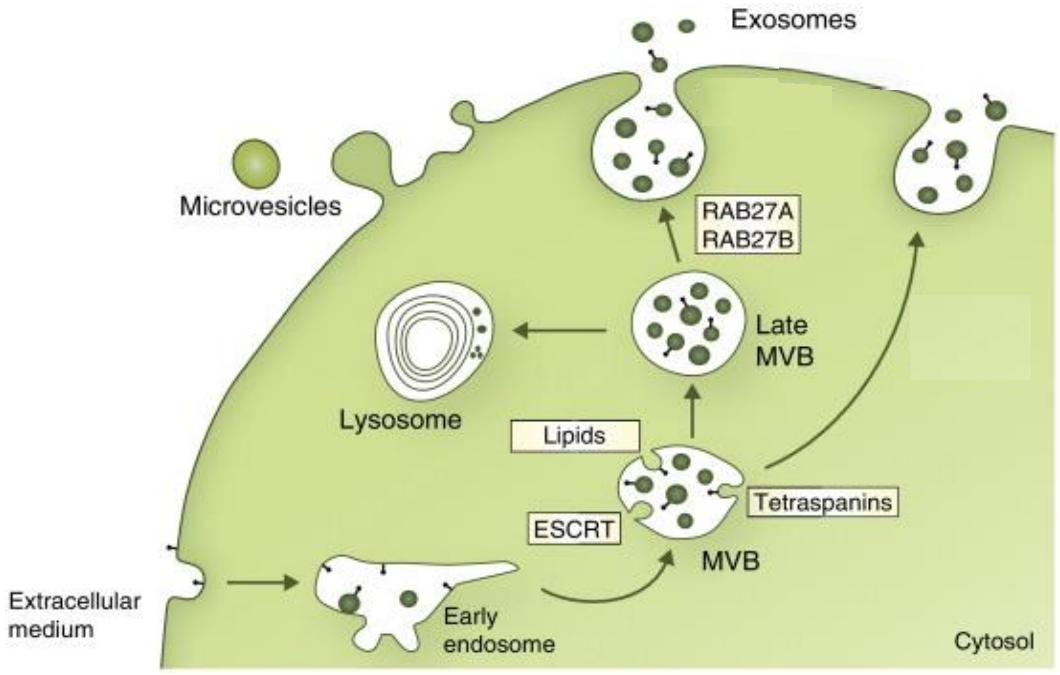

Figure 1.9 Exosome Biogenesis. Exosomes are formed as intraluminal vesicles of the multivesicular bodies by inward budding of the late endosomal membrane. This process is facilitated by ESCRT dependant and independent (tetraspanin and lipid mediated) mechanisms. MVBs can have degradative and secretory fates resultant from fusion with the lysosome and plasma membrane, respectively. The ILVs of secretory MVBs become exosomes. Microvesicles bud directly from the plasma membrane. Figure is adapted from Kowal et al. (2014)

infectivity. Thus exosomes may serve as a vehicle of transmission for the prion protein (Fevrier et al. 2014). Furthermore, mutant SOD-1 which misfolds and aggregates in amyotrophic lateral sclerosis can be secreted in exosomes from stably expressing cells and these exosomes are efficiently internalised by recipient cells (Grad et al. 2014). Moreover, alpha-synuclein is released in exosomes, and exosomal encapsulated alpha synuclein can be internalised by recipient SH-SY5Y cells (Alvarez-Erviti et al. 2011). Moreover, exosomal alpha-synuclein oligomers are preferentially taken up by H4 cells compared to free oligomers (Danzer et al. 2012). In each case sonication of the exosomes prevented the associated transmission, demonstrating that the intact vesicular structure of exosomes was necessary for their ability to transmit alpha-synuclein.

Collectively these observations identify exosomes as a functional conduit for the transfer of neurodegenerative associated proteins between cells.

1.10.5 Association of Tau protein with exosomes

The release of Tau protein in exosomes has been directly studied by a number of groups, with the first reports being published in 2012. Simon et al. (2012) demonstrated the release of exosome / microvesicle associated Tau when 4R Tau was overexpressed in COS-7 and M1C cells. Tau protein was also revealed to be intracellularly localised to compartments associated with exosome formation (TSG101, Hsp70, flotilin-1). This work was important as it identified Tau protein as able to readily associate with machinery orchestrating vesicular targeting and release. Also in 2012, Saman et al. demonstrated the release of exosomal Tau from M1C cells with inducible expression of 4R Tau. In this work the authors also demonstrated the presence of Tau protein in the exosomes isolated from the CSF of Alzheimer's disease post-mortem brains. Exosomal Tau from AD CSF was enriched in phosphoepitopes AT8 and AT270, and present as a multimeric and phosphorylated (pT181) species reminiscent of pathologically conformed Tau. Through their analysis of CSF from

different stages of AD progression, the authors concluded that exosomal Tau release may represent an early and specific process in AD pathophysiology.

On the other hand, other authors (Pooler et al. 2013; Dujarding et al. 2012) have raised questions about the release of Tau in exosomes from cultured cells. As such there is currently little consensus regarding the exact species of Tau that are released in exosomes, and whether pathological species are truly enriched in extracellular vesicles.

1.11 Potential intracellular mechanisms targeting tau protein to exosomes

1.11.1 Degradative pathways and exosomal Secretion

In terms of the mechanistic factors that may regulate the targeting of proteins, including Tau, to exosomes, is the consideration of the overlap between cellular degradative pathways and exosomal secretory pathways. Multivesicular bodies can be both degradative and secretory via their fusion with lysosomes and the plasma membrane, respectively (see **figure 1.10**). As such, the exosomal release of proteins may represent a mechanism for the clearance of harmful and damaged intracellular proteins (Baixauli et al. 2014). For instance, lysosomal compromise increase exosomal release of disease associated TDP-43, whilst its aggregation is increased by blocking exosome synthesis and secretion (Iguchi et al. 2016). Furthermore, inhibition of lysosomal function increases the exosomal targeting and release of alpha-synuclein (Alvarez-Erviti et al. 2011) further highlighting the co-ordination between autophagy and exosomal release of proteotoxins.

There is clear evidence that Tau protein can be degraded by autophagy and inhibition of autophagic pathways enhances Tau aggregation in neuronal cells (Hamano et al. 2008; Dolan & Johnson. 2010; Kruger et al. 2012). Moreover, lysosomal inhibition promotes the secretion of Tau protein from primary neurons (free release; Mohamed et al. 2014). These lines of evidence suggest that the targeting of Tau to exosomes and its secretion from cells

may be a regulated mechanism that relies on the balance between secretory and degradative pathways.

1.11.2 Use of chaperone mediated autophagy by Tau

Chaperone mediated autophagy (CMA) is a mechanism for the selective degradation of cytosolic proteins (unlike non-selective bulk macroautophagy). CMA occurs by an Hsc70 dependent targeting of substrates to lysosomal LAMP2A receptors, the target protein is then translocated through LAMP2A to the lysosomal lumen for degradation - the rate limiting step of CMA. Peptide motifs biochemically related to KFERQ direct target proteins for CMA through recognition by Hsc70 (Chiang et al. 1989; Dice. 1990). The cellular steps of CMA are displayed in **figure 1.10**.

Recent work has identified WT-2N4R-Tau as a bona-fide CMA substrate, demonstrated by its cellular accumulation upon LAMP2A knockdown and translocation into the lumen of isolated lysosomes (Caballero et al. 2017). Interestingly, the pathogenic P301L mutation prevented the degradation of Tau by CMA, and P301L Tau did not accumulate at the lysosomal membrane. Moreover, an aggregating fragment of Tau was demonstrated to use CMA in a nonconventional way whereby it was not translocated inside lysosomes, but held on the cytosolic surface for sequential proteolysis that liberated aggregating fragments (Wang et al. 2009). These observations identify WT forms of Tau as CMA substrates and reveal differences in the cellular degradation pathways of WT and pathogenic forms of Tau.

A distinct degradative mechanism that shares molecular components with CMA was described in 2011 by Sahu et al. Degradation of substrates in late endosomes and MVBs, termed ‘endosomal microautophagy’ was demonstrated to utilise endosomal machinery (ESCRT complexes) and Hsc70. Endosomal microautophagy was demonstrated as capable of degrading both folded and misfolded proteins, whereas CMA required the complete unfolding of proteins for their translocation, via LAMP2A, into the lysosomal lumen. This is interesting given the misfolding of Tau protein in disease.

Endosomal microautophagy is an interesting process with regards to exosomal targeting of client proteins because the intraluminal vesicles of multivesicular bodies may become exosomes upon fusion with the plasma membrane. Importantly, Sahu et al. (2011) demonstrated an enrichment of proteins with KFERQ - like motifs in exosomes versus the cytosol, indicating a specific enrichment mechanism. It was demonstrated that Hsc70 mediated targeting of proteins was the key figure of this enrichment mechanism demonstrating a selective character to this process.

The role of Hsc70 in the exosomal targeting of proteins is reinforced by observation that Hsc70 interaction promotes the co-sorting of transferrin receptor into exosome released from reticulocytes (Geminard et al. 2004). The hypothetical mechanism by which Hsc70 recruits proteins to ILVs for exosomal release is displayed in **figure 1.10**.

1.11.3 Tau Hsc70 interaction

As mentioned above, Hsc70 interacts with proteins at consensus motifs in the substrate protein which are biochemically related to the sequence KFERQ, motifs termed 'consensus CMA motifs' (Dice et al. 1990). This interaction has been long known to guide proteins for CMA degradation, but given the above discussion now has a role as a potential mechanism for guiding proteins to the ILVs of MVBs (Sahu et al. 2011). Tau protein is known to interact with Hsc70, a process first described in 2008 by Sarkar et al. In this work, the authors localised the site of Tau to interact with Hsc70 as within the hexapeptide motifs: ^{275}VQIINK^{280} and ^{306}VQIVYK^{311}, the same sets of residues important for Tau aggregation (von Bergen et al. 2000).

On the other hand, and in line with the points mentioned above, Tau protein contains two KFERQ consensus motifs (^{336}QVEVK^{340} and ^{347}KDRVQ^{351}), both of which are found in the microtubule binding domain of Tau (**figure 1.11**). Neutralising the charge and sequence identity of these motifs abrogated the co-immunoprecipitation of a pro-aggregating Tau fragment and Hsc70 (Wang et al. 2009).

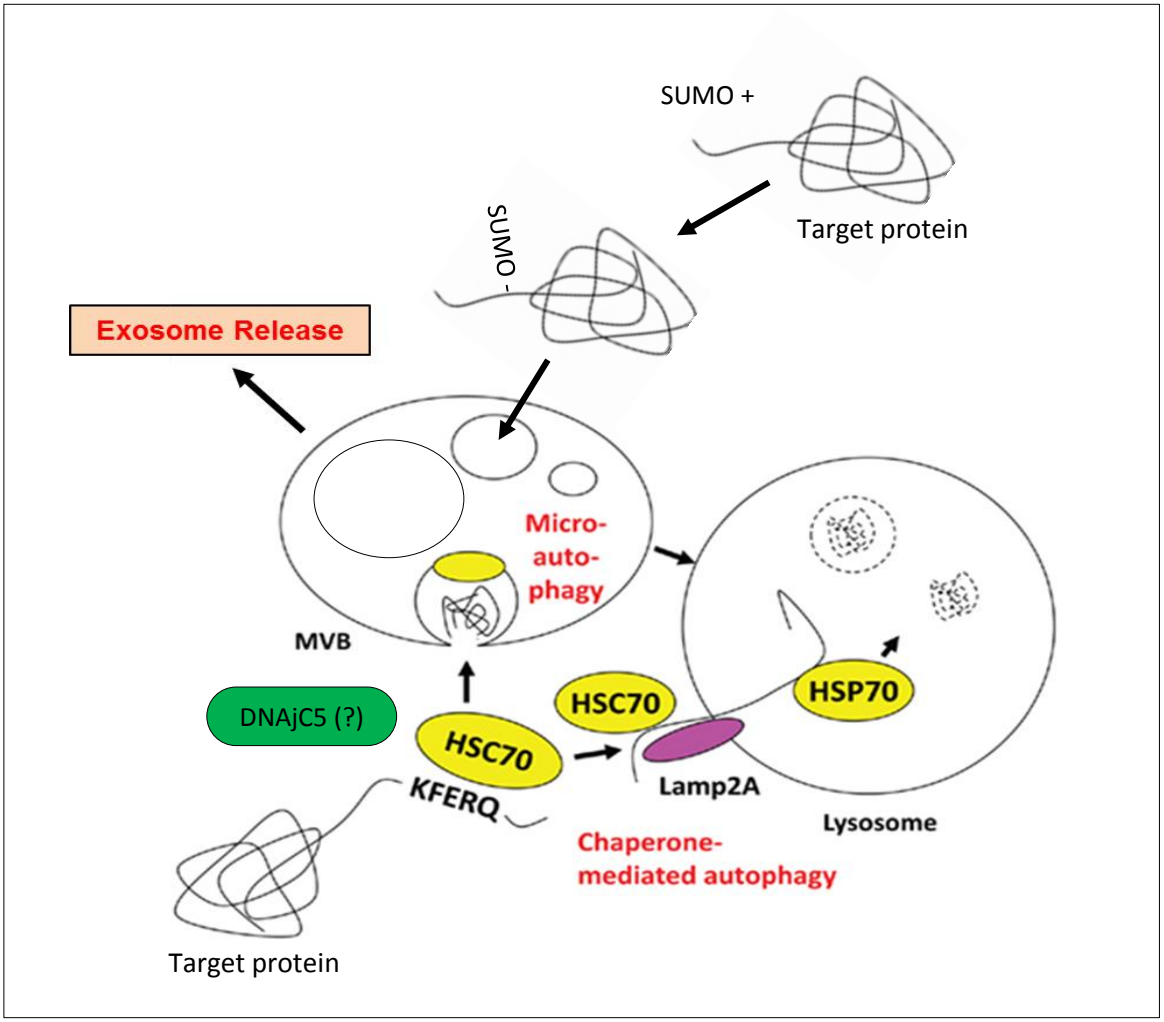

Figure 1.10 Cellular steps in CMA and putative mechanisms for targeting client proteins to exosomes. Target proteins containing KFERQ-like motifs are recognised by Hsc70 and delivered to lysosomes and translocated via LAMP2A into the lysosomal lumen for degradation, in the process termed 'chaperone mediated autophagy'. Alternatively, Hsc70 can target proteins to multivesicular bodies (MVB) in a process termed 'microautophagy' (Sahu et al., 2011). MVBs can have degradative and secretory fates, and the fusion of MVBs with the plasma membranes will release ILVs to the extracellular space as exosomes (top left).Tau contains two KFERQ motifs so is a candidate for this pathway (just one KFERQ motif is indicated). We are hypothesising a role for DNAjC5 in this process, as indicated by the green box. Alternatively, SUMOylation of proteins has been implicated in their exosomal targeting (Kunadt et al. 2015). SUMOylation of target proteins occurs by covalent attachment of SUMO to substrate proteins. This may then determine their sorting to the ILVs fated for release as exosomes (top right). This figure is adapted from Munz (2011).

The relative contribution of the CMA and hexapeptide motifs to Tau - Hsc70 interaction is therefore an unexplored area and suggests a redundancy in the interaction sites between Tau and Hsc70.

Collectively these lines of evidence implicate a role for Hsc70 in the targeting of client proteins to MVBs leading to their release in exosomes. This targeting potentially occurs through interaction of Hsc70 with consensus CMA motifs in client proteins (Sahu et al. 2011). Tau protein has been demonstrated to interact with Hsc70, a process in which its CMA motifs may play an important role (Wang et al. 2009). Therefore the evidence suggests that Hsc70 may play an important role in targeting Tau to exosomes.

1.11.4 Functional effects of Tau – Hsc70 interaction and the role of DNAjC5 in Tau secretion

The functional effects of Tau – Hsc70 interaction have been explored in detail. Hsc70 is known to recruit Tau that has dissociated from microtubules (Jinwal et al. 2010). Moreover, Tau and Hsc70 have been demonstrated to stimulate Tubulin assembly through the formation of an active complex (Fontaine et al. 2015). The functional effect of Tau – Hsc70 interaction is co-ordinated via co-chaperone, for instance BAG-1 expression prevents the proteasomal degradation of Tau (Elliot et al. 2007). On the other hand, CHIP (carboxyl terminus of the Hsc70-interacting protein), in complex with Hsc70 causes the ubiquitination of Tau and prevented Tau induced cell death (Shimura et al. 2004).

In terms of Tau secretion, the synaptic co-chaperone DNAjC5 has been demonstrated to potentiate Tau secretion from neuronal and non-neuronal cells, potentially forming part of the unconventional secretion of Tau, as discussed above (**1.9.2**). This process was shown to be dependent upon the interaction of Tau and Hsc70 and Tau – Hsc70 – DNAjC5 formed a heterotrimeric complex (Fontaine et al. 2016). Moreover, DNAjC5 is secreted in exosomes isolated from neuronal cells (Deng et al. 2017). DNAjC5 induced the secretion of two neurodegenerative disease proteins; SOD1 and huntingtin.

These findings implicate a role for DNAjC5 in the exosomal release of Tau protein from cells, a process which may involve the interaction of Tau with Hsc70. The hypothetical role of DNAjC5 in the exosomal secretion of Tau protein is illustrated in figure **1.10**.

1.11.5 SUMOylation

Covalent attachment of the small ubiquitin like modifier (SUMO) to lysine residues in consensus motifs of target proteins is a post-translational modification that can diversely modulate protein function through effects on sub-cellular targeting and by regulating adjacent post translational modifications (Krumova & Weishaupt, 2013).

SUMOylation of specific proteins may promote their exosomal targeting. For instance, exosomal forms of the protein heterogeneous nuclear ribonucleoprotein A2B1 (hnRNPA2B1) is SUMOylated, and its SUMOylation affects the targeting its substrate miRNAs to exosomal vesicles (Villarroya-Beltri et al. 2013). More directly, Kunadt et al. (2015) investigated the effects of SUMOylation on the release of proteins in exosomes. They observed that GFP-SUMO-2 constructs had increased exosomal release and exosomal release of SUMO used the ESCRT machinery. The authors generated SUMOylation deficient alpha-synuclein constructs and demonstrated their exosomal release to be significantly reduced. SUMOylation promoted the membrane binding of alpha-synuclein, potentially bringing it into close alignment with ESCRT complexes and promoting translocation into intraluminal vesicles (Kunadt et al. 2015).

The SUMOylation of Tau protein was first described in 2006 (Dorval & Fraser. 2006). SUMOylation of Tau occurs predominantly with SUMO-1, although SUMO-2 and SUMO-may also SUMOylate Tau at lower levels. Of the two consensus SUMOylation motifs in Tau ($_{339}$V**K**SE$_{342}$ and $_{384}$A**K**TD$_{387}$), lysine340 was demonstrated to be critical in Tau SUMOylation, with limited contribution from lysine385. The SUMOylation of Tau was inhibited by proteasome blockade, likely via increased ubiquitination under these conditions out-competing

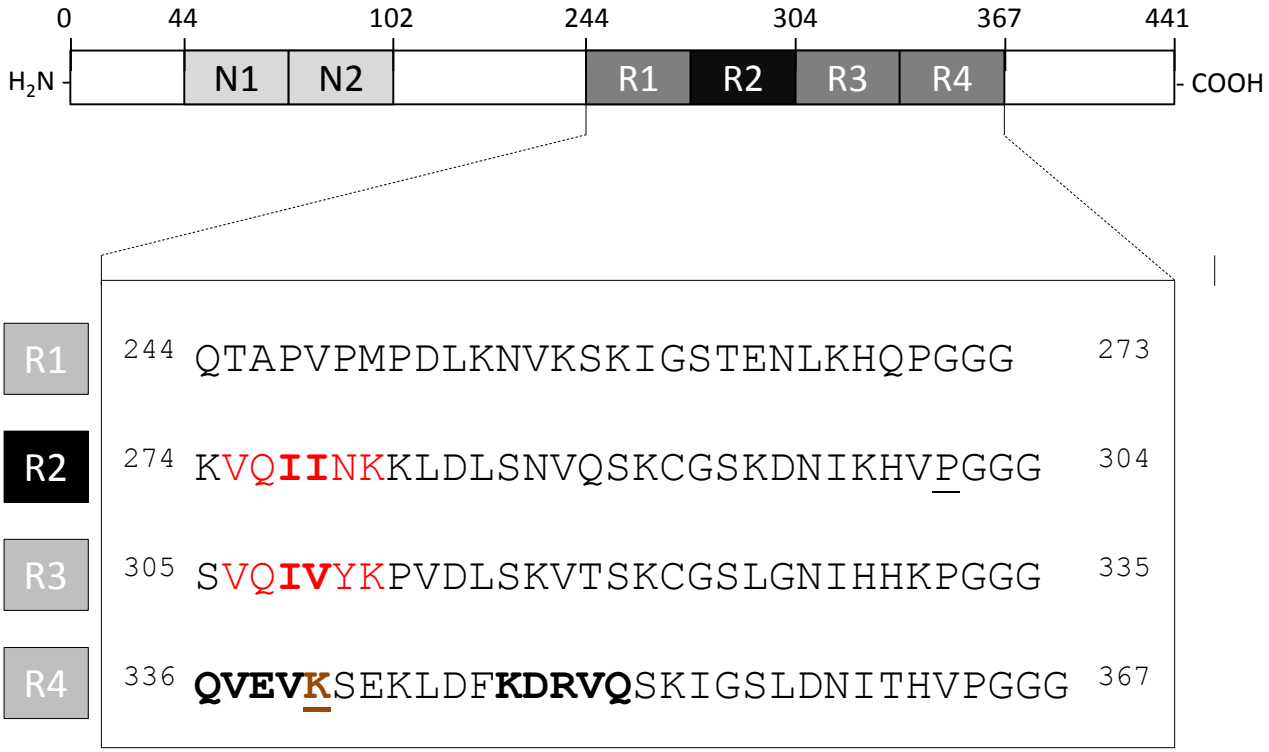

Figure 1.11 Schematic of 2N4R-Tau displaying residues involved in Hsc70 interaction and SUMOylation. The expanded section displays the four microtubule binding regions, of which the second is alternatively spliced. The two motifs identified in red (^{275}VQII^{278} and ^{306}VQIV^{309}) were identified as Sarkar et al. (2008) as being important for interaction with Hsc70. Deletion of the residues represented in red bold (^{277}II^{278} and ^{308}IV^{309}) disrupted Tau – Hsc70 binding. Putative consensus CMA motifs are both situated in the fourth repeat and are identified in bold (^{336}QVEVK^{340} and ^{347}KDRVQ^{351}). These motifs were identified as being important for Tau – Hsc70 interaction by Wang et al. (2009). Lysine^{340} , the target of Tau SUMOylation, which also composes the last residue of the first CMA motif, is displayed in brown underlined text (Dorval & Fraser. 2006). Location of proline^{301} in the second repeat is identified by underlined text. Mutation of P^{301} to leucine causes FTD-Tau and CBD.

SUMOylation. Consistent with this, Luo et al (2014) directly demonstrated that SUMOylation of Tau at lysine340 reduces the ubiquitination of Tau, demonstrating significant cross-talk between these two post translational systems. Luo et al. (2014) also demonstrated that SUMOylation of Tau increases its phosphorylation and stability, thereby promoting aggregation. This was contextualised by the observation that AT8 and SUMO-1 immunoreactivity co-localise in AD brain and that amyloid beta exposure promotes Tau SUMOylation. Collectively, these lines of evidence demonstrate that SUMOylation of Tau is a modification that has important consequences on the cellular handling of Tau, some of which may have disease relevance.

The role of Tau SUMOylation in its exosomal targeting is a currently unexplored area. But given the above observations there is a suggestion that SUMOylation of Tau may be a relevant process in its targeting to exosomes.

1.12 Hypotheses and aims and objectives

The above lines of evidence indicate a role for the transmission of pathological Tau between neurons in the progression of Alzheimer's disease and other Tauopathies. Increasing evidence demonstrates that Tau protein is secreted from cells by non-conventional pathways, of which exosomal release may be a component. Exosomes may be a key pathway for the spreading of Tau between neurons.

The release of proteins in exosomes may be regulated by the chaperone network, with roles being played by Hsc70 and DNAjC5. The exosomal release of proteins may also be determined by their SUMOylation.

From these observations we hypothesise the following:

Tau released in exosomes may be important for the transmission of Tau protein to naïve cells and has the potential to transmit Tau pathology. The targeting of Tau to exosomes

is a regulated process and may rely upon interaction with Hsc70 and co-chaperones and SUMOylation.

Our primary model system for addressing these hypotheses is the ectopic expression of various Tau isoforms in SH-SY5Y cells. The project is subdivided into the following aims:

1) Characterisation of SH-SY5Y clones with ectopic expression of various Tau isoforms (various Tau isoforms and constructs)
2) The characterisation of Tau release from cells, with a focus upon exosomal release
3) Investigation of the factors affecting the release of Tau in exosomes, including the role of hsc70 interaction and SUMOylation
4) Development of cell systems to assess the role of exosomal Tau in transmission of Tau to naïve cells

2 Material and methods

2.1 Chemicals and reagents

Unless otherwise stated, chemicals were obtained from Sigma, BDH, Invitrogen and Merck.

2.2 Plasmid preparation

The sources of the plasmids used in the project are detailed below (**table 2.1**). For plasmid amplification, 0.1 ng of plasmid was transformed into DH5α e-coli (Invitrogen) by a 45 second 42^{o}C heat pulse. Transformed e-coli were incubated in lysogeny broth (LB) broth (Sigma) with kanamycin or ampicillin depending upon bacterial selection (both at 50 µg / ml; see **table 2.1**) for 1 hour at 37^{o}C with 225 RPM shaking. After 1 hour the cells were pelleted by centrifugation at 8000 RPM for 5 minutes on a microfuge, resuspended in LB containing antibiotic and plated on LB-Agar plates containing the appropriate antibiotic (50 µg / ml). Plates were incubated overnight at 37^{o}C. Individual colonies were picked and grown into 5 ml LB containing antibiotic and shaken at 225 RPM overnight. Plasmid DNA was isolated by mini-prep (Qiagen) and concentration and purity was assessed by Nanodrop analysis (Thermo; see below section **2.3**). The insert sequence was confirmed by Sanger sequencing (Source Bioscience) with either commercially available or custom designed (Eurofins Genomics) primers. Glycerol stocks of clones expressing sequence verified plasmids were generated by mixing 850 µl of bacterial culture with 150 µl glycerol and vortexing which were flash frozen in liquid nitrogen. For large scale plasmid preparation, 150 ml of LB medium was inoculated with glycerol stocks of sequence verified clones and grown overnight at 37^{o}C with 225 RPM shaking. The culture was pelleted (3000 x g, 10 minutes) and plasmid DNA isolated by Gen-Elute Maxi-prep kit (Sigma).

2.3 Nanodrop analysis

1 µl of eluted plasmid DNA, or other DNA sample was pipetted onto the Nanodrop pedestal. Absorbance at 260 nm (A260) was read to assess DNA concentration. DNA purity

was assessed by analysing the ratio between A260: A280 (which was greater than 1.8 for pure DNA).

Table 2.1 List of constructs, their plasmids backbones and origin, used in this project

Construct	Backbone	Selection		Origin
		Bacterial	Mammalian	
Empty	pcDNA3.1	Ampicillin	G418	Purchased from Invitrogen
HA-0N3R-Tau	pCMV3-N-HA	Kanamycin	Hygromycin	Purchased from Sino Biologicals
0N3R-Tau	pEGFP-N1	Kanamycin	G418	Generated by RDS
2N3R-Tau	pEGFP-N1	Kanamycin	G418	Generated by RDS
WT-2N4R-Tau	pEGFP-N1	Kanamycin	G418	Generated by RDS
CMA3-2N4R-Tau	pEGFP-N1	Kanamycin	G418	Sequential SDM performed on WT-2N4R-Tau and then CMA1-2N4R-Tau
K340R-2N4R-Tau	pEGFP-N1	Kanamycin	G418	SDM performed on WT-2N4R-Tau
0N3R-GFP-Tau	pEGFP-N1	Kanamycin	G418	Generated by RDS
0N4R-GFP-Tau	pEGFP-N1	Kanamycin	G418	Generated by RDS
2N3R-GFP-Tau	pEGFP-N1	Kanamycin	G418	Generated by RDS
2N4R-GFP-Tau	pEGFP-N1	Kanamycin	G418	Generated by RDS
HA-P301L-2N4R-Tau	pcDNA3.1	Ampicillin	G418	Synthesised by Eurofins Genomics
CMA3-HA-P301L-2N4R-Tau	pcDNA3.1	Ampicillin	G418	SDM performed on HA-P301L-2N4R-Tau
DD-HA-P301L-2N4R-Tau	pcDNA3.1	Ampicillin	G418	Synthesised by Eurofins Genomics
RDΔK280-dsRED	pEGFP-N1	Kanamycin	G418	Generated by RDS
RDΔK280-eGFP	pDsRed-Monomer-N1	Kanamycin	G418	Generated by RDS
Hsc70-V5	pcDNA3.1	Ampicillin	G418	Purchased from Addgene
SUMO-1-His Tag	pcDNA3.1	Ampicillin	G418	Purchased from Sino Biologicals

2.4 Site directed mutagenesis

Mutagenesis was conducted according to manufacturer's guidelines (Agilent QuickChange Site Directed Mutagenesis Kit). 20 ng template DNA was mixed with 5 µl reaction buffer,

125 ng of forward and reverse primers containing the desired mutation(s) (HPLC purified, Eurofins Genomics; table **2.2**), 1 µl dNTPs, 1 µl PfuTurbo and made up to 50 µl with H_2O. The reaction was cycled 18 times (55°C anneal, 1 minute; 68°C extension 1 min / kb plasmid) and then digested for 1 hour at 37°C with Dpn1. 1 – 5 µl of the digested DNA was transformed into XL10-Blue cells and colonies were picked and amplified, and plasmid DNA was isolated and analysed for desired mutations.

Table 2.2 Primers used in site directed mutagenesis of Tau cDNA. Mutated sequences are in bold.

Mutation	Forward Primer	Reverse Primer
K340R	GTGGCCAGGTGGAAGTA**AGA**TCTGAGAAGCTTGACTTCAAG	CTTGAAGTCAAGCTTCTCAGA**TCT**TACTTCCACCTGGCCAC
CMA1	TAAACCAGGAGGTGGC**GCGGCG**GAAGTAAAATCTGAG	CTCAGATTTTACTTC**CGCCGC**GCCACCTCCTGGTTTA
CMA2	TGACTTCAAGGACAGA**GCCGCG**TCGAAGATTGGGTCC	GGACCCAATCTTCGA**CGCGGC**TCTGTCCTTGAAGTCA

2.5 Reverse transcription PCR and sequencing of Tau inserts

RNA was isolated from cell pellets (Qiagen) and reverse transcribed to cDNA (*Precision nanScript* Reverse Transcription kit, Primerdesign). PCR was performed by thermocycling a reaction of cDNA, 25 pmol (0.5 µM) specific primers (refer to **table 2.**3, Eurofins Genomics), 1U Taq polymerase (Peqlab), 0.2 mM dNTPs (Peqlab) in 10X buffer (100 mM Tris-HCl pH 8.8, 500 Mm KCl, 0.1% Tween 20 and 15 mM $MgCl_2$) made up to 50 µl in H_2O. The thermocycle program was as following: following an initial denaturation for 10 minutes at 94°C, 30 cycles of denaturation (94°C, 1 minute) annealing (52°C, 1 minute), and extension (72°C, 1.5 minutes, adjusted to length of product). A final 10 minutes extension at 72°C was performed. The PCR product was cleaned up (Qiagen) and sent for Sanger sequencing (Source Bioscience) with desired primers diluted to 3.2 pmol / µl (all primers were obtained from Eurofins Genomics). The primer sequences used to amplify Tau cDNAs are displayed in **table 2.3**. A schematic of the strategy used to amplify Tau cDNA is displayed in **figure 2.2**.

Table 2.3 Nucleotide sequences of primers used to amplify ectopic Tau cDNAs

Primer	Sequence	Primer	Sequence
TAU_03	GTCCGTACTCCACCCAAGTC	TAU_16	CTACAAACCCTGCTTGGC
TAU_09	CGCTACCGGACTCAGATC	TAU_17	ATGGTAAAACGAAGATCGCCA
TAU_10	GGCTGATTATGATCTAGAGTCG	TAU_15	GGCTGATTATGATCTAGAGTCG

2.6 Agarose gel electrophoresis

Tris-acetate EDTA buffer (TAE) buffer was made up at 40 mM Tris, 20 mM acetate 1 mM EDTA at pH 8.6. Agarose was added to Tris-acetate EDTA (TAE) buffer at 1 – 2 % (w/v) and solubilised by heat pulses in a microwave. Once cooled, SafeView at 1 µl / 10 ml (nbsbio) was added to the solution which was then poured into a gel tank electrophoresis system and allowed to gellate. To 9 µl DNA (0.3 - 1 µg; PCR product, plasmid) was added 1 µl 10 X DNA loading buffer (39% glycerol (v/v), 0.000125% bromophenol blue (w/v), 0.000125% xylene cyanol (w/v) 61% H_2O) and the reaction was loaded onto the agarose gel. The gel was submerged in TAE buffer and the tank was connected to an electrophoresis power pack system (Biorad) and ran at 100 V for 30 minutes. Nucleic acids were visualised with GelRed program on ChemiDoc imaging system (BioRad).

2.7 Cell lines

Normal SH-SY5Y cells were obtained from the European Collection of Authenticated Cell Cultures at passage 12. Clonal SH-SY5Y cells ectopically expressing various Tau constructs were donated by Rohan de Silva (IoN, UCL) or generated in house by the methodology detailed below (stable transfection of SH-SY5Y cells **2.12**). In house generated cell lines shared the name of the respective constructs listed in **table 2.1**. Tau constructs expressed by the respective SH-SY5Y cell lines are schematically represented in **figure 2.1** and specific details of the cell lines used in this study and their origins are given in **table 2.4**.

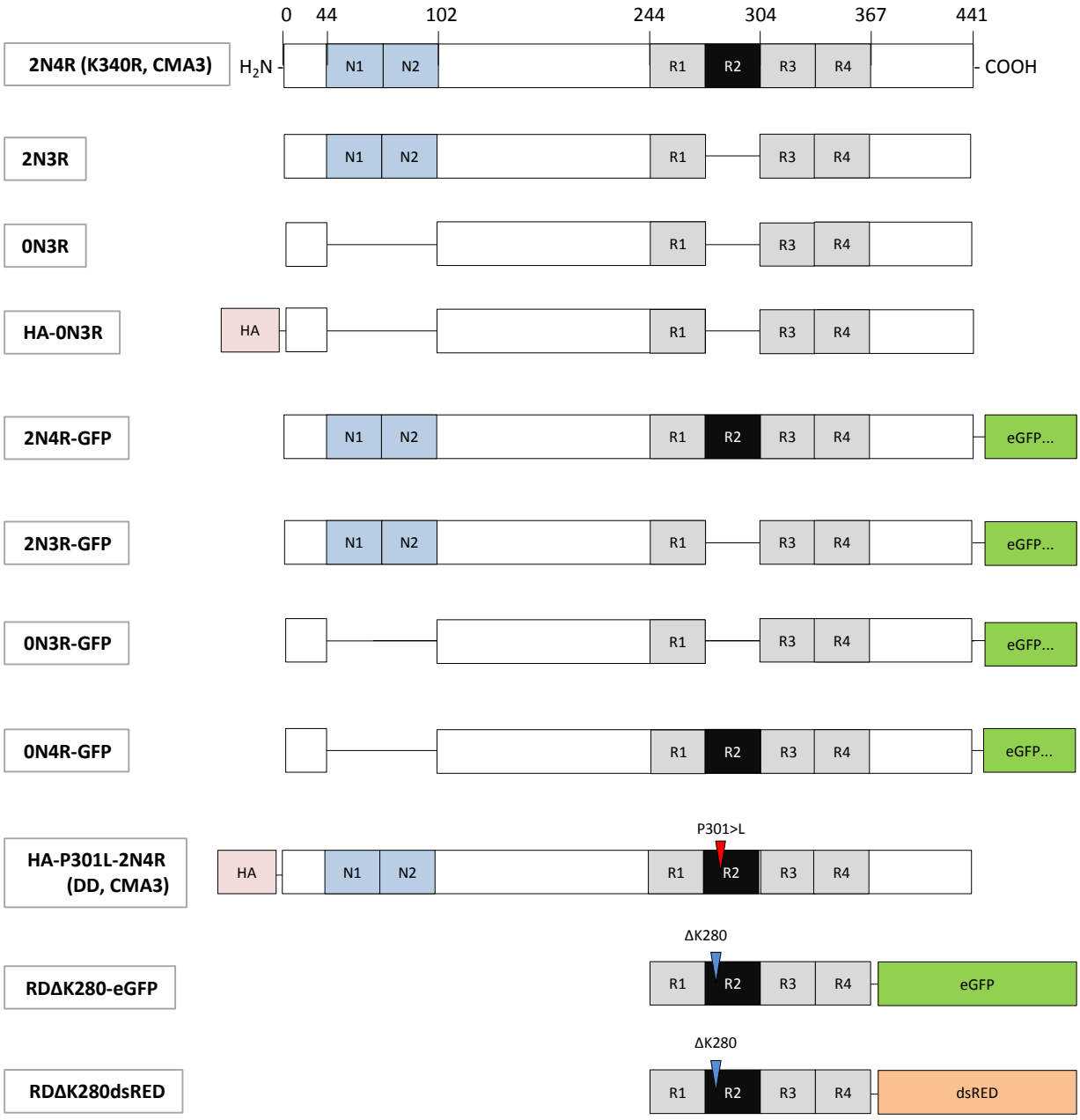

Figure 2.1 Schematic diagram of Tau constructs used in this study. Diagrams represent different Tau protein isoforms expressed in SH-SY5Y cells. Numbers above 2N4R-Tau diagram indicate amino acids. Blue and black boxes represent alternatively spliced N-terminal inserts and R2 microtubule binding region, respectively. Grey boxes represent constitutively expressed microtubule binding regions. C-terminal eGFP tags on full-length Tau isoforms are not represented to scale as indicated by the ellipsis. Constructs with specific mutations (i.e. K340R and CMA3-2N4R and DD and CMA3-P301L-2N4R) are indicated next to the WT construct from which they were generated by site directed mutagenesis of the underlying cDNA. More detail regarding the location of these mutations is indicated in the relevant results sections. Locations of P301>L and ΔK280 mutations are indicated by the red and blue arrows, respectively, in the appropriate constructs.

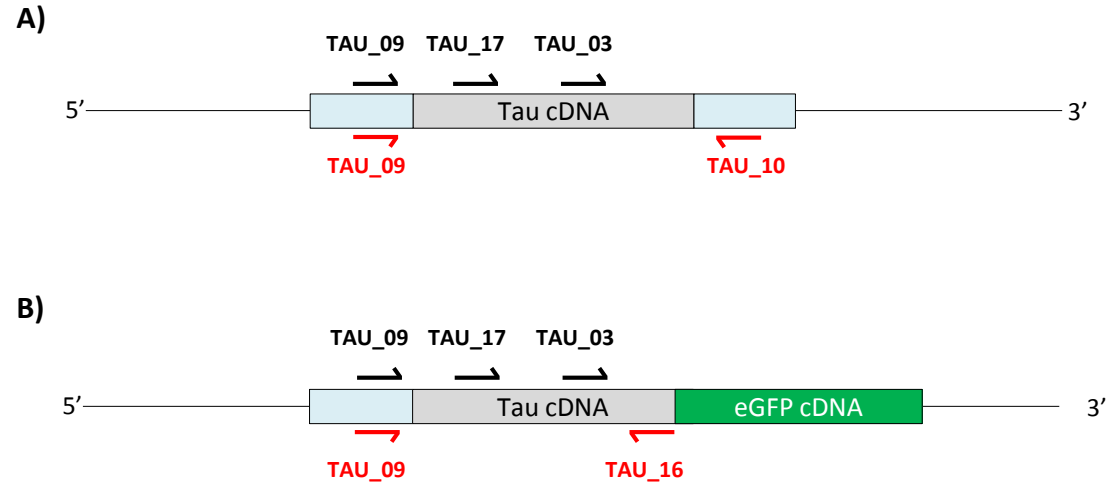

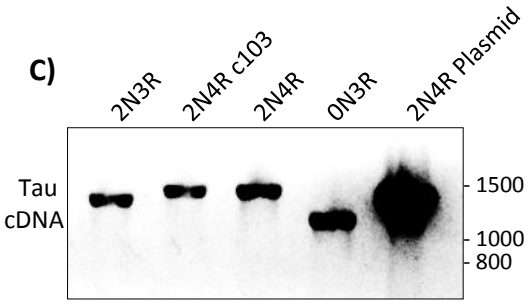

Template	Size (bp) Predicted	Observed
2N4R cDNA	1379	~1400
2N3R cDNA	1286	~1200
0N3R cDNA	1124	~1100

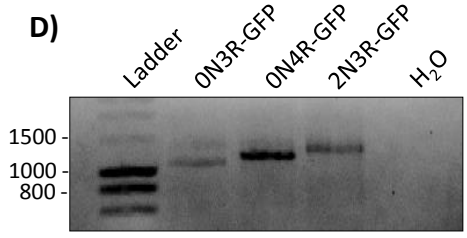

Template	Size (bp) Predicted	Observed
0N3R-GFP cDNA	1059	~1000
0N4R-GFP cDNA	1152	~1200
2N3R-GFP cDNA	1233	~1250

Figure 2.2 Strategy for PCR of Tau cDNA. Names and annealing locations of forward and reverse primers used to PCR amplify and sequence **A)** untagged Tau and **B)** C-terminally GFP tagged Tau cDNA inserted in pEGFP-N1 vectors. PCR primers are in red, sequencing primers are in black. Grey boxes indicate Tau cDNA, green box indicates eGFP cDNA and blue boxes indicate flanking pEGFP-N1 vector regions. Box sizes are not to scale. **C)** Agarose gel electrophoresis of PCR product using the above primers was performed on cDNA isolated from SH-SY5Y cells stably transfected with **C)** untagged Tau isoforms and **D)** C-terminally GFP tagged Tau isoforms. Tables on the right indicate predicted and observed product sizes for the respective PCR.

Table 2.4 SH-SY5Y cell lines used in the project and their origin. RDS – Rohan de Silva

Construct	Promoter	Clones Used	Origin
2N4R-Tau	CMV	c103, cB,	RDS
		c216.6, c218	Stable transfection
2N3R-Tau	CMV	n.a.	RDS
0N3R-Tau	CMV	n.a.	RDS
HA-0N3R-Tau	CMV	c113, c117	Stable transfection
K340R-2N4R-Tau	CMV	c102, c106, c205	Stable transfection
CMA3-2N4R-Tau	CMV	c103, c105, c111	Stable transfection
0N3R-GFP-Tau	CMV	n.a.	RDS
0N4R-GFP-Tau	CMV	n.a.	RDS
2N3R-GFP-Tau	CMV	n.a.	RDS
2N4R-GFP-Tau	CMV	n.a.	RDS
HA-P301L-2N4R-Tau	CMV	c1, c2, c8	Stable transfection
HA-P301L-CMA3-2N4R-Tau	CMV	c111	Stable transfection
HA-P301L-DD-2N4R-Tau	CMV	c108	Stable transfection
RDΔK280-Tau-dsRED-Tau	CMV	c9	Stable transfection
RDΔK280-Tau-eGFP-Tau	CMV	c8	Stable transfection

2.8 SH-SY5Y cell culture

Unless otherwise stated, all cell culture reagents were purchased from Life Technologies. SH-SY5Y clonal lines were cultured in DMEM:F12 (1:1) growth medium supplemented with 10% foetal bovine serum, non-essential amino acids (NEAA: 0.1 mM of: glycine, L-alanine, L-asaparagine, L-aspartic acid, L-glutamic acid, L-proline and L-serine) and penicillin (50 U/ml) and streptomycin (50 µg/ml) at 37°C and 5% CO_2. SH-SY5Y clones ectopically expressing Tau protein coupled to G418 resistance were routinely cultured in 400 µg/ml G418 (Sigma), and clones expressing Tau coupled to hygromycin resistance were cultured in 200 µg/ml hygromycin (Sigma). Growth under these conditions ensured stable expression of Tau protein over subsequent passages, and selection reagents were omitted 24 hours prior to experiments. For routine cell culture, cells were passaged at 80%

confluency via trypsinisation. Cells were washed once in PBS and following incubation for 2-5 minutes with trypsin (0.25% trypsin in Versene) and plates were tapped to encourage detachment of the cells. The trypsin was then neutralised in 9 volumes of normal growth medium, a fraction of which was either transferred to new vessels directly for continued culturing or pelleted for 10 minutes at 1000 rpm (200 x g). Pelleted cells were resuspended in an appropriate volume of medium and split between new plates. For certain experiments (i.e. transfections, co-culture) cells were counted prior to seeding, cells were counted (C-Chip NanoEnTek DHC-N01). Cell lines stocks were generated by resuspending cell pellets (from 1 x 10 cm plate) in 1 ml of freezing down medium (10% DMSO in FBS) and after being frozen initially at -80^{o}C were transferred to liquid nitrogen for long term storage. When collecting cell pellets for later analysis (for e.g. for SDS-PAGE or IP), the pellet was resuspended in PBS, and pelleted at 13,000 RPM on a microfuge for 10 minutes, the supernatant was discarded and the pellet stored at -80^{o}C until analysis.

2.9 Transwell co-culture

For transwell experiments donor cells were seeded on transwell inserts (Falcon, 1 µm pores) and grown for 24 hours. Recipient cells were seeded in 6 well plates and grown for 24 hours. After this time, the transwell insert containing the donor cells was moved into the 6 well plates where the recipient cells were growing. Bafilomycin treatment, where appropriate, was performed at this point, and cells were grown in transwell co-culture for 24 – 48 hours. Donor and recipient cells were then harvested separately by trypsinisation and pelleted.

2.10 Direct SH-SY5Y co-culturing

Two independent SH-SY5Y clones expressing Tau isoforms with different tags (e.g. HA-0N3R-Tau and 2N3R-GFP-Tau) were harvested, pelleted at 200 x g for 10 minutes, resuspended in growth medium and counted (NanoEntek). Volumes of cells equivalent to

500 – 200000 (for each clone) were then mixed by trituration in a 20 ml Universal tube and seeded on coverslips in 6 well plates (to give 1000 – 400000 cells / well). Bafilomycin treatment was performed the following day once cells had adhered and growth was continued for a further 24 – 48 hours. Co-cultures were then processed by ICC and analysed by fluorescent microscopy (**2.19** and **2.21**, respectively).

2.11 HEK293 cell culture

HEK293 cells were acquired from ATCC and cultured in DMEM supplemented with 10% foetal bovine serum, non-essential amino acids (NEAA: 0.1 mM of: glycine, L-alanine, L-asparagine, L-aspartic acid, L-glutamic acid, L-proline and L-serine) and penicillin (50 U/ml) and streptomycin (50 µg/ml) at 37°C and 5% CO_2. Routine culturing, passaging and freezing procedures were performed as with SH-SY5Y cells (section **2.8**)

HEK293 cells with inducible expression of alpha-Synuclein were induced with ponasterone A treatment. Cells were treated with ponasterone A for 48 hours prior to experiments, at 1 – 2.5 µM.

2.12 Cortical neuron cell culture

Primary neuronal cultures were prepared from E15 – E17 C57BL/6 mouse brains (Charles River). Dissociated cortical neurons were plated onto poly-L-Ornithine (Sigma) coated coverslips at a density of 1 cortex per 6 well plate, and cultured in Neurobasal Medium supplemented with serum free B27, GlutaMAX and antibiotic/antimycotic solution (Sigma) in a 37°C 5% CO2 incubator. Experiments were generally performed at ~12 DIV. A representative photograph of primary cortical mouse neurons as 10 DIV is shown in **figure 2.3**.

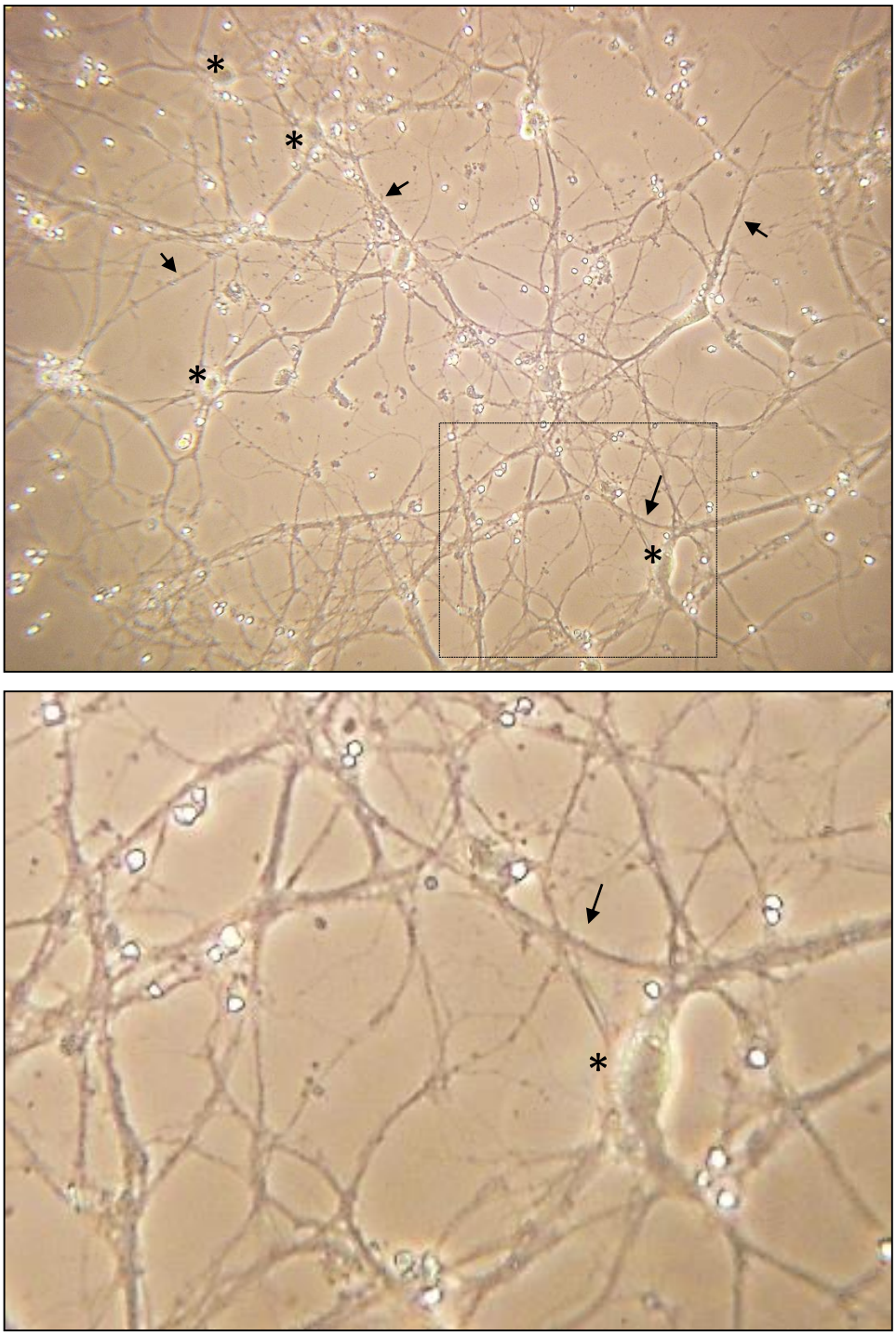

Figure 2.3 Phase contrast image of primary mouse cortical neurons in culture. Taken at 10 DIV. Arrows indicate neurites and asterisks indicate cell bodies. Boxed region is enlarged below.

2.13 Lysis of SH-SY5Y cells with nitrogen bomb

SH-SY5Y cells (1 – 4 x 10 cm of 90% confluent cells) were harvested by trypsinisation and pelleted by centrifugation at 200 x g for 10 minutes. The PBS washed pellet was resuspended in DMEM: F12 medium supplemented with NEAA and penicillin / streptomycin, or complete neurobasal medium (supplemented with B27 and antibiotic / anti-mycotic) at 1 ml / 10 cm. The resuspended cells were pressurised to 1400 psi in a nitrogen bomb and incubated for 30 minutes at 4^{o}C. The pressure was released and the resultant lysate was clarified at 3000 x g for 15 minutes, the supernatant was filtered through a 0.2 µm, and either supplemented with 10% FBS (for DMEM: F12 samples) and added to SH-SY5Y cells in culture, or added to cortical neurons in culture (for Neurobasal samples).

2.14 Stable transfection of SH-SY5Y

24 hours prior to transfection early passage number SH-SY5Y cells were plated in a 6 well plate at 50% confluence. 2.5 µg plasmid DNA was added to 375 µl DMEM/F12 (plain) and 5 µl Superfect (Qiagen), mixed and incubated for 10 minutes at room temperature, after which time it was added to the adherent cells growing in complete medium (containing 10% FBS, non-essential amino acids and penicillin-streptomycin). A mock transfection, containing no DNA was performed in parallel. The growth medium was changed 24 hours later and after a further 24 hours (48 hours from original transfection) transfected and mock transfected cells were each split onto 2 x 10 cm plates with fresh growth medium containing the appropriate selection reagent (200 µg/ml hygromycin or 400 µg/ml G418, see **table 2.1** for plasmid resistances). Colonies were allowed to expand and growth medium with selection reagent was frequently replaced. After ensuring that all mock transfected cells had died, sufficiently large (covering the field on 10 X phase contrast view) colonies from the transfected cells were selected with sterile cloning cylinders (Sigma),

transferred to 6 well plates and maintained in hygromycin / G418 containing medium. Clones were expanded for freezing down, and plated for immunocytochemical characterisation and pellets harvested for western blot characterisation.

2.15 Transient transfection of SH-SY5Y

2.15.1 Electroporation

Healthy cells growing under normal conditions were harvested by trypsinisation and counted (C-Chip DHC-N01, NanoEnTek). A volume corresponding to 5 x 10^5 cells was pelleted at 200 x g and the pellet was resuspended in buffer R (Thermo) and made up to a final volume of 10 µl with 1 µg plasmid DNA. When cells were co-transfected, as for Tau – Hsc70 co-immunoprecipitation experiments, 0.5 µg of each plasmid was used. Cells were electroporated under the optimal conditions of 1000 V, a bandwidth of 30, and 2 pulses (achieving efficiency of ~ 70%, **figure 2.3**). Electroporation equipment used was the Digital Bio Microporater MP-100 and electroporation reagents were purchased from Life Technologies

Electroporated cells were cultured in antibiotic free medium (DMEM:F12 supplemented with NEAA and 10% FBS) overnight and then medium was changed to either complete medium containing antibiotics for ICC analyses and immunoprecipitation experiments, or to optiMEM (containing penicillin / streptomycin) for exosomal isolation and analysis. Cells were then grown for a further 24 hours, after which time the determined analyses were performed.

2.15.2 Reagent mediated

For the SUMOylation experiments reagent mediated transfection of HEK293 cells was used. Plasmid DNA was incubated with XtremeGene HP transfection reagent (Roche) at a ratio of 1 µg DNA: 4 µl reagent in 100 µl optiMEM per 125,000 transfected cells. The mixture was

vortexed and incubated at room temperature for 15 minutes before being added dropwise to cells growing under normal conditions. Cells were incubated for 48 hours to allow protein expression prior to analysis.

2.15.3 Determining Optimal Conditions for Transfections

SH-SY5Y cells transfected under different conditions were analysed for efficiency of transfection. With reagent mediated transfection, the ratio of transfection reagent: plasmid DNA (µl : µg) was varied over 1:1 – 4:1, whilst with electroporation, the key parameters varied were voltage, bandwidth and pulse (set to: 1000, 30, 2 / 1200, 20, 3 or 1100, 30, 2). The transfected plasmid encoded WT-2N4R-Tau. Transfected cells were left to express the protein for 48 hours, after which time Dako Tau ICC was performed, with mock transfected (no plasmid DNA) and untransfected SH-SY5Y cells being used as negative controls. **Figure 2.4** displays the results of this optimisation of methodology, and established an optimal ratio of 4:1 (reagent: DNA) for reagent mediated transfections, and settings of 1000, 30, 2 (voltage, bandwidth, pulse) for transfection by electroporation. Electroporation was determined to be, in general, more efficient than reagent mediated transfection, with optimal conditions achieving ~70% efficiency, versus ~25% for reagent mediated transfection.

2.16 Vesicle depletion of bovine serum

FBS was mixed with DMEM: F12 (1:1) to a concentration of 50% and stored at 4^{o}C overnight. The serum – medium mixture was then centrifuged at 100,000 x g for 70 minutes at 4^{o}C and the supernatant was removed and diluted to 10% serum with DMEM F12 (1:1).

2.17 Exosome isolation

We adopted the methodology of Quah & O'Neill (2005) for exosome isolation from culture medium. 4 – 10 x 10 cm SH-SY5Y cells (with and without tau overexpression; number of

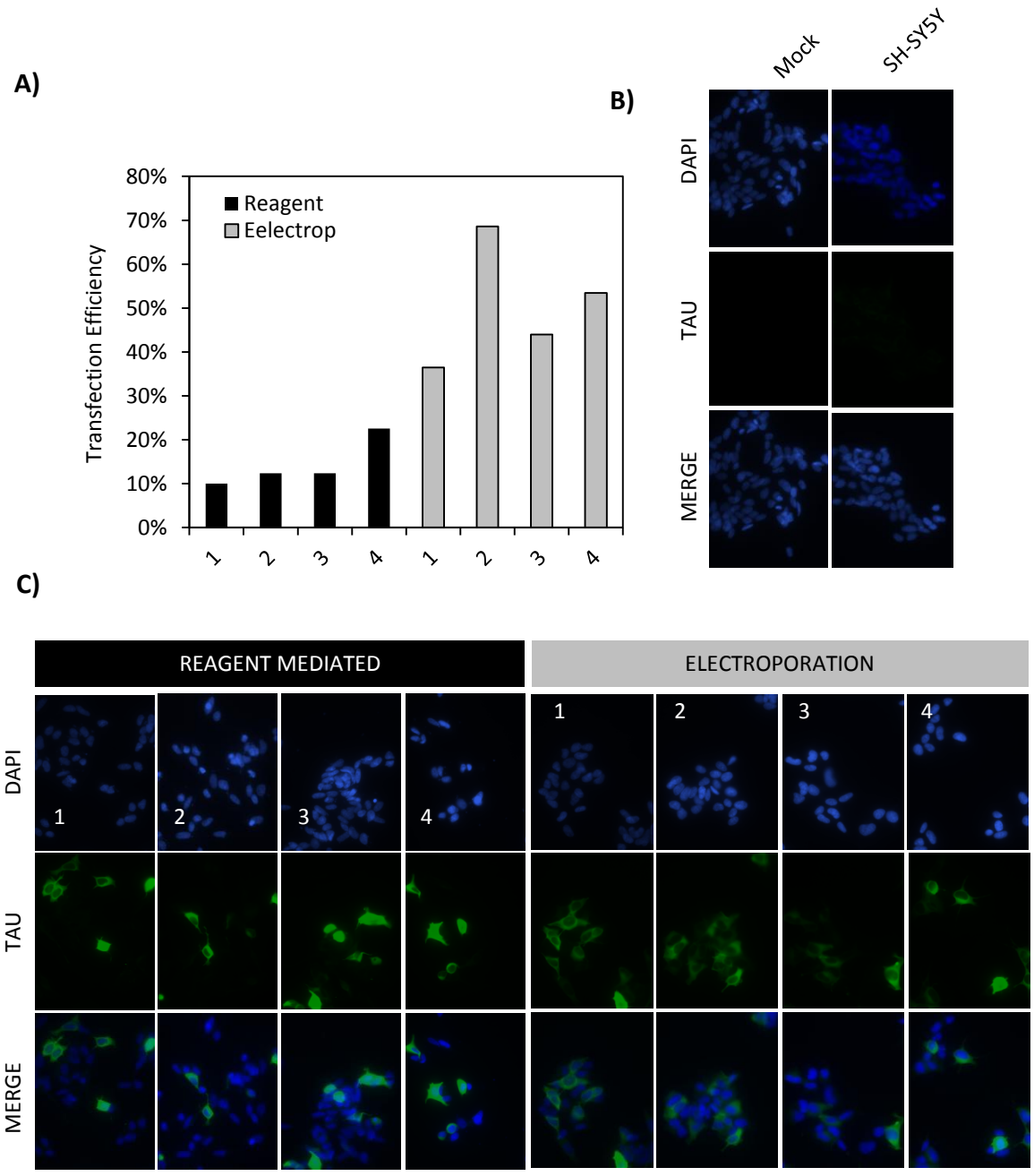

Figure 2.4 Optimisation of transient transfection in SH-SY5Y cells. **A)** Reagent mediated (grey bars) and electroporation mediated (black bars) transfection of SH-SY5Y cells was performed under a variety of conditions and transfection efficiency was quantified. Overall electroporation was determined to increase transfection efficiency relative to reagent mediated transfection. **B)** Mock transfected (with no plasmid DNA) and untransfected SH-SY5Y cells were used as negative controls in order to quantify transfection efficiency. **C)** cells transfected with WT-2N4R Tau under different conditions with reagent (left side) and electroporation (right side) were processed with Dako Tau immunocytochemistry and imaged by fluorescent microscopy. Numbers in graph and in ICC montages refer to transfection conditions. For reagent mediated transfection the ratio of reagent : plasmid DNA was varied at 1 = 1:1; 2 = 1:2; 3 = 1:3; 4 = 1:4. for electroporation the varied conditions were voltage, bandwidth and pulses, which were set at 1 = 1100, 30, 1; 2 = 1000, 30, 2; 3 = 1200, 20, 3; 4 = 1100, 30, 2.

plates used adapted to experimental constraints) were plated and grown until 60 - 80% confluent. At this time 7 ml optiMEM or DMEM : F12 (1:1) supplemented with 10% prespun foetal bovine serum (see above) (and NEAA and penicillin / streptomycin) was added to each plate. 24 hours later the medium was harvested and centrifuged at 2000 x g to remove cells and large debris. The supernatant was carried over and centrifuged sequentially at 12,000 x g (30 minutes, 4^{o}C) and 100,000 x g (70 minutes, 4^{o}C) (Beckman Coulter L8M ultracentrifuge, 70Ti rotor) to pellet cell debris and exosomes respectively. The exosomal pellet was resuspended in 2 ml PBS to wash and pelleted at 100,000 x g (70 minutes, 4^{o}C) (TLS-55 rotor). Exosome pellets destined for TRPS /Nanosight analysis were diluted to an appropriate concentration in PBS immediately and stored at 4^{o}C until analysis. Exosomal pellets for SDS-PAGE and immunoblotting analysis were stored at – 80^{o} C. When exosomes were isolated for treatment of recipient cells, isolation was performed under sterile conditions. Beckman ultracentrifuge tubes were sterilised by submersion in 100% etOH for 10 minutes, followed by rinsing with sterile PBS and then used as described above. Exosome pellets were resuspended in growth medium (different growth medium depending on the experiment and type of recipient cells).

2.18 Standardisation of exosome quantity and normalisation of exosomal Tau levels

Exosomes were isolated from the conditioned medium of SH-SY5Y cells from Between 4 - 10 plates per isolation. The number of plates used in each experiment is referred to in the text to allow comparison between samples. Wherever quantifications of exosomal Tau levels have been performed these data have been normalised to either a) an exosomal marker protein (for example, Alix) levels (see section **2.35**) or b) the protein content of the cells from which the exosomes were isolated, as determined by BCA or c) both. The

following equivalence allows translation between the units of measurement: 1 x 10 cm plate of SH-SY5Y at 80% confluence ≈ 6 x 10^6 SH-SY5Y cells ≈ 1 mg of cellular protein.

2.19 Nanoparticle tracking analysis (NTA) characterisation of exosomes

The Nanosight NS3000 instrument from Malvern instruments was used for NTA of exosomal preparations. This machine detects the Brownian motion of particles in suspension via laser beam induced light scatter, and relates this to particle size. For NTA exosomes were isolated from the 24 hour conditioned optiMEM of normal / 2N4Rc103 SH-SY5Y cells. The PBS washed exosomal pellet was resuspended in 1 ml PBS and diluted 1000X and loaded into the NTA cell. The NTA software version used was NTA 3.2 Dev Build 3.2.16 with the standard measurement script. For each sample three subsequent readings were taken and the mean, mode and standard deviation was calculated.

2.20 Tuneable resistive pulse sensing analysis (TRPS) characterisation of exosomes

The qNANO instrument from iZON science was used for TRPS analysis of exosomal preparations. In TRPS analysis, suspended particles flow through a nanopore across which an electrical current is established. The particles offer resistance to this current in proportion to their size. The amplitude and frequency of resistance events is therefore proportional to concentration and sizes of particles, respectively. For TRPS analysis exosomes were isolated from the 24 hour conditioned optiMEM of normal / 2N4Rc103 SH-SY5Y cells. The PBS washed exosomal pellet was resuspended in 200 µl and diluted 2 X in PBS. After establishing a basal current on the qNANO the instrument was calibrated with nanobeads of a known size (200 nm; CPC200 iZON science). The exosomal preparation was then loaded on the instrument and particles were counted. Software version 3.2.2.268 was used.

2.21 Proteinase K treatment of exosomes

Exosomes isolated under standard conditions were resuspended in 10 mM Tris-HCl (pH 8.0) and split into aliquots. One aliquot was designated 'untreated' and to the rest was added proteinase K (Sigma) to a final concentration of 1 μg/ml and to 1 aliquot was additionally added Tx-100 to a final concentration of 1%. Samples were then incubated at 37^{o}C for increasing periods of time. Reactions were inactivated by addition PMSF (final concentration 1 mM), SDS sample buffer and reducing agent followed by heating at 95^{o}C for 10 minutes. Samples were then separated by SDS-PAGE and analysed by immunoblotting for exosomal marker proteins and Tau. In experiments where the proteinase K mediated degradation rate of exosomal Tau was compared to that of exosomal supernatant (free) Tau, reactions were performed in larger volumes to accommodate for sufficient Tau in the supernatant. To allow analysis by SDS-PAGE, once the reaction had proceeded for 5 minutes, proteins were precipitated with trichloroacetic acid (100% w/v; Sigma) at a ratio of 0.7:1 (TCA : sample). Samples were vortexed and left on ice for 15 minutes prior to centrifugation at 13000 RPM for 30 minutes at 4^{o}C. The supernatants were discarded and the pellet allowed to air-dry over 1 hour. The pellets were then resuspended in 1 X sample buffer and reducing agent and heated to 70^{o}C followed by SDS-PAGE, transfer and immunoblotting analysis.

2.22 Lactate dehydrogenase assay

LDH activity was measured in the conditioned optiMEM medium from SH-SY5Y cells. NADH was made fresh each time the assay was performed and in basic conditions. To 96 well plates were added the following per well: potassium phosphate buffer pH 7.4 to 50 mM (stock made by mixing 200 mM KH_2P04 with 200 mM K_2PO_4 until pH reached 7.4), NADH to 200 μM and Tx100 to 0.1% (w/v). Samples were added to the wells and H_2O was added to give each well a consistent volume. After heating the plate to 37^{o}C for 10 minutes, sodium

pyruvate was added to all wells to a final volume of 250 µl and absorbance was read at 340 nm on a plate reader. Absorbance was read kinetically over 30 minutes and the rate of LDH activity was calculated from the linear region of absorbance / time plots.

2.23 3-(4,5-dimethylthiazol-2-yl)-2,5-diphenyltetrazolium bromide (MTT) assay

MTT assay was used to assess the viability of cortical neurons. Reduction of MTT to insoluble, purple coloured Formazan depends upon the function of oxidoreductases, the activity of which serves as a surrogate for cell viability. Medium was aspirated from cortical neurons growing in 96 well plates leaving 100 µl medium per well. To this medium was added 10 µl MTT (5 mg/ml in PBS) which was incubated for 4 hours at 37°C 5% CO_2. After this time, the Formazan crystals which had formed were resuspended with 100 µl isopropanol + 0.04 N HCl per well. Absorbance of the resuspended crystals was read at 570 nm from which the background reading at 670 nm was subtracted.

2.24 Immunocytochemistry

Cells were plated at 20 – 60 % confluence on coverslips in 6 well plates. Cell lines that had a tendency to clump were triturated and drawn through an 18 gauge needle to ensure a single cellular suspension prior to seeding. When ready for analysis, coverslips were removed from the wells and cells fixed in pre-warmed (37°C) 4% paraformaldehyde PBS (SantaCruz) for 20 minutes. Cells were permeabilised by incubation in 100% MeOH at -20°C for 15 minutes. After washing 3 times in PBS, cellular proteins were blocked in 10% normal goat serum (NGS) at 37°C in a humidified atmosphere for 45 minutes. Coverslips were drained of serum and incubated with primary antibody (**table 2.6**) diluted in PBS for 1 hour at 37°C in a humidified atmosphere. Following primary antibody incubation cells were washed 3 times in PBS and incubated with alexa-fluor (488 / 594) conjugated secondary

antibodies (Dako) in 2% NGS PBS for 1 hour. Cells were washed three times in PBS, drained and mounted on glass slides with 1 µg/ml DAPI Citifluor and sealed with nail polish.

2.25 Staining cortical neurons with CellMask orange

Cortical neurons in culture were treated with 1 µg / ml CellMask Orange (Thermo) diluted in NeuroBasal medium for 10 minutes at 37^{o}C 5% CO_2. Neurons were then processed by immunocytochemistry.

2.26 Fluorescence microscopy

For routine analysis of coverslips a Zeiss Axioplan microscope fitted with an LED illumination unit (QImaging wLS) fitted with red, green and blue filters was used. Images were captured using Micro-Manager software; exposure settings were adjusted such that no fluorescence was detected from negative control samples, and this same exposure threshold was applied to experimental conditions. Images were analysed using imageJ software.

2.26.1 Confocal microscopy

A Nikon Eclipse Ti confocal microscope with 405 nm, 488 nm and 561 nm lasers was used. Images were captured using the NiS elements software interface on which exposures and Z-stack parameters were set. Captured images were later analysed with FiJI software (Fiji is Just ImageJ).

2.26.2 Image analysis

2.26.2.1 Tubulin neurite analysis

SH-SY5Y clones expressing different forms of Tau were cultured at the same density on coverslips under normal conditions. ICC with anti-Tubulin (βiii-Tubulin, ab6046) was performed as described under section **2.24**. Images of SH-SY5Y cells fluorescently stained with anti-Tubulin antibody were acquired at the same intensity with microscope using

Micro Manager software. Images were opened in ImageJ and tubulin positive neurites (extending from the cell body) were counted. Total nuclei were also counted and the number of Tubulin positive neurites was normalised to total cell number.

2.26.2.2 Quantification of individual cellular fluorescence from microscope images

Stacked microscope images (i.e. containing blue and green channels; DAPI and Tau) of ICC stained SH-SY5Y cells were opened in ImageJ. The channels were split and the DAPI channel was turned into a binary image. Watershed function was performed as appropriate to separate closely apposed nuclei. Maximum points were then calculated from the bninarised DAPI image, and 'segmented particles' were outputted. The segmented particle image was then added to the 8-bit transformed 'green' (Tau) channel and segment lines approximated cellular boundaries. The integrated pixel density within each segment (corresponding to one cell) was then calculated by setting measurements and referring the measurement back to the original green image. The fluorescence intensity of each cell was calculated by correcting for cellular area and background fluorescence using the following formula:

CTFC (corrected total cell fluorescence) = Integrated density of area of interest – (mean background intensity X area of interest)

2.26.2.3 Plotting fluorescence intensity of line segments in ICC images

Line segments were drawn through several nuclei (randomly chosen) on ICC images using the line drawing tool on ImageJ. The fluorescence intensity of blue, green and red channels was plotted and the numerical values exported as a list. Numerical values were normalised to the maximum value for the respective channels and plotted on a scatter graph using Excel.

2.27 Preparation of samples SDS-PAGE analysis

2.27.1 Preparation of cell pellets

Cells were harvested by trypsinisation, followed by neutralisation in 9 volumes of growth medium and pelleted at 200 x g. The cell pellet was washed with 1 ml PBS and pelleted at 17k x g at 4^{o}C in microfuge tubes. The supernatant was discarded and the dry pellet was stored at -80^{o}C until analysis.

2.27.2 SDS solubilisation of cell pellets

For routine analysis of protein expression levels cell pellets were solubilised in 0.1% SDS (10mM Tris/HCl pH 7.4 containing protease inhibitors, and phosphatase inhibitors where appropriate – Thermo, Halt) on ice with pipetting and vortexing for 10 minutes. The lysate was sonicated briefly (1 pulse for 2 seconds, with probe-sonicator) to disrupt nuclear material and the resultant lysate was aliquoted and either stored (at -80^{o}C) or taken directly for BCA and SDS-PAGE analysis. In some experiments DNase treatment was used as an alternative (to sonication) to disrupt nuclear material and allow SDS-PAGE analysis of cellular protein. Lysates were incubated with DNase (0.1U / µg cellular protein) and DNase (diluted to 1 X) buffer (Promega) at 37^{o}C 30 minutes.

2.27.3 Tx100 extraction of cell pellets

Pellets were extracted in 1% Triton X-100 in 50 mM Tris, 150 mM NaCl (pH 7.6) (containing protease inhibitors – Thermo, Halt) on ice with pipetting and vortexing for 10 minutes. Lysates were clarified at 17k x g in a microfuge for 10 minutes at 4^{o}C. The supernatant containing extracted proteins was aliquoted and stored at -80^{o}C or used directly for BCA and SDS-PAGE analysis.

2.27.4 BCA assay

BSA standards of known protein concentration (0.05 – 1.0 µg/µl) and cell lysates (prepared as above) diluted in H_2O were pipetted into clear bottomed 96 well plates to final volumes of 25 µl. 200 µl BCA reagent (50 : 1 ratio of A : B, Thermo) was added to the wells and heated at 37^{o}C for 15 minutes. Absorbance was read at 562 nm on a plate reader (Biorad). Protein concentrations of known standards were plotted against absorbance at 562 nm using Excel and sample protein concentration was interpolated from the curve by linear regression.

2.28 Immunoprecipitation of Tau

Cell pellets were extracted in lysis buffer (1% Triton X-100 in 50 mM Tris, 150 mM NaCl pH 7.6 containing protease inhibitor cocktail), vortexed, and incubated on ice for ten minutes. Lysates were then clarified at 17k x g in a microfuge for ten minutes at 4^{o}C. The supernatant was taken to a fresh tube and to it was added 1 µl DAKO-Tau antibody (K9JA) and incubated overnight at 4^{o}C with rotation. The lysate-antibody mixture was incubated with 30 µl protein-G sepharose beads (Amersham Healthcare) for 2 hours at room temperature with rotation. Protein-G sepharose beads with bound antibody-antigen complex were pelleted for 2 minutes at 2000 x g and washed 4 times with lysis buffer. After the final wash, immunoprecipitating proteins were eluted with 20 µl IgG elution buffer pH 2.0 (Pierce) at room temperature for 10 minutes followed by centrifugation at 2000 x g for 2 minutes. The eluted proteins were either stored at -80^{o}C until further analysis or diluted in SDS sample buffer and separated by SDS-PAGE.

2.28.1 Determination of the linearity of immunoprecipitation of ectopic Tau

We aimed to determine if the immunoprecipitation of ectopic Tau protein from SH-SY5Y cell lysates followed a quantitatively linear pattern. As such the Tau signal detected from

immunoprecipitation reactions of decreasing quantities of 2N3R-GFP SH-SY5Y cells was analysed.

Normal SH-SY5Y cells and SH-SY5Y cells with ectopic expression of 2N3R-GFP-Tau were harvested, counted and pelleted. The cell pellets were extracted in 1% Tx100 to give defined concentrations of cells / volume. Decreasing volumes of the 2N3R-GFP SH-SY5Y cell lysate, from 80,000 to 800 cells were mixed with the normal SH-SY5Y cell lysate to give final quantities of 800,000 ± 9% cells / reaction. A consistent quantity of cells was used in each reaction so that the key variable was the quantity of ectopic 2N3R-Tau present. Proteins were then immunoprecipitated with DAKO-Tau and separated by SDS-PAGE followed by Tau12 immunoblotting. Input samples of the normal SH-SY5Y cells and 2N3R-GFP SH-SY5Y cells were also loaded and immunoblotted with Tau12 (**figure 2.5**)

From the 'INPUT' samples, a Tau12 cross reactive band from 2N3R-GFP SH-SY5Y cells was detected migrating at 88 kDa, detectable at high sensitivity (i.e. detected from as few as 800 cells by direct Tau12 western blot of cellular lysates; band '**a**' **figure 2.5 A**). This band was consistent with ectopic 2N3R-GFP-Tau. A 50 kDa Tau12 cross-reactive band from normal SH-SY5Y cells was also detected (band '**b**', **figure 2.5 A**). However this band was detected at a lower sensitivity, from 800,000 normal SH-SY5Y cells.

With immunoprecipitation, the Tau12 cross reactive band at 88 kDa, consistent with 2N3R-GFP Tau, could be reliably captured from SH-SY5Y lysate when the latter was 'spiked' with as few as 800 cells expressing the former. The range of detection was from 80,000 to 800 2N3R-GFP SH-SY5Y cells diluted in the lysate from a constant number of SH-SY5Y cells (800,000; **figure 2.5A**). Importantly, no Tau12 cross reactive bands were detected in the proteins precipitated from the lysate when DAKO-Tau antibody was included in the bead – lysate mixture, (Lane 1) thus demonstrating the immuno-specificity of the approach. Furthermore, over the detection range, the Tau12 signal arising from the 88 kDa band (i.e.

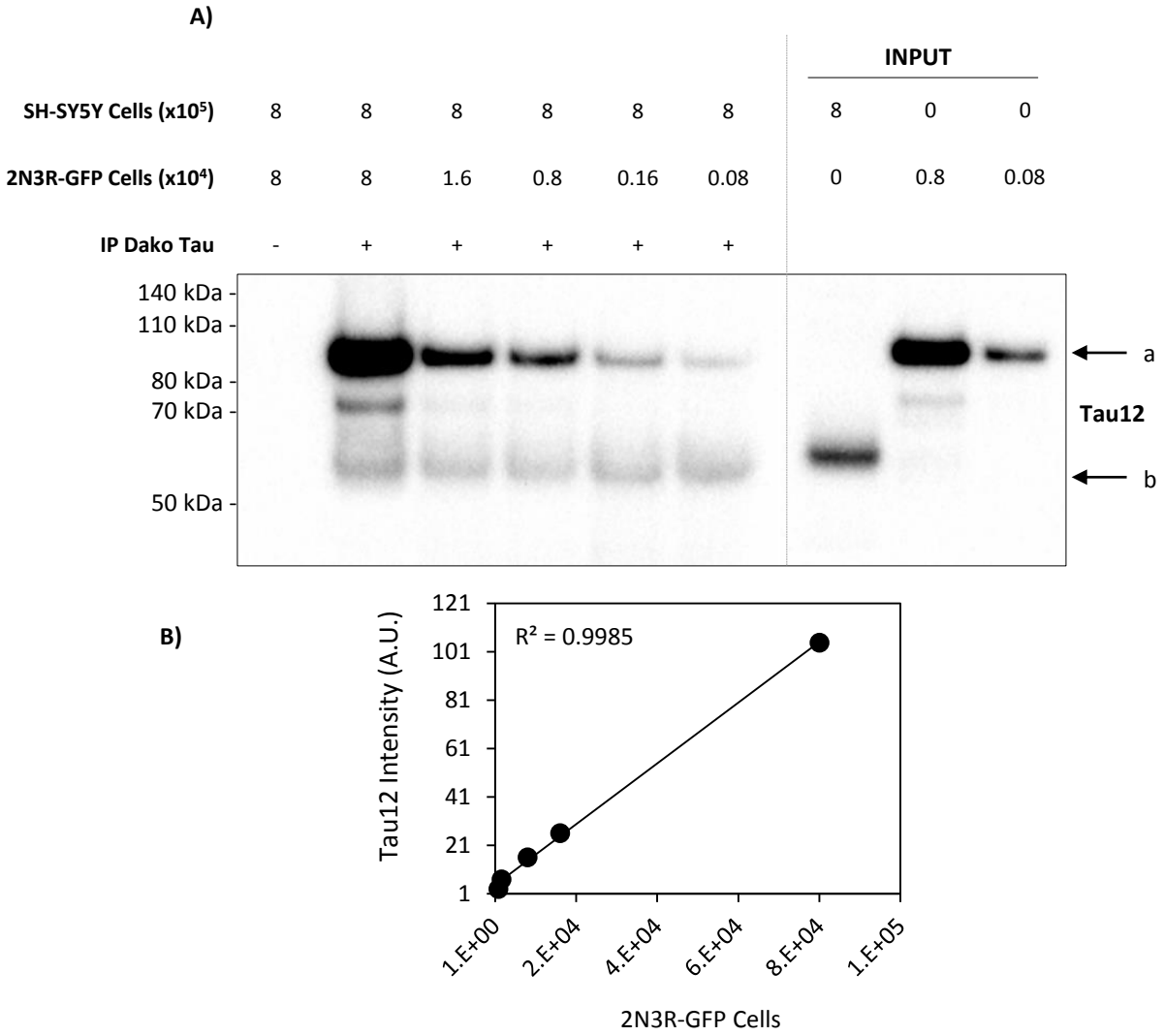

Figure 2.5 Validation of immunoprecipitation of Tau protein, and assessment of its quantifiability. A) DAKO-Tau immunoprecipitation of 2N3R-GFP lysate spiked into SH-SY5Y lysate. Lane one is the antibody control (i.e. no DAKO-Tau contained in the IP reaction). Tau12 cross reactive band consistent with 2N3R-GFP-Tau in the input is indicated by 'a' and endogenous Tau in normal SH-SY5Y cells is indicated by 'b'. **B)** Quantification of IPed 2N3R-GFP intensity correlated with input quantity.

that consistent with 2N3R-GFP-Tau) was quantifiably linear (r^2 = 0.9985; **figure 2.5 B**) demonstrating the fidelity of quantitation arising from this technique.

2.29 Co-immunoprecipitation

Co-immunoprecipitation methodology is adapted from Papkovskaia et al. (2012). Protein G agarose beads (Thermo) were rotated at 4^{o}C with antibody (1 µl DAKO-Tau) for 30 minutes and then centrifuged at 2000 x g for 2 minutes to pellet antibody-bead complexes. Subsequently, cell pellets were lysed in modified IP lysis buffer (50 mM Tris HCl pH 7.4), 270 mM sucrose, 1% NP-40, 1 mM EDTA, 1 mM EDTA, 1 mM benzamidine supplemented with protease inhibitor cocktail) and after incubating on ice for ten minutes, were clarified at 17k x g (on microfuge) for ten minutes at 4^{o}C. The supernatant was then added to the antibody-bead complexes and rotated for 2 hours at room temperature. The beads (and immunoprecipitating proteins) were then pelleted at 2000 x g for 2 minutes and washed 5 times with 1 ml wash buffer (modified IP lysis buffer supplemented with 150 mM NaCl) followed by pelleting at 2000 x g for 2 minutes. Residual wash buffer was aspirated and immunoprecipitating proteins were eluted with IgG elution buffer pH 2.0 (Thermo) at room temperature for five minutes, beads were pelleted at 2000 x g for 2 minutes, and the supernatant was transferred to fresh tubes and either stored at -80^{o}C or directly added to SDS sample buffer and reducing agent for SDS-PAGE.

2.30 Ni-NTA purification

Ni-NTA purification of His-tagged proteins was adapted from Dorval & Fraser (2006). 48 hours after transfection with SUMO-1-His and target proteins, HEK293 cells were harvested and pelleted. Pellets were washed with PBS and then lysed in lysis buffer (0.1 M NaH2PO4.H2O, 0.01 M Tris, 6 M Guanidine HCl, 10 mM imidazole, pH8 + protease inhibitors – Halt, Thermo) and to the lysates was added 50 µl of pre-washed Ni-NTA beads (washed in lysis buffer; Qiagen) and rotated for 2 hours at room temperature. Beads were

pelleted at 3000 x g for 3 minutes and washed 2 x with lysis buffer and 6 times with wash buffer (0.1M NaH2PO4.H2O, 0.01M Tris, 8M urea, 10 mM Imidazole, pH7) before elution in SDS sample buffer. Eluates were heated at 70^{o}C for 10 minutes and then analysed by SDS-PAGE.

2.31 Differential solubility protein extraction

Cell pellets were extracted in 1% Triton X-100 in 50 mM Tris, 150 mM NaCl (pH 7.6) (with protease inhibitor cocktail, Halt, Thermo) for 15 minutes on ice with vortexing and pipetting. Lysates were centrifuged at 50,000 x g for 30 minutes at 4^{o}C and the supernatant taken and designated as 'triton soluble fraction'. The pellet was washed with triton lysis buffer and centrifuged at 50,000 x g for 30 minutes at 4^{o}C. The triton insoluble pellet was solubilised in 1% SDS in 50 mM Tris, 150 mM NaCl (pH 7.6)) (containing protease inhibitors) and either DNase digested (Promega; see **2.24.2**) for 30 minutes at 37^{o}C or sonicated briefly (probe sonication, minimum volume 100 µl) to disrupt nuclear material, this sample was designated 'triton insoluble fraction'. Samples were prepared for SDS-PAGE and western blotted as described in **section 1.25**.

2.32 Fractionation of microtubules and cytoplasm

Cells were fractionated into cytoplasmic and microtubular components following established protocols (Derisbourg et al. 2015; Hamdane et al. 2003). Adherent SH-SY5Y cells were washed once in PBS and scraped into warmed microtubule stabilisation buffer (80 mM Pipes, pH 6.8, 1 mM $MgCl_2$,2mM EGTA, 30% glycerol, 0.1% Triton X-100 - with protease inhibitors cocktail, Halt, Thermo). The resultant lysate was ultracentrifuged at 100,000 x g (40,000 RPM with TLS-55 swing out rotor) for 20 minutes at 25^{o}C. The supernatant was taken and designated as the 'cytosolic' fraction, whilst the pellet, representing microtubular components was solubilised in RIPA buffer and probe sonicated to allow full resuspension. The resultant fractions were then analysed by SDS-PAGE. To

ensure the fidelity of this technique to isolate microtubules and lack of cytoplasmic contamination of the microtubular pellet, we performed SDS-PAGE and immunoblotting of cytosolic and microtubular fractions isolated from SH-SY5Y cells with Tubulin and GAPDH antibodies. The results of this validation are shown in **figure 2.6**. 96±0.5% of the GAPDH signal arouse from the cytoplasmic compartment, indicating minimal contamination of the pellet with cytoplasmic components. The 50 kDa Tubulin cross reactive band was distributed throughout the two compartments, with 28±5% arising from the pellet, representing 'polymerised' tubulin and 72±5% arising from the cytoplasmic compartment (**figure 2.6 B**). Tubulin immunostaining of SH-SY5Y cells revealed the presence of microtubular structures (arrows, **figure 2.6 B**) and treatment of these cells with the microtubule destabilising drug colchicine (at 0.1 μg/ml, Sigma) for 24 hours completely abolished the microtubular network (**figure 2.6 B**). Colchicine treatment decreased the amount of Tubulin pelleted at 100,000 x g in a time dependant manner (50% decrease at 2 hours, **figure 2.6 D** and **E**). Collectively these findings validated usage of the microtubule fractionation assay in SH-SY5Y cells.

2.33 Dephosphorylation of cell lysates

Protein de-phosphorylation of cellular lysates was performed with calf intestinal alkaline phosphatase (CIP; New England Biolabs). Cell pellets were extracted in 0.1% Tx-100 Tris-HCl (pH 8, supplemented with protease inhibitor cocktail, Halt, Thermo) and clarified at 1317k x g for 10 minutes at 4^{o}C. Supernatants were incubated with CIP at 1U / μg cellular protein with CIP buffer (New England Biolabs) for 30 minutes at 37^{o}C. Control samples were lysed in the same way, but lysis buffer was additionally supplemented with protein phosphatase inhibitor cocktail (Halt, Thermo) and the samples were not subjected to CIP treatment.

2.34 Preparation of human brain samples

Brain samples were obtained from Parkinson's UK Brain Bank. Ethical approval from Wales Research Ethics Committee (Ref. No. 08/MRE09/31+5) covered this analysis. The gender, age at death and post mortem delay of the brain samples used in this study are displayed in **table 2.5**.

Table 2.5 Brain samples used in this project

Sample ID	Age at Death	M/F	Post mortem delay
3014	87	F	13 hours
3074	87	M	31 hours
3050	79	F	32 hours

10 – 50 mg of human hippocampi were weighed in microfuge tubes. Proteinaceous material was extracted in RIPA buffer supplemented with protease inhibitor cocktail at 100 µl / 10 mg brain tissue. Samples were sonicated and fibrous / insoluble material was allowed to settle. BCA analysis was performed on the supernatants which were then diluted with SDS sample buffer and reducing agent and heated to 70^{o}C for 10 minutes prior to separation by SDS-PAGE.

2.35 SDS-PAGE and Western blotting

To volumes of lysate containing 10 – 20 µg of protein was added LDS sample buffer (Novex) and reducing agent (Novex) diluted in H_2O to consistent final volumes (25 – 30 µl depending on well volume). Samples were heated at 70^{o}C for ten minutes in a heat block, centrifuged (17K x g for 5 minutes), and loaded on NuPage^{TM} Novex^{TM} bis-tris protein gels (either 4-12% gradient gels, or 12% linear gels) alongside 5 µl molecular weight standard (PageRuler). Samples were electrophoresed for 45 minutes (4-12% gels) or 90 minutes (12% gels) at 200 V (BioRad power pack) in MES buffer (Novex). Proteins were transferred onto PVDF membranes at 30 V for 1 hour in Towbins buffer (25 mM Tris, 190 mM glycine,

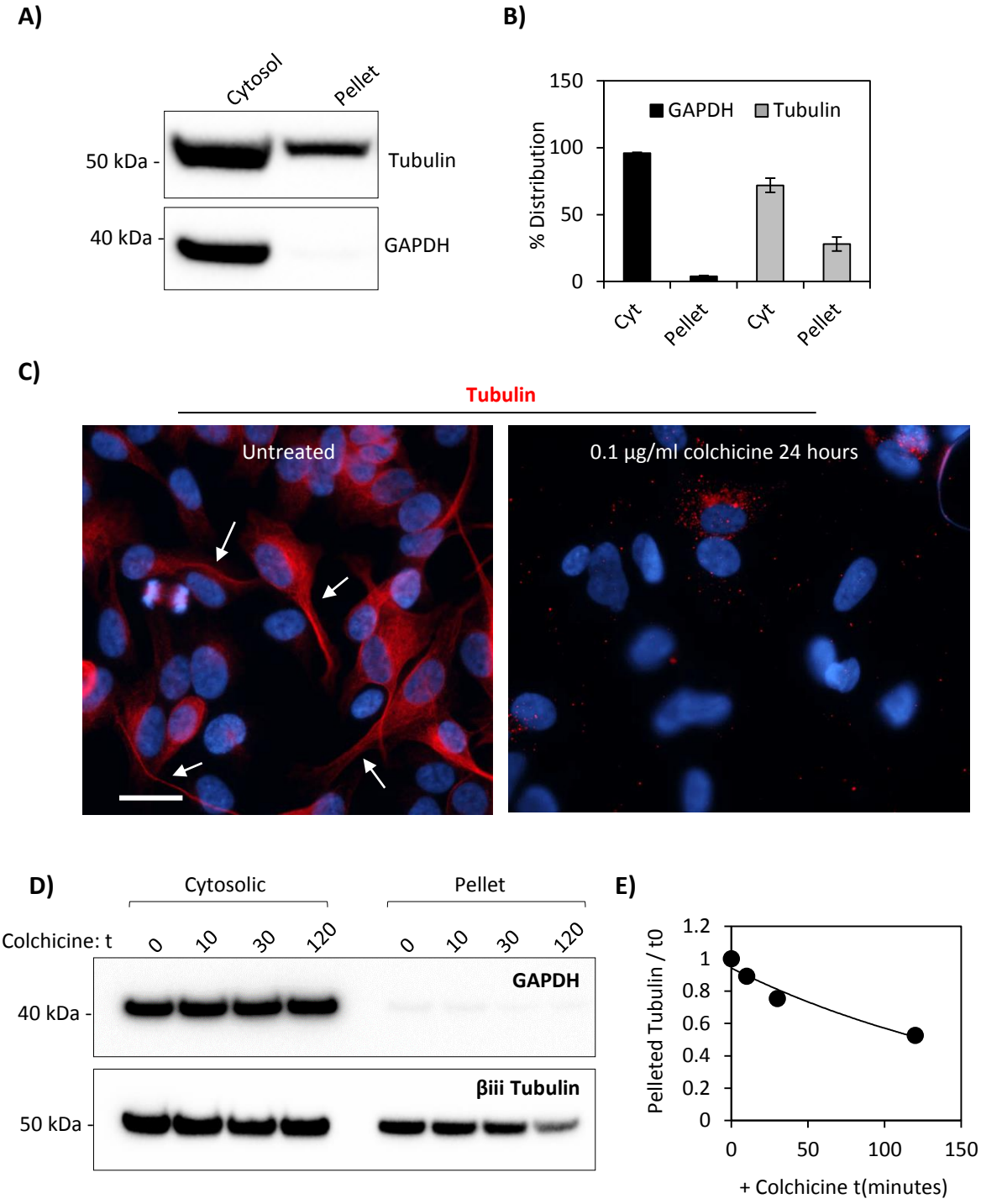

Figure 2.6 Fractionation of microtubules and cytosol from SH-SY5Y cells. A) Western blot of cytosolic and microtubular (pellet) isolated from SH-SY5Y cells by ultracentrifugation (100,000 x g) of cells lysed under microtubule stabilising conditions. Each fraction was solubilised in 100 µl and equal proportions were loaded on the gel. **B)** Quantification of distribution of Tubulin and GAPDH between cytosolic and microtubular (pellet) compartments (mean ± SEM, n=3). **C)** Tubulin – Tau co-immunostaining of SH-SY5Y cells ectopically expressing 2N4R-Tau, untreated and treated for 24 hours with 0.1 µg/ml colchicine. Scale bar 10 µm. **D)** Cytosolic and microtubular fractions were prepared and analysed as in A), from SH-SY5Y cells treated with colchicine (0.1 µg/ml) for increasing periods of time. **E)** The amount of Tubulin in the pellet relative to t0 was quantified for SH-SY5Y treated with colchicine for increasing periods of time.

20% MeOH) using the XCell transfer system. Membranes containing transferred proteins were placed into tubes and blocked for 45 minutes by rolling in 10% milk PBS. Primary antibodies (**table 2.7**) diluted in 5% milk 0.2% PBS-Tween20 (PBS-T) were added to the membranes and incubated for 1 hour at room temperature or overnight at 4^{o}C with rolling. Following primary antibody incubation the membranes were washed 3 times 10 minutes with 0.4% PBS-T and incubated with HRP-conjugated secondary antibodies (**table 2.7**) diluted in 5% milk 0.2% PBS-T for 45 minutes with rolling. Membranes were washed 3 times for 10 minutes each time with 0.4% PBS-T. For sensitive detection of proteins, membranes were incubated with 1 ml ECL reagent (Luminata Forte Western HRP substrate; EMD Millipore) for 1 minute prior to development. For less sensitive detection of proteins, Pierce ECL Western blotting substrate was used. Blots were incubated with Pierce ECL reagent for 5 minutes with rolling. Blots were developed with ChemiDoc imaging system (BioRad) using either 'chemi' or 'chemi-high sensitivity' programs with signal accumulation mode, calibrated to the signal intensities. Molecular weight protein standards markers were captured using the 'colorimetric' protocol on the ChemiDoc imaging system.

Western blots were analysed using ImageLab software (BioRad). Molecular weight analysis was performed by merging the chemiluminescent and colorimetric images and generating a standard curve for the size markers. Sizes of protein bands in the samples were interpolated from this curve. Protein abundance was quantified by densitometric integration of band intensity from non-saturated bands, using ImageLab software.

2.36 Blue-Native PAGE

Cultured cells growing under normal conditions were washed once with cold PBS and scraped directly into modified IP buffer (50 mM Tris HCl (pH 7.4), 270 Mm sucrose, 1% NP-40, 1 mM EDTA, 1 mM benzamidine supplemented with protease and phosphatase inhibitor cocktail, Halt, Thermo) on ice. The scraped cells were transferred to a tube and

incubated on ice for 15 minutes with gentle vortexing to promote lysis. Lysates were then clarified at 1k x g or 17k x g for 10 minutes at 4^{o}C and the supernatants containing soluble and oligomeric proteins were diluted in NativePAGE sample buffer (Thermo). Samples were then separated on a 4-16% bis-tris native PAGE gel (Thermo) at 150 V for 20 minutes after which time the cathode buffer was changed and electrophoresis was resumed for a further 80 minutes. The gel was removed from its cassette and denatured for 20 minutes in 66 mM $NaHCO_3$, 2% SDS (w/v) 2% β-mercaptoethanol (v/v) and then washed for 10 minutes in transfer buffer (20% v/v MeOH, 25 mM Tris pH 8.8, 0.2 M glycine) before being transferred to PVDF membrane at 30 V for 1 hour. The membranes were then subjected to immunoblotting as described in section **2.32**.

2.37 Dot blot

Nitrocellulose membrane (PerkinElmer PROTRAN, 0.45 µm pore size) was assembled into BioRad dot blot apparatus and washed twice with PBS. Samples of conditioned medium (clarified at 12,000 x g for 30 minutes) were loaded onto the nitrocellulose membrane and vacuum was applied. The membrane was washed once more with PBS. Membranes were then blocked and immunoblotted and-developed in the same manner as for western blotting (section **2.32**). In order to assess the linearity of the dot blot technique to detect extracellular Tau, normal SH-SY5Y cells and SH-SY5Y cells with ectopic expression of 2N4R-Tau were grown in 6 well plates in optiMEM growth medium for 24 hours. The 24 hour conditioned medium was harvested, centrifuged at 2000 x g for ten minutes to remove whole cells and debris and loaded on dot blot in increasing quantities, from 100 – 500 µl. The membrane was immunoblotted with Tau12 antibody. Tau12 immunoreactivity was detected in the conditioned medium from SH-SY5Y cells expressing 2N4R-Tau at all volumes loaded (**figure 2.7**). At the same exposure time no Tau12 immunoreactivity was detected in the conditioned medium from normal SH-SY5Y cells at any volume,

demonstrating the specificity of the signal. Quantification of the intensity of Tau12 immunoreactivity detected from the increasing volumes of 2N4R-Tau SH-SY5Y conditioned optiMEM demonstrated it to follow a linear relationship (r^2 = 0.9959; **figure 2.7 B**).

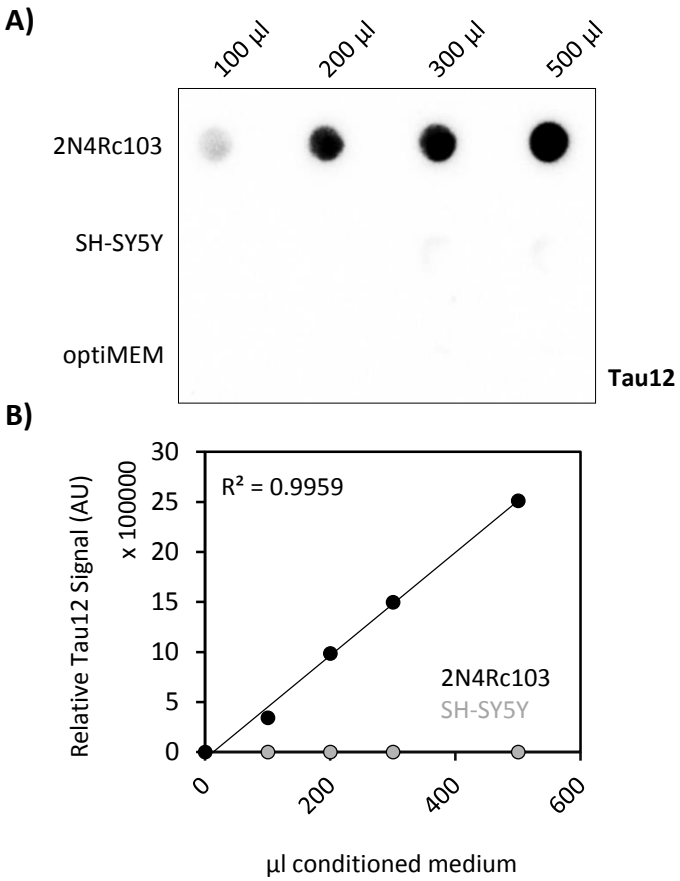

Figure 2.7 Validation of dot-blot for quantifying extracellular Tau. WT-2N4R-Tau c103 and normal SH-SY5Y cells at 80% confluence in a 6 well plate were grown in 2 ml optiMEM for 24 hours. The conditioned medium was centrifuged at 2000 x g for 10 minutes and loaded on **A)** dot blot at increasing quantities, following vacuum, membranes were immunoblotted with Tau12. Plain optiMEM was also loaded to give an indication of background signal. **B)** Tau12 intensity was quantified and background signal (from optiMEM alone) was subtracted. Values were then plotted against volume of conditioned medium loaded.

Table 2.6 Antibodies used in the project

Antibody Name and Reference	Immunogen and epitope	Species/ Clonality	WB Dilution	ICC Dilution	Primary Uses
Dako Tau, A0024	C-terminal Tau, AA 244-441	Rabbit, pAB	1:10000	1:500	Routine detection of Tau in cells and exosomes. Dako Tau used for IP
Tau12, MAB2241	N-terminal Tau, AA epitope = 6-18	Mouse, mAB	1:10000	1:500	
Tau46, #4019 CST	C-terminal Tau, epitope = AA 404-441	Mouse, mAB	1:1000		
pT205 Tau, STJ90426, St John's Laboratory	Synthesised peptide derived from HuTau around the phosphorylation site of T205	Rabbit, pAB	1:1000		Detection of phosphorylated forms of Tau
pS356 Tau, STJ90422, St John's Laboratory	Synthesised peptide derived from HuTau around the phosphorylation site of S356		1:1000		
pT181 Tau, STJ90425, St John's Laboratory	Synthesised peptide derived from HuTau around the phosphorylation site of T181	Rabbit, pAB	1:1000		
Tau RD4, 05-804 Clone 1E1/A6 Millipore	Bovine thyroglobulin-conjugated synthetic peptide corresponding to amino acids 275-291 (VQIINKKLDLSNVQSKC) of human Tau (4-repeat isoform RD4).	Mouse, mAB	1:1000		Detection of 4R containing Tau isoforms
Flotilin-1, ab41927	Human flotilin-1 residues 1-100	Rabbit, pAB	1:1000		Characterisation and marking of extracellular vesicles / exosomes
Alix, ABC40 Millipore	GST-tagged recombinant fragment corresponding to 479 amino acids from the C-terminal half of mouse AIP1/Alix.	Rabbit, pAB	1:5000		
Hsc70		Rabbit, pAB	1:1000		
Tsg101, (C-2): sc-7964	amino acids 1-138 representing full length tsg 101 (tumour susceptibility gene 101) of mouse origin	Mouse, mAB	1:200		
CD-81, (B-11): sc-166029	amino acids 90-210 of human CD81	Mouse, mAB	1:100		
GAPDH, 6C5 ab8245	Rabbit muscle GAPDH	Mouse, mAB	1:10000		Loading controls and compartment markers (e.g. cytoplasm, nucleus and microtubules)
Actin, ab3280	Unavailable	Mouse, mAB	1:5000		
βiii Tubulin, ab6046	Synthetic peptide conjugated to KLH derived from within residues 1 - 100 of Human beta Tubulin.	Rabbit, pAB	1:5000	1:1000	
Histone H3, ab1791	Synthetic peptide corresponding to Human Histone H3 aa 100 to the C-terminus	Rabbit, pAB	1:1000		
GFP, ab290	Recombinant full length GFP	Rabbit, pAB	1:1000	1:1000	Detection of ectopically expressed proteins with the respective tags
V5, 46-0705 Invitrogen	V5 synthetic peptide: Gly-Lys-Pro-Ile-Pro-Asn-Pro-Leu-Leu-Gly-Leu-Asp-Ser-Thr-.	Mouse, mAB	1:1000	1:500	
RFP, ab62341	Recombinant full length protein corresponding to RFP.	Rabbit, pAB	1:1000	1:1000	
FLAG Tag, A00187-200, Genscript	Synthetic peptide (DYKDDDDK)	Mouse, mAB	1:5000	1:1000	
HA, Covance MMS-101R	Monoclonal antibody HA.11 (HA, 16B12, flu tag) was	Mouse, mAB	1:5000	1:1000	

	raised against the twelve amino acid peptide CYPYDVPDYASL.				
LC3B, ab48394	Synthetic peptide corresponding to Human LC3B (N terminal, between residues 1-100).	Rabbit, pAB	1:2000		Investigating starvation and autophagy
SUMO-1, Ab32058	A synthetic peptide corresponding to residues near the C-term of human SUMO-1.	Rabbit, mAB	1:1000	1:300	Detecting SUMO-1 and SUMOylated proteins
Anti-Rabbit HRP (Dako)			1:3000		Secondary Ab for western blot
Anti-Mouse HRP (Dako)			1:3000		
Anti-Mouse Alex-Fluor 594 / 488 (Invitrogen)				1:300 – 1:500	Secondary Ab for ICC
Anti-Rabbit Alex-Fluor 594 / 488 (Invitrogen)				1:300 – 1:500	

3 Results 1: Analysis of the exosomal release of Tau protein from SH-SY5Y Clones

3.1 Introduction and Aims

Our model system for studying the exosomal release of Tau protein was SH-SY5Y clones with ectopic expression of Tau isoforms. SH-SY5Y cells also express Tau protein endogenously (Umberti et al. 1997) but at low levels relative to human brain (Zhong et al. 1999). In this chapter we therefore aimed to rigorously characterise ectopic and endogenous Tau expression in our SH-SY5Y clones by ICC and Western blotting analysis. The enrichment of exosomes from culture medium is classically performed by differential ultracentrifugation of conditioned medium. Exosomes are characterised by their size, 30 – 140 nm – and expression of protein markers (Thery et al. 2002). We aimed to isolate exosomes from the conditioned medium of SH-SY5Y cells and characterise them in these terms. The exosomal release of Tau protein from cell cultures has previously been reported (Saman et al. 2012; Simon et al. 2012), however there is some debate and ambiguity over this process (Dujardin et al. 2014). In this chapter we aimed to rigorously characterise the exosomal release of Tau protein from SH-SY5Y cells. We aimed to investigate which isoforms of Tau were released in exosomes from SH-SY5Y cells and to analyse the species of Tau released from cells in exosomes and how these compared to the cellular Tau species.

Overall the aims for this chapter were:

1) Characterise Tau expression in normal SH-SY5Y cells and SH-SY5Y cells with ectopic Tau expression
2) Characterise exosomes isolated from the conditioned medium of SH-SY5Y cells
3) Analyse the presence of Tau protein in exosomes isolated from SH-SY5Y with ectopic Tau expression

4) Investigate the isoforms and species of Tau released in exosomes, including endogenous Tau from SH-SY5Y cells

3.2 Characterisation of stable, ectopic expression of WT-2N4R-Tau in SH-SY5Y clones

SH-SY5Y cells stably transfected with cDNA encoding 2N4R-Tau (termed 'WT-2N4R-Or SH-SY5Y') were obtained from R. de Silva (see methods for full details). We began by characterising the Tau expression in these cells by immunocytochemistry, Western blotting and verification of the inserted cDNA sequence.

3.2.1 Immunocytochemical characterisation of WT-2N4R-Tau SH-SY5Y Cells

Normal and WT-2N4R-Or SH-SY5Y cells were subjected to immunostaining with the polyclonal Tau antibody DAKO-Tau. DAKO-Tau immunoreactivity was detected by fluorescent microscopy in the cytoplasm and neurites of stained cells (**figure 3.1 A**). Staining of the normal SH-SY5Y population was heterogeneous: some cells had high intensity staining whereas some cells had no detectable staining (**white arrows** and **arrowheads**, respectively, **figure 3.1 A**).

Under conditions where no evident Tau staining was detected in normal SH-SY5Y cells (i.e. at lower exposure), intense DAKO-Tau immunostaining was detected from 2N4R-Or SH-SY5Y cells (**figure 3.1 B,** middle column, row 1 and 2, respectively) with 63±3% of WT-2N4R-Or cells demonstrating detectable levels of DAKO-Tau immunostaining.

To identify if the WT-2N4R-Or SH-SY5Y population was purely clonal we sub-cloned the line. Most clones failed to propagate, however we identified one clone that continued to grow: WT-2N4R-c103 (**2N4Rc103**). DAKO-Tau immunocytochemical analysis of 2N4Rc103 demonstrated similar heterogeneity to the parental WT-2N4R-Or line (**figure 3.1 B,** bottom row, middle column) with 67±9% of cells staining above the highest level of endogenous SH-SY5Y staining.

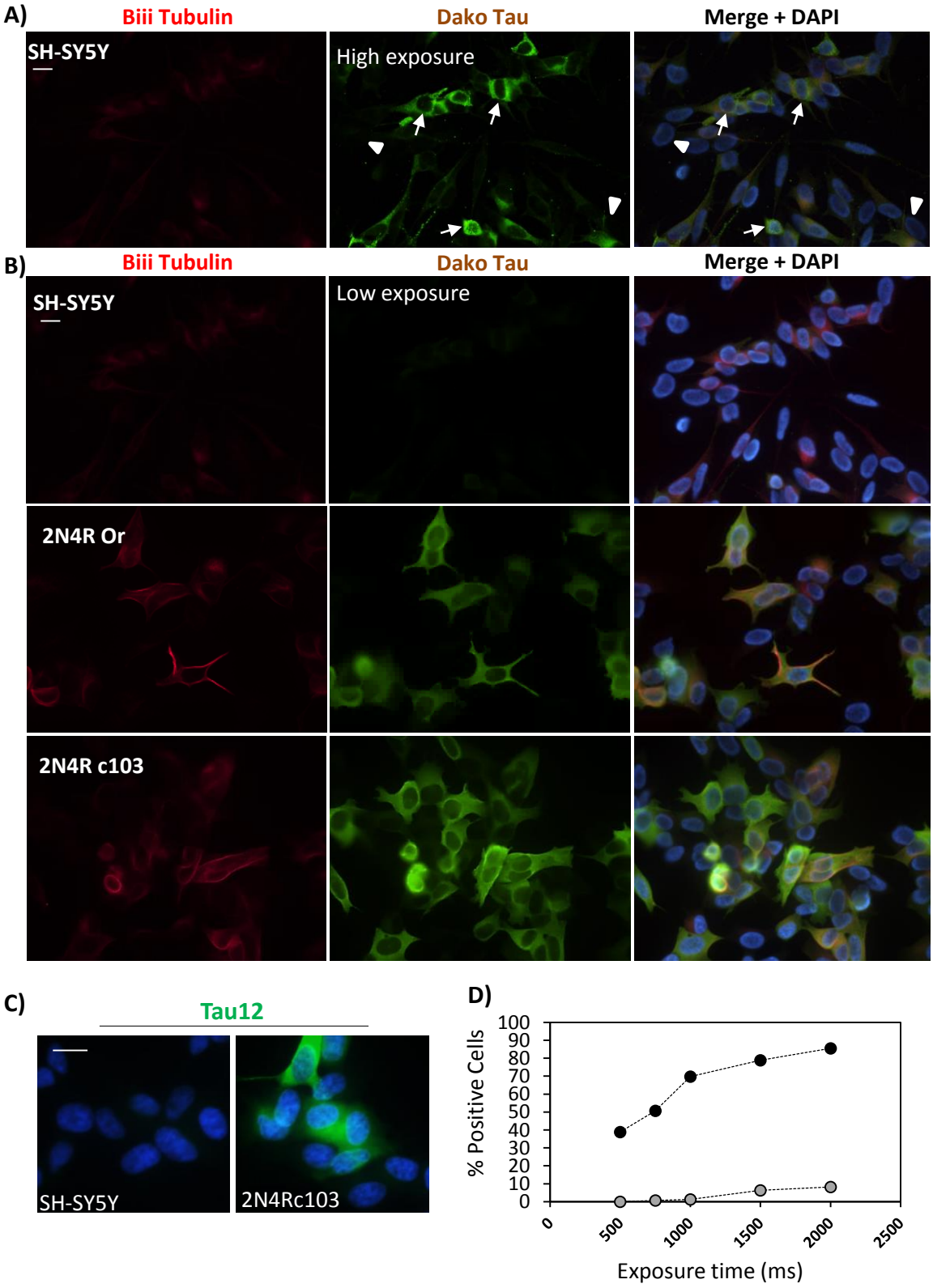

Figure 3.1 Immunocytochemical characterisation of Tau expression in normal and WT-2N4R-Tau expressing SH-SY5Y cells. A) DAKO-Tau immunostaining of normal SH-SY5Y cells at high exposure times. White arrows and arrowheads indicate high and low Dako-Tau intensity cells, respectively. **Ai)** DAKO-Tau immunostaining of normal (SH-SY5Y), WT-2N4R-Or and 2N4Rc103 SH-SY5Y cells at low exposure (relative to **A**). **C)** 2N4R-c103 SH-SY5Y immunostaining with Tau12 antibody. **D)** Quantitation of positively Tau12 Immunostained cells calculated at increasing exposure settings for normal (grey circles) and WT-2N4R-c103 (black circles) SH-SY5Y cells. Each data-point is the average of four fields (>150 cells for each line counted in total). Scale bars 10 µm.

2N4Rc103 cells also demonstrated positive immunostaining with the N-terminal Tau12 antibody. Staining was detected in the cytoplasm and neurites and cells and demonstrated similar heterogeneity to that observed with DAKO-Tau immunostaining (**figure 3.1 C**). We sequentially increased the exposure time of Tau12 immunostained normal and 2N4Rc103 SH-SY5Y and quantified the percentage of positive cells at each exposure. At the shortest exposure (500 ms), 0% of SH-SY5Y cells had detectable Tau12 staining, which increased to 10% at the highest level of exposure (2000 ms). Percentage of 2N4Rc103 SH-SY5Y cells with detectable DAKO-Tau staining increased from 40% to 90% over the same exposure range. Whilst we cannot be sure that all cells were ectopically expressing Tau, these findings demonstrated that at least 81% of 2N4Rc103 SH-SY5Y cells had levels of Tau expression higher than the highest level of endogenous SH-SY5Y Tau expression.

3.2.2 Sequencing inserted cDNA from WT-2N4R-Tau SH-SY5Y Cells

Cellular mRNA from 2N4Rc103 SH-SY5Y cells was isolated and reverse transcribed and ectopic 2N4R-Tau cDNA was amplified by PCR with specific primers. Agarose gel electrophoresis confirmed amplification of a product of the expected size (i.e. ~1500 BP, same as the product obtained from the WT-2N4R-Tau plasmid, **black box, figure 3.2 A)** and Sanger sequencing confirmed the product to be the correct sequence for WT-2N4R-Tau cDNA (see **appendix 1.1** for full sequence and alignment with reference sequence).

3.2.3 Western blotting analysis of WT-2N4R-Tau c103 SH-SY5Y Cells

To characterise Tau expression in normal and 2N4Rc103 SH-SY5Y cells by SDS-PAGE, cells were loaded at 1 and 20 µg, respectively. Two Tau12 cross reactive bands were detected in normal SH-SY5Y cells; a major band migrating at 51 kDa and a minor band migrating at 56 kDa (**red dashed box**, **figure 3.2 B**). Tau12 cross reactivity from 2N4Rc103 SH-SY5Y cells was detected as one major band migrating at 65 kDa (**green box**, **figure 3.2 B**).

The Tau ladder containing all six Tau isoforms (Sigma; loaded at 1 ng) separated into 4 Tau12 cross reactive bands which were identified as peaks '**A**',' **B**','**C**' and '**D**' (**figure 3.2 B**). The calculated molecular weights of these bands were 65, 61, 57 and 53 kDa, respectively (**figure 3.2 C** and **D)** which were larger than the predicted molecular weights of Tau isoforms calculated at 46 kDa, 43 kDa, 43 kDa, 40 kDa, 40 kDa and 37 kDa for 2N4R,1N4R, 2N3R, 0N4R, 1N3R and 0N3R, respectively (**figure 3.2 D**) . This however is consistent with previous reports (Guo et al. 2017) which identify the Tau isoforms 2N4R, 1N4R, 2N3R, 0NR, 1N3R and 0N3R as migrating at 67 kDa, 59 kDa, 62 kDa, 52 kDa, 54 kDa and 48 kDa, respectively. Therefore, the migration of bands 'A' and 'D' in our gel were consistent with 2N4R and 0N3R-Tau, respectively, whilst bands 'B' and 'C' were consistent with 1N4R / 2N3R and 0N4R / 1N3R-Tau isoforms, respectively (**figure 3.2 D**).

The major Tau12 reactive species from normal SH-SY5Y cells co-migrated with band 'D' of the Tau ladder, which was therefore consistent with SH-SY5Y cells endogenously expressing 0N3R-Tau. Tau12 immunoreactivity from 2N4Rc103 SH-SY5Y cells co-migrated with band 'A' of the Tau ladder, therefore consistent with this band representing ectopically expressed 2N4R-Tau.

To assess the stability of ectopic Tau expression, 2N4Rc103 SH-SY5Y cells were grown in the presence or absence of G418 (selection reagent for this clone) for the duration of 20 passages. Western blot analysis of Tau levels at 1, 10 and 20 passages indicated a reduction in Tau expression levels when cells were grown in the absence of G418 (0.3 times and 0.5 times P0 with DAKO-Tau and Tau12 staining, respectively; relative to GAPDH levels). In the presence of G418, however, Tau expression levels remained stable (**figure 3.2 E**). 2N4Rc103 SH-SY5Y cells were therefore routinely cultured in G418, except just prior to experiments.

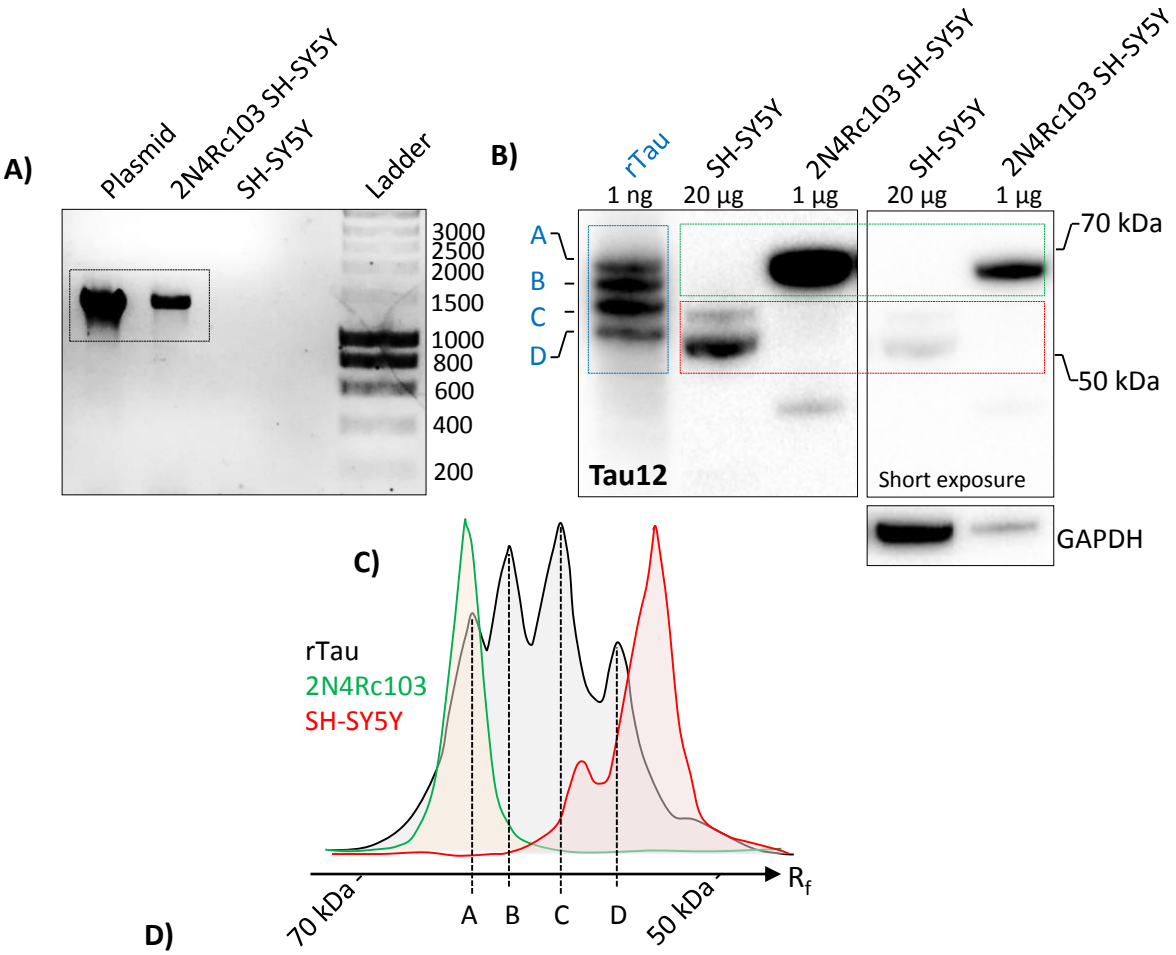

D)

Isoform	Expected Mr (kDa)	Published Mr (kDa)	rTau	SH-SY5Y	2N4Rc103
2N4R	45.8	67	A – 65		64
1N4R	42.9	59	B – 61		
2N3R	42.6	62			
0N4R	40	52	C – 57	56	
1N3R	39.7	54			
0N3R	36.7	48	D – 53	51	

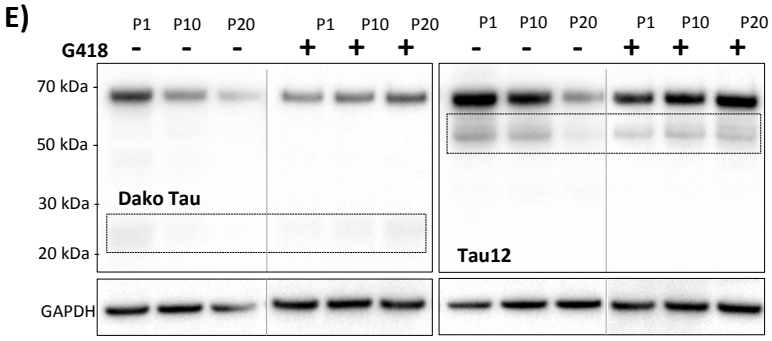

Figure 3.2 Characterisation of Tau expression in normal and WT-2N4R-c103 SH-SY5Y cells. **A)** agarose gel electrophoresis of PCR amplified ectopic 2N4R-Tau cDNA from 2N4Rc103 SH-SY5Y cells. Used for sequencing. **B)** Tau12 Western blotting of normal (SH-SY5Y; 20µg) and 2N4Rc103 (1 µg) SH-SY5Y cells. 'rTau' = recombinant Tau ladder containing all six Tau isoforms. **C)** Analysis of molecular weight profile or recombinant Tau isoforms separated by SDS-PAGE (band identities A – D are as in **B**) and Tau isoforms in normal (SH-SY5Y) and 2N4Rc103 SH-SY5Y cells. **D)** Interpolated and aligned molecular weight profiles of recombinant, endogenous and ectopic Tau, using reference values from the literature (Guo et al., 2017) as comparison points. **E)** Western blotting of Tau levels in WT-2N4R-c103 SH-SY5Y over increasing passage number (P1 – P20), in the absence and presence of G418. Dashed boxes indicate potential Tau fragments.

3.2.4 Analysis of the optimal conditions for solubilisation of ectopically expressed WT-2N4R-Tau

In order to determine the origin of potential Tau fragments detected in **figure 3.2 E** (**dashed boxes**) we compared the Tau species detected when WT-2N4R-Tau c103 SH-SY5Y cells were solubilised under different conditions.

Initially, adherent 2N4Rc103 SH-SY5Y cells were directly lysed in Triton X-100, clarified and separated by SDS-PAGE. Under these conditions, we detected a single Tau band migrating at 67kDa cross-reactive with N and C-terminal Tau antibodies and a polyclonal Tau antibody (Tau12, Tau46 and Dako Tau**,** respectively**, black box, 'Tx100 direct', figure 3.3 B**) that was consistent with expression of the full-length (FL) WT-2N4R-Tau in 2N4Rc103 SH-SY5Y cells (**figure 3.3 A** shows a schematic of antibody epitopes in 2N4R-Tau). A minor band migrating at 50 kDa was also detected with Tau12 immunoblotting (**green arrow, 'Tx100 direct', figure 3.3 Bi**). The major 67 kDa (with Tau12, Tau46 and DAKO-Tau IB) and the minor 50 kDa (with Tau12 IB) bands were also detected when 2N4Rc103 SH-SY5Y cells were pelleted prior to extraction in Tx100 (**black box** and **green arrow**, respectively, **'Tx100 pelleted', figure 3.3 B**) and the quantity of Tau extracted under these conditions was the same (relative to GPADH, **figure 3.3 C**), indicating that pelleting *per se* did not affect Tau species detected.

When 2N4Rc103 SH-SY5Y cell pellets were prepared for SDS-PAGE by solubilisation in 0.1% SDS followed by DNase treatment, the major 67 kDa (Tau12, Tau46 and DAKO-Tau cross reactive) and minor 50 kDa (Tau12 cross reactive) bands were also detected (**black box** and **green arrow,** respectively, **'SDS + DNase', figure 3.3 B**). Under these conditions the intensity of the 67 kDa band was significantly reduced to 70±0.04% and 76±0.05% of that detected under Tx100-direct conditions, for DAKO-Tau and Tau46, respectively (no differences observed with Tau12 antibody**, figure 3.3 C**).

Under these conditions we also detected DAKO-Tau and Tau46 cross reactive species migrating at 46 kDa and 37 kDa, respectively (**figure 3.3 Bii and iii, red** and **blue arrows**). These bands were not detected however, when SDS solubilised cell pellets were sonicated prior to SDS-PAGE, indicating that these species represented artefacts generated during DNase treatment (**'sonication'** vs. **'DNase', figure 3.3 D**). Moreover, sonication of 0.1% SDS solubilised 2N4Rc103 cell pellets retained the quantity of 67 kDa full-length 2N4R-Tau detected (as compared to Tx100 extraction, data not shown graphically).

To determine if any Tau remained in the pellet following Tx100 extraction, the pellet was solubilised in SDS, sonicated and analysed by DAKO-Tau IB. H3 and GAPDH immunoblot of Tx100 soluble and insoluble fractions demonstrated mutual exclusivity of these markers, demonstrating lack of cross contamination between the two fractions (**figure 3.3 D**). When loaded at the same proportion as the soluble fraction, DAKO-Tau cross-reactive bands were not detected in the Tx100 insoluble pellet of 2N4Rc103 SH-SY5Y cells (**figure 3.3 D, TxS:1, TxP:1**) When loaded at a 1:10 ratio (soluble: insoluble) however, a 67 kDa DAKO-Tau cross reactive band was detected in the insoluble fraction which was calculated to represent <1% of total detected Tau (**figure 3.3 Di, TxS:1, TxP:10**). H3 and GAPDH immunoblot of Tx100 soluble and insoluble fractions demonstrated mutual exclusivity of these markers, demonstrating lack of cross contamination between the two fractions (**figure 3.3 D**).

These observations demonstrated that either extraction of cell pellets in Tx100, or solubilisation with 0.1% SDS followed by sonication were appropriate methods for preparing 2N4Rc103 SH-SY5Y cell pellets for SDS-PAGE analysis. These methods were not equivalent though, as a small proportion of Tau (<1%) was deemed Tx100 insoluble.

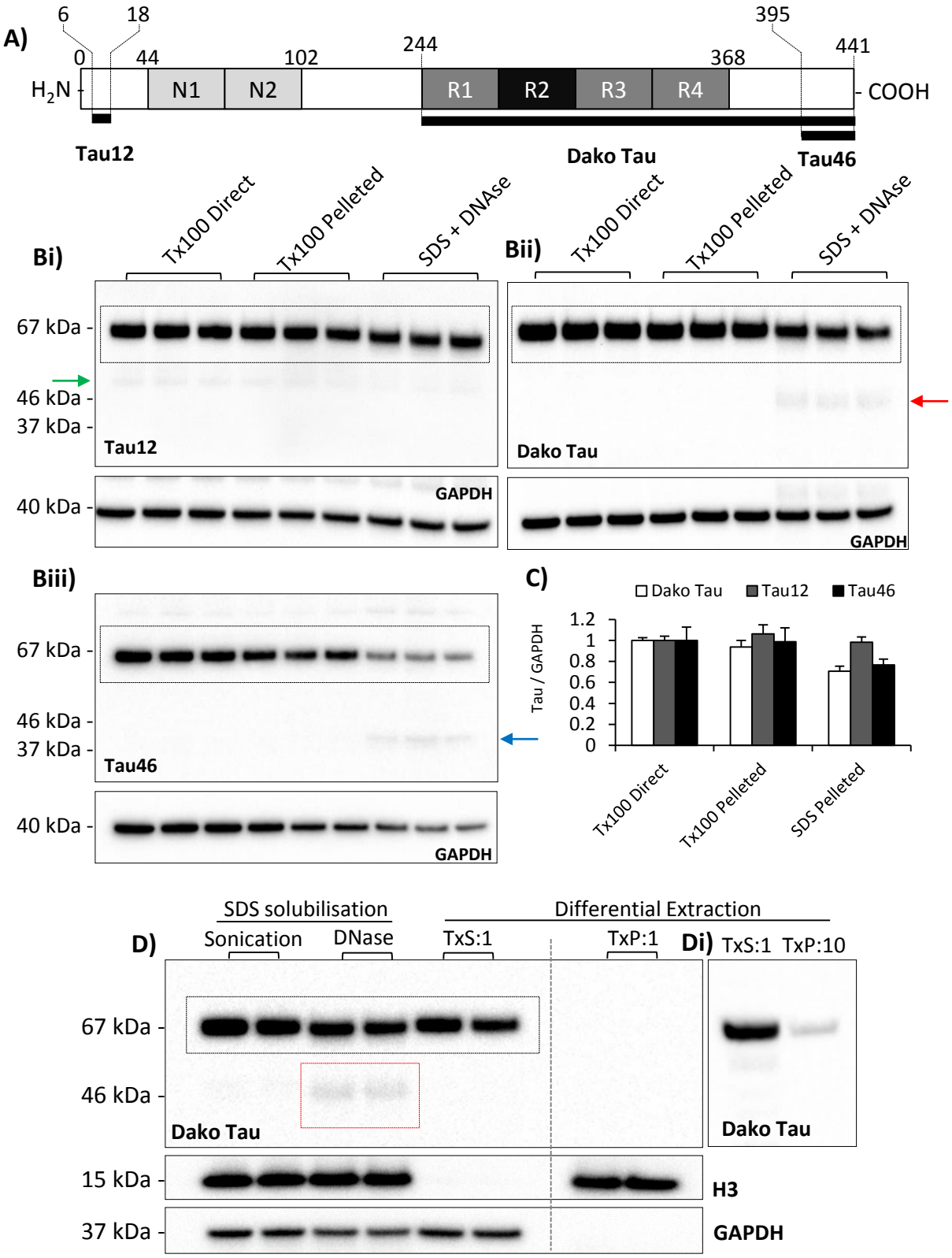

Figure 3.3 Comparison of preparation procedures of stably expressed 2N4R-Tau for SDS-PAGE analysis. A) Diagram of full length 2N4R Tau and the epitope of Tau12, and the immunogenic regions for Dako Tau and Tau46. Numbering refers to amino acid positions. **B)** Western blotting of 2N4Rc103 SH-SY5Y cells (20 µg), solubilised in SDS or extracted in Tx100, with three different Tau antibodies **i)** Tau12, **ii)** DAKO-Tau, **iii)** Tau46. Full-length 2N4R-Tau is indicated by the black dashed box, C-terminal fragments detected with DAKO-Tau and Tau46 are indicated by red and blue arrows, respectively. Green arrow indicates a Tau band detected only with Tau12. **C)** Levels of Tau protein were quantified (relative to GAPDH) and normalised to 'Tx100 Direct' condition and are shown graphically (mean ± SEM, n=3). **D)** Western blotting of 2N4Rc103 SH-SY5Y cells solubilised in SDS followed by either DNase treatment or sonication, or extracted in Tx100. With DAKO-Tau, GAPDH and H3 antibodies. 10 % of total volume (i.e. ~10 µg cellular protein) was loaded. The triton insoluble pellet was further solubilised in SDS and loaded at a 1:1 or **Di)** 10:1 ratio with soluble protein..

3.2.5 Phosphorylation of ectopic 2N4R-Tau

Tau protein function is regulated by phosphorylation and we next aimed to investigate the phosphorylation state of ectopically expressed 2N4R-Tau. 2N4Rc103 SH-SY5Y Tx100 (1%) extracts treated with phosphatase inhibitors or calf intestinal phosphatase (CIP; to dephosphorylate proteins) were subjected SDS-PAGE and immunoblotted using three antibodies detecting phosphorylated Tau residues; pS356, pT181 and pT205. One immunoreactive band was detected with each of the antibodies migrating at 65 kDa, consistent with full length 2N4R-Tau (**figure 3.4 A,** right hand blot, **arrow**). Immunoreactivity with the phospho-antibodies was abolished when cell pellets were pre-treated with CIP, thereby demonstrating the specificity of the signal (**figure 3.4 A,** right hand blot). Furthermore, when detected with the phospho-independent Tau12 antibody, the Tau cross-reactive species in the CIP treated lysates was more electrophoretically mobile than the untreated, phosphorylated form (**lower arrow** vs. **upper arrow, figure 3.4 A)**. Dephosphorylated Tau was 2.1±0.5 kDa smaller than phosphorylated Tau from 2N4Rc103 SH-SY5Y cells (**figure 3.4 B**), a significant decrease of 3±0.8% (**figure 3.4 C**, mean ± SEM, n=3, p=0.008). These findings showed that ectopically expressed Tau in 2N4Rc103 SH-SY5Y cells was phosphorylated and this contributed to the apparent molecular weight of ectopically expressed Tau.

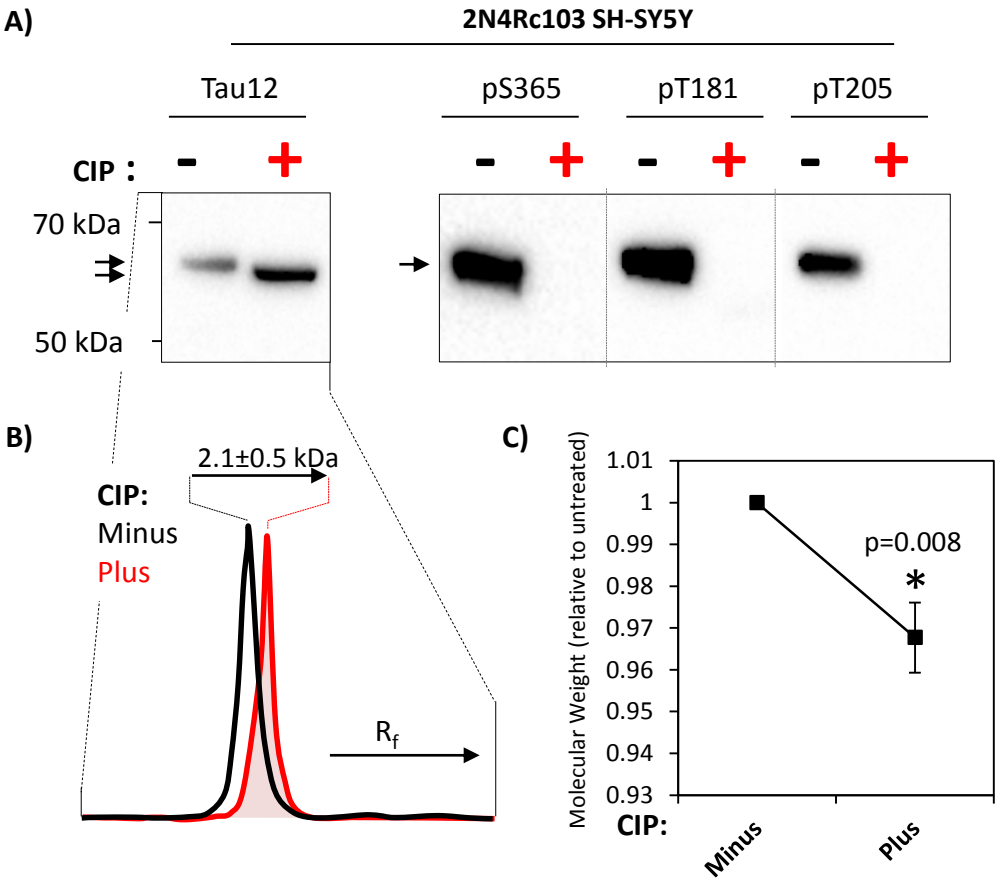

Figure 3.4 Analysis of Tau phosphorylation and impact on electrophoretic mobility. A) Western blot analysis of 2N4Rc103 cells treated with either protein phosphatase inhibitors or dephosphorylated with calf intestinal phosphatase (CIP). De-phosphorylated Tau and Tau Phosphorylated (at S365, T181 and T205) are indicated by the upper and lower arrows, respectively. **B)** Densitometric peaks of Tau12 reactive bands, with and without CIP treatment. **C)** Relative Molecular weights of Tau12 bands with and without CIP treatment were interpolated and normalised to untreated weight (mean ± SEM, n=4, paired Student's T-test used for statistical analysis).

3.2.6 Microtubule binding of endogenous and ectopic Tau in SH-SY5Y cells

Tau's most well defined physiological function is the stabilisation of microtubules; we therefore asked how ectopic Tau expression affected the microtubule network. Cytosolic (supernatant) and microtubular (pellets) fractions from normal and 2N4Rc103 SH-SY5Y cells were prepared by ultracentrifugation and analysed by immunoblotting (see **methods 1.23**). Tubulin was detected in the cytosolic and microtubular fractions of ultracentrifuged cells, representing monomeric and polymeric tubulin, respectively (**figure 3.5 A**). In normal SH-SY5Y cells, 28±5.3% of total tubulin was polymeric and in 2N4Rc103 SH-SY5Y cells, it was similar at 29.7±5.5% (mean ± SEM, n=3, **figure 3.5 B**) indicating that stable expression of WT-2N4R-Tau was not significantly affecting the polymerisation of tubulin. Moreover, ectopic Tau expression did not affect the levels of total tubulin in SH-SY5Y cells (**figure 3.5 C**). Endogenous SH-SY5Y Tau was detected in the cytosolic and microtubular fractions from ultracentrifuged cells, consistent with free and microtubular bound forms of Tau, respectively (**lower arrows, figure 3.5 A**). Tau12 cross reactivity (at 67 kDa) was also detected in the cytosolic and microtubular fractions from 2N4Rc103 SH-SY5Y cells (**upper arrows, figure 3.5 A**). As a percentage of total Tau levels, WT-2N4R-Tau was more associated with microtubular fractions than was endogenous SH-SY5Y Tau (**figure 3.5 D**, 34±9% vs 20±5%, mean ± SEM, n=3 for WT-2N4R, n=4 for SH-SY5Y) however this difference did not reach statistical significance.

Tau phosphorylated at T181 was detected in the cytosolic, but not microtubular fraction from 2N4Rc103 SH-SY5Y cells, (**figure 3.5 E**) consistent with phosphorylation disrupting Tau – microtubule interaction.

Overall these observations indicated that ectopic 2N4R-Tau expression did not significantly affect the tubulin monomer to polymer ratio in SH-SY5Y cells. Moreover, the association of endogenous and ectopic Tau with microtubules was similar in terms of proportionality.

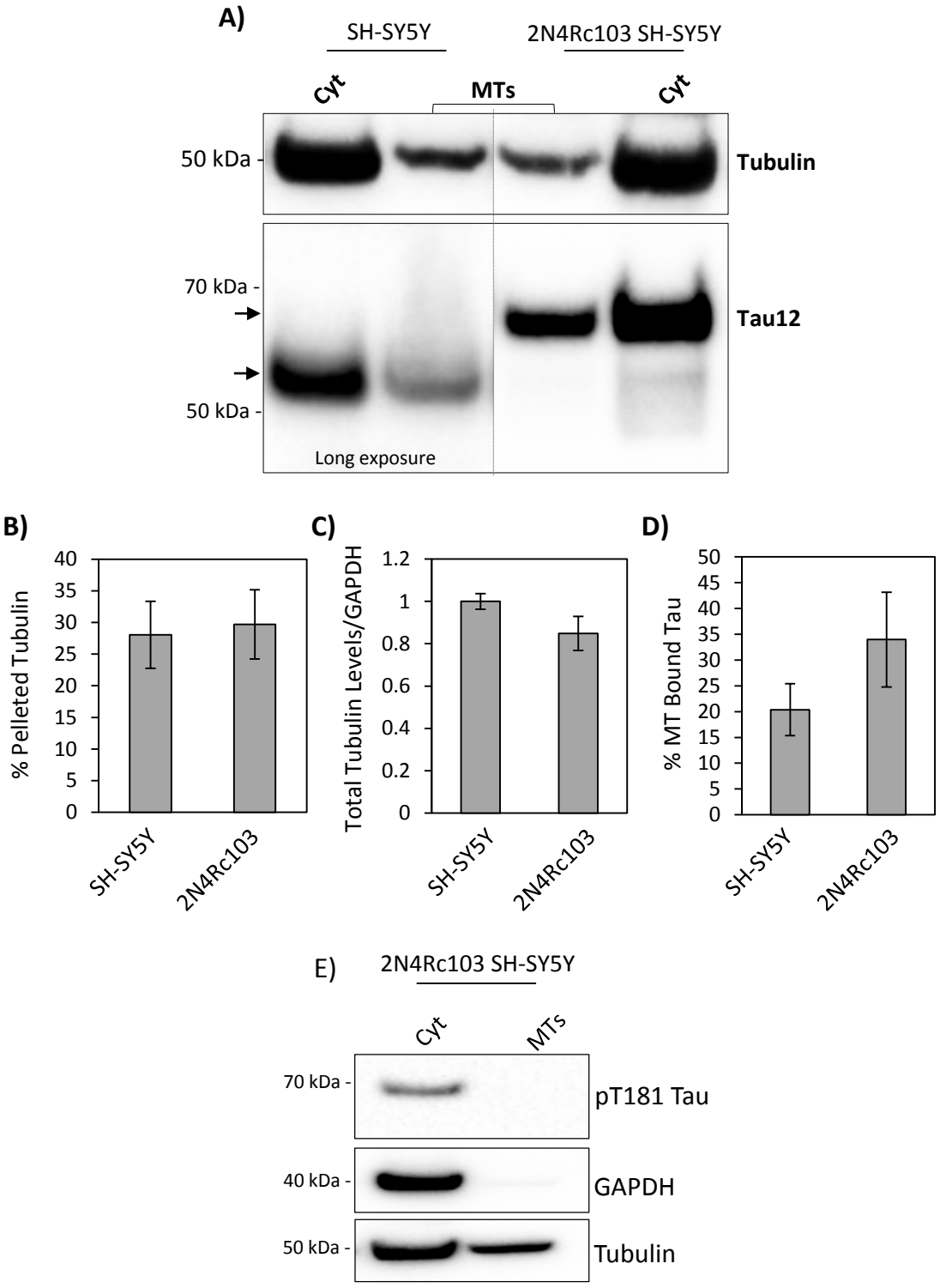

Figure 3.5 Analysis of tubulin polymers and microtubule associated Tau in normal and 2N4Rc103 SH-SY5Y cells. A) Western blotting analysis of cytosolic (Cyt) and microtubular (MTs) fractions isolated from normal and WT-2N4R-c103 SH-SY5Y cells by ultracentrifugation. Equal proportions of cytosolic and microtubular fractions were loaded. **B)** Total tubulin levels (i.e. cytosolic + microtubular) quantified from normal and WT-2N4R-c103 SH-SY5Y cells (normalised to normal). **C)** Percentage of pelleted tubulin from normal and WT-2N4R-c103 SH-SY5Y cells. **D)** Percentage of endogenous and ectopic Tau co-pelleting with microtubules (all quantitation n=3, except microtubule bound Tau from normal SH-SY5Y n=4, mean ± SEM; ('2N4Rc103' in graph labels refers to 2N4Rc103 SH-SY5Y clone). **E)** Western blotting of phosphorylated Tau (T181) in the cytosolic and microtubular fractions isolated from WT-2N4R-c103 SH-SY5Y cells.

3.2.7 Analysis of Tau expression in human brain

The Tau expression in normal and 2N4Rc103 SH-SY5Y cells and human hippocampi (from healthy, aged adults) was compared by western blotting. Samples were prepared for SDS-PAGE by solubilisation in 0.1% SDS followed by sonication. Human hippocampal samples demonstrated six Tau12 cross reactive bands, three of which migrated within the limits of the recombinant Tau ladder, with apparent molecular weights 59, 54, and 50 kDa (**red arrows, figure 3.6 A**) suggesting that they represented full-length Tau isoforms. Three lower bands were detected migrating at 42 kDa, and 39 kDa and 36 kDa (**purple arrows** and **black arrows,** respectively, **figure 3.6 A**). The major Tau12 cross reactive band from 2N4Rc103 cells was detected migrating at 63 kDa and a minor band was detected at 42 kDa, which therefore co-migrated with the 42 kDa band from the hippocampal lanes (**purple arrows, figure 3.6 A**). Normal SH-SY5Y lysates exhibited one Tau12 immunoreactive band, migrating at 53 kDa (**brown arrow, figure 3.6 A**).

There was a large variation in the levels of Tau in the hippocampal samples, which were 38±16 times higher than endogenous SH-SY5Y Tau levels when expressed relative to βiii Tubulin. However, there was no significant difference between the Tau levels in the 2N4Rc103 SH-SY5Y cells and the hippocampal samples (**figure 3.6 C**) suggesting that ectopic Tau expression in 2N4Rc103 SH-SY5Y cells was within physiological limits.

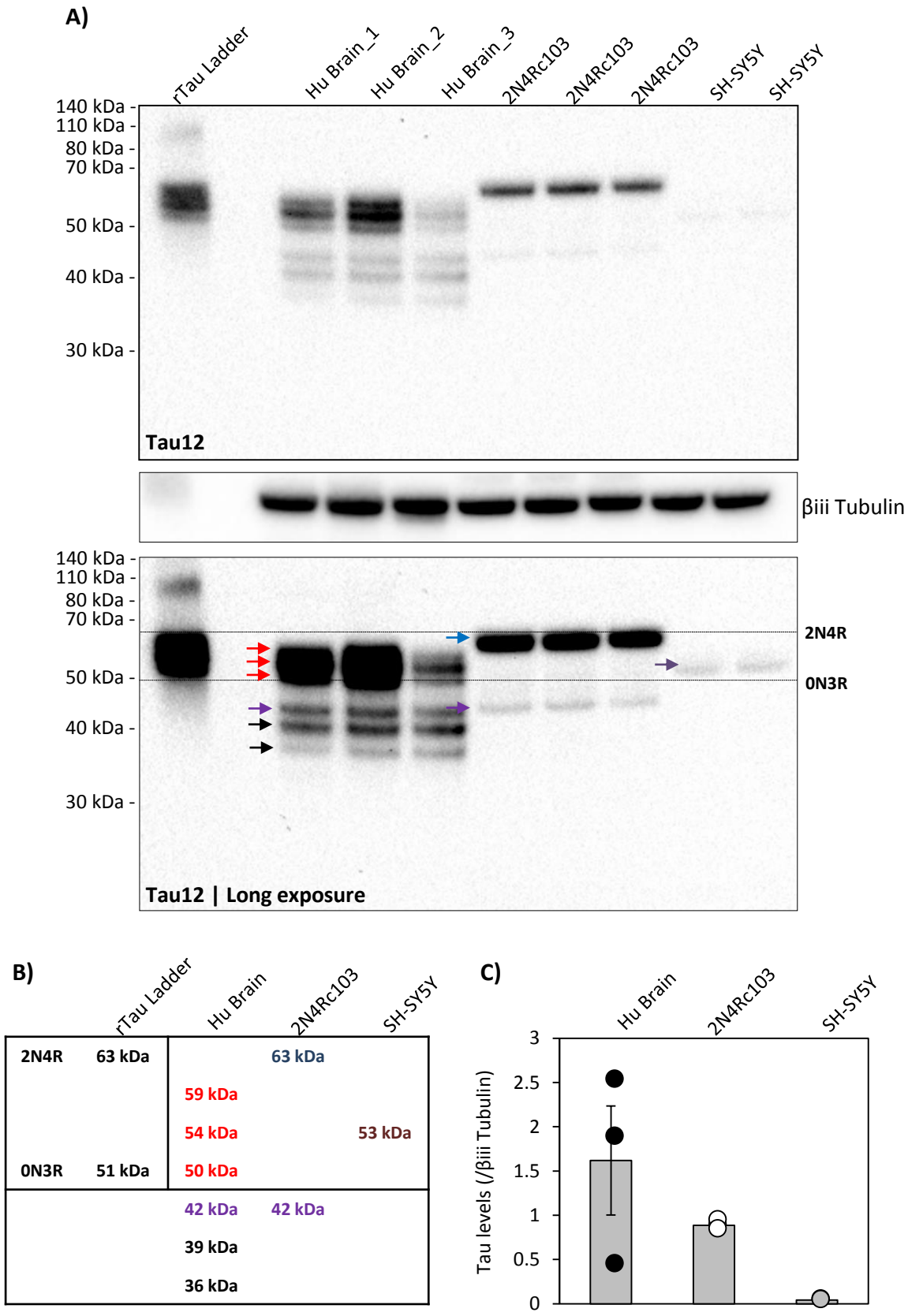

Figure 3.6 Comparison of Tau expression in human hippocampi, 2N4Rc103 and normal SH-SY5Y cells. A) Western blotting analysis of human hippocampi, WT-2N4R-c103 SH-SY5Y cells and normal SH-SY5Y cells with Tau12 and βiii Tubulin antibodies. Samples were solubilised in 0.1% SDS followed by sonication and 20 µg of protein was loaded / lane. Lower blot presents a longer exposure: Black dashed lines mark the upper and lower limits of the recombinant Tau ladder. Coloured arrows indicate Tau12 cross-reactive bands in the different samples. **B)** Interpolated molecular weights of the Tau bands in the different samples. The migration of 2N4R-Tau and 0N3R-Tau was determined from the recombinant Tau ladder. Text colour in the table corresponds with coloured arrows on the gel. **C)** Tau levels in the three samples (hippocampi n=3, normal SH-SY5Y n=2, and WT-2N4R-Tau c103 SH-SY5Y n=3) quantified relative to βiii Tubulin and normalised to normal SH-SY5Y levels (mean ± SEM).

3.3 Release of tau in exosomes from SH-SY5Y cells

3.3.1 Characterisation of exosomes isolated from SH-SY5Y cells

Exosomes were isolated from the 24 hour conditioned optiMEM from 10 x 10 cm of normal and 2N4Rc103 SH-SY5Y cells by differential ultracentrifugation (Thery et al. 2002; Quah & Neil. 2005). The enriched exosomes were subjected to nanoparticle tracking analysis (NTA) which revealed the exosome population to be enriched in vesicles ~100 nm in diameter. The mode vesicle size was 83.4±4.1 nm and the mean vesicle size was 130.9 ± 3.5 nm, a discrepancy indicating a positive skew – the population contained some larger vesicles with peaks at 200-300 and ~350 nm. These larger particles however represented a minority of the population (**figure 3.7A**). Tuneable resistive pulse sensing (TRPS) was also used to interrogate the size distribution of our exosome population. TRPS and nanosight analyses were in broad agreement, demonstrating enrichment of vesicles ~100 nm, although TRPS gave larger values for the particle mode (128 nm for normal SH-SY5Y and 117 for WT-2N4Rc103 SH-SY5Y cells) and mean (154 nm for normal SH-SY5Y and 152 nm for WT-2N4Rc103 SH-SY5Y cells) size than NTA (**figure 3.7 B** and **C**). Furthermore, the size distribution of the exosomal population isolated from the conditioned medium of normal and 2N4Rc103 SH-SY5Y cells were broadly similar (**purple** and **red distributions**, respectively, in **figure 3.7 B**). Overall, these results demonstrated the enrichment of vesicles, consistent in size with that of exosomes (see **Introduction 1.8.2**), from the conditioned optiMEM medium of SH-SY5Y cells.

Next, the expression of protein markers in the exosomal population was interrogated using western blotting, which demonstrated the detection of Alix (100 kDa), Tsg101 (50 kDa), CD-81 (21 kDa), Hsc70 (70 kDa) and Flotilin-1 (50 kDa) cross reactivity in the exosome pellet (**figure 3.7 D**), consistent with the presence of exosomes.

3.3.2 Presence of Tau in exosomes isolated from 2N4R-c103 SH-SY5Y cells

The enriched exosome pellets isolated from the 24 hour conditioned optiMEM of normal and 2N4Rc103 SH-SY5Y cells were subjected to SDS-PAGE and immunoblotted with Tau12 antibody. No specific Tau12 immunoreactivity was detected in the exosomes isolated from the conditioned optiMEM of normal SH-SY5Y cells (left lane, **figure 3.7 D**). A major Tau12 immunoreactive band migrating at 65 kDa and a minor band migrating at 55 kDa were however detected in the exosomes isolated from the conditioned optiMEM of 2N4Rc103 SH-SY5Y cells (**upper** and **lower arrows**, respectively, **figure 3.7 E**). These findings demonstrated that ectopically expressed Tau was released in exosomes from 2N4Rc103 SH-SY5Y cells.

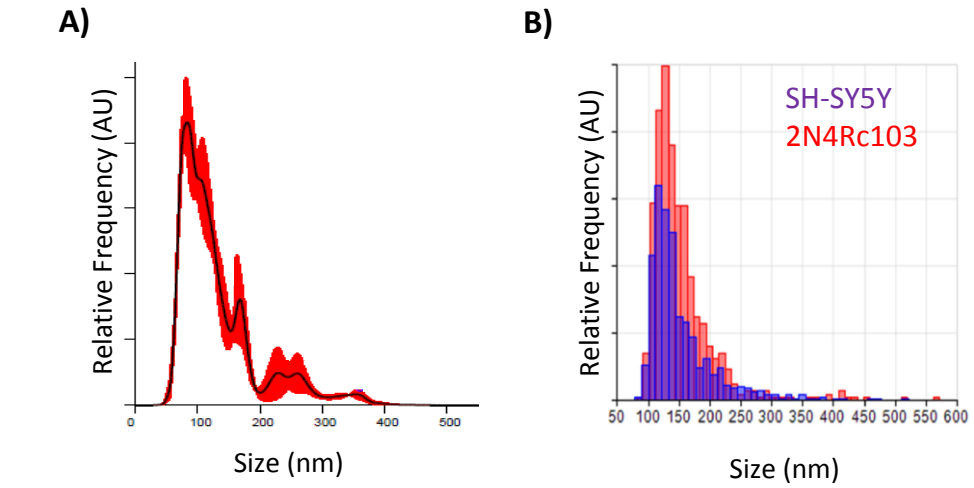

C)

Technology	Mode size	Mean size
Nanosight NTA	83±4 nm	131±6 nm
qNANO TRPS	117-128 nm	152-154 nm

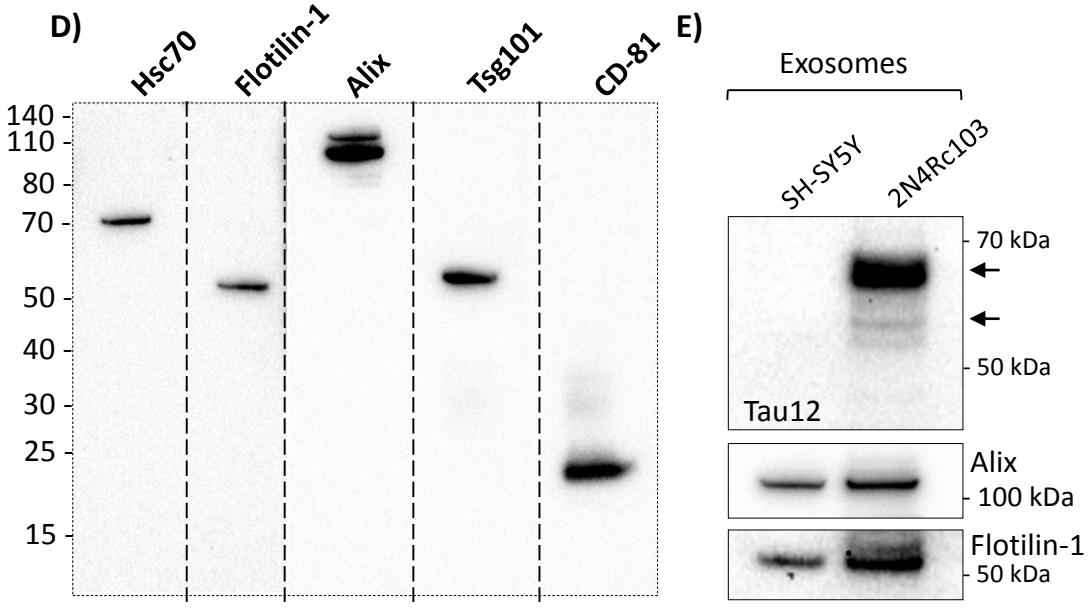

Figure 3.7 Characterisation of exosomes isolated from the conditioned medium (CM) of SH-SY5Y cells. Exosomes isolated from the 24 hour conditioned optiMEM of SH-SY5Y cells by differential ultracentrifugation were analysed by **A)** NTA Nanosight analysis (black line represents mean and red line standard deviation) and **B)** tuneable resistive pulse sensing analysis. **C)** Mode and mean particle sizes as assessed by these respective technologies. For qNANO TRPS the lower and higher values refer to the sizes of particles in the exosome populations from 2N4Rc103 and normal SH-SY5Y cells, respectively. **D)** Western blotting analysis of exosomes isolated from the 24 hour conditioned optiMEM of SH-SY5Y cells for the presence of specific protein markers (exosomes from 5 x 10 cm CM / lane loaded). **E)** Western blotting of exosomes isolated from normal and 2N4Rc103 SH-SY5Y cells with Tau12, Alix and flotilin-1 antibodies (exosomes from 10 x 10 cm CM / lane loaded). Arrows indicate Tau12 reactive bands.

3.3.3 Effects of optiMEM and prespun growth medium on exosomal Tau release

OptiMEM is a standard medium used to study exosomal release from cell cultures. However it is a reduced serum growth medium so we investigated if growth in these conditions was affecting the exosomal release of Tau from SH-SY5Y cells. In order to grow SH-SY5Y cells under normal conditions (i.e. 10% serum – FBS), DMEM F12 growth medium was supplemented with 10% FBS that had previously been ultracentrifuged at 100, 000 x g to remove co-sedimenting bovine particles (growth medium prepared in this way is hereon referred to a 'prespun medium'). Normal and 2N4Rc103 SH-SY5Y cells (80% confluent, 10 x 10 cm of each) were grown in optiMEM or prespun medium and exosomes were isolated from the 24 hour conditioned medium by differential ultracentrifugation and analysed for the presence of Tau.

No specific Tau12 cross-reactive bands were detectable in the exosomes isolated from the conditioned medium of normal SH-SY5Y cells, regardless of growth condition (Tau12 immunoblotting, **figure 3.8 A**). Two Tau12 cross reactive bands were detected in the exosomes isolated from the conditioned optiMEM of 2N4Rc103 SH-SY5Y cells, a major band of 65 kDa and a minor band of 55 kDa (**upper** and **lower arrows**, respectively, **'opti'** lane, **figure 3.8 A**). The same pattern of Tau12 cross-reactivity was detected in the exosomes isolated from the 24 hour conditioned medium of 2N4Rc103 SH-SY5Y cells cultured in prespun medium (**'prespun'** lane**, figure 3.8 A)**, demonstrating that exosomal Tau release was occurring under normal growth conditions, and in the same pattern as when cells were grown in optiMEM.

When normalised to the total cellular protein of the cultured cells from which the isolated exosomes were released (i.e. BCA on the cultured cells), exosomal Tau levels from 2N4Rc103 SH-SY5Y cells were 1.6±0.2 times higher in exosomes isolated from cells cultured in prespun medium compared to when cells were cultured in optiMEM (mean ± SEM, n=4, p=0.04, **figure 3.8 B**). When normalised to exosomal Alix levels, exosomal Tau levels were

significantly increased 3.3±0.4 times by growth in prespun medium compared to optiMEM (**figure 3.8 C**, mean ± SEM, n=5, *p*=0.0002). However, exosomal Alix levels were significantly reduced when cells were cultured in prespun medium, representing 0.4±0.06 times that of when cells were cultured in optiMEM (levels normalised to cellular BCA assay, mean ± SEM, n=6, $p=2.6x10^{6}$, **figure 3.8 B**) thereby potentially exaggerating the magnitude of the calculated Tau increase. Moreover, this suggested that growth in optiMEM medium may have affected the composition of exosomes released by cultured cells, consistent with recent reports (Liu et al. 2017).

Collectively these observations demonstrated that Tau was released in exosomes isolated from 2N4Rc103 SH-SY5Y cells grown under normal conditions, and that the qualitative pattern of exosomal Tau release was the same from cells cultured in optiMEM and prespun serum.

3.3.4 Effect of optiMEM on intracellular Tau levels and autophagy

Prolonged culture in optiMEM (>48 hours) affected cellular morphology (increased number and length of neurite projections), decreased cellular growth rate and reduced adherence (data not shown, anecdotal observations) so we investigated if 24 hour culture time (i.e. that used for exosome isolation experiments) affected intracellular Tau levels and / or starvation induced autophagy in 2N4Rc103 SH-SY5Y cells.Tau12 immunoblotting of cellular lysates indicated that intracellular Tau levels did not differ between cells grown in optiMEM or prespun medium for 24 hours (**figure 3.9 A** quantified in **figure 3.9 B**, prespun levels 0.84±0.2, mean ± SEM vs optiMEM grown cells, n=3). Total LC3 levels were also unaffected between growth conditions (**figure 3.9 C**) and LC3II did not accumulate under either condition, indicating that optiMEM did not induce cellular starvation (LC3II accumulated with 6 hour bafilomycin treatment, indicating the fidelity of detection in this system, **lower arrow, figure 3.9 A**). Growth in reduced serum medium (i.e. optiMEM) therefore did not affect cellular Tau levels or induce autophagy.

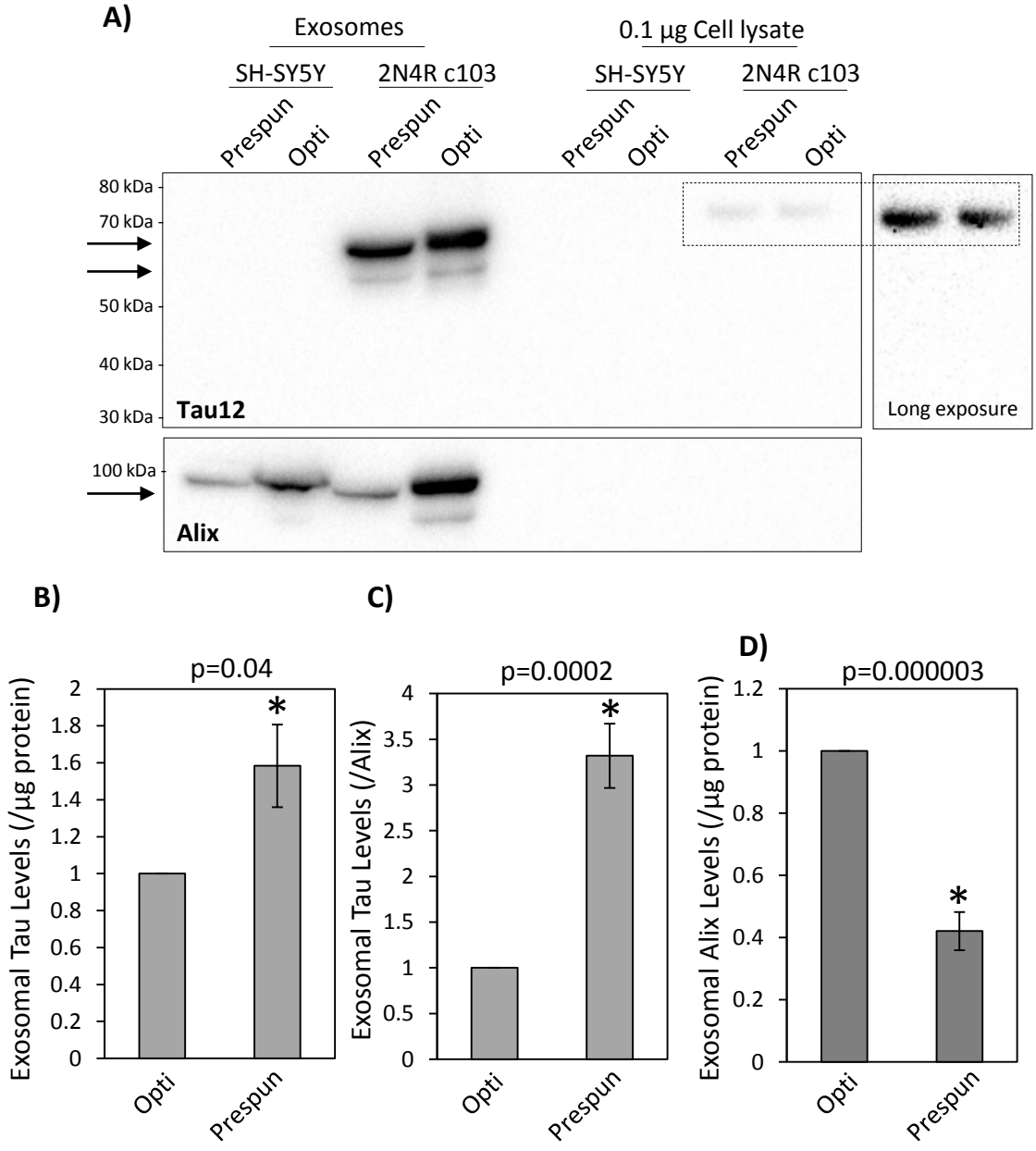

Figure 3.8 Analysis of the effects of growth medium on the exosomal release of Tau. A) Western blot analysis of the exosomes isolated from the 24 hour conditioned optiMEM ('Opti') and prespun ('Serum') medium (from 10 x 10 cm plates) from normal and WT-2N4R-c103 SH-SY5Y cells. 0.1 µg cellular lysate also loaded. **B)** Tau levels in exosomes isolated from conditioned optiMEM ('Opti') and prespun ('Serum') medium of WT-2N4R-c103 SH-SY5Y cells. Tau intensity expressed relative to cellular protein levels (n=4) and **C)** exosomal Alix levels (n=5) and normalised to 'optiMEM' condition (mean ± SEM, Student's T-test). **D)** Exosomal Alix levels from exosomes isolated from the conditioned medium of SH-SY5Y cells grown in optiMEM ('Opti') or prespun ('Serum') medium. Alix intensity expressed relative to cellular protein levels and normalised to 'optiMEM' condition (mean ± SEM, n=6, Student's T-test)

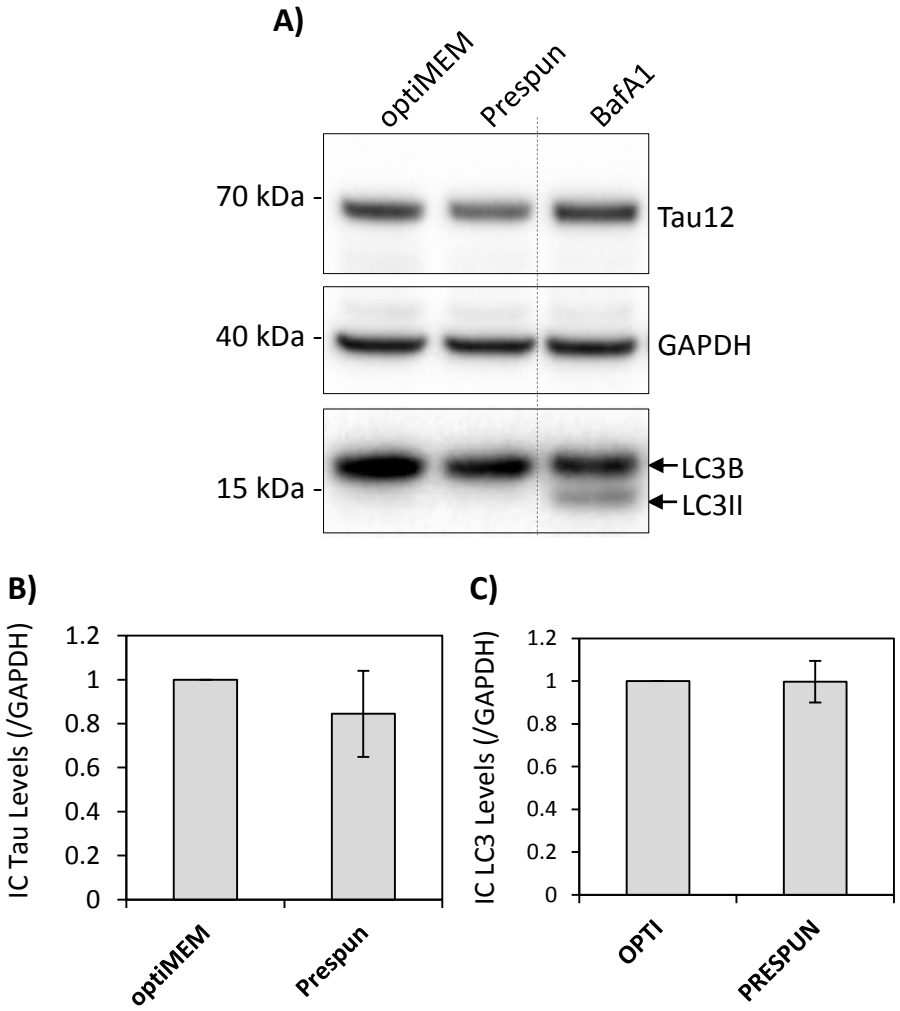

Figure 3.9 Effects of growth medium on intracellular Tau levels and autophagy induction. **A)** Western blot analysis of 2N4Rc103 SH-SY5Y cells grown in optiMEM (24 hours), prespun medium (24 hours) and treated with bafilomycin A1 (100 nM, 6 hours, in normal growth medium) with Tau12, GAPDH and LC3B antibodies. 20 µg protein loaded / lane **B)** Quantification of cellular Tau and **C)** LC3 levels from 2N4Rc103 SH-SY5Y cells grown in optiMEM or prespun medium. Band intensities expressed relative to GAPDH and normalised to 'optiMEM' condition (mean ± SEM, n=3, no significant differences observed, Student's T-test).

3.3.5 Analysis of the exosomal release of endogenous SH-SY5Y Tau

Endogenous Tau was not detectable in the exosomes isolated from the conditioned optiMEM from 10 x 10 cm plates of normal SH-SY5Y cells (~60 million cells, **figure 3.7 D**), regardless of growth in optiMEM or prespun medium (**figure 3.8 A**). In order to detect endogenous Tau, exosomes were isolated from the conditioned optiMEM of 45 x 10 cm plates (315 ml) of normal SH-SY5Y cells. The exosomal pellet was immunoprecipitated with DAKO-Tau and analysed by western blotting, in parallel the same analysis was performed on the exosomes isolated from the conditioned optiMEM of 5 x 10 cm plates (35 ml) of 2N4Rc103 SH-SY5Y cells, and 2 μg and 0.2 μg normal and 2N4Rc103 SH-SY5Y cell lysates, respectively.

Cellular and exosomal Tau from 2N4Rc103 SH-SY5Y cells was detected as major Tau12 cross reactive bands migrating at 68 kDa and 64 kDa, respectively (bands **A** and **A'**, **figure 3.10 A**). Additional minor Tau12 reactive bands were detected in the 2N4Rc103 cells and exosomes, migrating at 52 kDa and 54 kDa, respectively (bands **B** and **B'**, respectively, **figure 3.10 A**).

Endogenous Tau was IP'd from SH-SY5Y cell lysates as a 54 kDa Tau12 cross reactive protein (**band C, figure 3.10 A**). A 53 kDa Tau12 cross reactive band was also detected from the SH-SY5Y exosomes, the migration of which was commensurate with intracellular SH-SY5Y Tau. This demonstrated the exosomal release of endogenous SH-SY5Y Tau (**band C', figure 3.10 A**).

To confirm the relative quantities of exosomes analysed from normal and 2N4Rc103 SH-SY5Y cells, a fraction (corresponding to exosomes from 5 x 10 cm) of the exosomes was taken prior to IP and subjected to immunodetection with anti-Alix (**figure 3.10 C**). The relative exosomal release of endogenous and ectopic Tau from SH-SY5Y cells was calculated which demonstrated that exosomal Tau from 2N4Rc103 SH-SY5Y cells was 20 times greater than endogenous Tau (relative to Alix, n=1, **figure 3.10 D**). This was similar in magnitude to

difference between cellular endogenous Tau and ectopic 2N4R-Tau (21±0.7 times**, figure 3.6 C**). Overall these findings confirmed the exosomal release of endogenous SH-SY5Y Tau in proportion to cellular Tau levels.

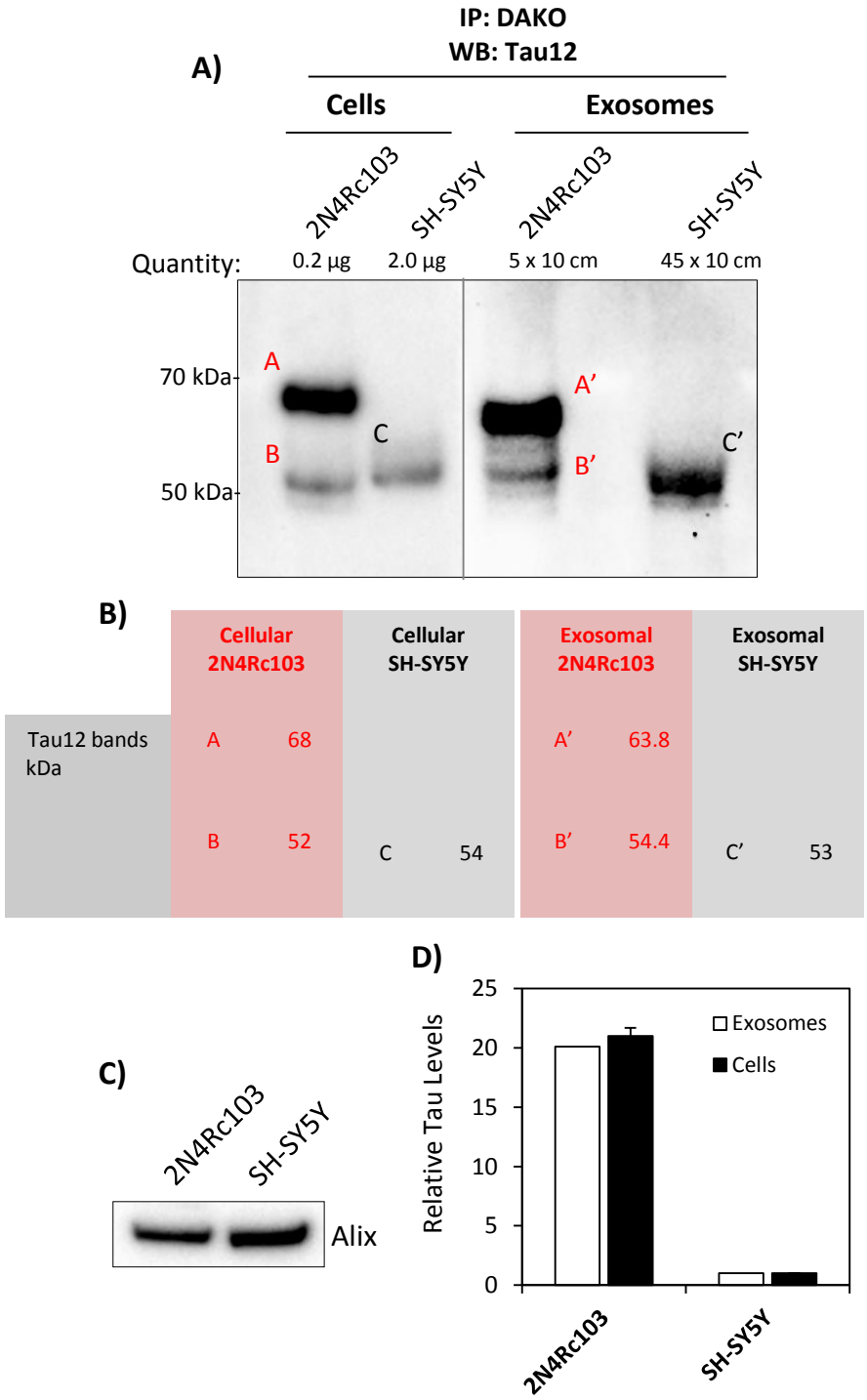

Figure 3.10 Analysis of the exosomal release of endogenous Tau from normal SH-SY5Y cells. A) Western blot analysis of the exosomes isolated from the 24 hour conditioned optiMEM from 2N4Rc103 (5 x 10 cm = 35 ml) and normal (45 x 10 cm = 315 ml) SH-SY5Y cells. Exosomes were lysed in 0.1% Tx100 and DAKO-Tau IP'd prior to SDS-PAGE. Cellular lysates from 2N4Rc103 (0.2 µg) and normal (2.0 µg) SH-SY5Y cells were also DAKO-Tau IP'd and analysed. **B)** Interpolated molecular weights of Tau12 reactive bands in the cellular and exosomal fractions from 2N4Rc103 and normal SH-SY5Y cells identified in **A)**. **C)** Alix immunoblotting of a fraction (corresponding to the exosomes from 5 x 10 cm) of the DAKO-Tau IP input material. **D)** Comparison of the relative amounts of cellular (black bars) and exosomal (white bars) Tau between normal and 2N4Rc103 SH-SY5Y cells. Exosomal Tau (n=1) expressed relative to exosomal Alix and cellular Tau (mean ± SEM, n=3) expressed relative to GAPDH levels, and normalised to levels from the respective normal SH-SY5Y fraction.

3.3.6 Analysis of extracellular and intracellular Tau12 reactive species

The above findings suggested a discrepancy between the molecular weights of intracellular and exosomal Tau12 cross reactive species from 2N4Rc103 SH-SY5Y cells (**figure 3.10 A** and **B**). To more closely examine this discrepancy, cellular lysates and exosomal fractions from 2N4Rc103 SH-SY5Y cells were loaded adjacently on SDS-PAGE. In addition to analysing the exosomes from the conditioned optiMEM of 2N4Rc103 SH-SY5Y cells, Tau present in the exosome supernatant was analysed following DAKO-Tau IP which represented non-pellet-able or 'free' extracellular Tau.

Major Tau12 cross reactive bands were detected in the cell lysates, free and exosomal fractions from 2N4Rc103 SH-SY5Y cells migrating at 65 kDa, and 62 kDa and 61 kDa, respectively (**black** – cellular, and **red** – extracellular, **arrows** and peaks, **figure 3.11 A**). Minor Tau12 reactive bands were also detected in cell lysates (50 kDa) and extracellular fractions (free – 50 kDa, exosomal – 55 kDa; **grey arrows, figure 3.11 A**). The extracellular major Tau12 reactive bands were more electrophoretically mobile than the major cellular Tau12 cross reactive band. Free Tau was 4±0.4 kDa smaller than cellular Tau (6±1.3% smaller, mean ± SEM, n=6 p=0.0001) whilst exosomal Tau was 3.4±0.5 kDa smaller than cellular Tau (5±1.3% smaller, mean ± SEM, n=6 p=0.001, **figure 3.11 B**).

Densitometric analysis, quantification and correction for loading demonstrated that exosomal Tau represented 1.2±0.5% of all extracellular Tau post 12k x g centrifugation (mean ± SEM, n=6, **figure 3.11 C**) released from 2N4Rc103 SH-SY5Y cells.

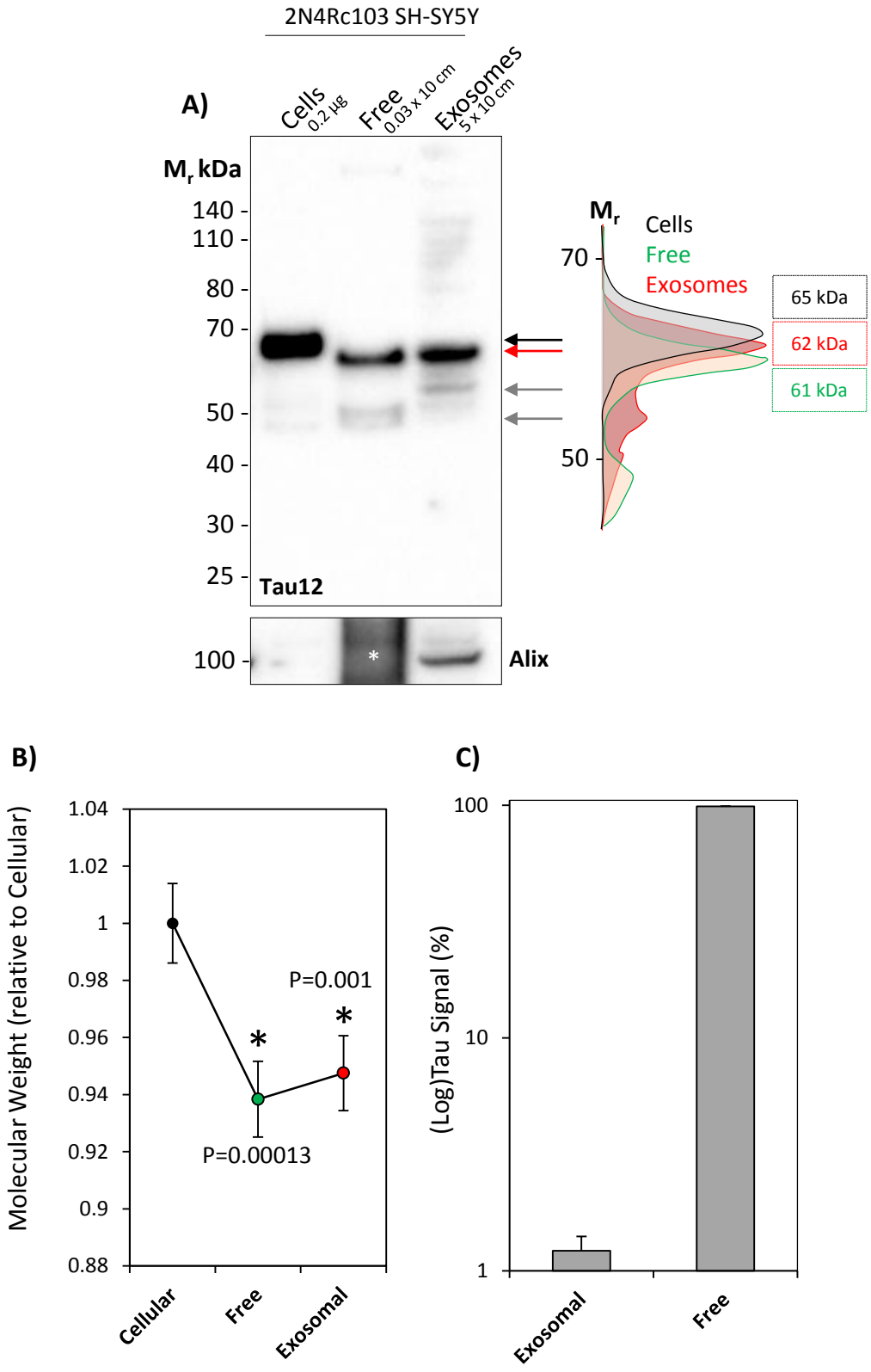

Figure 3.11 Analysis of the cellular and extracellular Tau12 cross reactive species from 2N4Rc103 SH-SY5Y cells. A) Tau12 western immunoblotting analysis of cell lysates (0.1 µg), Free (DAKO-Tau IP 0.3 x 10 cm, exosome supernatant), and Exosomal (5 x 10 cm exosomal pellet) Tau from 2N4Rc103 SH-SY5Y cells. Molecular weight size peak of Cellular (black), Free (green) and Exosomal (red) Tau are shown to the right. Alix immunoblot displayed beneath, white asterisks indicates IgG cross-reactivity from the immunoprecipitated conditioned medium. **B)** Interpolated molecular weights (kDa) of cytosolic, free and exosomal WT-2N4R-Tau from WT-2N4R-c103 SH-SY5Y cells normalised to cytosolic molecular weight (mean ± SEM, n=6). Student's T-test was used for statistical analysis. **C)** Quantification of distribution of Tau protein between the Exosomal and Free fractions, whereby 'Free' corresponds to Tau in the post-exosomal supernatant. Calculated by densitometry of Western blot analyses of free and exosomal fractions and correcting for volumes (mean ± SEM, n=6).

3.3.7 Analysis of exosomal Tau with N- and C-terminal antibodies

To investigate if extracellular Tau was full length (FL) we analysed extracellular fractions from 2N4Rc103 SH-SY5Y cells with Tau12 and Tau46 antibodies, directed to the N and C-termini respectively (epitope of Tau12 and immunogen of Tau46 displayed in **figure 3.12 A**). Initially, the sensitivity of these antibodies to detect Tau from 2N4Rc103 SH-SY5Y cells was established by immunoblot of titrated lysates. This revealed that Tau12 was approximately twice as sensitive as Tau46, these antibodies detecting Tau from 0.1 and 0.2 µg of 2N4Rc103 cell lysate, respectively (**red boxes, figure 3.12 A**).

Accordingly, Tau12 cross reactive bands were detected in 0.2 µg cellular lysate, exosome supernatant from 0.03 x 10 cm plates (IP'd with DAKO-Tau) and exosomes from the conditioned medium of 5 x 10 cm plates migrating at 67 kDa, 61 kDa and 62 kDa, respectively. This demonstrated the presence of N-terminally intact Tau in the respective fractions (**black** and **red arrows**, respectively, **figure 3.12 B**).

A Tau46 cross reactive band was detected in 0.52 µg of cellular lysate from 2N4Rc103 SH-SY5Y cells migrating at 67 kDa, confirming the cellular expression FL-Tau (**blue arrow**, **figure 3.12 B**). Extracellular fractions were loaded as to surpass the threshold of Tau46 sensitivity (free: 0.08 x 10 cm, IP DAKO-Tau; exosomal: 24 hour conditioned optiMEM from 13 x 10 cm plates) however neither free nor exosomal fractions demonstrated any detectable Tau46 cross reactivity, suggesting the absence of Tau46 cross reactive Tau species in the extracellular fractions of 2N4Rc103 SH-SY5Y cells. These observations are consistent with the suggestion that the majority of free and exosomal Tau species from 2N4Rc103 SH-SY5Y cells lacked a portion of the C-terminus which corresponded to the epitope of Tau46 (**figure 3.12 A**).

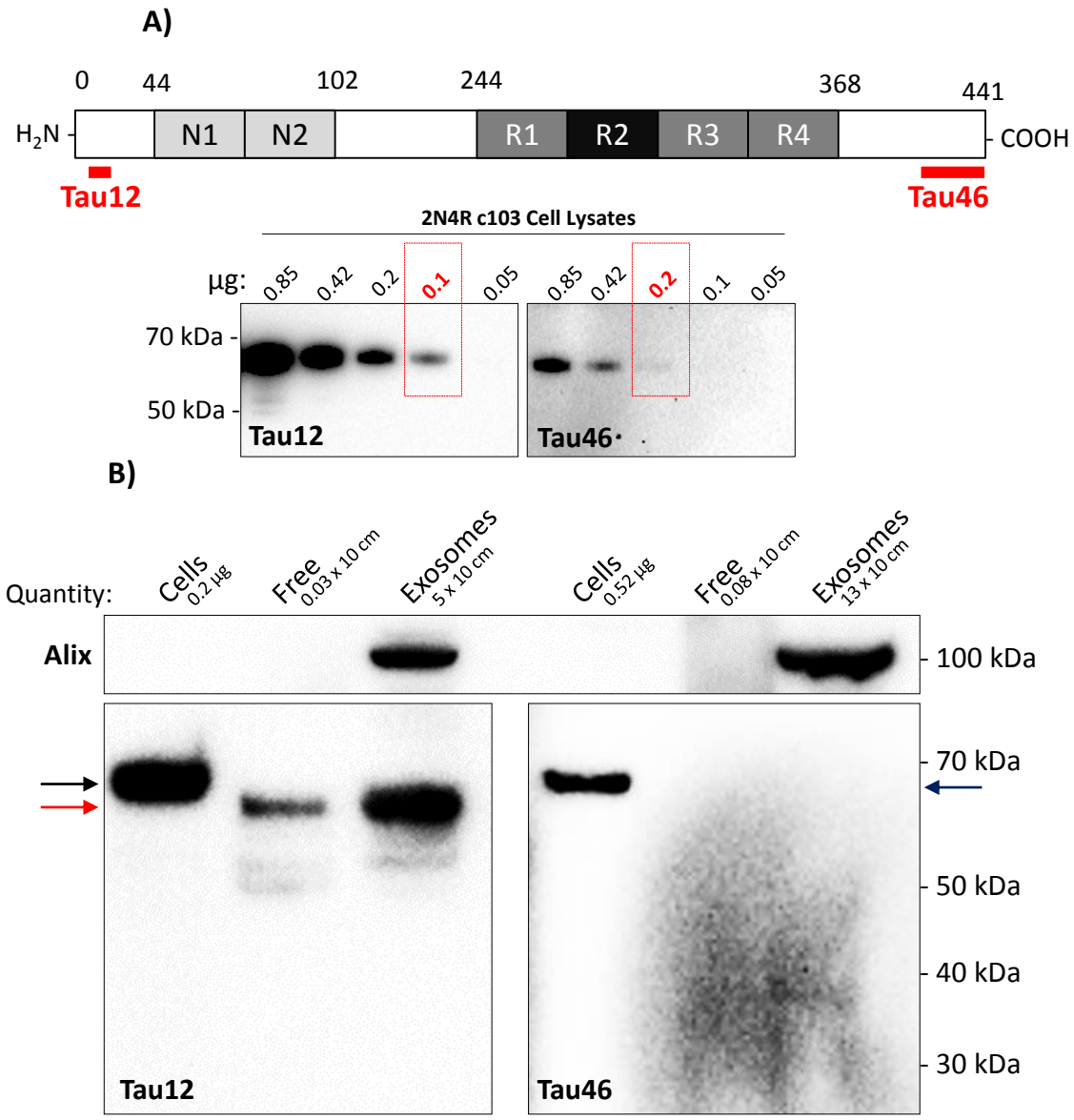

Figure 3.12 Analysis of the cross reactivity of intracellular and extracellular Tau species with N and C-terminal Tau antibodies. A) Schematic of Tau12 and Tau46 epitopes on 2N4R-Tau and determination of the sensitivity of these antibodies to detect Tau in 2N4Rc103 SH-SY5Y cell lysates. Lower limits of detection for the respective antibodies are indicated by the red boxes. **B)** Western blot analysis of cellular, free and exosomal fractions from 2N4Rc103 SH-SY5Y cells. 0.2 / 052 µg cellular lysate, DAKO-Tau IPed exosome supernatant from 0.03 / 0.08 x 10 cm plates and exosomes from 24 hour conditioned optiMEM from 5 / 13 x 10 cm plates cells were loaded in the Tau12 blot and Tau46 blot respectively. The major Tau12 reactive bands from cellular and extracellular (free and exosomal) fractions are indicated by the black and red arrows, respectively. Tau46 reactive band in the cellular fraction is indicated by the blue arrow.

3.3.8 Analysis of the association of Tau with the exosomal membrane

To analyse the location of exosomal associated Tau, exosomes isolated from 2N4Rc103 SH-SY5Y conditioned optiMEM were treated with protease K for increasing periods of time (1 µg / ml for 5, 10, 30 and 60 minutes, exosomes from 5 x 10 cm plates / reaction) under the assumption that intraluminal proteins would be protected from digestion (Cvjetkovic et al. 2016).

Western blotting of protease K treated exosomes demonstrated that after an initial decrease of signal of 40% over 5 minutes, exosomal Alix signal remained stable over the remaining 60 minutes of protease K treatment. Moreover, permeabilisation of exosomes by addition of Tx100 (final concentration 1%) to the protease K reaction caused a substantial drop in exosomal Alix levels consistent with the intra-luminal location of Alix protein (**figure 3.13 A**, quantified in **figure 5.13 B**).

Exosomal associated Tau signal underwent a similar pattern to Alix with protease K treatment; an initial decrease of 50% over 5 minutes was observe, which was followed by a relatively stable signal over 60 minutes that was nullified by vesicle permeabilisation with Tx100 (1% final concentration – **figure 3.13 A**, quantified in **figure 3.13 B**).

Next we studied the relative degradation rates of exosomal and free Tau by protease K digestion of the respective fractions (i.e. 5 x 10 cm exosomes from 24 hour conditioned optiMEM and 300 µl exosome supernatant). Exosomal Tau and Alix were resistant to protease K digestion, an effect nullified by Tx100 treatment (1% final concentration – **upper** and **lower arrows, respectively, figure 3.13 C**). Exosome supernatant Tau, however, was completely degraded by protease K over 5 minutes, consistent with its unprotected 'naked' location (**figure 3.13 C**).

These observations are consistent with exosomal Tau isolated from the conditioned medium of 2N4Rc103 SH-SY5Y cells being located intraluminally.

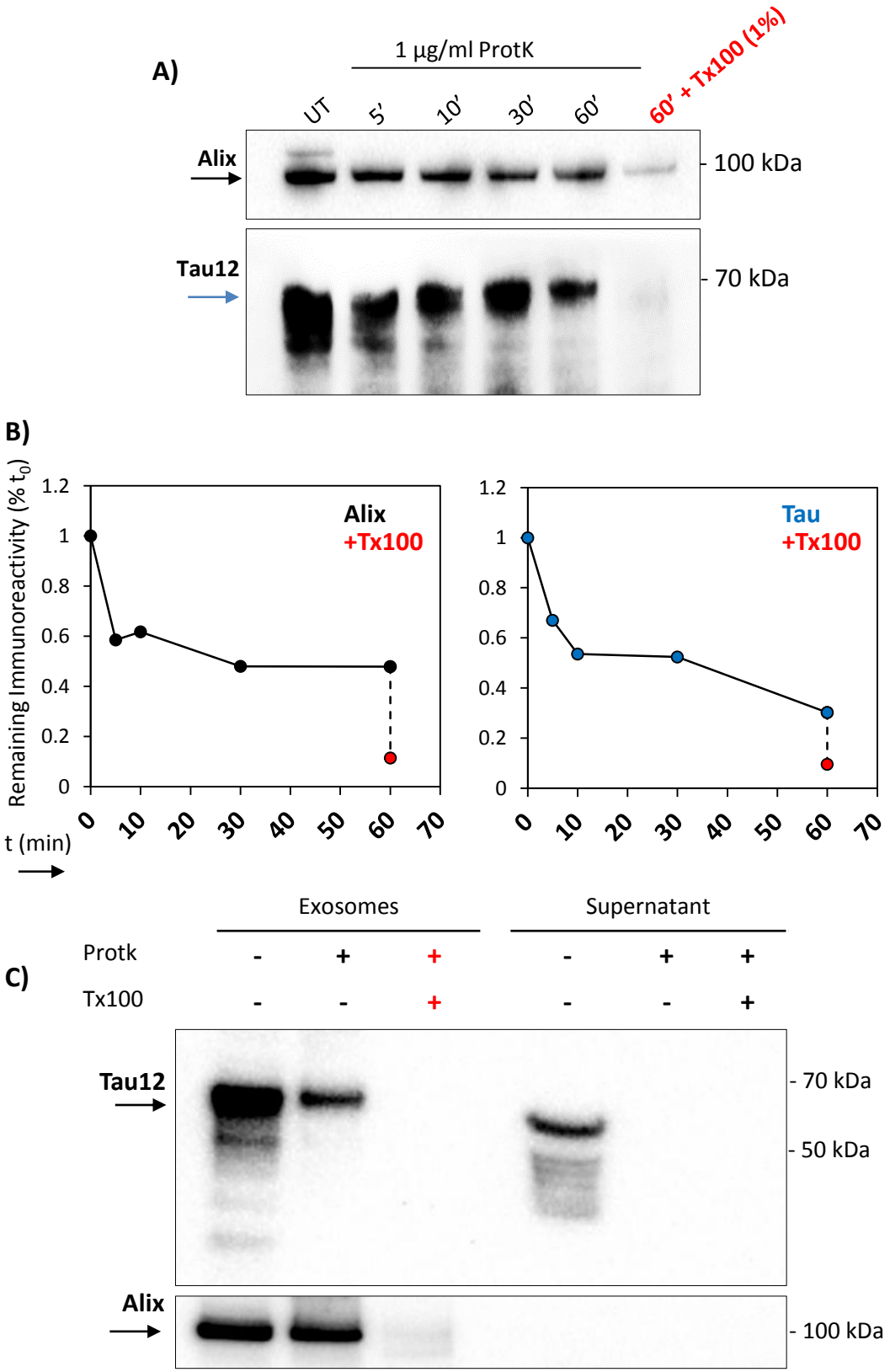

Figure 3.13 Analysis of the location of exosomal WT-2N4R-Tau. A) Western blot of WT-2N4R-c103 SH-SY5Y exosomes treated with protease K for increasing periods of time. Reactions which included Tx100 are indicated by the red box. Exosomes from 5 x 10 cm (24 hour conditioned optiMEM) were loaded / lane. **B)** Quantification of Alix (left) and Tau (right) levels with increasing time of protease K treatment, normalised to untreated value (n=1). Red circle data point represents treatment for 60 minutes in the presence of 1% Tx100. **C)** Western blot of Protease K treated exosomal and 'free' (exosomal supernatant Tau) fractions from WT-2N4R-c103 SH-SY5Y cells. Exosomes from 5 x 10 cm (24 hour conditioned optiMEM) and from 300 µl exosome supernatant (24 hour conditioned optiMEM) were loaded / lane.

3.3.9 Characterisation of SH-SY5Y clones stably expressing 0N3R and 2N3R-tau

We next sought to analyse the exosomal release of other Tau isoforms. Initially, SH-SY5Y clones with stable ectopic expression of 0N3R, HA-0N3R and 2N3R-Tau were analysed by immunostaining. 2N3R and 0N3R-Tau and HA-0N3R-Tau SH-SY5Y cells demonstrated DAKO-Tau and HA immunostaining, respectively, at exposure times when no evident staining was detected from normal SH-SY5Y cells (**figure 3.14 A,** % of cells with clear expression of ectopic Tau: 0N3R ≈ 60%, 2N3R ≈ 94%, 2N4Rc103 ≈ 67%, HA-0N3R = 100%). Staining was observed in the cytoplasm and neurites of cultured cells (**white arrowheads** and **arrows**, respectively, **figure 3.14 A**).

In order to confirm the sequence of inserted Tau cDNA in the respective clones, we isolated mRNA and performed reverse transcription followed by PCR to amplify ectopic Tau cDNA (see methods **figure 2.2** for agarose gel electrophoresis of PCR products). Sanger sequencing confirmed the correct sequence of 0N3R and HA-0N3R-Tau. 2N3R-Tau however exhibited a S383P mutation and an 18 amino acid C-terminal truncation. We factored these findings into downstream interpretations of these 2N3R-Tau SH-SY5Y cells.

Cell pellets of 0N3R, HA-0N3R, 2N3R and 2N4Rc103 SH-SY5Y cells were solubilised in 0.1% SDS, sonicated and analysed by Western blotting. Major Tau12 cross reactive species were detected from 0N3R and 2N3R SH-SY5Y cells migrating at 49 kDa and 57 kDa, respectively (**black** and **green arrows** respectively, **figure 3.14 Bi**). The same pattern of immunoreactivity was detected by DAKO-Tau immunoblotting (although DAKO-Tau also detected a minor band from 0N3R SH-SY5Y cells; **lower grey arrow, figure 3.14 Bii**) suggesting that 2N3R-Tau and 0N3R-Tau existed predominantly as single species when ectopically expressed in SH-SY5Y cells. (HA)-0N3R and 2N3R-Tau isoforms migrated anomalously in SDS-PAGE, with observed kDa's significantly larger than predicted kDa's as displayed in **table 3.1**.

Table 3.1 Predicted M_R of Tau isoforms and observed M_R when expressed in SH-SY5Y cells

Isoform	Predicted kDa	Published kDa	Observed kDa (n)
0N3R	37	48	49±1 (3)
(HA)-0N3R	38	n.a.	52 (2)
2N3R	43 (- 2 kDa)	62	57±0.7 (3)

The Tau12 immunoreactive band from HA-0N3R SH-SY5Y cells migrated ~2 kDa heavier than the Tau12 cross-reactive band from 0N3R-Tau SH-SY5Y cells, consistent with the presence of an N-terminal HA tag. The migration of 2N3R-Tau was slightly smaller than previous reports (57 vs 62 kDa – table 3.1) which may be due to the C-terminal truncation described above (18 amino acids ≈ 1.8 kDa) and electrophoresis conditions. Overall, therefore, these findings are consistent with previous reports (Guo et al. 2017; Goedert & Jakes. 1990) and suggested that the major Tau12 immunoreactive species in 0N3R, HA-0N3R and 2N3R-Tau SH-SY5Y cells to represent full length species of the respective isoforms.

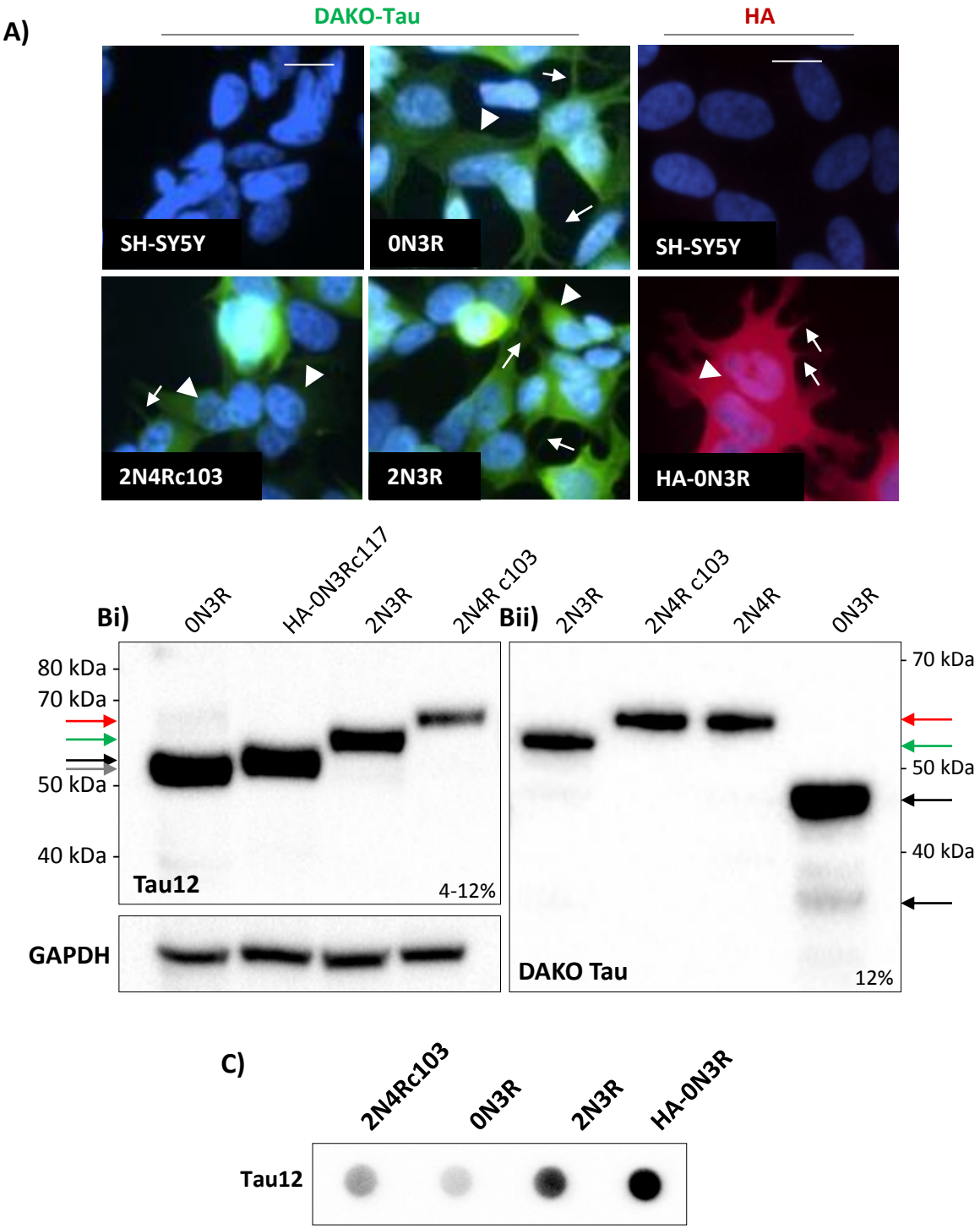

Figure 3.14 Characterisation of SH-SY5Y clones ectopically expressing 2N3R and 0N3R Tau isoforms. A) DAKO Tau and HA immunocytochemical analysis of SH-SY5Y with stable expression of 0N3R and 2N3R-Tau and HA-0N3R-Tau, respectively. Arrows and arrowheads indicate neuritic and cytoplasmic staining, respectively. Scale bars 10 µm **Bi)** Tau12 (left) and **Bii)** DAKO Tau (right) Western blotting of cellular lysates from SH-SY5Y cells with stable expression 0N3R, HA-0N3R (Tau12 only), 2N3R and 2N4R Tau (20 µg protein loaded / lane). **C)** Dot blot analysis of 24 hour conditioned optiMEM from SH-SY5Y clones expressing various Tau isoforms (1/10th - 200 µl – of conditioned medium from 1 well of a 6 well plate was loaded).

3.3.10 Analysis of exosomal Tau release from 0N3R-Tau and 2N3R-Tau SH-SY5Y cells

Exosomes were isolated from the 24 hour conditioned optiMEM (10 x 10 cm) from 0N3R and 2N3R SH-SY5Y cells and analysed by SDS-PAGE followed by Tau12 immunoblotting. Specific Tau12 immunoreactive bands were detected in the exosomes from all the clones (**figure 3.15 A**). Exosomal Tau from 2N3R-Tau SH-SY5Y cells was detected as one band at 56 kDa (**green arrow, figure 3.15 A**) and exosomal Tau from 0N3R-Tau SH-SY5Y cells was detected as two bands, a major band of 55 kDa and a minor band of 43 kDa (**black arrows, figure 3.15 A**).

These findings demonstrated that Tau was released in exosomes from SH-SY5Y cells expressing 0N3R and 2N3R-Tau, and that the migration of the exosomal Tau species were consistent with the ectopically expressed Tau isoforms. Levels of Tau12 immunoreactivity from 2N3R and HA-0N3R SH-SY5Y (not shown in blot, see **figure 3.16 A**) exosomes were similar to those from 2N4Rc103 SH-SY5Y, at 0.6±0.1 (mean ± SEM, n=2) and 0.8±0.1 (mean ± SEM, n=3) times respectively. 0N3R-Tau was exosomally released at 2±0.05 (mean ± SEM, n=2) times the release of WT-2N4R-Tau (all values normalised to cellular BCA, **figure 3.15 B**).

3.3.11 Detection of a non-specific exosomal protein with DAKO-Tau immunoblot

DAKO-Tau immunoblot of the lysates of SH-SY5Y cells expressing 2N3R, and 2N4R-Tau and 2N3R-Tau with a C-terminal GFP tag (see below, **3.3.13**, for full characterisation) detected major bands whose migration was consistent with full-length species of the respective isoforms (2N3R-GFP, 80 kDa; 2N3R, 57 kDa; 2N4R, 67 kDa; **asterisks** – **figure 3.15 A** and see above, **figure 3.14 Bii**). Moreover, endogenous Tau from SH-SY5Y cells was not detected at this exposure.

DAKO-Tau immunoblot of exosomes isolated from the conditioned optiMEM of the same cells, however, detected a single 70 kDa band in all samples. A co-migrating band of similar intensity was also detected in the exosomes isolated from the conditioned medium of

normal SH-SY5Y cells thus arguing against the identity of this band as Tau protein. These results demonstrated that DAKO-Tau detected a non-specific protein in the exosomes isolated from SH-SY5Y cells and therefore designated the use DAKO-Tau for western blot analysis of exosomal Tau release as unsuitable (**figure 3.15 D**).

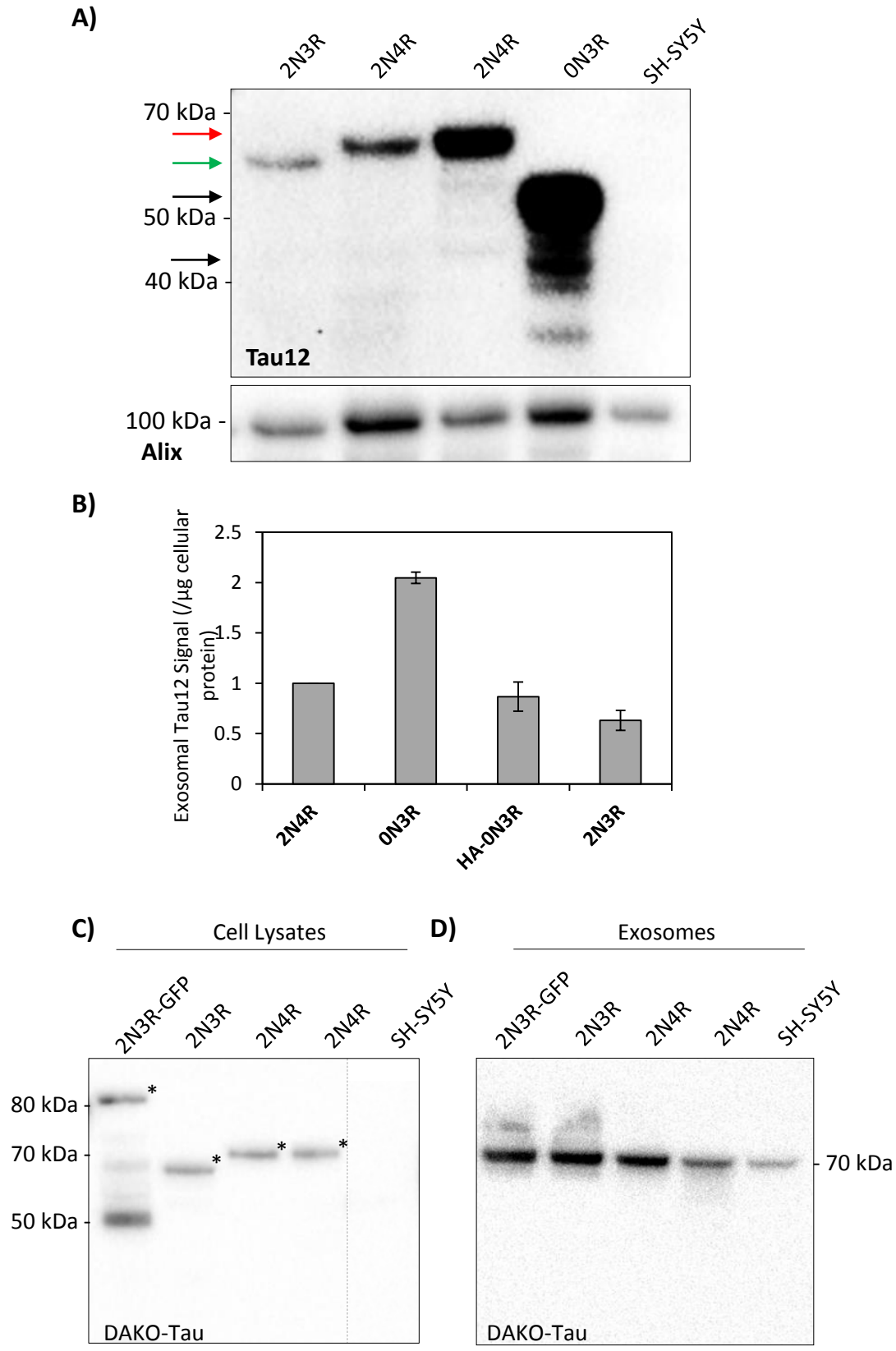

Figure 3.15 Analysis of exosomal Tau release from 0N3R, HA-0N3R and 2N3R Tau SH-SY5Y cells. A) Western blot analysis of exosomes isolated from the 24 hour conditioned optiMEM of SH-SY5Y clones with expression of 2N3R, 2N4R and 0N3R Tau (10 x 10 cm / lane). Arrows indicate major Tau12 reactive bands (red = 2N4R, green = 2N3R, black = 0N3R) **B)** Relative levels of major Tau12 reactive bands detected in the exosomes isolated from the 24 hour conditioned optiMEM from respective SH-SY5Y clones (values expressed relative to cellular protein levels and normalised to 2N4Rc103 levels, mean ± SEM, n=3 for 0N3R and 2N3R, n=2 for HA-0N3R). **C)** DAKO-Tau immunoblot of 20 µg cellular protein from the respective SH-SY5Y clones (same blot as figure 3.14 Bii, cropped differently) and **D)** of exosomes from the respective SH-SY5Y clones. Exosomes were isolated from the 24 hour conditioned optiMEM from 10 x 10 cm plates of each line. Arrow indicates a 70 kDa molecular weight band detected indiscriminately in the exosomes isolated from the conditioned medium of all cell lines.

3.3.12 Analysis of cellular and extracellular molecular weight profiles of Tau12 cross reactive species from 0N3R, HA-0N3R and 2N3R-Tau SH-SY5Y Cells

To compare the migration profiles of intracellular and extracellular Tau species, cell lysates (0.2 µg), exosome supernatant (DAKO-Tau IP'd exosome supernatant 24 hour conditioned optiMEM, 0.03 x 10 cm) and exosomes (5 x 10 cm, 24 hour conditioned optiMEM) from 0N3R, HA-0N3R, 2N3R and 2N4Rc103 SH-SY5Y cells were loaded adjacently on SDS-PAGE. As shown above (**figure 3.10, figure 3.11 and figure 3.12**) major Tau12 bands detected in extracellular fractions from 2N4Rc103 SH-SY5Y cells were more electrophoretically mobile than from cellular lysates (**figure 3.16 A** and **B**). Similarly, exosomal Tau from 2N3R-Tau SH-SY5Y cells was slightly more mobile than intracellular Tau on SDS-PAGE (**figure 3.16 A,** 57±1 kDa vs. 58±0.6 kDa, n=2**, figure 3.16 B**), however stably expressed 2N3R-Tau exhibited a C-terminal mutation (of 18 amino acids, described above) which must be considered when interpreting these results. Exosomal 0N3R and HA-0N3R Tau proteins migrated similarly to their intracellular counterparts (0N3R: 52.3 vs 52.9 kDa, cells vs exosomes**;** HA-0N3R: 54 vs 55 kDa, cells vs exosomes**, figure 3.16 A** and **B**). Tau12 reactive species were not detected from the DAKO-Tau IP'd exosome supernatant of 0N3R and HA-0N3R SH-SY5Y cells (**asterisks** – **figure 3.16 A**). However, direct Tau12 dot-blot of the 24 hour conditioned optiMEM demonstrated the presence of extracellular Tau12 reactive species from 0N3R and HA-0N3R-Tau SH-SY5Y cells (see above – **figure 3.14 C**). We cannot comment further on the identity of these species. Overall these results demonstrated that there were no significant size differences between cellular and exosomal Tau12 immunoreactive species from 0N3R, HA-0N3R and 2N3R-Tau SH-SY5Y cells.

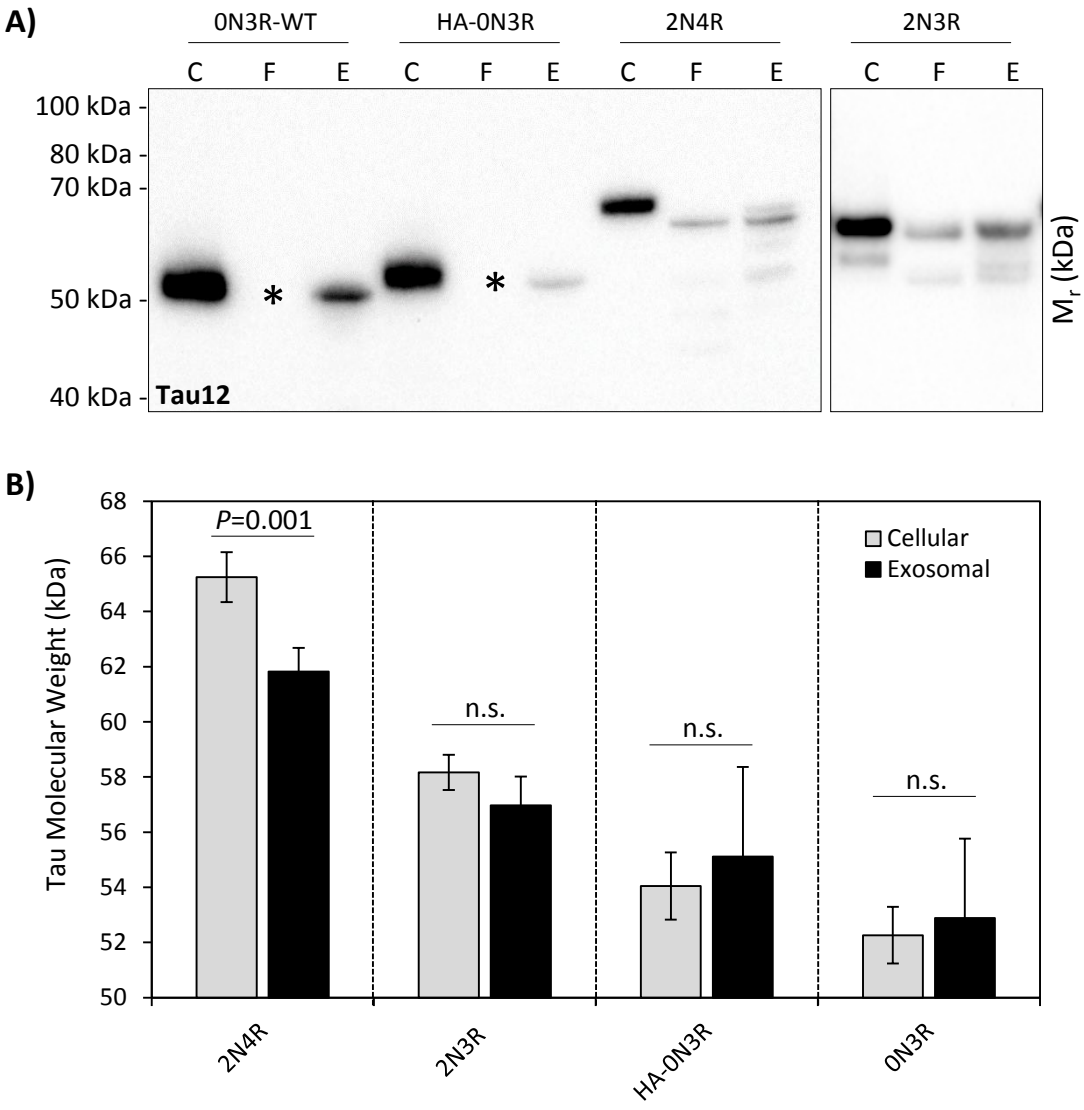

Figure 3.16 Analysis of molecular weight of cellular and extracellular Tau12 immunoreactive species from 0N3R, HA-0N3R and 2N3R-Tau SH-SY5Y cells. A) SDS-PAGE and Western blot analysis of adjacently loaded cellular ('C' – 0.2 µg), free ('F' – 0.03 x 10 cm exosome supernatant DAKO-Tau IP'd) and exosomal ('E' – 24 hour conditioned optiMEM, 5 x 10 cm) fractions from SH-SY5Y clones expressing the respective Tau isoforms. Asterisks indicate lack of Tau12 immunoreactivity in DAKO-Tau IP'd exosome supernatant from 0N3R and HA-0N3R SH-SY5Y cells. **B)** Interpolated molecular weights of major Tau12 reactive bands detected in the cellular and exosomal fractions of 0N3R (n=3), HA-0N3R (n=2) 2N3R (n=2) and 2N4Rc103 (n=6) SH-SY5Y cells (mean ± SEM, Student's T-test).

3.3.13 Characterisation of SH-SY5Y clones with ectopic expression of C-terminally GFP tagged tau isoforms

Next we analysed the exosomal release of Tau isoforms with C-terminal GFP tags. To characterise Tau expression, SH-SY5Y clones with ectopic expression of 0N3R-GFP, 0N4R-GFP, 2N3R-GFP and 2N4R-GFP were fixed and GFP fluorescence directly analysed by fluorescence microscopy. 2N4Rc103 SH-SY5Y cells displayed no direct GFP fluorescence whereas 0N3R-GFP, 0N4R-GFP, 2N3R-GFP and 2N4R-GFP cells had detectable levels of GFP fluorescence in the cytoplasm and neurites of analysed cells (**white arrowheads** and **white arrows,** respectively**, figure 3.17 A**) reflecting ectopic Tau-GFP expression. Rt-PCR of ectopically expressed Tau isoforms followed by Sanger sequencing demonstrated the correct sequence identity for 0N4R-GFP and 0N3R-GFP, whilst 2N3R-GFP exhibited a 36E>G mutation (see methods **figure 2.2** for agarose gel of rt-PCR products).

0N3R-GFP, 0N4R-GFP, 2N3R-GFP, 2N4R-GFP and 2N4Rc103 SH-SY5Y adherent cells growing in culture were lysed directly in 1% Tx100 with protease inhibitors, separated by SDS-PAGE and Tau-GFP expression was analysed by Western blotting with DAKO-Tau, Tau12 and GFP antibodies.

Numerous cross-reactive bands were detected from each SH-SY5Y clone. The highest molecular weight band from each clone was detected with DAKO-Tau, Tau12 and GFP antibodies (**green boxes, figure 3.17 B** and **C –** 2N4R-GFP with DAKO-Tau only). The molecular weight of this band was different for each isoform in a pattern consistent with the alternatively spliced regions. Thus, this band from 2N4R-GFP SH-SY5Y cells was 6 kDa heavier than that from 2N3R-GFP, which was in turn 8 kDa heavier than that from 0N4R-GFP. The 0N4R-GFP band was 3 kDa heavier than that from 0N3R-GFP. Furthermore, the molecular weight profiles of these bands were consistent with the molecular weights of the respective untagged Tau isoforms added to the calculated molecular weight of GFP (27

kDa). The molecular weight and cross-reactivity profiles of these bands therefore suggested they constituted the respective full length Tau-GFP isoforms, as summarised in **table 3.2**.

Table 3.2 Summary of hypothetical molecular weight profiles of full-length Tau and GFP constructs and Tau / GFP cross reactive bands detected from Tau-GFP SH-SY5Y cells

		Molecular Weight			
		0N3R-GFP	**0N4R-GFP**	**2N3R-GFP**	**2N4R-GFP**
Hypothetical	Untagged	48 kDa	52 kDa	62 kDa	67 kDa
	GFP	27 kDa	27 kDa	27 kDa	27 kDa
	Untagged + GFP	75 kDa	79 kDa	89 kDa	94 kDa
Detected	Tau12, DAKO-Tau, GFP	77 kDa	80 kDa	88 kDa	94 kDa

A band doublet was also detected from 0N3R-GFP, 0N4R-GFP, and 2N3R-GFP SH-SY5Y cells with DAKO-Tau and Tau12 antibodies, but not with GFP antibody (**black box, figure 3.17 B**). These bands also migrated consistent with the alternatively spliced regions of Tau. The lower band from this doublet ran close to the molecular weight for the corresponding untagged, full length forms of the respective proteins, whereas the upper band ran higher than this. This band doublet was also detected from 2N4R-GFP SH-SY5Y cells; the lower band of the doublet migrated commensurate with untagged 2N4R-Tau from 2N4Rc103 cell lysate (~68 kDa) which was loaded adjacently, whereas the upper band ran higher than this (~73 kDa; **black box, figure 3.17 C**). These findings suggested that the lower band of the doublet from the Tau-GFP SH-SY5Y clones corresponded to the respective untagged Tau isoforms (i.e. without the C-terminal GFP tag) and that the upper band represented the full-length Tau isoforms with some of the C-terminal GFP tag. These findings are summarised in **table 3.3**.

Table 3.3 Summary of molecular weight profiles of lower molecular weight Tau12 and DAKO-Tau cross reactive band doublets detected from Tau-GFP SH-SY5Y cells. The weights of the two bands are separated with a forward slash ('/').

		Molecular Weight (kDa)			
		0N3R-GFP	**0N4R-GFP**	**2N3R-GFP**	**2N4R-GFP**
Hypothetical	Untagged	48	52	62	67
Detected	Tau12, DAKO-Tau,	52 / 61	56 / 62	61 / 65	68 / 73

A protein band at 50 kDa cross reactive to DAKO-Tau and GFP antibodies was also detected (**red box, figure 3.17 Bi, Biii**). This band was not differentially mobile between the isoforms, and therefore most likely represented a form of Tau-GFP that was cleaved in the N-terminus of Tau, downstream of the second repeat and containing some or potentially all of the GFP Tag (schematically represented in **figure 3.17 E, red box).** A 30 kDa band cross reactive with only GFP antibody was detected in all the Tau-GFP clones that likely represented cleaved GFP (**blue box, figure 3.17 Biii,**). There were no major differences between the intracellular expression levels of each isoform (**figure 3.17 D**). A summary and interpretation of the Tau species detected in the Tau-GFP SH-SY5Y clones is displayed in **figure 3.17 E**.

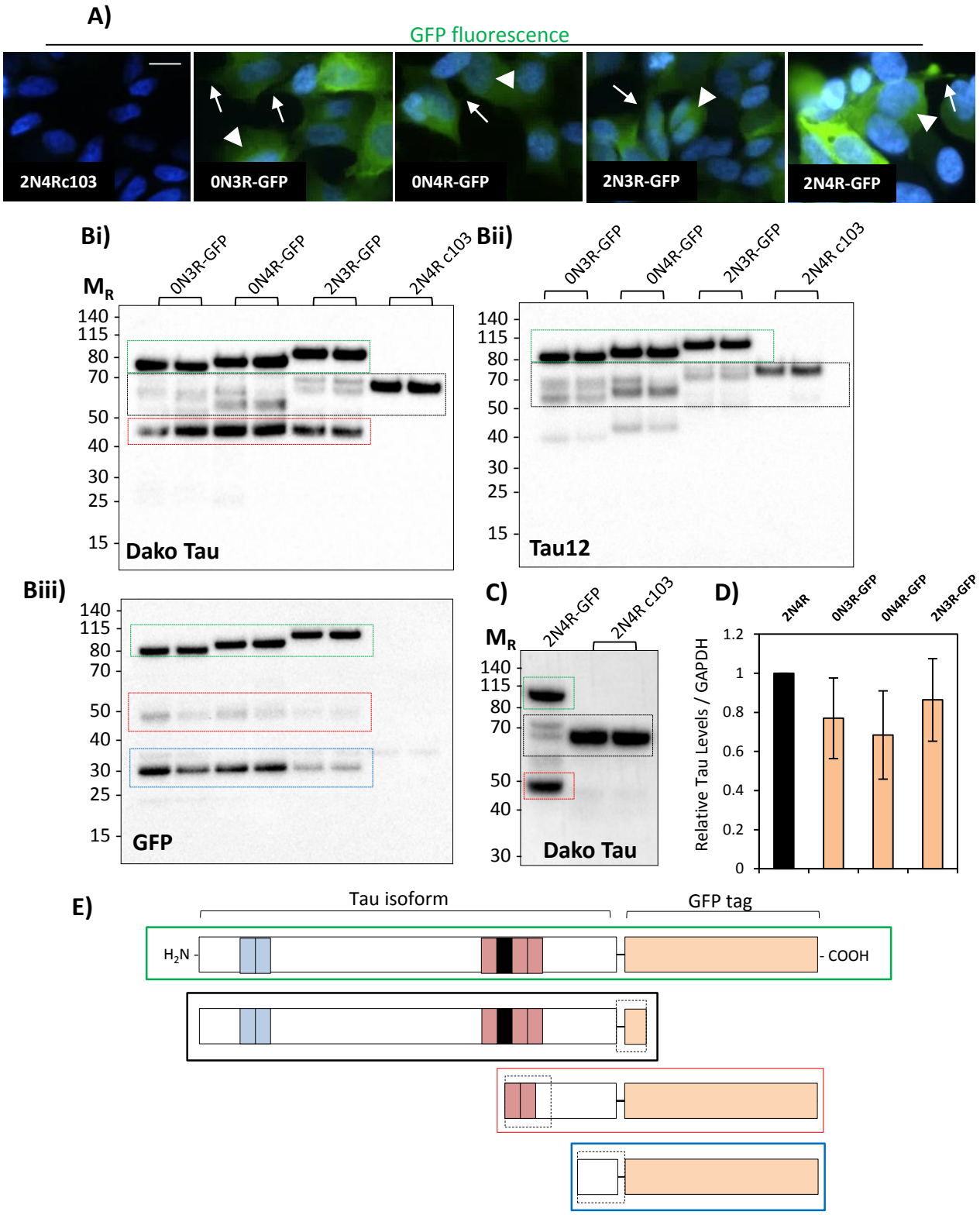

Figure 3.17 Characterisation of SH-SY5Y clones stably expressing C-terminal GFP tagged Tau constructs. A) Analysis of direct GFP fluorescence of PFA fixed SH-SY5Y clones expressing 0N3R-GFP, 2N3R-GFP, 0N4R-GFP and 2N4R-GFP Tau (2N4Rc103 negative control). White arrows and arrowheads indicate neuritic and cytoplasmic fluorescence, respectively. Scale bar 10 µm **B)** Western immunoblotting analysis SH-SY5Y clones (20 µg) stably expressing 0N3R-GFP, 0N4R-GFP and 2N3R-GFP with DAKO Tau **(i)**, Tau12 **(ii)** and GFP **(iii)** antibodies. Green boxes represent FL-Tau-GFP constructs, black boxes correspond to a C-terminally truncated Tau-GFP construct. Red box indicates an N-terminally cleaved Tau-GFP product and blue box represents cleaved GFP. Loading order in **(iii)** is as in **(i)**. **C)** DAKO-Tau Western blot of adjacently separated 2N4R-GFP and 2N4Rc103 SH-SY5Y cells. **D)** Levels of expression of Tau-GFP constructs quantified relative to GAPDH and normalised to 2N4Rc103 Tau expression levels. (Only top bad indicated by the green boxes was quantified; mean ± SEM, n=3-5). **E)** Schematic model of Tau-GFP processing in SH-SY5Y cells. Each diagram corresponds to a species detected in the cells by Western blotting, identified by the correspondence between the box colours enclosing the constructs. Black dashed boxes represent *regions* of cleavage, the precision of which was defined by the level of analysis.

3.3.14 Analysis of exosomal release of C-terminally GFP tagged tau isoforms

Exosomes were isolated by differential ultracentrifugation from the 24 hour conditioned optiMEM medium from 0N3R-GFP, 2N3R-GFP, 0N4R-GFP and 2N4R-GFP SH-SY5Y cells (5 x 10 cm plates / isolation) and loaded adjacently to their corresponding cellular lysates (0.2 µg) on SDS-PAGE.

Tau12 cross reactive species were detected in the exosomes isolated from 0N3R-GFP (**black arrow, figure 3.18 A**), 0N4R-GFP (**blue arrow, figure 3.18 A**), 2N3R-GFP (**red arrow, figure 3.18 A**) and 2N4R-GFP (**green arrow, figure 3.18 A**) SH-SY5Y cells. One major Tau band was detected in the exosomes from each SH-SY5Y clone (minor bands were also detected which are analysed in **figure 3.19**), all of which co-migrated with the corresponding cellular major Tau12 cross reactive band consistent with the full-length protein; 0N3R-GFP at 77 kDa, 0N4R-GFP at 79 kDa, 2N3R-GFP at 88 kDa and 2N4R-GFP at 94 kDa. This demonstrated that there were no differences in the molecular weights of the major cellular and exosomal Tau12 reactive bands from Tau-GFP SH-SY5Y clones (**figure 3.18 B**), unlike that observed for Tau species detected from 2N4Rc103 SH-SY5Y cells and exosomes.

It was noted however, that the C-terminally directed Tau46 antibody did not cross react with 0N3R-GFP, 0N4R-GFP, or 2N3R-GFP cellular lysates, but did cross react with 2N4Rc103 SH-SY5Y lysates (at 67 kDa – FL protein), suggesting a steric hindrance of Tau's C-terminal by the GFP tag (**figure 3.18 C**).

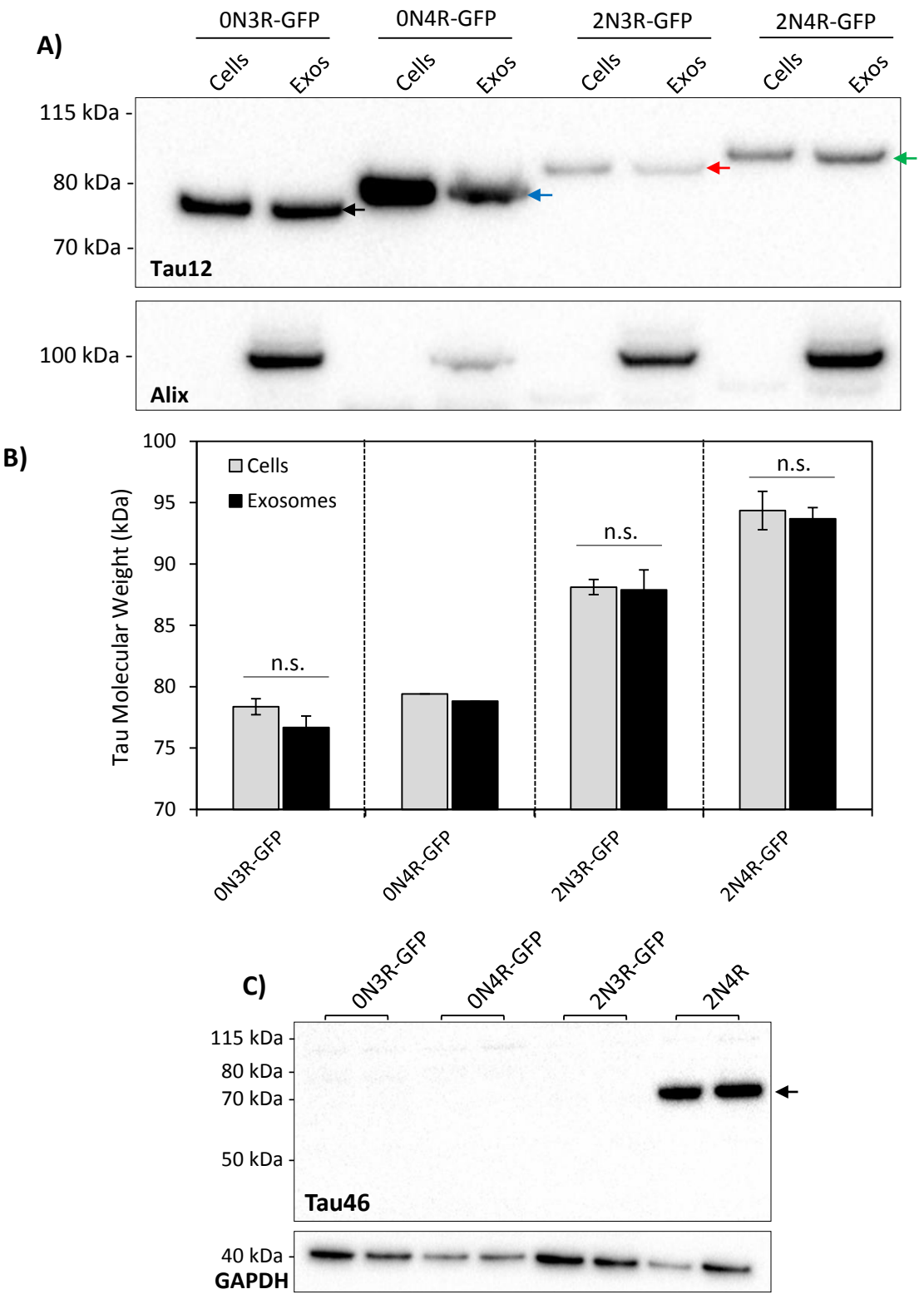

Figure 3.18 Analysis of exosomal release of C-terminally tagged GFP-Tau proteins from stably expressing SH-SY5Y cells. A) Western immunoblotting analysis of adjacently separated cellular (0.2 µg) and exosomal (24 hour conditioned optiMEM, 5 x 10 cm) fractions from SH-SY5Y cells with stable expression of C-terminally GFP tagged Tau proteins; Major Tau12 reactive species in the exosomes are indicated: 0N3R-GFP (black arrow), 0N4R-GFP (blue arrow), 2N3R-GFP (red arrow) and 2N4R-GFP (green arrow). **B)** Interpolated molecular weights of cellular and exosomal major Tau12 cross reactive proteins in the cell lysates (grey bars) and exosomes (black bars) from 0N3R-GFP (n=3), 0N4R-GFP (n=1), 2N3R-GFP (n=3) and 2N4R-GFP (n=2) SH-SY5Y cells. **C)** Western blotting of cell lysates of 0N3R-GFP, 2N3R-GFP, 0N4R-GFP and 2N4Rc103 (untagged, below) SH-SY5Y clones with Tau46 antibody (20 µg / lane).

3.3.15 Exosomal release of C-terminally cleaved 2N4R-GFP Tau species

We next aimed to investigate the minor Tau12 cross-reactive species released in the exosomes from 2N4R-GFP SH-SY5Y cells, and to compare them with those detected from 2N4Rc103 SH-SY5Y cells. Cellular (0.2 µg), free (220 µl, DAKO-Tau IP exosome supernatant) and exosomal (24 hour conditioned optiMEM, 5 x 10 cm) fractions from the respective SH-SY5Y clones were loaded adjacently on SDS-PAGE.

Tau12 cross-reactive species migrating consistent with the full length forms of 2N4R-GFP and 2N4R-Tau, at 96 kDa and 67 kDa, respectively, were detected in the cell lysates of the correspondent SH-SY5Y clones (bands '**A**' and '**B**', respectively, **figure 3.19 A**). As demonstrated previously (**figure 3.10 A, figure 3.11, figure 3.12**) extracellular Tau12 cross reactive species from 2N4Rc103 SH-SY5Y cells were smaller than the cellular Tau species, migrating at 62 kDa (band '**C**', **figure 3.19 A**). The major Tau12 cross reactive band detected in the exosomes from 2N4R-GFP SH-SY5Y conditioned medium was consistent with the full length protein, migrating at 96 kDa, this band was also detected in the exosome supernatant from these cells (band '**A**', **figure 3.19 A**).

Minor Tau12 cross-reactive species were also detected in the free and exosomal fractions from 2N4R-GFP SH-SY5Y cells, one of which was detected both in the cell lysates and exosomes and was migrating heavier than FL-2N4R-Tau at ~74 kDa and thus represented a species of Tau caused by cleavage within the GFP molecule (**asterisks, figure 3.19 A**).

The other minor exosomal Tau12 cross-reactive band, however, co-migrated with the major Tau12 cross reactive species detected in the extracellular fractions from 2N4Rc103 SH-SY5Y cells, at 62 kDa (band '**C**', **figure 3.19 A**). This band therefore represented a species of exosomal 2N4R-GFP Tau cleaved at the C-terminus of Tau and its co-migration with the exosomal Tau12 cross reactive band from 2N4Rc103 SH-SY5Y cells suggested a common mechanism of formation. Moreover, this band was not detected in the cell lysates of either

cell population which therefore demonstrated that the 62 kDa band represented an exclusively extracellular (exosomal and free) Tau species (band '**C**', **figure 3.19 B**).

3.3.16 Analysis of Exosomal Tau release from SH-SY5Y cells transiently expressing WT-2N4R-Tau

We next examined the exosomal release of Tau from SH-SY5Y transiently transfected WT-2N4R-Tau plasmid. DAKO-Tau immunostaining demonstrated ectopic Tau expression in 40% of cells transfected cells at 48 hours. Expression was detected in the cytoplasm and neurites of stained cells (**white arrowheads** and **white arrows**, respectively, **figure 3.20 A**). Transient ectopic Tau expression was also analysed by Western blotting, which demonstrated one Tau12 immunoreactive band co-migrating with stably expressed Tau in 2N4R-c103 SH-SY5Y cells, at 67 kDa (**black arrow**, **figure 3.20 B**), demonstrating expression of full-length ectopic 2N4R-Tau. Tau12 immunoreactivity from transiently transfected cells was calculated to be 40% as intense as that detected in stably expressing 2N4Rc103 SH-SY5Y cells, relative to GAPDH (**figure 3.20 B**).

For the final 24 hours of expression (48 hours total) transiently transfected cells were grown in optiMEM growth medium from which exosomes were isolated by differential ultracentrifugation. One Tau12 cross reactive band was detected in the exosomes from the conditioned medium of stably expressing 2N4R c103 SH-SY5Y cells, and a co-migrating Tau12 band was detected in the exosomes from transiently expressing SH-SY5Y cells (**red arrow, figure 3.20 C**). The exosomal Tau12 cross reactive band from transiently expressing SH-SY5Y cells was more smaller than Tau12 cross reactive band detected in the cells, migrating at 62 kDa (vs. 67 kDa) the same as that from 2N4Rc103 SH-SY5Y cells (**red arrow**, **figure 3.20 B**). Exosomal Tau levels from transiently expressing SH-SY5Y cells was 2.3 times greater than that from stably expressing cells when expressed relative to Alix levels, and 1.7 times greater when expressed relative to cellular protein levels (n=1, **figure 3.20 D**, Alix levels were roughly equal between stably and transiently expressing cells when expressed

relative to BCA, data not shown). We have studied exosomal Tau release from SH-SY5Y cells with transient Tau expression a number of times (see chapter 4), however the quantitative comparison with exosomal Tau release from stably expressing SH-SY5Y cells was performed only once, a caveat which must be considered when interpreting the above data.

3.3.17 Analysis of relationship between cellular protein expression levels and exosomal release

To directly investigate the relationship between the intracellular protein expression levels and exosomal release in the absence of an inducible Tau expression model, we took advantage of HEK293 cells with inducible (ponasterone A) HA-α-Synuclein (HA-Syn) expression. HA-Syn expression in HEK293 cells was induced for 48 hours with increasing concentrations of ponasterone A and cells were harvested, lysed and subjected to HA immunoblotting. HA immunoblot revealed one band on SDS-PAGE migrating at 17 kDa only when cells were treated with Ponasterone A, the migration of this band was consistent with HA-α-Synuclein (**black arrow, figure 3.21 A**). The intensity of this band increased in a concentration dependant manner with Ponasterone A concentration, and followed a linear relationship (r^2=0.98, **figure 3.21 B**).

No HA immunoreactivity was detected in exosomes isolated from the conditioned medium (optiMEM, 24 hours) of untreated HEK293 cells, or from those treated with 0.5 µM ponasterone A, despite detection in the cell lysates. HA immunoreactivity was faintly detected in the exosomes isolated from the conditioned medium from HEK cells induced with 1 µM ponasterone A and strongly detected in the exosomes from those treated with 2.5 µM ponasterone A (**red arrow, figure 3.21 A**, quantified in **figure 3.21 C**). A correlation analysis between intracellular levels of HA immunoreactivity in the cells and levels in the exosomes suggested that exosomal release occurred when intracellular levels reached a threshold (indicating a 'step function', **figure 3.21 D**).

A)

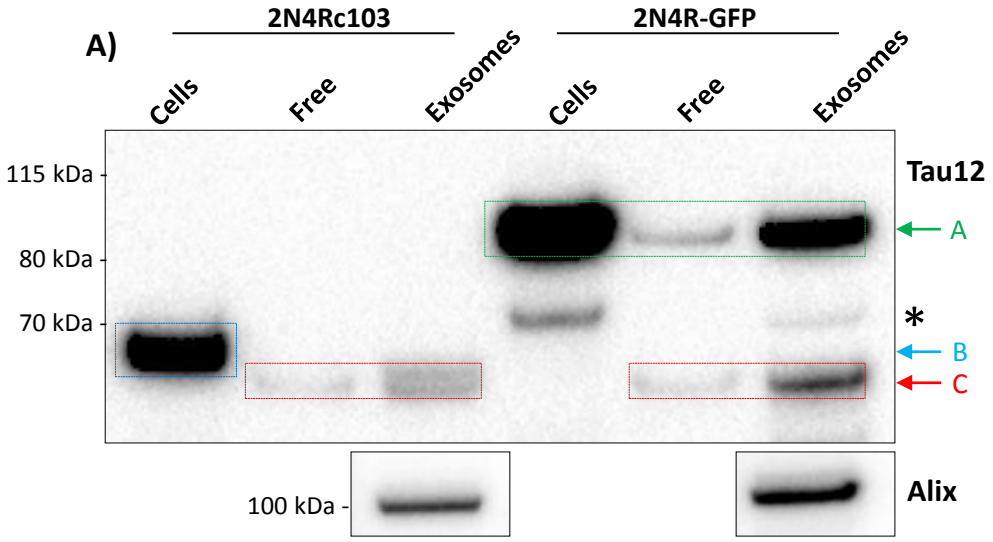

B)

	2N4Rc103			2N4R-GFP		
Band	**IC**	**Free**	**Exo**	**IC**	**Free**	**Exo**
A	n.a.			✓	✓	✓
B	✓	×	×	×	×	×
C	×	✓	✓	×	✓	✓

Figure 3.19 Comparative analysis of intracellular and extracellular Tau12 immunoreactive species from 2N4Rc103 and 2N4-GFP SH-SY5Y cells. A) Immunoblotting of cellular (0.2 µg), free (220 µl exosome supernatant, DAKO-Tau IP'd), and exosomal fractions (24 hour conditioned optiMEM from 5 x 10 cm) isolated from 2N4Rc103 and 2N4R-GFP SH-SY5Y cells. **B)** Analysis of the distribution of cellular, free and exosomal Tau species derived from 2N4Rc103 and 2N4R-GFP SH-SY5Y cells. Bands are those as identified in **A)**. Ticks and crosses represent the detection and lack of detection, respectively, of the identified band in each fraction (IC = intracellular, Exo = exosomal).

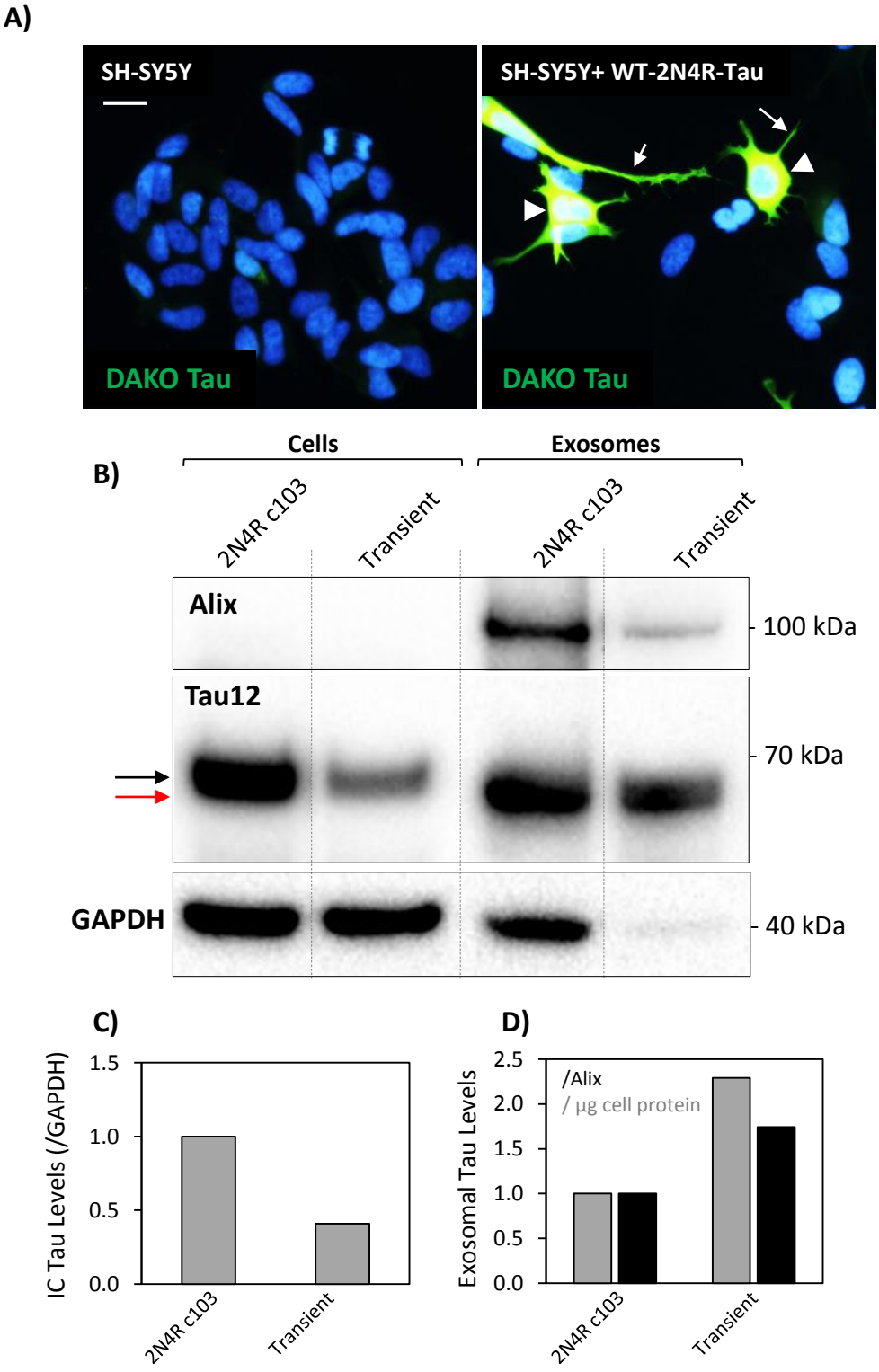

Figure 3.20 Comparison of exosomal Tau release from SH-SY5Y cells stably and transiently expressing WT-2N4R-Tau. A) DAKO-Tau immunocytochemical analysis of untransfected SH-SY5Y cells and SH-SY5Y cells electroporated with WT-2N4R-Tau plasmid and grown for 48 hours. Scale bar 10 µm. **B)** Western blotting analysis of cellular (10 µg) and exosomal fractions (24 hour conditioned optiMEM) isolated from SH-SY5Y cells with stable (5 x 10 cm) and transient (15 x 10^6 cells) WT-2N4R-Tau expression. Black and red arrows indicate major cellular and exosomal Tau12 reactive species, respectively. **C)** Quantification of levels of intracellular Tau12 reactive species in SH-SY5Y cells with stable (2N4Rc103) and transient expression of 2N4R-Tau (expressed relative to GAPDH and normalised to stable levels in 2N4Rc103 SH-SY5Y cells; n=1). **D)** Quantification of exosomal Tau levels isolated from the 24 hour conditioned medium of SH-SY5Y cells with stable (2N4Rc103) and transient 2N4R-Tau expression (expressed relative to Alix levels – grey bars – and cellular µg protein levels – white bars – and normalised to levels from 2N4Rc103 cells).

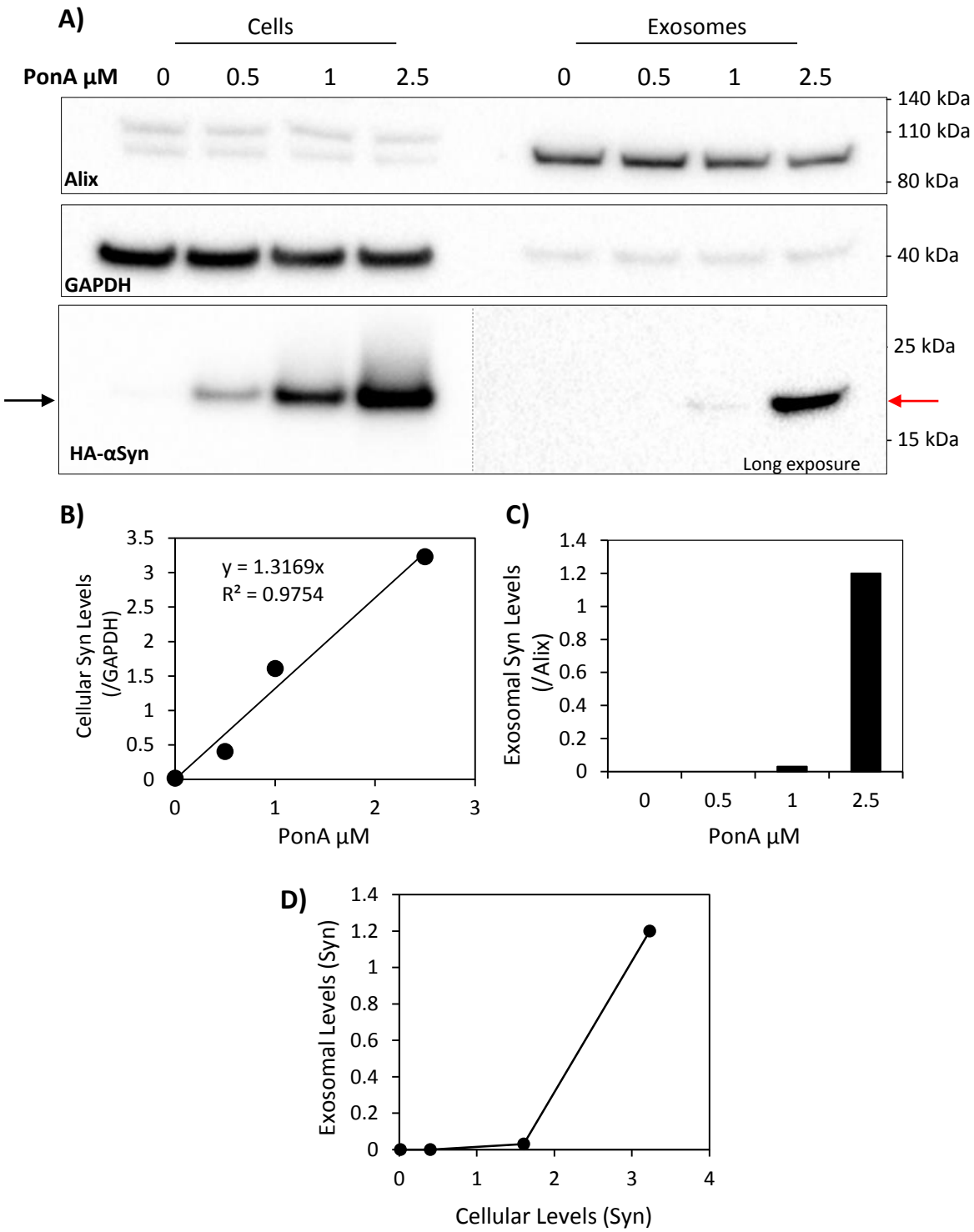

Figure 3.21 Analysis of exosomal alpha-synuclein release from HEK293 cells with inducible expression of alpha-synuclein. A) Western blotting analysis of cellular extracts (Tx100 extracts, 20 µg / lane; left side) and exosomes (24 hour conditioned optiMEM, 5 x 10 cm / lane; right side) from un-induced and induced HEK293 cells with inducible alpha-synuclein expression. Cells were induced with increasing concentrations of Ponasterone A for 48 hours and exosomes isolated during the last 24 hours of induction (in optiMEM). **B)** Correlation of Ponasterone A concentration used for induction with cellular alpha-synuclein expression levels (alpha-synuclein levels are expressed relative to GAPDH). **C)** Quantification of exosomal α-Synuclein levels (relative to Alix) isolated from the conditioned optiMEM of inducible HEK293 cells treated with increasing concentrations of Ponasterone A. **D)** Correlation of cellular alpha-synuclein levels (expressed relative to GAPDH) with exosomal alpha-synuclein levels (expressed relative to exosomal Alix).

4 Results 2: Analysis of factors affecting the exosomal release of Tau protein

4.1 Introduction and aims

The release of Tau protein in exosomes may be regulated by a number of factors. In this chapter we aimed to establish some of the key pathways that influence exosomal release of Tau protein from SH-SY5Y cell models.

The lysosomal and exosomal pathways share common components (Sahu et al. 2012) we thus aimed to assess the impact of lysosomal inhibition on exosomal Tau release.

The P301L mutation in Tau is known to cause frontotemporal dementia-Tau and other neurodegenerative Tauopathies (Hutton et al. 1999). We aimed to investigate how the P301L mutation affected the exosomal release of Tau.

The interaction of Tau and Hsc70 has been previously demonstrated; however the residues identified as important for this interaction have varied between published reports. Sarkar et al. (2008) identified residues within the hexapeptide motifs of Tau as central to Hsc70 interaction, whereas Wang et al. (2009) demonstrated a role of the consensus CMA motifs. In this chapter we aimed to establish the role of the CMA and hexapeptide motifs in the interaction of Tau and Hsc70 with the purpose of investigating how Tau – Hsc70 interaction affected the exosomal targeting of Tau. Hsc70 function is modulated by the concerted action of co-chaperones, such as DNAjC5. DNAjC5 has previously been shown to influence the free secretion of Tau protein (Fontaine et al. 2016) and the exosomal secretion of Huntingtin and SOD protein (Deng et al. 2017). We therefore aimed to investigate the effect of DNAjC5 on the exosomal release of Tau protein and how this was influenced by Tau – Hsc70 interaction.

SUMOylation has been identified as a post-translational modification that regulates the exosomal sorting of proteins, among them α-Synuclein protein (Kunadt et al. 2016). Tau

protein undergoes SUMOylation (Dorval & Fraser. 2006; Luo et al. 2014) and we therefore aimed to assess if SUMOylation played a role in the exosomal release of Tau protein.

Overall the aims for this chapter were:

1) Investigate the influence of the P301L mutation on the exosomal release of Tau
2) Determine the role of Tau – Hsc70 interaction in the exosomal targeting of Tau
3) Study how DNAjC5 affected the exosomal release of Tau protein
4) Investigate the role of Tau SUMOylation in its exosomal release

4.2 Effect of bafilomycin treatment on exosomal Tau release from SH-SY5Y cells

We next assessed the effects of bafilomycin treatment on exosomal Tau release. SH-SY5Y cells stably expressing WT-2N4R-Tau were grown in prespun medium ± 200 nM bafilomycin for 24 hours. Western blot analysis of cellular lysates from untreated 2N4Rc103 SH-SY5Y cells revealed a major Tau12 cross reactive band migrating at 67 kDa, consistent with full length 2N4R-Tau (**upper arrow, figure 4.1 A**). A minor band migrating at 57 kDa was also detected in untreated 2N4Rc103 SH-SY5Y cells (**lower arrow, figure 4.1 A**). Levels of the major band were unaffected by 24 hour bafilomycin treatment (**figure 4.1 B**) whereas the minor band at 57 kDa was undetectable with bafilomycin treatment, suggesting its formation to be dependent upon lysosomal function. The exosomes from the 24 hour conditioned media (prespun) of untreated and 200 nM bafilomycin A1 treated 2N4Rc103 SH-SY5Y cells were isolated by differential ultracentrifugation and analysed by Tau12 immunoblot. A Tau12 cross reactive band at 62 kDa was detected in the exosomes isolated from the conditioned media of untreated and bafilomycin treated cells (**arrow, figure 4.1 C**) consistent with exosomal release of 2N4R-Tau. Levels of this band were increased in the exosomes isolated from the conditioned medium of bafilomycin treated 2N4Rc103 SH-SY5Y cells by 4.1±0.7 times (mean ± SEM, n=3, p=0.014) and 9.5±0.7 times (mean ± SEM, n=3) when expressed relative to exosomal Alix levels and cellular protein content, respectively (figure **4.26 B** and **C**). Moreover, levels of the 88 kDa Tau12 cross reactive band detected in the exosomes isolated from 2N3R-GFP SH-SY5Y conditioned medium was increased by bafilomycin treatment (48 hours, 200 nM in normal medium for 24 hours and optiMEM for 24 hours) by 4.6 times compared to untreated (relative to Alix levels, **figure 4.26 B**). Collectively these results suggested that lysosomal compromise by bafilomycin treatment potentiated the exosomal release of Tau protein from SH-SY5Y cells.

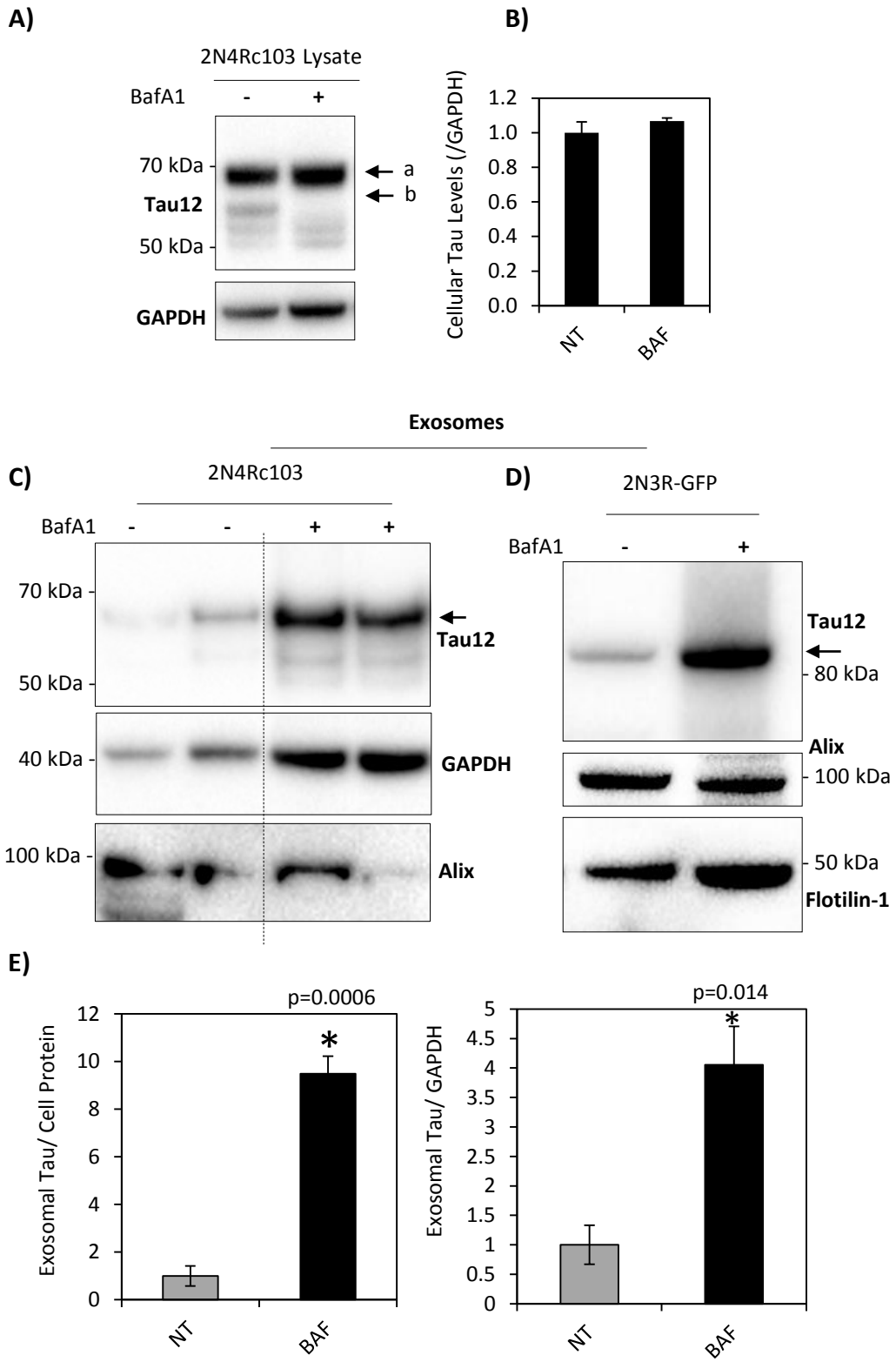

Figure 4.1 Effects of bafilomycin treatment on the exosomal Tau release from 2N4R-Tau and 2N3R-GFP-Tau SH-SY5Y cells. A) Western blot analysis of 2N4Rc103 SH-SY5Y cells untreated and treated with 200 nM bafilomycin A1 for 24 hours. Upper and lower arrows indicate major and minor Tau12 cross reactive bands, respectively. **B)** Quantification of the intensities of the major Tau12 cross reactive band from untreated and bafilomycin A1 treated 2N4Rc103 SH-SY5Y cells (200 nM, 24 hours). **C)** Western blotting analysis of exosomes isolated from 2N4Rc103 and **D)** 2N3R-GFP SHSY5Y cells untreated and treated with bafilomycin. Treatment was performed for 24 hours in prespun medium for 2N4Rc103 cells, and 48 hours in (24 hours in normal and 24 hours in optiMEM) for 2N3R-GFP cells. **E)** Quantification of exosomal Tau release from bafilomycin treated WT-2N4R-c103 SH-SY5Y cells. Values are expressed relative to cell protein (left graph) and exosomal GAPDH (right graph) and normalised to non-treated (NT) mean (mean ± SEM, n=3, Student's T-test).

4.3 Analysis of the exosomal release of P301L-Tau

4.3.1 Characterisation of SH-SY5Y cells stably expressing P301L-2N4R-Tau

We generated SH-SY5Y cells with stable expression of HA-P301L-2N4R-Tau (hereafter referred to as 'P301L-2N4R-Tau') by transfection of SH-SY5Y cells with the plasmid encoding for this Tau construct and selection of G418 resistant colonies.

HA immunocytochemical analysis of three of these clones revealed strong cytoplasmic and neurite immunoreactivity that was absent in normal SH-SY5Y cells (arrowheads and arrows, **figure 4.2 A**). Quantification of percentage of positive cells revealed P301L-2N4R-Tau clones c1, c2 and c8 as being 96%, 84% and 100% positive for HA immunoreactivity, respectively. Western blotting revealed two Tau12 cross reactive bands in the three P301L-2N4R-Tau SH-SY5Y clones: a major band migrating at 70 kDa and a minor band migrating at 50 kDa (**figure 4.2 A,** bands '**A'** and '**B**', respectively). The migration of the major band was marginally shifted upward relative to the major Tau12 cross reactive band from WT-2N4R-Tau SH-SY5Y cells (by 1 kDa) due to the N-terminal HA-tag. Moreover, HA immunoblot of P301-2N4R-Tau c2 SH-SY5Y cells also detected major and minor cross reactive bands migrating at 70 kDa and 50 kDa, respectively, which were therefore consistent with the Tau12 cross reactive species (bands '**A**' and '**B**' respectively, **figure 4.2 C**) and demonstrated the minor species to represent an N-terminal fragment of ectopically expressed P301L-2N4R-Tau. These findings also supported the interpretation that the major Tau12 and HA cross reactive band detected from P301L-2N4R-Tau SH-SY5Y clones (at 70 kDa) represented FL-P301L-2N4R-Tau. This band from P301L-2N4R-Tau SH-SY5Y cells was 1.43±0.15 times more intense than the major Tau12 band from WT-2N4R-Tau SH-SY5Y cells, when quantified relative to GAPDH, suggesting that P301L-2N4R-Tau was expressed at a higher level than WT-2N4R-Tau in SH-SY5Y cells (mean ± SEM, n=3, p=0.02, **figure 4.2 D**).

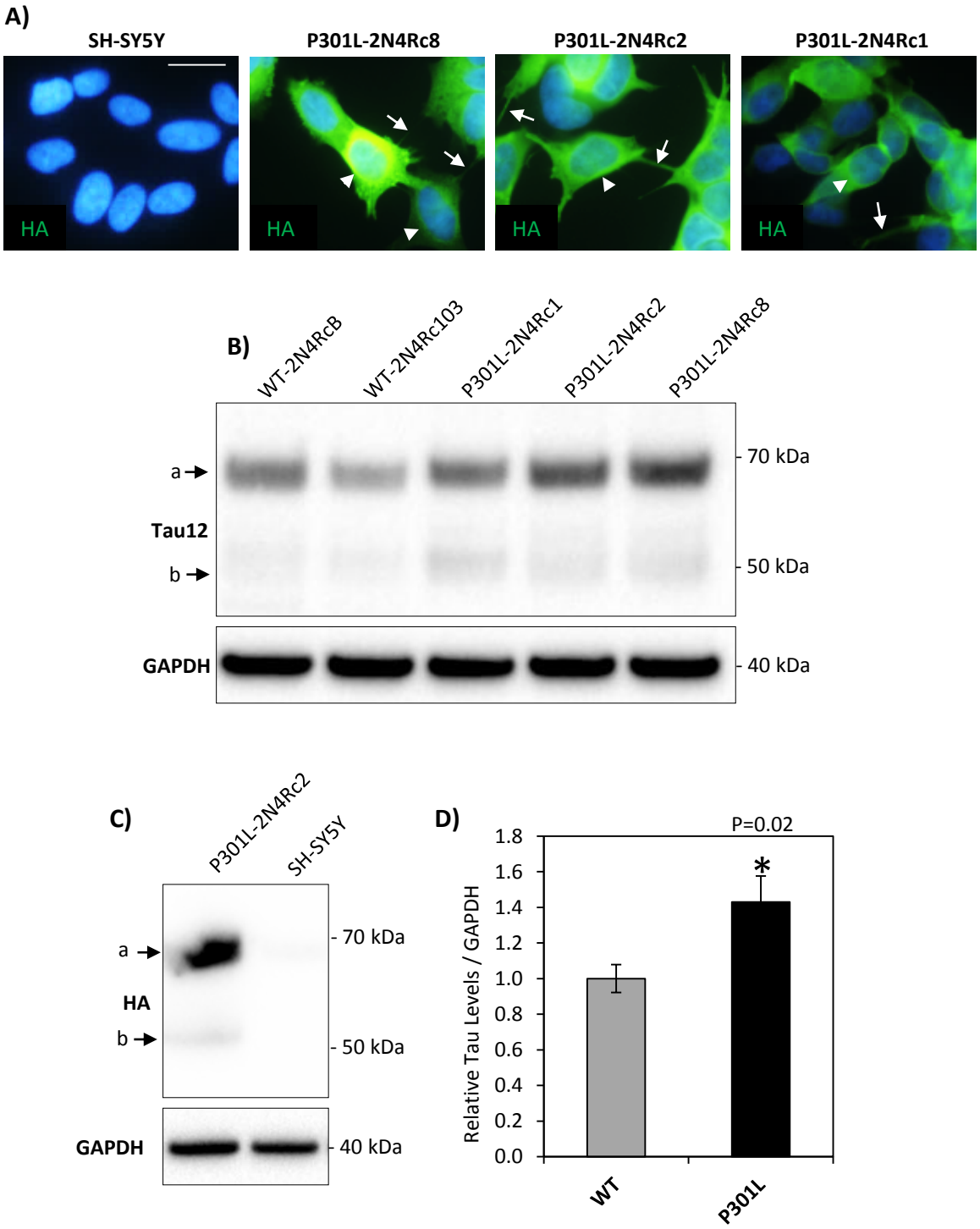

Figure 4.2 Characterisation of SH-SY5Y clones stably expressing HA-P301L-2N4R-Tau. A) HA immunostaining analysis of (HA)-P301L-2N4R-Tau SH-SY5Y clones. White arrowheads and arrows indicate cytoplasmic and neuritic HA staining, respectively. **B)** Western blot analysis of WT and HA-P301L SH-SY5Y clones (20 µg protein loaded / lane). Upper and lower arrows indicate major and minor Tau12 reactive bands, respectively. **C)** HA immunoblotting analysis of HA-P301L-2N4R-Tau c2 SH-SY5Y cells. **D)** Quantification of Tau levels in WT and HA-P301L-Tau SH-SY5Y clones. Values expressed relative to GAPDH and normalised to WT mean (mean ± SEM, WT n=6, P301L n=3, Student's T-test).

4.3.2 Analysis of Tau oligomerisation

To assess Tau oligomerisation in WT-2N4R and P301L-2N4R-Tau SH-SY5Y cells, proteins were extracted in native lysis buffer and separated by native-PAGE followed by immunoblotting with Tau antibodies. 1 ng of recombinant Tau (containing all 6 Tau isoforms) was also separated, in order to reveal the behaviour of monomeric Tau in this system (Tau ladder was reduced – 2-ME – and denatured – 90^{o}C 10 minutes – prior to analysis).

DAKO-Tau immunoreactivity from the recombinant Tau ladder appeared as a smear on native-PAGE, suggesting this system was unable to separate distinct Tau isoforms present in the same sample. DAKO-Tau cross reactive bands from WT-2N4R-Tau and P301L-2N4R-Tau SH-SY5Y cells were detected co-migrating within the limits of the Tau ladder, suggesting them to represent monomeric Tau from these cells (**green box,** band '**A**'**, figure 4.3 A**). DAKO-Tau cross reactive species from P301L-2N4R-Tau SH-SY5Y cells were also detected above the upper limit of the Tau ladder (and also from WT-2N4R-Tau SH-SY5Y cells, but less intensely), consistent with the detection of native Tau reactive species of higher molecular weight (HMW) than monomeric Tau from these cells (**red box,** '**HMW**' **figure 4.3 A**). Boiling the cell lysate prior to native-PAGE dissociated these HMW species such that under these conditions all Tau immunoreactive species (Tau12) from P301L-2N4R-Tau SH-SY5Y cells co-migrated with the lower band (band '**A**', **figure 4.3 B**). These observations are consistent with higher molecular weight (HMW) oligomeric Tau species as composing this Tau immunoreactivity ('HMW' – higher molecular weight – **figure 4.3 B**). Clarification of the cellular lysate at 1k x g vs 17k x g did not make a large difference to the composition of the Tau12 cross reactive band pattern detected from P301L-2N4R-Tau SH-SY5Y cells ('**HMW**' figure **4.3 B**).

The validity of native-PAGE to accurately resolve Tau species of different molecular weights was investigated by analysis of SH-SY5Y cells with ectopic expression of a truncated Tau protein. The repeat domain of Tau (RD-Tau) with a C-terminal dsRed tag contains 349 amino acids, 105 fewer than 2N4R-Tau (**figure 2.1** for a schematic diagram). The lowest molecular weight DAKO-Tau cross reactive band detected from SH-SY5Y cells with ectopic expression of RD-dsRed-Tau migrated further in native-PAGE than that from WT-2N4R-Tau and P301L-2N4R-Tau SH-SY5Y cells (band '**B**', **figure 4.3 A**), demonstrating the resolvability of differently sized Tau species in this system. Moreover, the repeat domain of Tau is known to undergo aggregation when expressed in cultured cells (Wang et al. 2007; Wang et al. 2009) and DAKO-Tau cross reactivity consistent with higher molecular weight Tau species were detected from RD-dsRed-Tau SH-SY5Y cells on native-PAGE (**figure 4.3 A**). Collectively, these findings support the interpretation that native-PAGE accurately separated monomeric Tau species and Tau species of higher molecular weight – such as oligomers – from SH-SY5Y cells with stable Tau expression.

We calculated the level of Tau oligomerisation in P301L-2N4R-Tau SH-SY5Y cells by expressing the density of Tau immunoreactivity composing the 'HMW' region relative to that co-migrating with the Tau ladder (termed 'monomer'; band '**A**' vs. '**HMW**', **figure 4.3 A** and **B**). This analysis demonstrated an increased HMW to monomer ratio in P301L-2N4R-Tau SH-SY5Y cells compared to WT-2N4R-Tau SH-SY5Y cells of 4.8±1 times, suggesting that stably expressed P301L-2N4R-Tau had increased oligomerisation relative to WT-2N4R-Tau when stably expressed in SH-SY5Y cells (mean ± SEM, n=3, p=0.01, **figure 4.3 C**).

We also assessed Tau oligomerisation in WT-2N4R-Tau and P301L-2N4R-Tau SH-SY5Y cells by dot blot of untreated and bafilomycin treated cellular lysates (prepared under native conditions) with the oligomer specific antibody T22 (Lasagna-Reeves et al. 2012a). No T22 immunoreactivity was detected from untreated WT-2N4R-Tau SH-SY5Y cells, whereas T22

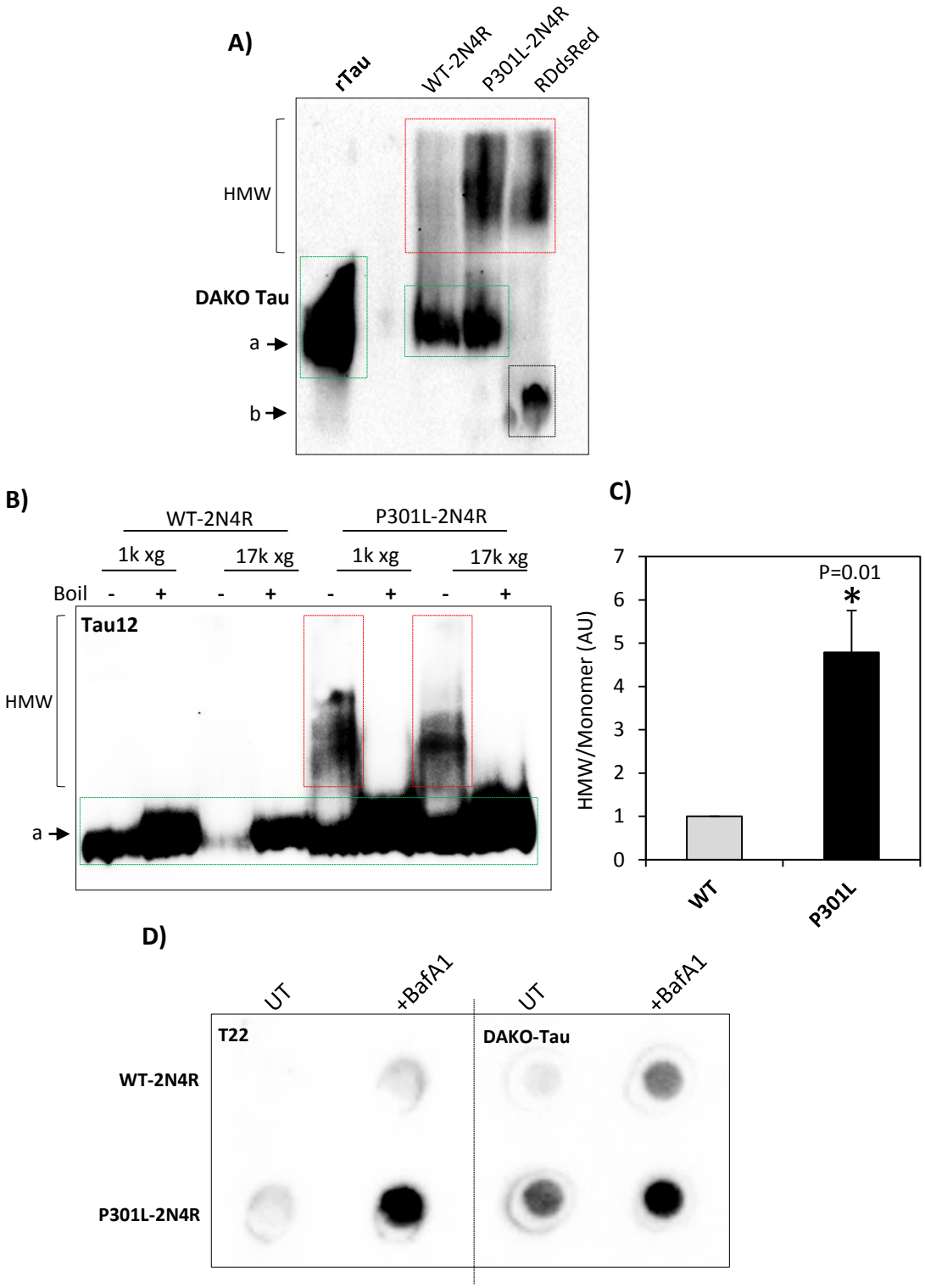

Figure 4.3 Analysis of Tau oligomerisation in P301L-2N4R-Tau SH-SY5Y cells. A) Native-PAGE analysis of recombinant Tau (rTau; all six isoforms) and WT-2N4R, P301L-2N4R and repeat domain (RD)-Tau expressing SH-SY5Y cells. Green dashed boxes and 'A' arrow indicate the migration of recombinant Tau (lane 1) and commonly migrating bands in WT-2N4R and HA-P301L-2N4R SH-SY5Y cells (lanes 2 and 3, respectively;). Red dashed box and 'HMW' indicates DAKO-Tau reactive species of higher molecular weight ('HMW'). Black dashed box and 'B' indicates a lower molecular mass band detected from RD-dsRed-Tau SH-SY5Y cells (1 ng recombinant Tau and 20 µg cell lysates loaded). **B)** Native-PAGE analysis of WT-2N4R-Tau and HA-P301L-2N4R-Tau SH-SY5Y cells. Cell lysates were boiled or not, and clarified at different speeds (1k and 17k x g). 'A' and green dashed box indicate a commonly migrating band detected in all samples and red dashed boxes 'HMW' indicate higher molecular mass Tau12 reactive species (20 µg / lane). **C)** Quantification of Tau oligomerisation levels in WT-2N4R-Tau and HA-P301L-Tau SH-SY5Y cells. Values obtained by expressing 'HMW' Tau intensity relative to band 'A' and normalised to WT-2N4R (mean ± SEM, n=4, Student's T-test). **D)** Dot-blot analysis of untreated and bafilomycin treated (100 nM 42 hour) WT-2N4R and HA-P301L-2N4R expressing SH-SY5Y cells with oligomer (T22; 50 µg loaded) and total (DAKO; 10 µg loaded) Tau antibodies.

cross reactivity was detected from untreated P301L-2N4R-Tau SH-SY5Y cells (**figure 4.3 D,** left side). T22 immunoreactivity was detected in bafilomycin treated (100 nM for 42 hours) WT-2N4R-Tau SH-SY5Y cells, and strongly detected in bafilomycin treated P301L-2N4R-Tau SH-SY5Y cells, suggesting that lysosomal compromise increased Tau oligomerisation. Bafilomycin treatment also increased total Tau levels for both WT and P301L-Tau as assessed by DAKO-Tau dot-blotting of the same samples (**figure 4.3 D, right side**).

Overall these findings suggested that stable P301L-2N4R-Tau SH-SY5Y cells had higher levels of Tau oligomerisation that WT-2N4R-Tau SH-SY5Y cells.

4.3.3 Analysis of the Exosomal Tau release from P301L-2N4R-Tau SH-SY5Y cells

Exosomes were isolated from the 24 hour conditioned optiMEM from 5 x 10 cm plates of P301L-2N4R-Tau SH-SY5Y cells, and separated on SDS-PAGE alongside DAKO-Tau immunoprecipitated exosome supernatant (0.03 x 10 cm) and cellular lysate (1 µg). Western blotting demonstrated the detection of Tau12 cross reactive bands in the exosomes and exosome supernatant from P301L SH-SY5Y cells, which migrated further than the major Tau12 reactive band detected in the cell lysate (**black** and **red arrows**, respectively, **figure 4.4 A**). The results of the molecular weight analysis are shown in **table 4.1**.

Table 4.1 Molecular weight analysis of cellular and extracellular Tau12 cross reactive species from WT-2N4R-Tau and (HA)-P301L-2N4R-Tau SH-SY5Y cells (interpolated from **figure 4.4**)

	M_r of Tau12 cross reactive bands	
	WT-2N4R-Tau	**(HA)-P301L-2N4R-Tau**
Cellular	69 kDa	70 kDa
Free	64 kDa	67 kDa
Exosomal	65 kDa	67 kDa

The molecular weight profiles of cellular and extracellular Tau12 reactive species from P301L-2N4R-Tau SH-SY5Y cells therefore followed the same qualitative pattern as those from WT-2N4R-Tau SH-SY5Y cells. The increased molecular weights of (HA)-P301L-2N4R-Tau species relative to the correspondent WT-2N4R-Tau species reflected the N-terminal HA tag in the former, which accounted for ~1 kDa of the molecular weight.

Next, the exosomes from two WT-2N4R-Tau SH-SY5Y clones (WTc103 and WTcB) and from three P301L-2N4R-Tau SH-SY5Y clones (P301Lc1, P301Lc2 and P301Lc8) were isolated (5 x 10 cm of each) from the 24 hour conditioned optiMEM and analysed by Tau12 western blotting. Tau12 cross reactivity was detected in the exosomes from all clones as one major band, migrating at 62 kDa and 64 kDa for WT and P301L clones, respectively.

The levels of exosomal Tau from P301L-2N4R-Tau SH-SY5Y cells was calculated to be 6±1.1 times higher than from WT-2N4R-Tau SH-SY5Y cells when expressed relative to Alix, suggesting P301L-Tau was exosomally released at a greater rate than WT-Tau (mean ± SEM, n=4, p=0.00042, **figure 4.4 C**).

Plotting the levels of cellular Tau expression versus the levels of exosomal Tau from a number of WT-Tau SH-SY5Y clones revealed no clear correlation between these parameters (r^2=0.05, **figure 4.4 D**). Incorporation of the values from the P301L clones into this plot demonstrated that cellular Tau expression in P301L-2N4R-Tau clones was within the limits of WT-Tau expression, whereas P301L-2N4R-Tau clones were sharply differentiated from WT-Tau SH-SY5Y clones by their levels of exosomal Tau (black diamonds, **figure 4.4 D**).

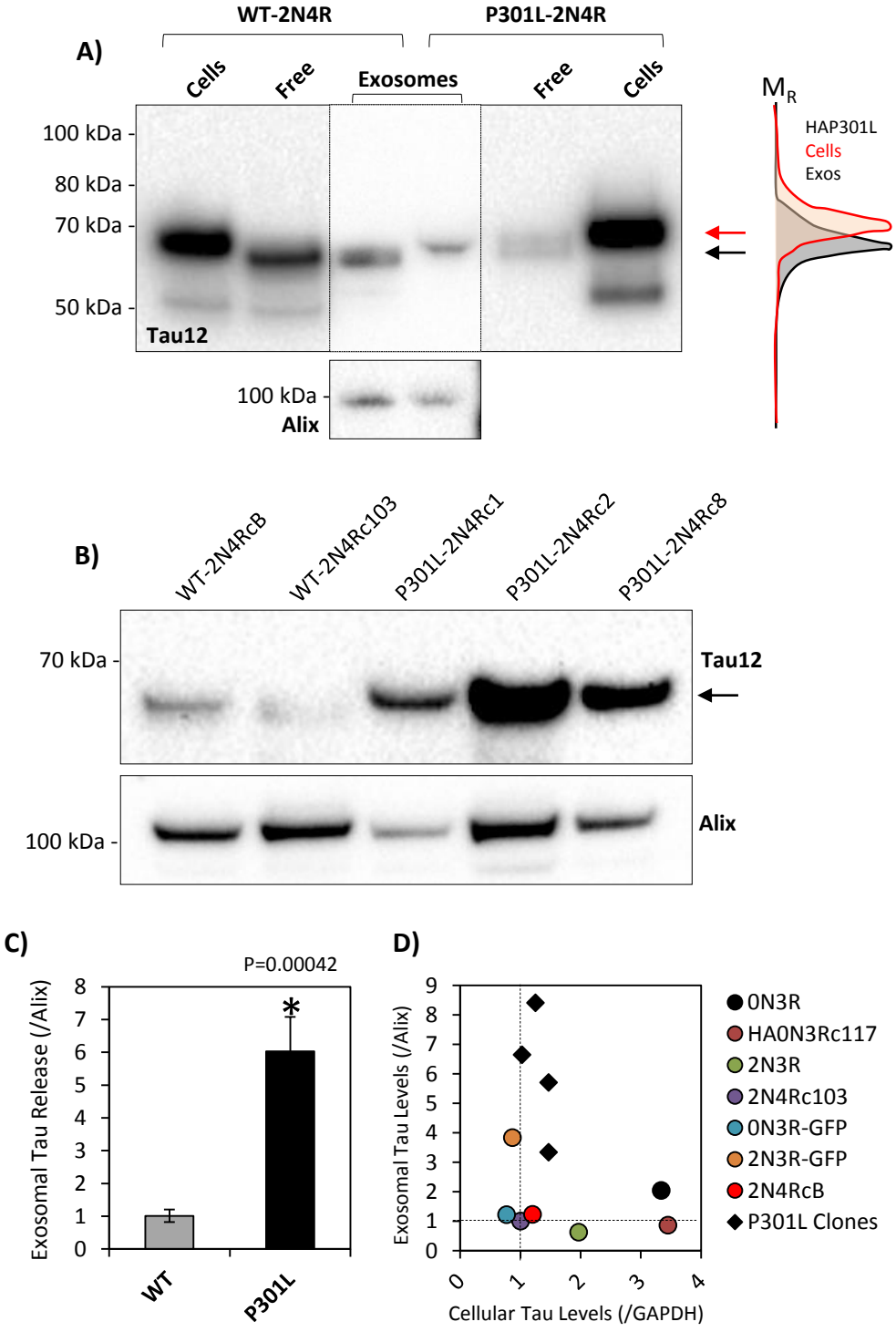

Figure 4.4 Analysis of Exosomal Tau release from P301L-2N4R-Tau SH-SY5Y cells. A) Western blot analysis of cellular (1 µg), exosomal supernatant (DAKO-Tau IP of 220 µl) and exosomal (5 x 10 cm) WT-2N4R and P301L-2N4R-Tau from SH-SY5Y cells. Upper arrow indicates the major cellular and extracellular Tau12 reactive bands, respectively. Peak analysis of these major bands from the cells and exosomes is displayed to the right. **B)** Western blot analysis of WT-2N4R and P301L-2N4R-Tau exosomal release from independent clonal lines. Arrow indicates major Tau12 reactive band.**C)** Quantification of WT and HA-P301L exosomal Tau levels. Values expressed relative to Alix and normalised to WT-2N4R mean (mean ± SEM, WT n=6, P301L n=4, Student's T-test). **D)** Correlation analysis of cellular and exosomal Tau levels from WT clones (coloured circles) and P301L clones (black diamonds). Cellular Tau expressed relative to GAPDH and exosomal Tau expressed relative exosomal Alix, normalised to WT-2N4R levels.

4.4 Analysis of the role of Hsc70 interaction in the exosomal release of Tau

4.4.1 Co-immunoprecipitation of Tau and Hsc70 in SH-SY5Y cells

To analyse their interaction, WT-2N4R-Tau and Hsc70-V5 were transiently co-expressed in SH-SY5Y cells by electroporation and grown for 48 hours. DAKO-Tau and V5 co-immunostaining revealed specific immunoreactivity from both channels in transfected cells only (**figure 4.5 A**). Moreover, patterns of V5 and DAKO-Tau immunoreactivity were overlapping demonstrating that individual cells co-expressed Tau and Hsc70-V5 (yellow arrows, **figure 4.5 A**).

Transiently co-transfected SH-SY5Y cells were lysed, immunoprecipitated with DAKO-Tau and analysed by Western blotting. Tau12 and V5 immunoreactive bands migrating at 67 kDa and 72 kDa, respectively, were detected in the 'input' sample confirming the expression of Tau and Hsc70-V5 in the cells (**figure 4.5 B**). The 67 kDa Tau12 cross reactive band was successfully IP'd from the transfected cells by DAKO-Tau in an antibody specific manner. Moreover, Hsc70-V5 was co-immunoprecipitated by DAKO-Tau pull-down, demonstrated by the detection of a V5 cross reactive band at 72 kDa in an antibody specific manner (**black** and **red arrows**, respectively, **figure 4.5 A**) thus confirming the interaction of Tau and Hsc70.

4.4.2 Effect of CMA3 Tau mutations on Hsc70 co-immunoprecipitation

Consensus CMA motifs in client proteins have been identified as important for interaction with Hsc70. Tau protein has two such motifs – ^{336}**QV**EVK^{340} and ^{347}KDR**VQ**^{351} – CMA1 and CMA2, which are located within the fourth microtubule binding repeat of Tau (**figure 4.5 C**). We aimed to assess the contribution of these motifs to the interaction of Tau with Hsc70.

^{336}**QV**EVK^{340} and ^{347}KDR**VQ**^{351} were mutated to ^{336}**AA**EVK^{340} and ^{347}KDRV**AA**^{351} by site directed mutagenesis of the underlying 2N4R-Tau cDNA. The mutations corresponding to ^{336}**QV**EVK^{340} to ^{336}**AA**EVK^{340} were introduced first, followed by mutation of ^{347}KDR**VQ**^{351} ^{347}KDRV**AA**^{351}. Introduction of the correct mutations was confirmed by Sanger sequencing of the cDNA (**figure 4.5 C**). The mutated form of the protein was termed 'CMA3-2N4R-Tau'.

CMA3-2N4R-Tau / WT-2N4R-Tau were transiently co-expressed alongside Hsc70-V5 in SH-SY5Y cells by electroporation, and after 48 hours of expression cells were immunoprecipitated with DAKO-Tau. V5 and Tau12 cross reactive bands were detected in the inputs of each immunoprecipitation reaction at 72 kDa and 67 kDa, respectively, demonstrating the expression of Tau and Hsc70-V5 in the lysates (**figure 4.5 C**, '**input**'). 67 kDa Tau12 immunoreactivity was detected in the DAKO Tau IP'd samples from SH-SY5Y cells transfected with WT-2N4R-Tau or CMA3-2N4R-Tau, demonstrating immunoprecipitation of the respective forms of Tau. The 72 kDa V5 cross reactive band was co-IP'd from SH-SY5Y cells transiently expressing WT-2N4R-Tau and Hsc70-V5, demonstrating the coIP of Hac70-V5 (**figure 4.5 C**, '**IP:DAKO-Tau'**). The level of Hsc70-V5 co-immunoprecipitated from SH-SY5Y cells transiently expressing CMA3-2N4R-Tau and Hsc70-V5 were 80±12% lower than that co-immunoprecipitated from SH-SY5Y co-expressing WT-2N4R-Tau and Hsc70-V5 (**figure 4.5 E**). Therefore the co-immunoprecipitation of Hsc70-V5 with DAKO-Tau was significantly disrupted by mutation of the two CMA motifs in Tau, suggesting these motifs were important for Tau – Hsc70 interaction.

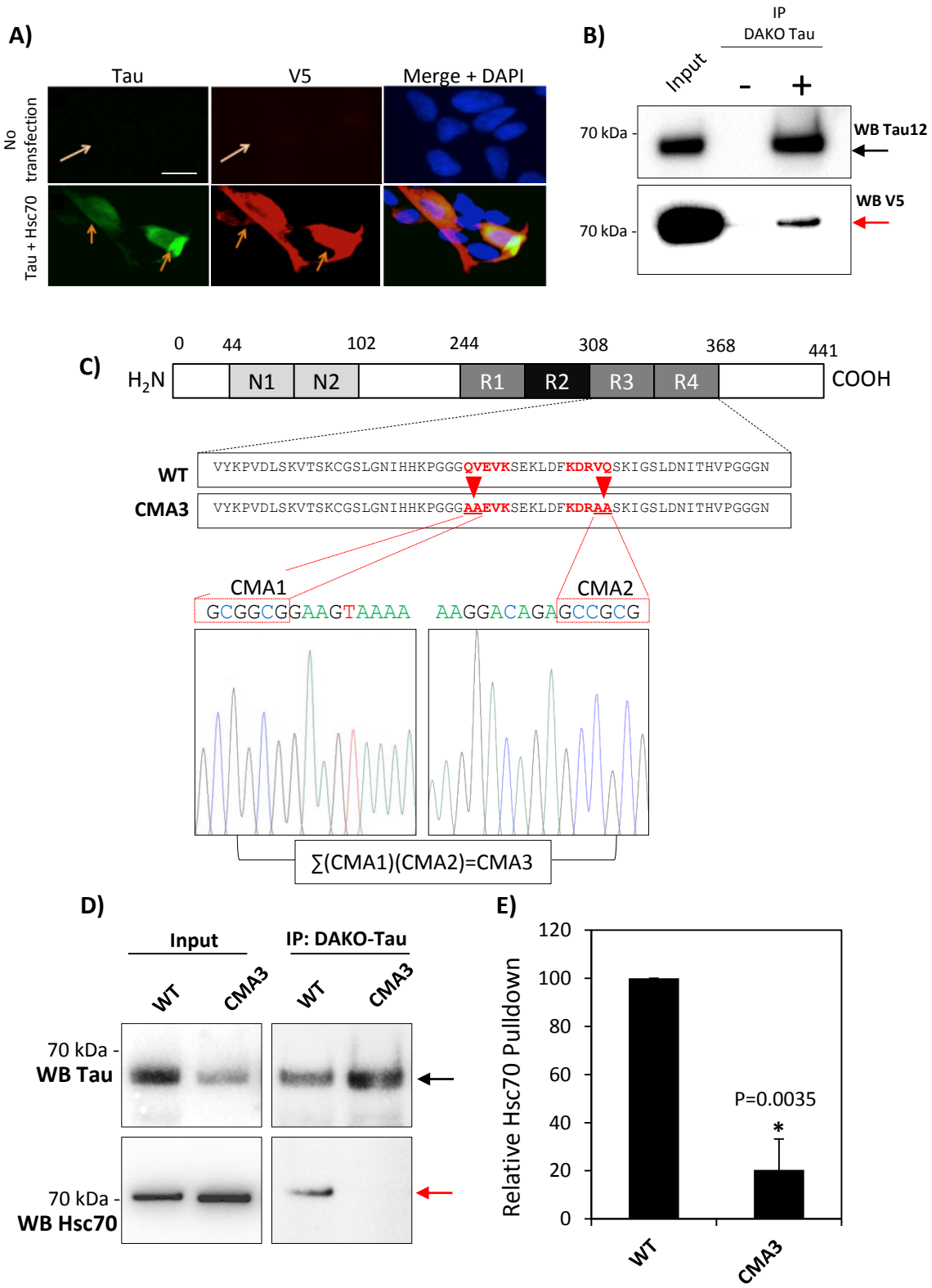

Figure 4.5 Co-immunoprecipitation analysis of Tau – Hsc70 interaction and role of CMA motifs. A) DAKO-Tau and V5 co-immunostaining analysis of untransfected and 2N4R-Tau – Hsc70-V5 co-transfected SH-SY5Y cells. **B)** DAKO-Tau co-immunoprecipitation and Western blot analysis of SH-SY5Y cells transiently co-transfected with WT-2N4R-Tau and Hsc70-V5 (for 48 hours). SDS-PAGE separated immunoprecipitating proteins were analysed for their cross reactivity with Tau12 (upper, black arrow) and V5 (lower, red arrow) antibodies (1/40th of the input and all of the IP eluate from ~10 x 10^6 transfected cells was loaded). **C)** Schematic diagram WT-2N4R-Tau protein indicating putative CMA motifs: ^{336}QVEVK^{340} and ^{347}KDRVQ^{351} in red text. These motifs were mutated to ^{336}AAEVK^{340} and ^{347}KDRVAA^{351} by substitution of the underlying 2N4R-Tau cDNA sequence, as displayed in the chromatogram (confirmed by Sanger sequencing). The mutated form of the protein was termed 'CMA3-2N4R-Tau'. (N = N-terminal insert, R = microtubule binding repeat). **D)** DAKO-Tau co-immunoprecipitation and Western blot analysis of SH-SY5Y cells transiently co-transfected with WT-2N4R-Tau or CMA3-2N4R-Tau and Hsc70-V5. Immunoprecipitating proteins were analysed for their cross reactivity with Tau12 (upper, black arrow) and Hsc70-V5 (lower, red arrow). (1/40th of the input and all of the IP eluate from ~10 x 10^6 transfected cells was loaded). **E)** Quantification of Hsc70-V5 pull-down from SH-SY5Y cells co-transfected with Hsc70-V5 and WT-2N4R-Tau or CMA3-2N4R-Tau. Co-IP'd Hsc70 levels expressed relative to IP'd Tau levels and normalised to WT levels (mean ± SEM n=3, Student's T-test).

4.4.3 Characterisation of SH-SY5Y cells with stable expression of CMA3-2N4R-Tau

SH-SY5Y cells were transfected with CMA3-2N4R-Tau plasmid and selected by growth in G418. Resistant colonies were selected, expanded, and analysed for their expression of Tau protein. In parallel, additional clones expressing WT-2N4R-Tau protein were generated – WT-2N4Rc216.6 and c218.

SDS-PAGE and western immunoblotting with Tau12 revealed a Tau12 immunoreactive band migrating at ~67 kDa in all WT-2N4R-Tau and CMA3-2N4R-Tau SH-SY5Y clones, consistent with expression of FL-2N4R-Tau (**arrow**, **figure 4.6 A**). Levels of this Tau12 cross reactive band were higher in CMA3-2N4R-Tau SH-SY5Y clones than in WT-2N4R-Tau clones (**figure 4.6 B**). Combined data demonstrated that the level of Tau12 cross reactivity levels in CMA3-2N4R-Tau SH-SY5Y cells was 5.1±0.9 times higher than in WT-2N4R-Tau SH-SY5Y cells (mean ± SEM, n=9, *p*=0.0002, expression of all clones was normalised to WT mean, **figure 4.6 C**).

WT-2N4R-Tau and CMA3-2N4R-Tau SH-SY5Y clones were further characterised by immunocytochemistry with DAKO Tau. Using normal SH-SY5Y cells as a control to allow gating of the exposure threshold to detect predominantly overexpressed Tau, detection of Tau protein above endogenous levels was observed in all the analysed WT and CMA3 clones (**figure 4.7 A**).

Intra-clonal heterogeneity of DAKO-Tau staining intensity was observed, including in normal SH-SY5Y populations. This was indicated by the presence more highly fluorescent cells (**white arrowheads** in **figure 4.7 A**). To quantify this heterogeneity we integrated the fluorescence intensity of individual cells using an adapted ImageJ protocol (example of this protocol applied to segment cells is shown in **figure 4.7 B**)). The DAKO-Tau immunofluorescence intensities of the cellular populations was represented as box and whisker plots. This analysis revealed the Tau expression in normal SH-SY5Y cells followed a

positive skew, suggesting that many cells had lower levels of Tau expression and fewer cells had higher levels (**figure 4.7 C,** enlarged region).

WT-2N4R-Tau and CMA3-2N4R-Tau SH-SY5Y clones all exhibited few highly fluorescent cells and the median values from each ectopic Tau line exceeded the maximum value from normal SH-SY5Y cells, consistent with Tau overexpression in these clones. Furthermore, the median values from each CMA3-2N4R-Tau SH-SY5Y clone were higher than those from each WT-2N4R-Tau SH-SY5Y clone, and the box-plots representing from the CMA3-2N4R-Tau SH-SY5Y population were overall shifted upward relative to the WT-2N4R-Tau SH-SY5Y clone plots (**figure 4.7 C**) These observations were consistent with higher intracellular Tau expression CMA3-2N4R-Tau SH-SY5Y clones than in WT-2N4R-Tau SH-SY5Y clones.

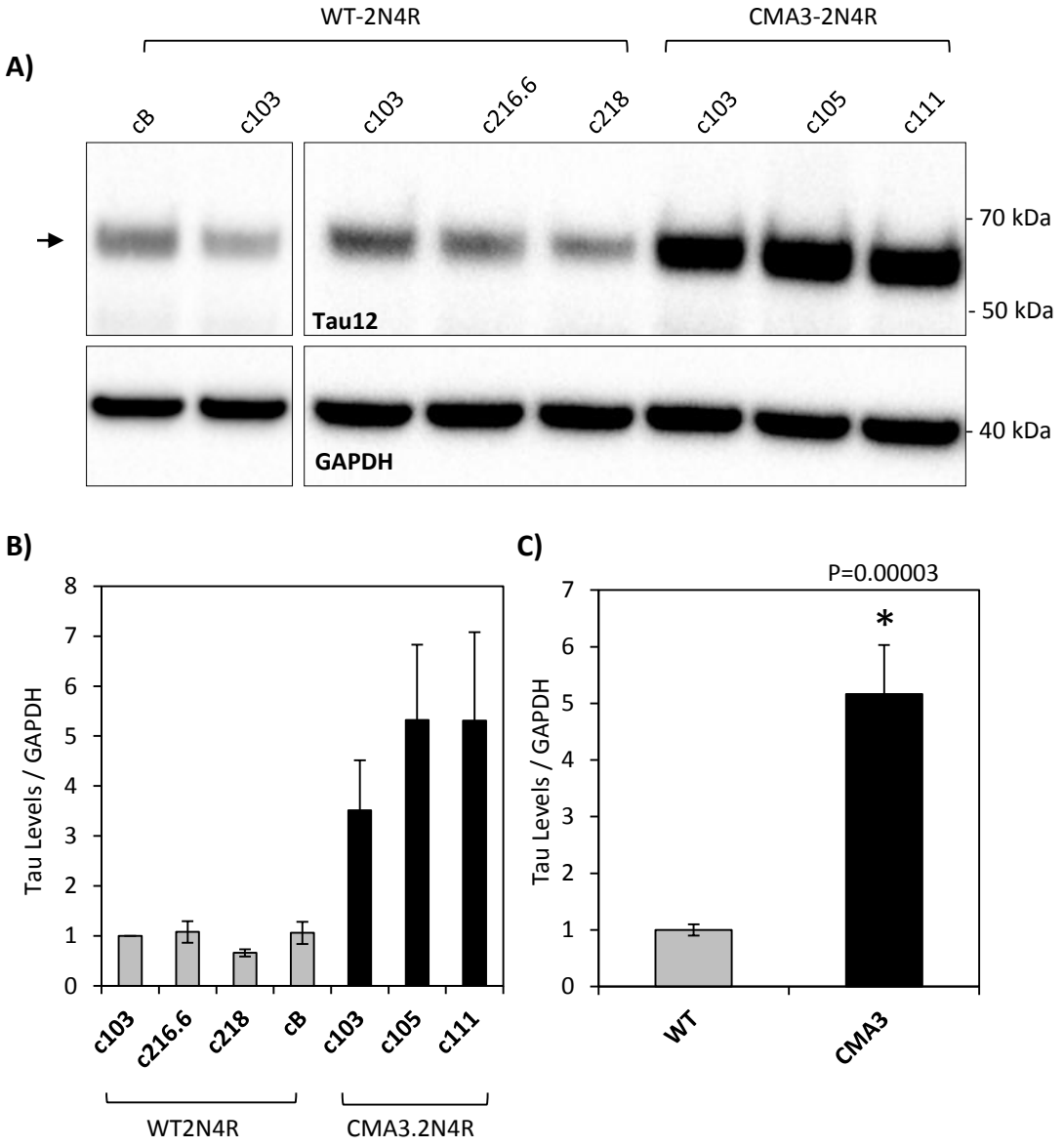

Figure 4.6 Western blot analysis of SH-SY5Y clones expressing WT-2N4R and CMA3-2N4R-Tau. A) Tau12 western blotting of independent SH-SY5Y clones stably expressing WT-2N4R-Tau / CMA3-2N4R-Tau (3 clones of each; 20 µg cellular protein loaded / lane). Black arrow indicates major Tau12 immunoreactive band. **B)** Relative quantification of Tau12 immunoreactivity from WT-2N4R-Tau and CMA3-2N4R-Tau SH-SY5Y clones. Levels expressed relative to GAPDH and normalised to WT-2N4Rc103 levels (mean ± SEM, n=3). **C)** Combination and statistical analysis of Tau expression levels in WT-2N4R and CMA3-2N4R SH-SY5Y cells (combination of three clones for each, mean ± SEM, n=9, Student's T-test).

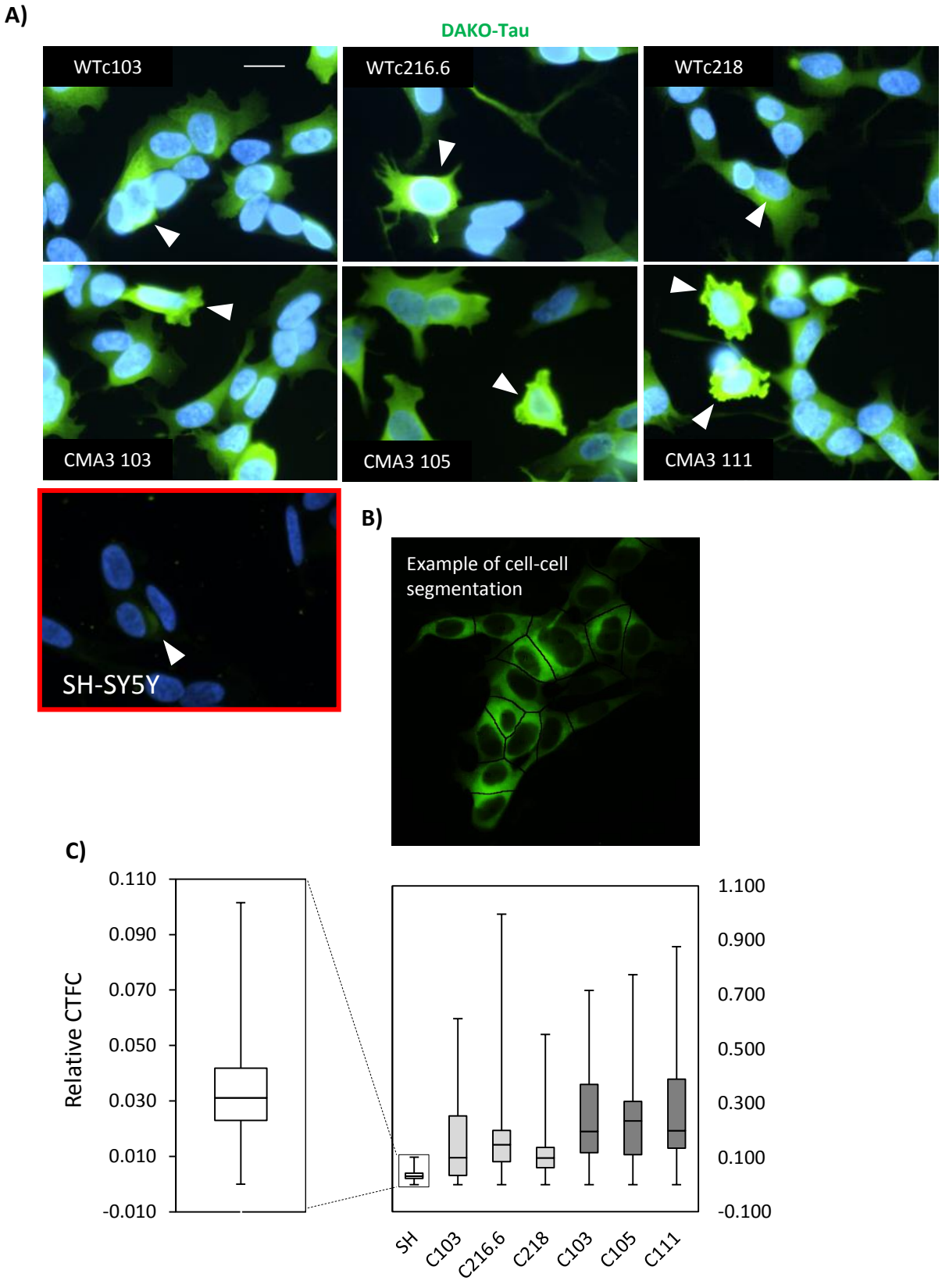

Figure 4.7 Immunocytochemical analysis of SH-SY5Y clones expressing WT-2N4R-Tau and CMA3-2N4R-Tau. A) Fluorescent microscopy images of DAKO-Tau immunostained SH-SY5Y cells expressing WT-2N4R-Tau (top row) and CMA3-2N4R-Tau (bottom row) and normal SH-SY5Y cells (outlined by the red box). Cells with higher intensity DAKO-Tau staining are indicated by white arrowheads. **B)** Segmentation of individual cells by an adapted image J protocol. Spaces enclosed by black borders constituted regions of interest from which DAKO-Tau fluorescence intensity was integrated. **C)** Box-plot representations of DAKO-Tau immunofluorescence profiles from the respective SH-SY5Y clonal populations (normal SH-SY5Y – white bars, WT-2N4R-Tau SH-SY5Y – light grey bars, CMA3-2N4R-Tau – dark grey bars; >80 cells counted / box plot).

4.4.4 Effect of lysosomal inhibition on steady state Tau levels in normal, WT-2N4R-Tau and CMA3-2N4R-Tau SH-SY5Y cells

We treated normal, WT-2N4R-Tau and CMA3-2N4R-Tau SH-SY5Y clones with bafilomycin (an inhibitor of the lysosomal H^+ ATPase; 200 nM 48 hours) and analysed the effects on intracellular Tau12 cross reactive band levels. In normal SH-SY5Y cells, levels of the Tau12 immunoreactive band corresponding to endogenous Tau were increased 2.1±0.4 times by bafilomycin treatment (mean ± SEM, n=3, *p*=0.03) (**figure 4.8 A** band '**B**' and quantified in **figure 4.8 B**). Levels of the 67 kDa Tau12 cross reactive band in WT-2N4R-Tau SH-SY5Y cells corresponding to ectopic 2N4R-Tau were increased by bafilomycin treatment by a similar magnitude to that observed for endogenous Tau (2±0.1 times, mean ± SEM, n=3 *p*=0.0065, Student's t-test, **figure 4.8 A** band '**A**' quantified in **figure 4.8 B**). However, bafilomycin A1 treatment did not significantly affect levels of the major Tau12 cross reactive band detected from CMA3-2N4R-Tau SH-SY5Y cells (**figure 4.8 A** and **B**). These observations suggested that endogenous and ectopic WT Tau, but not CMA3 Tau were degraded by lysosomally dependant mechanisms in SH-SY5Y cells.

4.4.5 Total secretion of Tau from WT-2N4R-Tau and CMA3-2N4R-Tau SH-SY5Y clones

We subjected the 24 hour conditioned medium (optiMEM) from WT-2N4R-Tau and CMA3-2N4R-Tau SH-SY5Y clones to dot-blot analysis. Tau12 cross reactivity was detected in the conditioned medium of all clones tested (**figure 4.8 D**). Quantification revealed an increase in the release of CMA3-2N4R-Tau compared to WT (2.8±0.8 vs 1±0.3, n=6), although this effect did not reach statistical significance (*p*=0.07, Student's t-test; **figure 4.8 D**).

We noted the detection of an extra Tau12 cross reactive band from WT-2N4Rc218 SH-SY5Y cells (**asterisk, figure 4.8 A**). This band was not detected from any of the other clones, and as we could not confirm the identity of this band, WT-2N4Rc218 SH-SY5Y cells were excluded from further analysis.

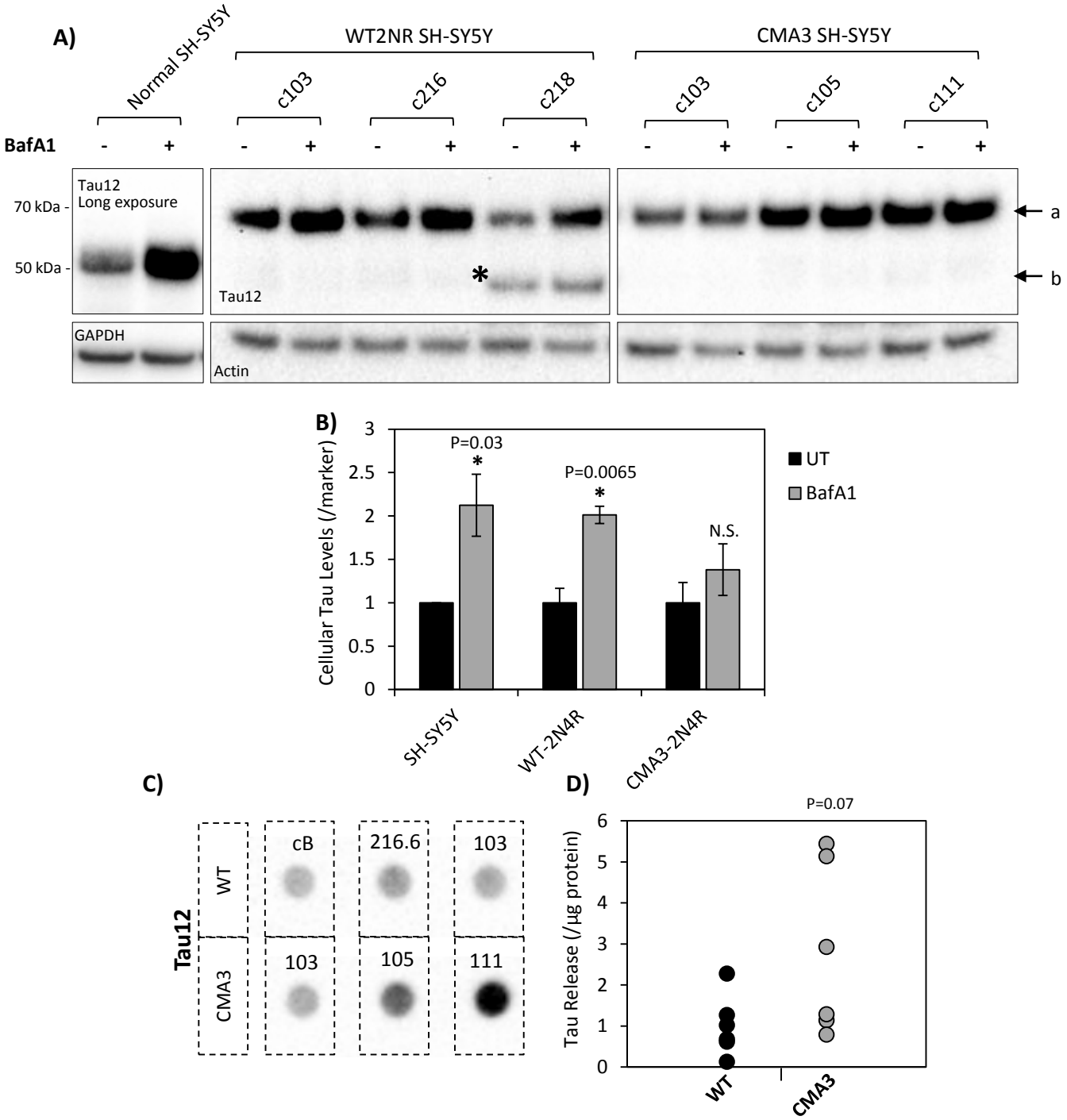

Figure 4.8 Analysis of the degradation and secretion of Tau from WT-2N4R-Tau and CMA3-2N4R-Tau SH-SY5Y cells. A) Western blot analysis of bafilomycin treated normal, WT-2N4R and CMA3-2N4R Tau SH-SY5Y cells (48 hours 200 nM bafilomycin). Upper and lower arrows indicate major Tau12 reactive bands from WT/CMA3-2N4R and normal SH-SY5Y cells, respectively. Molecular weight markers apply to all panels. Asterisk indicates anomalous Tau12 reactive band identified in WT-2N4Rc218 SH-SY5Y cells (20 µg protein loaded / lane). **B)** Levels of Tau12 major immunoreactive species from normal, WT-2N4R and CMA3-2N4R Tau SH-SY5Y cells untreated (black bars) and treated (grey bars) with 200 nM bafilomycin. Normal SH-SY5Y Tau12 levels are expressed relative to actin, and WT-2N4R and CMA3-2N4R Tau12 levels are expressed relative to GAPDH and all values are normalised to corresponding untreated values (mean ± SEM, n=3 i.e. 3 repeats for normal SH-SY5Y and 3 independent clones for WT-2N4R and CMA3-2N4R SH-SY5Y cells, Student's T-test). **C)** Dot-blot analysis of 24 hour conditioned optiMEM from WT-2N4R and CMA3-2N4R-Tau SH-SY5Y cells (200 µl ≈ 1/10th of the medium was loaded from 6 well plates). **E)** Quantification of total extracellular Tau from WT-2N4R and CMA3-2N4R-Tau SH-SY5Y cells. Values are expressed relative to cellular protein levels (n=6, 2 independent repeats for 3 independent clones of WT-2N4R and CMA3-2N4R SH-SY5Y cells).

4.4.6 Analysis of exosomal Tau release from CMA3-2N4R-Tau SH-SY5Y clones

We isolated exosomes from the 24 hour conditioned optiMEM from three WT-2N4R-Tau and three CMA3-2N4R-Tau SH-SY5Y clones. Tau12 cross reactive bands were detected in the exosomes from all WT-2N4R-Tau and CMA3-2N4R-Tau SH-SY5Y clones as a major band of 62 kDa and a minor band of 55 kDa. ('**A**' and '**B**', respectively **figure 4.9 A).** We calculated the relative levels of the major Tau12 band in the exosomes from individual WT-2N4R-Tau and CMA3-2N4R-Tau SH-SY5Y cells (expressed relative to cellular protein levels). Exosomal Tau levels were normalised to those from WT-2N4Rc103 SH-SY5Y cells, and levels were demonstrated to be similar from WT-2N4RcB and CMA clones c103 and c105. Exosomal Tau levels were reduced from WT-2N4Rc216.6 SH-SY5Y cells and levels from CMA3-2N4Rc111 SH-SY5Y cells exhibited large variability (**figure 4.9 D**).

Combining the data from individual clones revealed no significant difference in the exosomal Tau levels from WT-2N4R-Tau and CMA3-2N4R-Tau SH-SY5Y cells (1±0.3 times vs1.5±0.6 times, respectively; normalised to WT mean; mean ± SEM, n=9, *p*=0.5, **figure 4.8 C**).

A correlation analysis of intracellular Tau levels vs. exosomal Tau levels for a variety of clones expressing various WT-Tau isoforms demonstrated a lack of relationship between these two parameters (R^2=0.0485, **figure 4.9 D**). Furthermore, plotting the results from the CMA3-2N4R-Tau clones into this analysis showed that CMA3 clones were more sharply differentiated from WT-2N4R-Tau clones by their intracellular expression levels, rather than by exosomal Tau release.

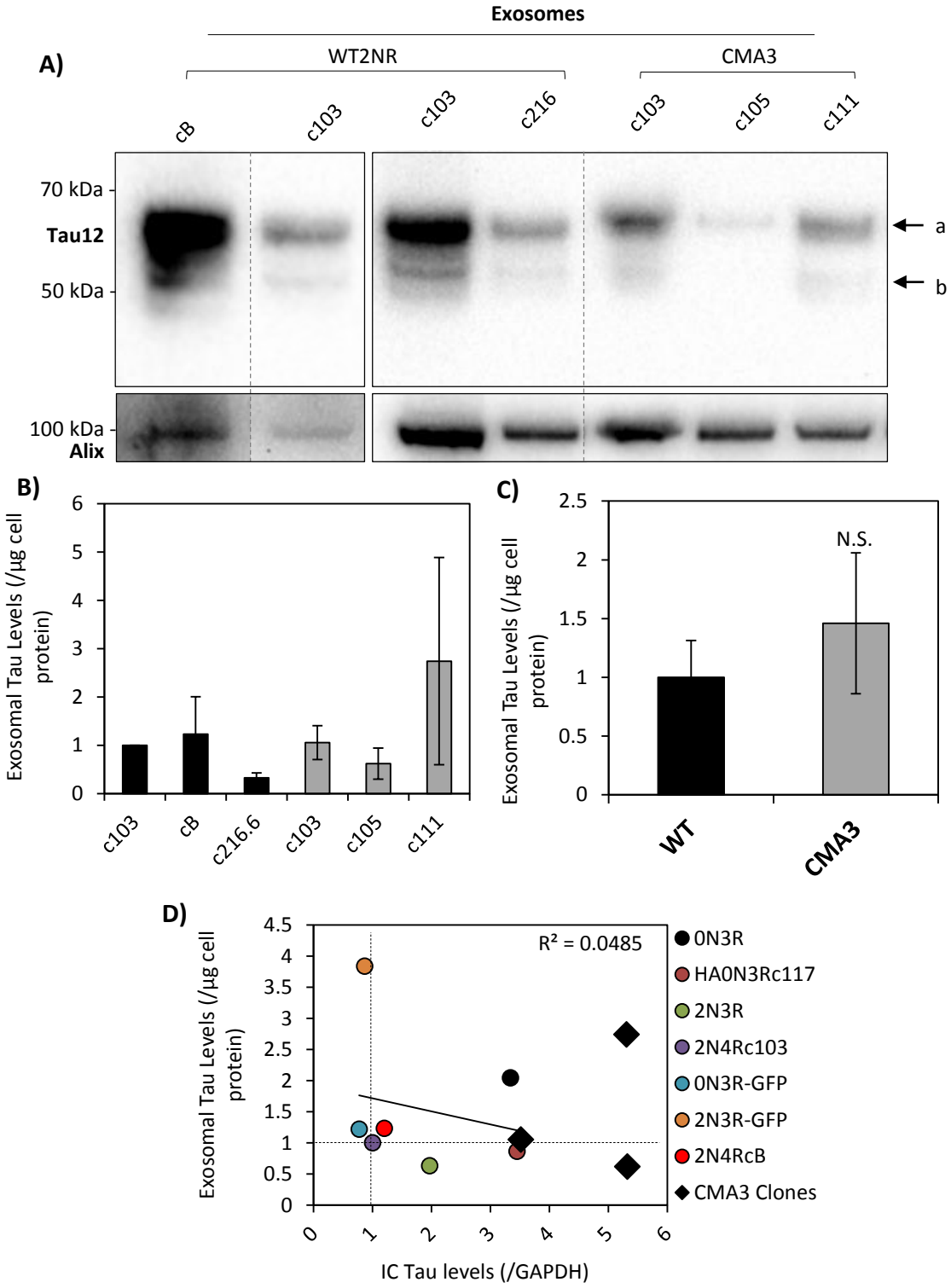

Figure 4.9 Analysis of exosomal Tau release from WT-2N4R and CMA3-2N4R SH-SY5Y clones. A) Western blot analysis of exosomes isolated from 24 hour conditioned optiMEM (5 x 10 cm / lane) SH-SY5Y cells with stable expression of WT-2N4R-Tau (cB, c103 and c216.6) and CMA3-2N4R-Tau (c103, c105, c111). Size markers are consistent between the two blots. Upper and lower arrows indicate major and minor Tau12 reactive bands, respectively. **B)** Quantification of exosomal Tau levels from individual WT-2N4R and CMA3-2N4R SH-SY5Y clones, levels expressed relative to cellular protein levels and normalised to WT-2N4R-c103 (mean ± SEM, WTcB n=4, WTc216.6 n=3, CMA3c103 n=3, CMA3c105 n=3, CMA3 c111 n=2). **C)** Combined quantification and statistical analysis of exosomal Tau release from WT-2N4R and CMA3-2N4R-Tau SH-SY5Y clones (values expressed relative to cellular protein levels and normalised to WT-2N4R mean; mean ± SEM, WT n=11, CMA3 n=8, Student's T-test). **D)** Correlation analysis of intracellular Tau levels (to GAPDH) and exosomal Tau levels (to cellular protein levels) for WT clones (coloured circles) and CMA3 clones (grey boxes). Values are normalised to WT-2N4R-c103 for both parameters.

4.4.7 Effects of optiMEM and prespun medium on exosomal Tau release from CMA3-2N4R-Tau SH-SY5Y cells

As previously demonstrated (**figure 3.8**), exosomal Tau release from WT-2N4R-Tau SH-SY5Y cells was increased when the cells were grown in DMEM F12 supplemented with prespun serum compared to optiMEM growth medium (2.1±0.37 times, mean ± SEM, n=3, *p*=0.04 Student's t-test, Western blot **figure 4.10 A**) and quantified in **figure 4.10 B**). We determined the effect of prespun growth medium on the exosomal release of Tau from CMA3-2N4R-Tau c105 SH-SY5Y cells by isolating the exosomes from the 24 hour conditioned optiMEM and prespun medium (5 x 10 cm / isolation). CMA3-2N4R-Tau c105 cells were used owing to good growth and detectable levels of Tau in the exosomes isolated from the conditioned optiMEM of these cells (**figure 4.10 A**). Levels of the 64 kDa exosomal Tau12 cross reactive band from CMA3-2N4R-Tau SH-SY5Y cells isolated from prespun conditioned medium were 0.18±0.06 (mean ± SEM, n=3) times that of when cells were grown in optiMEM (*p*=0.0001, Student's t-test, quantified in **figure 4.10 C**). Thus growth in serum caused a decrease in the exosomal release of Tau from CMA3-2N4R-Tau SH-SY5Y, an opposite effect that occurred for WT-2N4R-Tau SH-SY5Y cells.

Growth in OptiMEM did not induce intracellular accumulation of LC3-II in either WT or CMA3 SH-SY5Y clones (**figure 4.10 E**). Moreover, total LC3 levels were not different between optiMEM and prespun growth conditions (**figure 4.10 F**). Thus growth in optiMEM vs serum did not differentially affect WT and CMA3 SH-SY5Y clones in terms of starvation induced autophagy. Moreover, both SH-SY5Y populations responded to 6 hour bafilomycin treatment with accumulation of LC3-II indicating no gross differences in autophagic flux (**figure 4.10 D**). However CMA3-2N4R-Tau SH-SY5Y cells exhibited significantly lower levels of the LC3 cross reactive band than that detected from WT-2N4R-Tau SH-SY5Y cells (0.47±0.1 vs 1±0.05, mean ± SEM, n=3, *p*=0.0029, Student's t-test, **figure 4.10 F**).

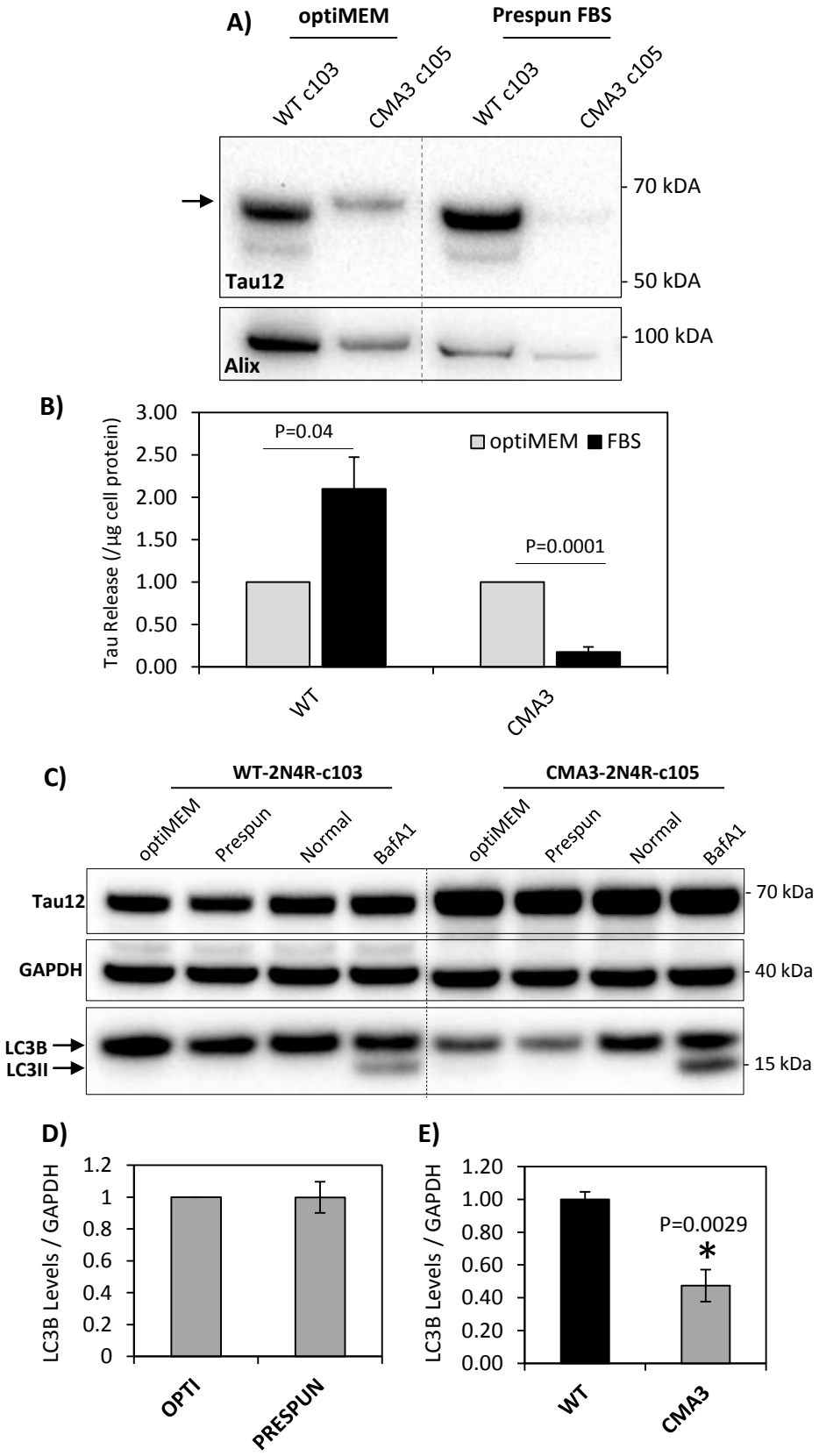

Figure 4.10 Analysis of the effects of optiMEM and prespun growth medium on exosomal Tau release from WT-2N4R and CMA3-2N4R SH-SY5Y cells. A) Western blotting of exosomes isolated from 24 hour conditioned optiMEM (5 x 10 cm; left side) or prespun medium (5 x 10 cm; right side) from WT-2N4R-c103 and CMA3-2N4R-c105 SH-SY5Y cells. Arrow indicates major Tau12 reactive band. **B)** Quantification of exosomal Tau levels from WT and **C)** CMA3-2N4R-Tau SH-SY5Y cells when grown in optiMEM or prespun medium, values expressed relative to cellular protein levels and normalised to 'optiMEM' levels (mean ± SEM, n=3). **D)** Western blot analysis of WT-2N4R and CMA3-2N4R SH-SY5Y cells grown under different conditions: optiMEM – 24 hours, prespun medium – 24 hours, normal growth medium – 24 hours, bafilomycin A1 – 100 nM in normal medium for 6 hours. 20 µg protein loaded / lane. **E)** Quantification of LC3B levels from SH-SY5Y cells grown in optiMEM and prespun growth medium (24 hours; levels expressed relative to GAPDH and normalised to optiMEM levels, mean ± SEM, n=4). **F)** Quantification of LC3B levels in WT-2N4R and CMA3-2N4R SH-SY5Y cells (levels expressed relative to GAPDH and normalised to WT mean, mean ± SEM, n=4, Student's T-test).

4.4.8 Exosomal Tau release from SH-SY5Y transiently expressing CMA3-2N4R-Tau

SH-SY5Y cells were transiently transfected with either WT or CMA3-2N4R-Tau plasmid for 48 hours. 24 hours into expression, medium was changed to either optiMEM or prespun medium and cells were grown for a further 24 hours. Exosomes were then isolated from this 24 hour conditioned optiMEM / prespun medium by differential ultracentrifugation (4 x 10 cm plates ~ 15 x 10^6 cells / isolation).

DAKO-Tau immunostaining of transfected SH-SY5Y cells displayed more intense immunoreactivity than in normal, untransfected SH-SY5Y cells (**white arrows; figure 4.11 A**, transfection efficiency ~40 – 60%). Tau12 immunoblot detected a major band migrating at 67 kDa in SH-SY5Y cells transfected with WT-2N4R-Tau / CMA3-2N4R-Tau, consistent with expression of the respective full-length proteins (**black arrow, figure 4.11 B**). Tau12 cross reactivity was detected in the exosomes isolated the conditioned medium of SH-SY5Y cells transiently transfected with WT-2N4R-Tau and CMA3-2N4R-Tau migrating as a major band of 62 kDa and a minor band of 55 kDa. This same pattern of immunoreactivity was observed regardless of growth in optiMEM or prespun growth medium (**upper** and **lower red arrows**, respectively, **figure 4.11 C**). Similar to that observed from SH-SY5Y cells with stable expression of Tau, exosomal Tau12 immunoreactivity from SH-SY5Y cells transiently expressing WT-2N4R-Tau and CMA3-2N4R-Tau was more electrophoretically mobile than the correspondent cellular forms (62 kDa vs. 67 kDa).

There was no difference in the exosomal levels of Tau12 immunoreactivity between SH-SY5Y cells transfected with WT-2N4R-Tau and CMA3-2N4R-Tau, regardless of whether cells were grown in optiMEM or prespun medium (**figure 4.11 D** and **E**, respectively).

These observations suggested that CMA mutations in Tau did not affect its exosomal release.

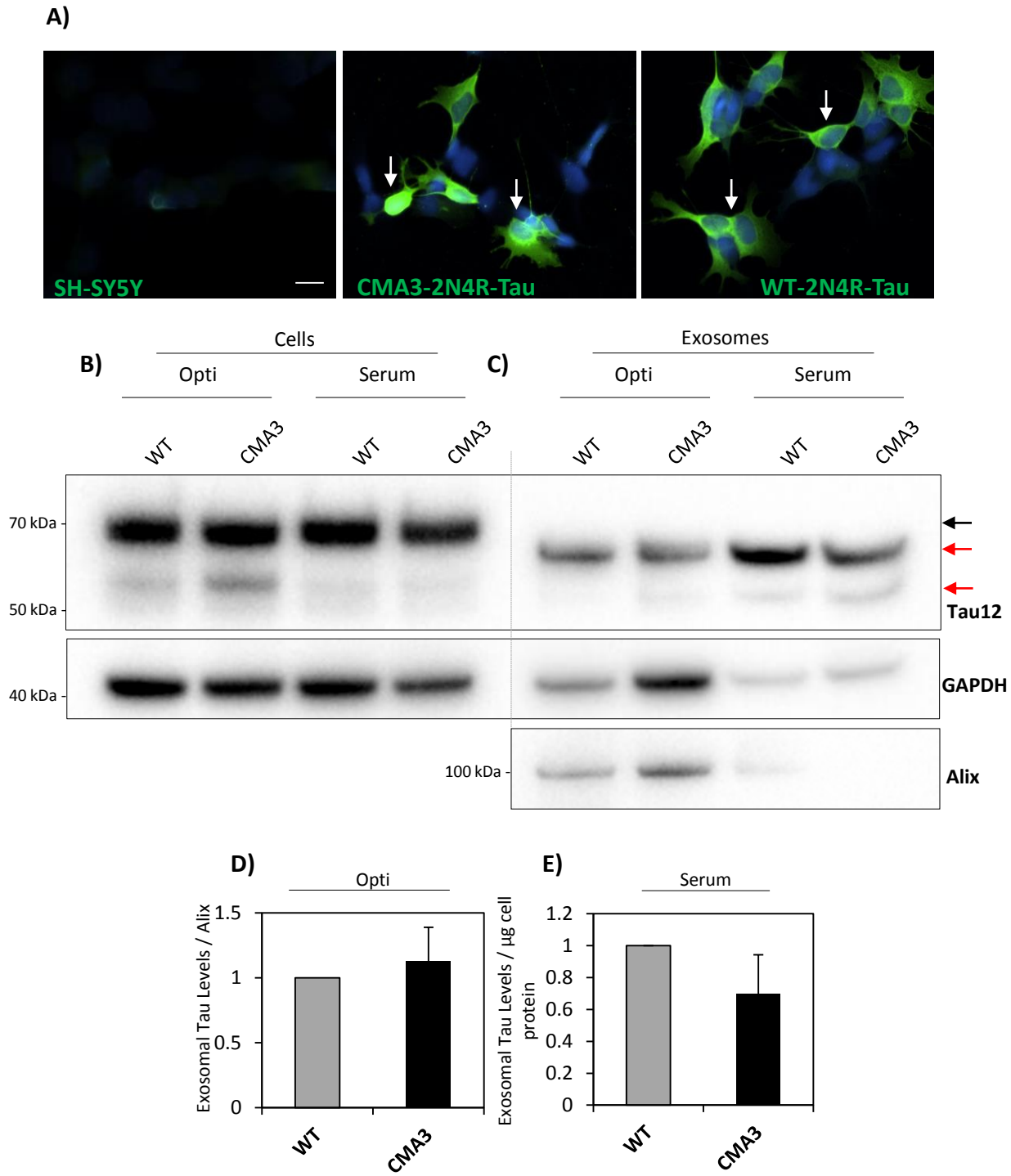

Figure 4.11 Analysis of the exosomal Tau release from SH-SY5Y cells transiently expressing WT-2N4R-Tau and CMA3-2N4R-Tau. A) DAKO Tau immunocytochemical analysis of SH-SY5Y cells electroporated with WT-2N4R-Tau and CMA3-2N4R-Tau (48 hours), alongside untransfected SH-SY5Y cells. **B)** Western blotting analysis of transfected cells (10 µg) and **C)** exosomes (24 hour conditioned medium from 15 x 10^6 cells) from SH-SY5Y cells transiently expressing WT-2N4R-Tau and CMA3-2N4R-Tau. Cells expressed for 48 hours following electroporation, and exosomes were isolated from the conditioned medium of the last 24 hours (either optiMEM – 'Opti' – or prespun –'serum' – growth medium). **D)** Quantification of exosomal WT-2N4R-Tau and CMA3-2N4R-Tau levels isolated from the conditioned optiMEM (expressed relative to Alix; normalised to WT levels, mean ± SEM, n=3) and **E)** prespun medium (expressed relative to cellular protein levels; normalised to WT levels, mean ± SEM, n=2) of transiently expressing SH-SY5Y cells.

4.4.9 Co-IP analysis of DDP301L-2N4R-Tau and Hsc70 interaction

Other residues in Tau have been implicated in Hsc70 interaction, namely two sets of residues which sit inside the hexapeptide motifs – ^{275}VQ**II**NK^{278} and ^{306}VQ**IV**YK^{309} (Sarkar et al. 2008; important residues in **bold**, outline in **Figure 4.12 A**). We obtained a cDNA sequence encoding P301L-2N4R-Tau with a deletion of these two sets of residues, which was termed 'DD-P301L-Tau' (DD = double deletion; confirmed by Sanger sequencing, **figure 4.12 A**).

Alongside this, the CMA3 mutations described above (**figure 4.4**) were inserted into the P301L-2N4R-Tau cDNA backbone to generate CMA3-P301L-Tau.

P301L, DDP301L or CMA3-P301L Tau was transiently co-expressed with Hsc70-V5 in SH-SY5Y cells and 48 hours later cells were lysed and IP'd with DAKO-Tau.

Tau12 and V5 immunoreactivity were detected in the inputs from all samples, migrating at 67 kDa and 72 kDa in SDS-PAGE, respectively, demonstrating expression of Tau and Hsc70-V5 in the respective samples (**figure 4.12 B**). Moreover, the 67 kDa Tau12 immunoreactive band was IP'd from SH-SY5Y cells transfected with P301L, DD-P301L or CMA3-P301L-Tau, consistent with IP of the respective forms of Tau.

V5 immunoreactivity migrating commensurate with Hsc70-V5 (72 kDa) was co-IP'd from SH-SY5Y cells co-transfected with P301L-Tau and Hsc70-V5. However, significantly less 72 kDa V5 immunoreactivity was co-IP'd from SH-SY5Y cells co-transfected with DD-P301L-Tau and Hsc70-V5 (20±11%, mean ± SEM, n=3, p=0.0017, **figure 4.12 C**) suggesting that disruption of the hydrophobic motifs in P301L-Tau impaired association with Hsc70-V5.

CMA3 mutations inserted into P301L-2N4R-Tau, however, did not affect the coIP of Hsc70-V5 immunoreactivity (138% of WT, n=1, **figure 4.12 C**) in contrast to our findings with CMA3 mutations inserted into WT-2N4R-Tau.

These findings suggested that DD mutations in P301L-2N4R-Tau significantly reduced the interaction of Tau and Hsc70 in SH-SY5Y cells. Furthermore, CMA3 mutations, previously demonstrated to disrupt WT-2N4R-Tau – Hsc70 interaction, did not affect the interaction of P301L-2N4R-Tau with Hsc70, however this finding was only n=1, which must be considered when interpreting this result.

4.4.10 Analysis of Tau expression and exosomal Tau release from DDP301L-2N4R-Tau SH-SY5Y cells

Clonal lines with stable ectopic expression of DD-P301L-Tau were generated by transfection of SH-SY5Y cells and selection of G418 resistant colonies. DAKO-Tau immunocytochemical analysis of DDP301L cells demonstrated immunoreactivity in the cytoplasm and neurites of stained cells, in a similar pattern to that detected from P301L-Tau SH-SY5Y cells (**white arrowheads** and **arrows**, respectively, **figure 4.13 A**).

Tau12 Western blotting of DD-P301LTau (c108) SH-SY5Y cells demonstrated a major cross reactive band migrating at 67 kDa and a minor band migrating at 50 kDa (**figure 4.13 C**). Levels of the major Tau12 reactive band did not differ significantly from that detected in P301L-Tau (c102) SH-SY5Y cells (**figure 4.13 C**).

Exosomes were isolated from the 24 hour conditioned optiMEM from P301L-Tau and DDP301L-Tau SH-SY5Y cells by differential ultracentrifugation (5 x 10 cm plates). Western blotting demonstrated the presence of a Tau12 cross reactive band migrating at 65 kDa in the exosomes from both SH-SY5Y populations (**figure 4.13 D**). Quantification revealed that exosomal Tau levels from DDP301L-Tau SH-SY5Y cells were 0.6±0.2 and 0.86±0.2 times that of levels from P301L-Tau SH-SY5Y cells, when expressed against cellular protein and exosomal Alix levels, respectively (mean ± SEM, n=3, **figure 4,13 E, figure 4.13 F**). Statistical analysis (Student's T-test) indicated that the DD mutations did not significantly affect the levels of exosomal Tau release.

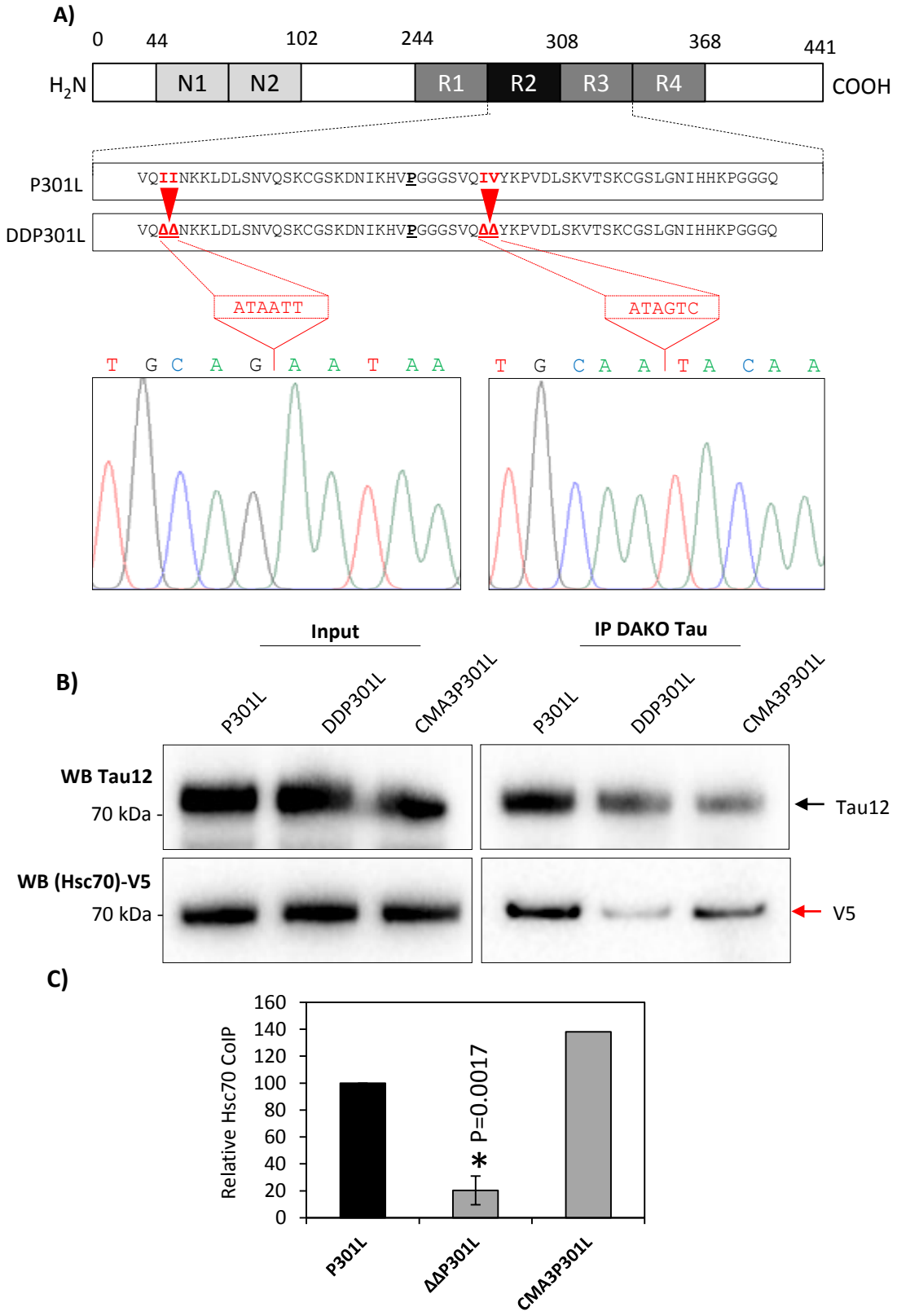

Figure 4.12 Co-immunoprecipitation analysis of P301L-2N4R-Tau – Hsc70 interaction and role of hydrophobic motifs. A) Schematic diagram of P301L-2N4R-Tau showing hydrophobic motifs important for interaction of Tau with Hsc70: ^{277}II^{278} and ^{308}IV^{309} in red (Sarkar et al., 2008). These motifs were deleted by deletion of the underlying genetic code, as shown in the chromatogram (confirmed by Sanger sequencing). The mutated form of the protein was termed 'DD-P301L-Tau' ('DD' = double deletion). **B)** DAKO-Tau immunoprecipitation and Western blot analysis of SH-SY5Y cells transiently co-transfected with Hsc70-V5 and P301L, DD-P301L or CMA3-P301L (electroporated for 48 hours). Immunoprecipitated proteins were analysed by immunoblotting with Tau12 and V5 antibodies. Black and red arrows indicate IP'd Tau12 and co-IP'd V5 cross-reactive species, respectively (1/40th of the input and all of the IP eluate from 15 x 10^6 cells was loaded). **C)** Quantification of V5 immunoreactivity levels co-IP'd with P301L, DD-P301L and CMA3-P301L (mean ± SEM, DDP301L n=3, CMA3P301L n=1, V5 levels expressed relative to IP'd Tau12 levels and normalised to 'P301L'; Student's T-test).

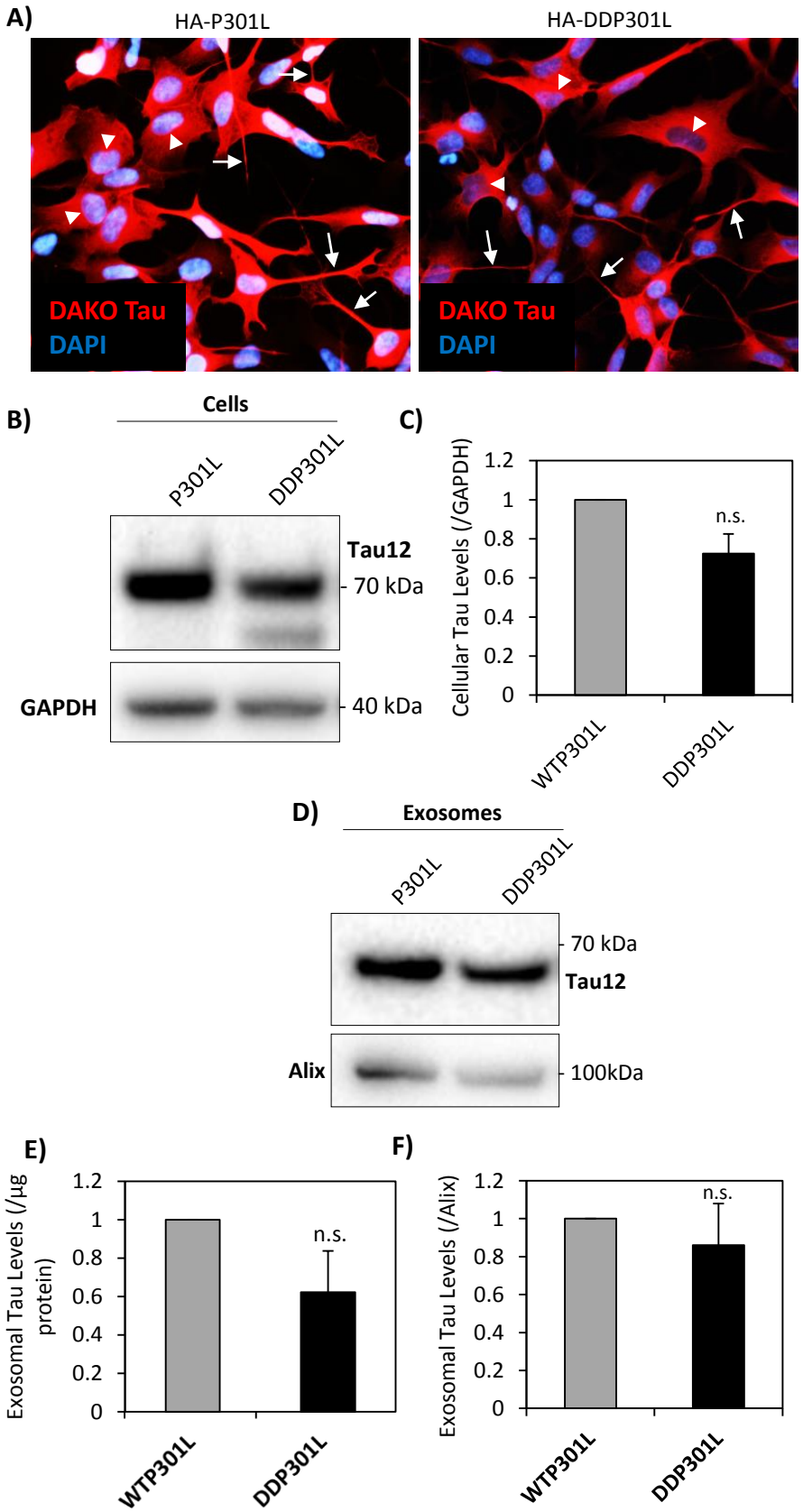

Figure 4.13 Characterisation of SH-SY5Y cells stably expressing DD-P301L-Tau and analysis of exosomal Tau release from DD-P301L-Tau SH-SY5Y cells. A) DAKO-Tau immunocytochemical analysis of SH-SY5Y cells stably expressing HA-3P10L-2N4R (c2) and DDP301L-2N4R-Tau. White arrows and arrowheads indicate neuritic and cytoplasmic staining, respectively. **B)** Western blot analysis of stably expressed P301L and DDP301L-2N4R-Tau (20 µg cellular protein loaded / lane). **C)** Quantification of Tau expression levels in P301L and DDP301L-2N4R-Tau. Values are expressed relative to GAPDH and normalised to P301L levels (mean ± SEM, n=3, Student's T-test). **D)** Western blot analysis of exosomes isolated from the 24 hour conditioned optiMEM of SH-SY5Y stably expressing P301L-2N4R-Tau and DDP301L-2N4R-Tau (5 x 10 cm / lane). **E)** Quantification of exosomal P301L and DD-P301L-Tau levels. Values are expressed relative to µg cellular protein and **F)** exosomal Alix and normalised to P301L levels (mean ± SEM, n=3, Student's T-test).

4.5 Analysis of the effects of DNAjC5 expression on exosomal Tau release

We next investigated the role of the Hsc70 co-chaperone DNAjC5 in the exosomal release of Tau protein.

4.5.1 Effect of DNAjC5 on steady state Tau levels WT-2N4R-Tau SH-SY5Y cells

DNAjC5-FLAG was transiently expressed in WT-2N4R-c103 SH-SY5Y cells for 48 hours and expression was analysed by Western blotting and ICC. In cellular lysates, FLAG immunoreactivity was detected as major and minor bands migrating at 30 kDa and 60 kDa, respectively, consistent with monomeric and dimeric forms of DNAjC5 (bands '**A**' and '**B**', respectively, **figure 4.14 A**)

Levels of the 67 kDa major Tau12 cross reactive band from 2N4Rc103 SH-SY5Y cells were unaffected by DNAjC5 expression (**figure 4.14 A** and **B**).

ICC analysis demonstrated that mock transfected (pcDNA3.1) 2N4Rc103 SH-SY5Y cells exhibited no FLAG staining, whereas 50% of DNAjC5 transfected 2N4Rc103 SH-SY5Y cells demonstrated intense FLAG staining 48 hours after transfection and no FLAG staining was detected in mock (pcDNA3.1) transfected cells. We noted the appearance of FLAG positive 2N4Rc103 SH-SY5Y cells that exhibited relatively less intense DAKO-Tau staining than surrounding, untransfected cells (**arrow**, **figure 4.15 A**). We plotted the intensities of DAPI, DAKO-Tau and FLAG staining along line segments drawn through several nuclei of ICC images of mock and DNAjC5 transfected cells (ImageJ software). Cells were elucidated in this analysis by DAPI peaks (**grey line, figure 4.15 B**). Mock transfected cells did not show FLAG staining above background levels, however DAKO-Tau staining was heterogeneous with some cells exhibiting less intense staining (**arrow**, top graph, **figure 4.15 B**). DNAjC5 transfected 2N4Rc103 SH-SY5Y cells also exhibited some cells with low intensity DAKO-Tau staining, some of which did not co-stain with FLAG (transfection efficiency ~50%; **arrow**, bottom graph, **figure 4.15 B**). However there were a preponderance of low intensity DAKO-

Tau stained 2N4Rc103 SH-SY5Y cells, that exhibited high intensity FLAG immunostaining (**asterisks**, **figure 4.15 B**), supporting our visual analysis. These findings suggested that individual 2N4Rc103 SH-SY5Y cells transfected with DNAjC5 may have had lower levels of Tau expression, despite DNAjC5 expression having no impact on the global levels of Tau expression in 2N4Rc103 SH-SY5Y cells (**figure 4.14 B**).

4.5.2 Effect of DNAjC5 expression on total and exosomal Tau release from 2N4Rc103 SH-SY5Y cells

24 hour conditioned optiMEM from WT-2N4R-c103 SH-SY5Y cells transiently transfected with DNAjC5 was analysed by dot-blotting ($1/10^{th}$ - 200 µl of the medium from 500,000 cells). Tau12 immunoreactivity was detected in the conditioned medium from all cells, levels of which was increased by DNAjC5 expression by 1.7±0.4 times (mean ± SEM, n=3, *p*=0.05, **figure 4.16 B**). LDH activity in the medium from the same cells was unaffected by DNAjC5 expression suggesting a specific effect on promoting Tau secretion, and not passive release depending on cell death (**figure 4.15 C**).

Exosomes were isolated from the 24 hour conditioned optiMEM (4 x 10 cm, ~15 x 10^6 cells) from DNAjC5 transfected WT-2N4R-Tau c103 SH-SY5Y cells, and exosomal Tau was analysed by Tau12 immunoblotting. A major Tau12 immunoreactive band migrating at 62 kDa was detected in the exosomes from mock and DNAjC5 transfected cells. Levels of this band were increased 2.2±0.3 times with DNAjC5 expression, when expressed relative to cellular protein (mean ± SEM, n=3, *p*=0.0098, **figure 4.16 E**). When expressed relative to exosomal Alix levels the increase was more modest and variable at 1.9±0.57 times (mean ± SEM, n=3, *p*=0.27, **figure 4.16 F**) which may have been due to effects of DNAjC5 on exosomal Alix levels, which were variably increased by DNAjC5 expression (1.9±0.5 times, **figure 4.15 G**). Overall these results demonstrated that DNAjC5 increased total and exosomal Tau release from 2N4Rc103 SH-SY5Y cells.

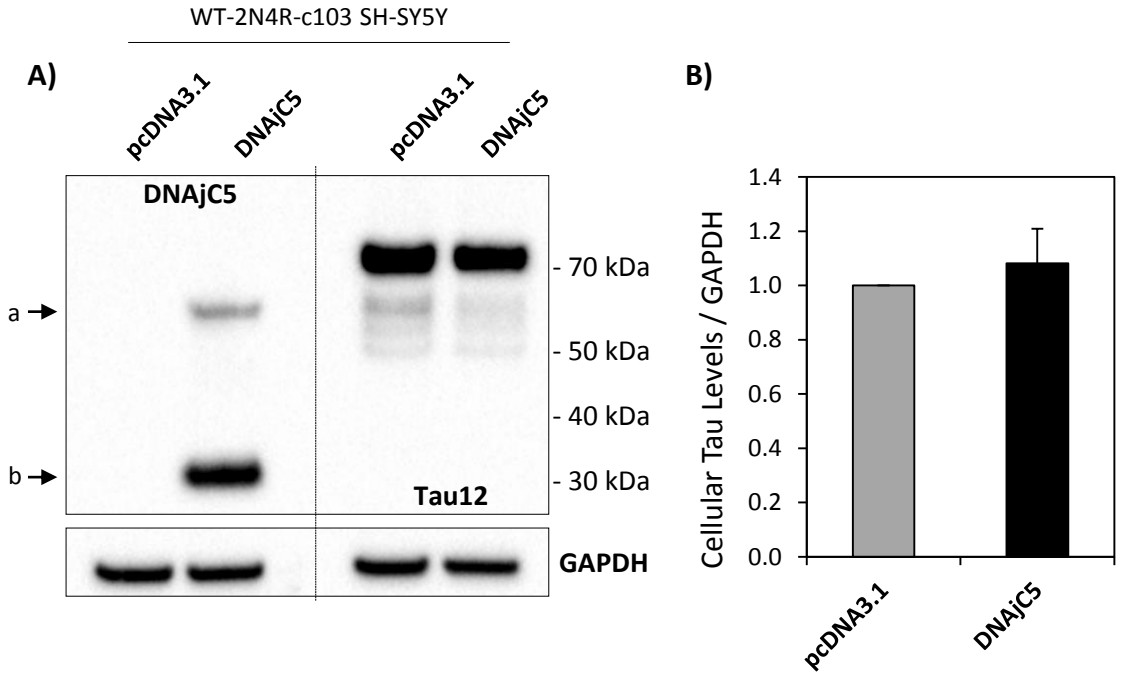

Figure 4.14 Analysis of the effects of DNAjC5 expression on steady state Tau levels in WT-2N4R-Tau SH-SY5Y cells. A) Western blot analysis of WT-2N4R-c103 SH-SY5Y cells transfected with DNAjC5 (electroporation, 48 hours; 20 µg loaded /lane) with FLAG antibody (left side) and Tau12 (right side). Lower and upper arrows indicate major and minor FLAG cross-reactive bands, respectively. **B)** Quantification of Tau expression levels from WT-2N4R-c103 SH-SY5Y transiently expressing DNAjC5 (48 hr). Values expressed relative to GAPDH and normalised to pcDNA3.1 control transfection (mean ± SEM, n=3, 20 µg cellular protein loaded).

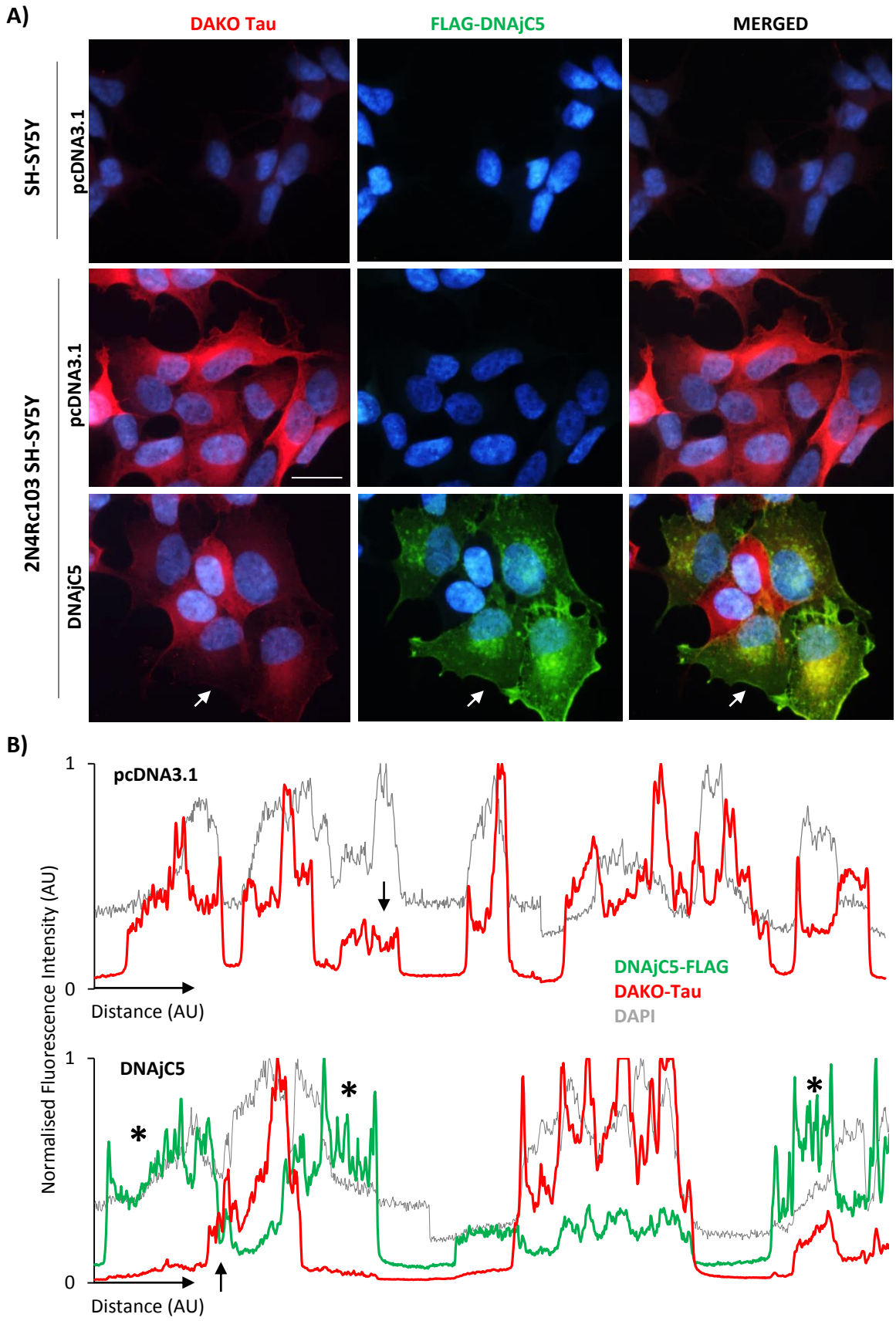

Figure 4.15 DAKO-Tau and FLAG co-immunostaining analysis of WT-2N4R-c103 SH-SY5Y cells transiently transfected with DNAjC5-FLAG. A) DAKO-Tau (red) and FLAG (green) co-immunostaining analysis of WT-2N4R-c103 SH-SY5Y cells transiently expressing DNAjC5 (48 hours). Arrow indicates a strong FLAG reactive and weak DAKO-Tau co-reactive cell. **B)** Fluorescence intensity profiles of DAKO-Tau and DAPI staining in pcDNA3.1 transfected WT-2N4R-c103 SH-SY5Y cells, and DAPI, DAKO-Tau and FLAG staining in DNAjC5 transfected WT-2N4R-c103 SH-SY5Y cells. Peaks are plotted by integration of intensity through lines of the ICC images. Arrows indicate profiles of untransfected cells with low intensity Tau staining, and asterisks indicate DNAjC5 transfected cells with low intensity Tau staining.

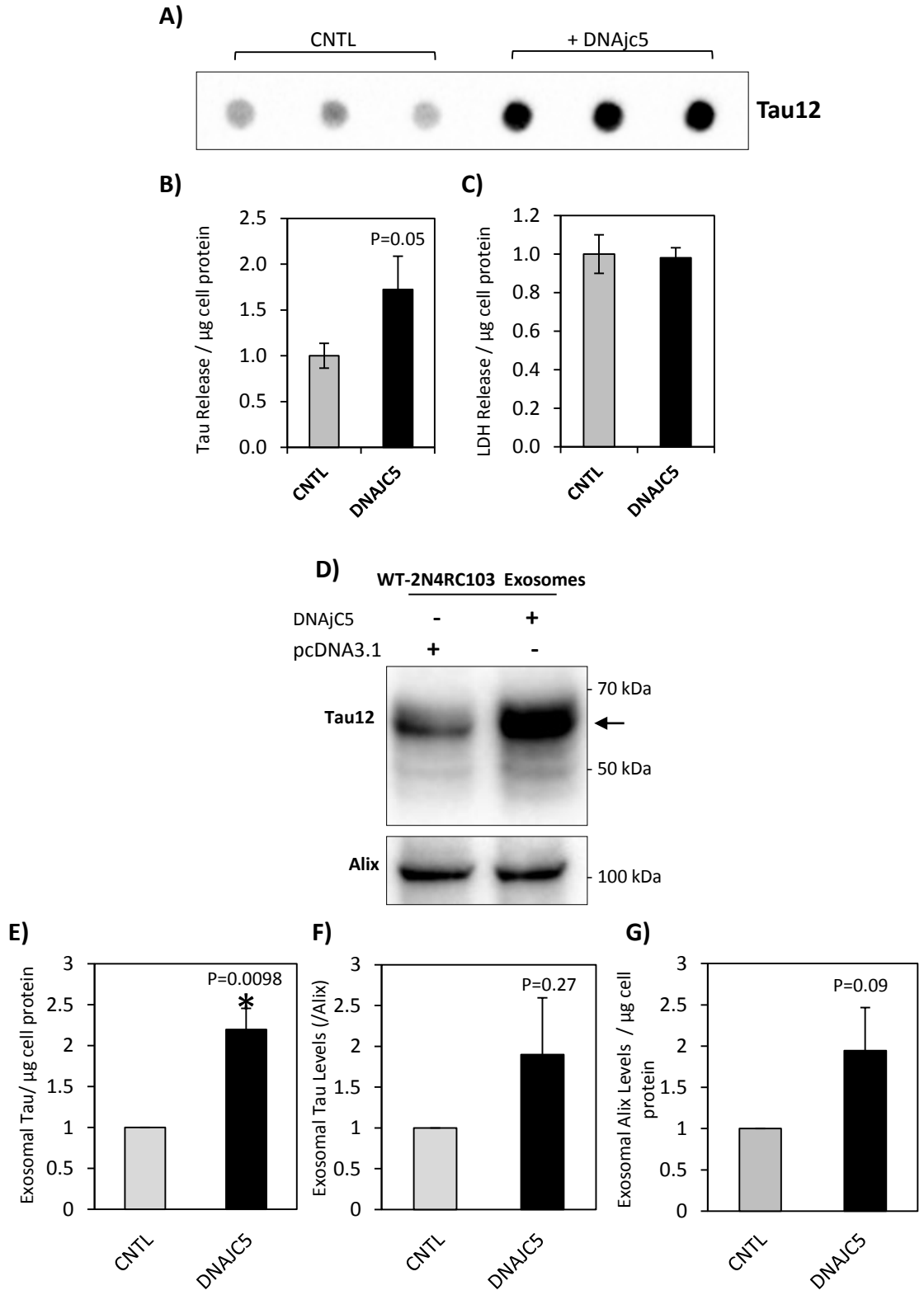

Figure 4.16 Analysis of the effects of DNAjC5 expression on total and exosomal Tau release from WT-2N4R-Tau SH-SY5Y cells. A) Dot blot analysis of 24 hour conditioned optiMEM from control and DNAjC5 transfected 2N4Rc103 SH-SY5Y cells (200 µl ≈ 1/10th of the conditioned medium from 6 well plate / dot). **B)** Quantification of Tau secretion from WT-2N4R-c103 SH-SY5Y cells transiently expressing DNAjC5, levels are expressed relative to cellular protein and normalised to control transfection mean (mean ± SEM, 3 technical replicates, Student's T-test). **C)** Quantification of LDH activity in the medium of control and DNAjC5 transfected cells, levels are expressed per ml relative to cellular protein and normalised to control mean (mean ± SEM, 3 technical replicates). **D)** Western blot analysis of exosomes isolated from WT-2N4R-c103 SH-SY5Y cells transiently expressing DNAjC5. DNAjC5 expressed for 48 hours and exosomes isolated from the conditioned optiMEM of the last 24 hours expression from ~15 x 10^6 cells. **E)** Quantification of exosomal Tau levels from WT-2N4R-c103 cells transiently expressing DNAjC5. Levels expressed relative to cellular protein levels and **F)** exosomal Alix levels, normalised to control transfection (pcDNA3.1) levels (mean ± SEM, n=3, Student's T-test). **G)** Quantification of exosomal Alix levels from SH-SY5Y cells transiently expressing DNAjC5 . Levels are expressed relative to cellular protein and normalised to control transfection levels (mean ± SEM, n=8).

4.5.3 Effect of DNAjC5 expression on steady state Tau levels and exosomal Tau release in DDP301L-2N4R-Tau SH-SY5Y cells

To explore the role of Tau – Hsc70 interaction in DNAjC5 mediated exosomal Tau release, DNAjC5-FLAG was transiently expressed in P301L and DDP301L SH-SY5Y cells for 48 hours. A 30 kDa specific FLAG immunoreactive band was detected in the transfected cell lysates, consistent with expression of monomeric DNAJC5-FLAG. Levels of the 67 kDa Tau12 immunoreactive band from both P301L-Tau and DD-P301L-Tau SH-SY5Y cells were unaffected by DNAjC5-FLAG expression demonstrating that DNAjC5 expression did not affect global Tau expression levels in either cell population (**figure 4.17 A** and **B**).

By ICC, DNAjC5 transfected cells displayed strong FLAG immunoreactivity which was not detected in mock transfected cells. FLAG staining was detected throughout the cytoplasm and neurites of the cells. Transfection efficiency for P301L-Tau and DD-P301L-Tau SH-SY5Y cells was 28% and 40%, respectively. Similar to that observed in 2N4Rc103 SH-SY5Y cells, FLAG expression in P301L-Tau SH-SY5Y cells associated with cells with low intensity DAKO-Tau staining (**white arrows, figure 4.17 C**) whereas FLAG immunoreactive DD-P301L-Tau SH-SY5Y cells also displayed colocalisation with high intensity DAKO-Tau immunostaining (**white arrowheads, figure 4.17 C**).

The intensities of DAKO-Tau and FLAG immunostaining across line segments drawn through several nuclei of ICC images from DNAjC5 transfected P301L and DD-P301L-2N4R-Tau SH-SY5Y cells were plotted. As observed with WT-2N4R-Tau c103 SH-SY5Y cells, P301L-2N4R-Tau SH-SY5Y cells with intense FLAG immunostaining demonstrated low intensity DAKO-Tau immunostaining (**arrows**, top graph, **figure 4.18 B**). Although some DNAjC5 transfected P301L-2N4R-Tau SH-SY5Y cells demonstrated high immunostaining with both DAKO-Tau and FLAG antibodies (**asterisks**, top graph, **figure 4.18 B**) there were a preponderance of cells with this pattern of immunostaining observed in the DNAjC5 transfected DD-P301L-

2N4R-Tau SH-SY5Y cells (**asterisks**, bottom graph, **figure 4.18 B**). These findings suggested that at the single cell level, DNAjC5 expression differentially affected the pattern of DAKO-Tau immunoreactivity from P301L-2N4R-Tau and DD-P301L-2N4R-Tau SH-SY5Y cells, despite having no effects on the global levels of expression of Tau in either cell population.

Exosomes were isolated from the 24 hour conditioned optiMEM of P301L-Tau and DDP301L SH-SY5Y cells transiently transfected with DNAjC5-FLAG demonstrated major Tau12 cross reactivity at 62 kDa. The levels of this band detected from P301L-Tau SH-SY5Y exosomes was increased with DNAjC5-FLAG expression by 2.4±0.5 times (mean ± SEM, n=2). Levels of Tau12 immunoreactivity detected in exosomes from DD-P301L-Tau SH-SY5Y exosomes, however, were unaffected by DNAjC5-FLAG expression (0.7±0.4 times mean ± SEM, n=2; **figure 4.19 A** and **B**)

Collectively these results demonstrated that DNAjC5-FLAG expression potentiated exosomal Tau release from WT-2N4R-Tau and P301L-2N4R-Tau SH-SY5Y cells. On the other hand, DNAjC5-FLAG expression did not affect exosomal Tau release from DD-P301L-2N4R-Tau SH-SY5Y cells.

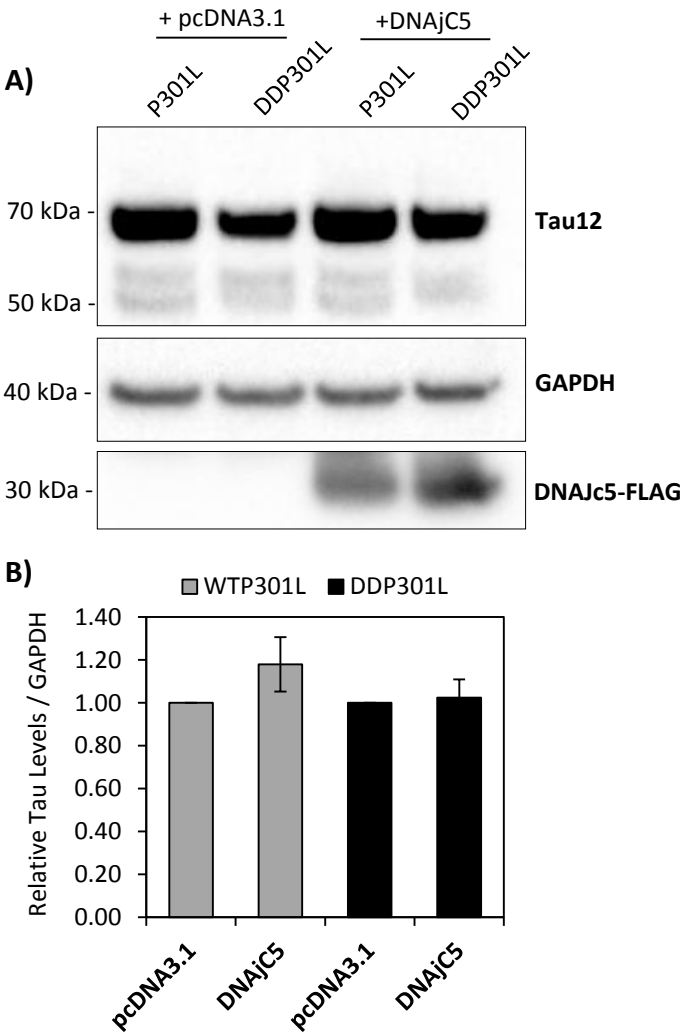

Figure 4.17 Analysis of the effects of transient DNAjC5 expression on steady state Tau levels in P301L-2N4R-Tau and DDP301L-2N4R-Tau SH-SY5Y cells. **A)** Western blot analysis of P301L and DD-P301L SH-SY5Y cells transiently transfected with DNAjC5 (48 hour electroporation, 20 µg / lane). B) Quantification of steady state Tau levels in DNAjC5 transfected P301L / DD-P301L SH-SY5Y cells. Values are expressed relative to GAPDH and normalised to the control transfection for each construct (mean ± SEM, n=3, no significant differences, Student's T-test).

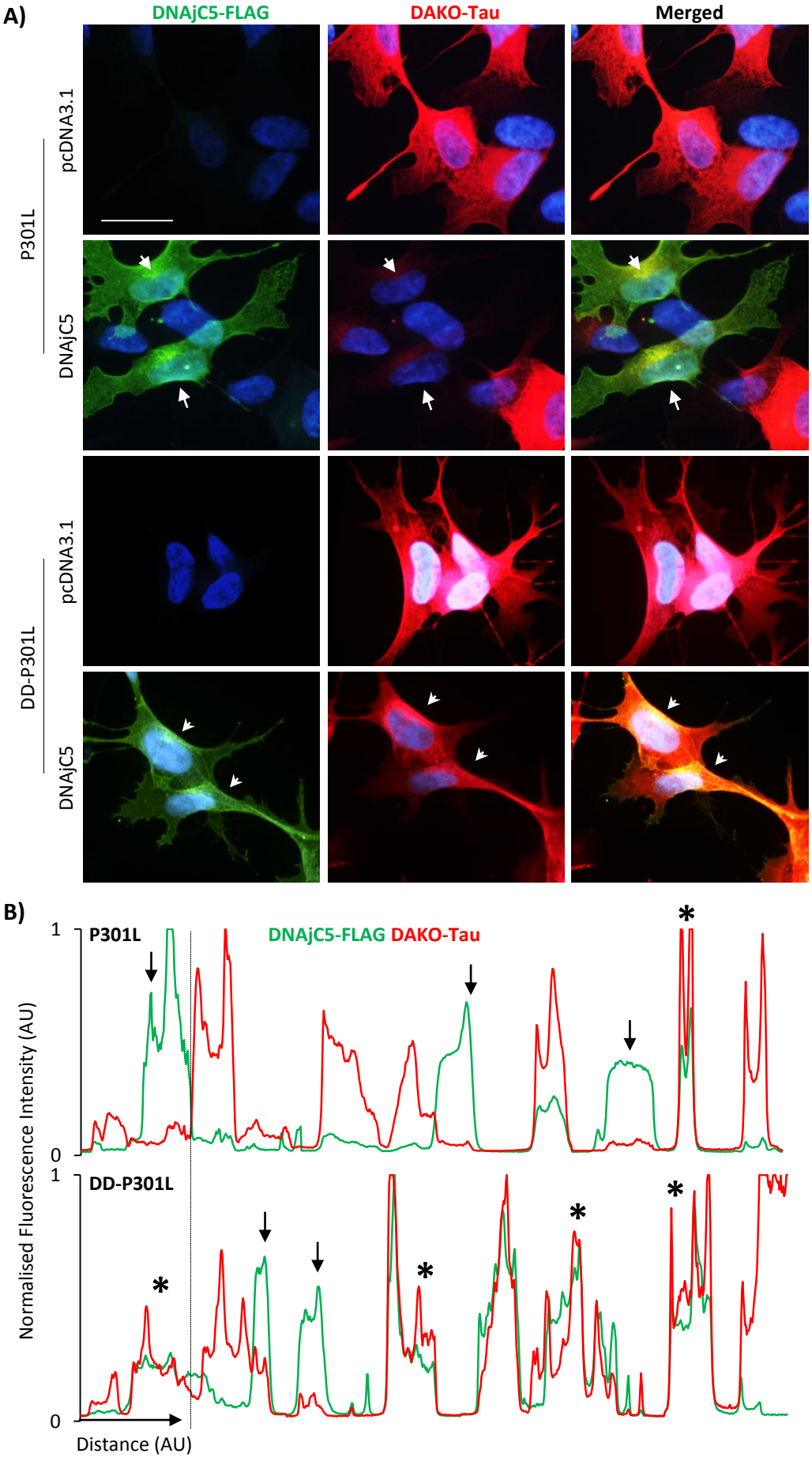

Figure 4.18 DAKO-Tau and FLAG co-immunostaining analysis of P301L-2N4R-Tau and DD-P301L-2N4R-Tau SH-SY5Y cells transiently transfected with DNAjC5-FLAG. A) ICC analysis of mock (pcDNA3.1) and DNAjC5 transfected P301L/DD-P301L-Tau SH-SY5Y cells. **B)** Intensity profiles of DAKO-Tau (red) and FLAG (green) fluorescence through lines of ICC images of DNAjC5 transfected P301L/DD-P301L-Tau SH-SY5Y cells. Peaks represent individual cell (as indicated by the black dashed line). Arrows indicate cells with low DAKO-Tau and high FLAG intensity, and asterisks indicate cells with high DAKO-Tau and high FLAG intensity.

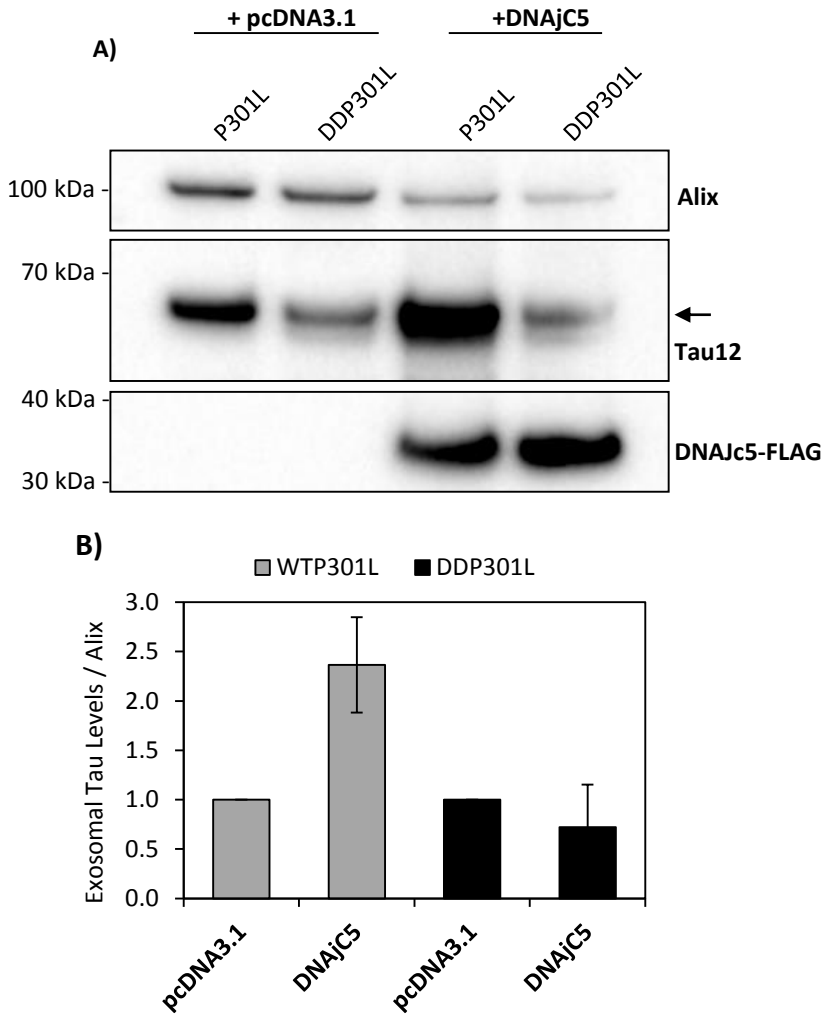

Figure 4.19 Analysis of the effects of transient DNAjC5 expression on exosomal Tau release from P301L and DD-P301L Tau SH-SY5Y cells. A) Western blot analysis of exosomes isolated from P301L and DD-P301L Tau expressing SH-SY5Y cells transiently transfected with DNAjC5 (electroporation for 48 hours, exosomes harvested from the conditioned optiMEM of the last 24 hours of expression; 15 x 10^6 cells; arrow indicates major Tau12 reactive band). **B)** Quantification of exosomal P301L and DD-P301L Tau levels from SH-SY5Y cells transiently expressing DNAjC5. Values are expressed relative to Alix and normalised to control transfection (mean ± SEM, n=2).

4.5.4 Effect of DNAjC5 expression on exosomal Tau release from CMA3-2N4R-Tau SH-SY5Y cells

We next investigated whether DNAjC5 mediated exosomal Tau release was dependent upon Tau – Hsc70 interaction via Tau's CMA motifs. DNAjC5-FLAG was transiently expressed in CMA3-2N4R SH-SY5Y cells (stably expressing CMA3-Tau) for 48 hours. A FLAG cross reactive band migrating at 30 kDa was detected in the CMA3-2N4R-Tau SH-SY5Y cells transfected with DNAjC5-FLAG, consistent with the expression of DNAjC5 monomer in these cells (**figure 4.20 A**).

During the last 24 hours of DNAjC5-FLAG expression (48 hours total), CMA3-2N4R-Tau SH-SY5Y cells were cultured in optiMEM from which exosomes were isolated. A major 62 kDa Tau12 cross reactive band was detected in the exosomes from mock transfected and DNAjC5-FLAG transfected cells. The intensity of this band was increased 3.4 X and 1.4 X relative to cellular protein and exosomal Alix levels, respectively, in the presence of DNAjC5-FLAG expression (**figure 4.20 B** and **C**).

DNAjC5-FLAG expression therefore promoted exosomal Tau release from CMA3-2N4R-Tau SH-SY5Y cells, which suggested that DNAjC5 mediated exosomal Tau release occurred independently of the CMA motifs in Tau.

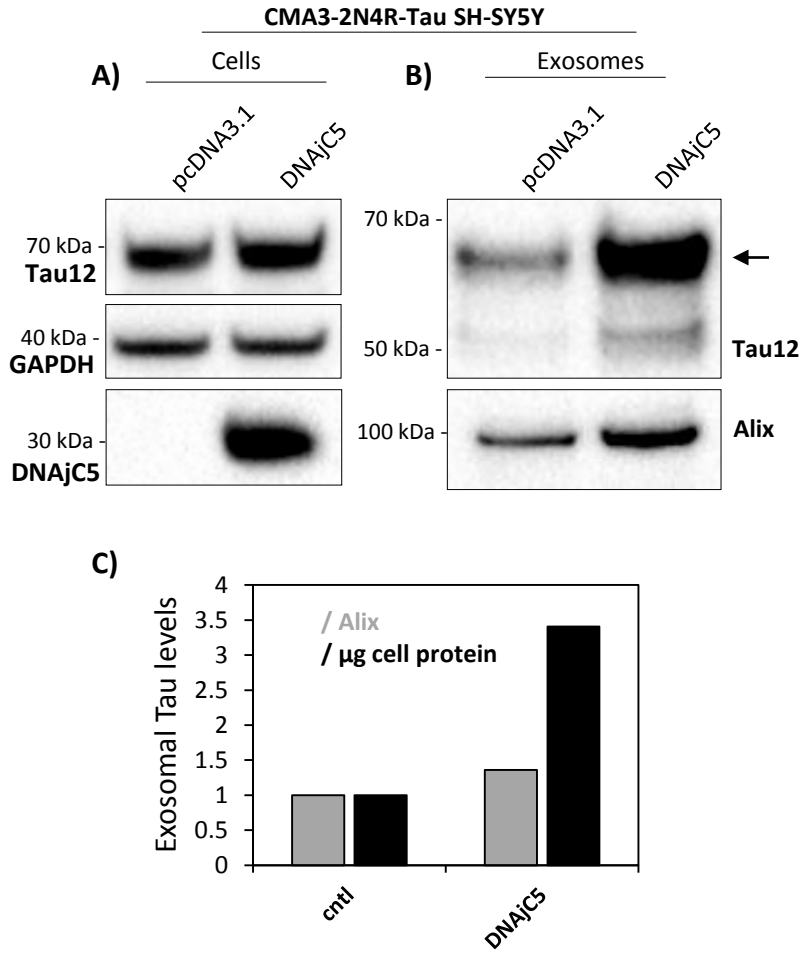

Figure 4.20 Analysis of the effects of transient DNAjC5 expression on the exosomal release of Tau from CMA3-2N4R-Tau SH-SY5Y cells. A) Western blot analysis of cell lysates (20 µg) and **B)** exosomes (24 hour conditioned optiMEM from 15 x 10^6 cells) from CMA3-2N4R-Tau SH-SY5Y cells transiently expressing DNAjC5 (electroporation for 48 hours, exosomes isolated during the last 24 hours; arrow indicates major Tau12 reactive band). **B)** Quantification of exosomal CMA3-2N4R-Tau levels with transient DNAjC5 expression. Values are expressed relative to Alix (grey bars) and cellular protein (black bars) and normalised to control transfection levels (n=1).

4.6 Analysis of the role of SUMOylation in the exosomal release of Tau

4.6.1 Analysis of Tau SUMOylation in HEK293 cells

SUMOylation of proteins has been identified as an exosomal sorting determinant (Kunadt et al. 2016). Tau protein has been reported to undergo SUMOylation (Dorval & Fraser. 2006; Luo et al. 2014) so we therefore aimed to investigate the role of SUMOylation in the exosomal release of Tau protein from SH-SY5Y cells.

The primary amino acid sequence and secondary structure of SUMO-1 are displayed in **figure 4.21 A**. We adopted a nickel purification methodology to study proteins SUMOylated by ectopically expressed SUMO-1-His in HEK293 cells (methods **2.25**; Dorval & Fraser. 2006). In order to characterise their cross-reactivity profiles, SUMO-1-His and WT-2N4R-Tau were transiently transfected (separately) in HEK293 cells. SUMO-1 and Tau12 immunoblot demonstrated specific cross reactivity at 15 kDa and 67 kDa, respectively, consistent with monomeric SUMO-1-His and full-length WT-2N4R-Tau expression in the respectively transfected cells (**figure 4.21 B**).

After 48 hours of expression, SUMO-1-His transfected HEK293 cells were lysed and nickel precipitated (Ni-NTA beads – Qiagen) to concentrate SUMO-1-His and conjugated (SUMOylated) proteins. SUMO-1 Western blot of Ni-NTA precipitated lysates demonstrated a SUMO-1 cross reactive band migrating at 15 kDa and diffuse cross reactivity migrating at higher molecular weights, consistent with the pulldown of SUMO-1-His monomer and SUMOylated proteins, respectively (**arrow** and **bracket**, respectively, **figure 4.21 C**) thereby demonstrating the SUMOylation of proteins with ectopic SUMO-1-His in HEK293 cells.

HEK293 cells (co)-transfected with varying combinations WT-2N4R-Tau and SUMO-1-His (48 hours) were lysed and His-tagged proteins were Ni-NTA purified. A 67 kDa Tau12 cross reactive band was detected in the lysates of WT-2N4R-Tau transfected and WT-2N4R-Tau / SUMO-1-His co-transfected cells (band '**b**', **figure 4.21 D**). A co-migrating band was

detected in the Ni-NTA pulldown of HEK293 cells transfected with only WT-2N4R-Tau. The pulldown of this 67 kDa band was suggested as non-specific, as these cells expressed no His-tagged proteins. However, an 80 kDa Tau12 cross reactive band was detected in the NiNTA pulldown from HEK293 cells co-transfected with WT-2N4R-Tau and SUMO-1-His. The migration of this band was consistent with the conjugation of SUMO-1 to 2N4R-Tau (67 kDa + 15 kDa ≈ 80 kDa). Moreover, this band was not detected in the NiNTA pulldown of HEK293 cells transfected with WT-2N4R-Tau and was thus consistent with SUMOylated 2N4R-Tau protein (band '**a**' **figure 4.21 D**). This finding confirmed the SUMOylation of WT-2N4R-Tau protein by SUMO-1-His.

4.6.2 Analysis of the SUMOylation of K340R-2N4R-Tau

Previous report identified K340 as they key SUMOylation site in Tau protein (Dorval & Fraser. 2006; Luo et al. 2014). Site directed mutagenesis was used to mutate K340>R and the sequence was confirmed by Sanger sequencing, the mutated protein was termed 'K340R-2N4R-Tau' (**figure 4.21 E**). WT-2N4R-Tau or K340R-2N4R-Tau were co-transfected with SUMO-1-His into HEK293 cells. DAKO-Tau and SUMO-1 co-immunostaining of co-transfected cells revealed positive immunostaining in the respective channels (**figure 4.22 A**). Moreover, SUMO-1 and DAKO-Tau immunoreactivity were generally co-expressed in the same cells. However the proteins exhibited different sub-cellular localisations; SUMO-1 immunoreactivity was predominantly nuclear, whilst DAKO-Tau staining was detected primarily in the cytoplasm (**figure 4.22 A**). HEK293 cells are small cells, and Tau expression generally filled the extent of the cytoplasm which appeared in some cells as a small ring around the nucleus, whilst in others as a structure with numerous protrusions (**asterisks** and **plus** symbol, respectively, **figure 4.22 A**).

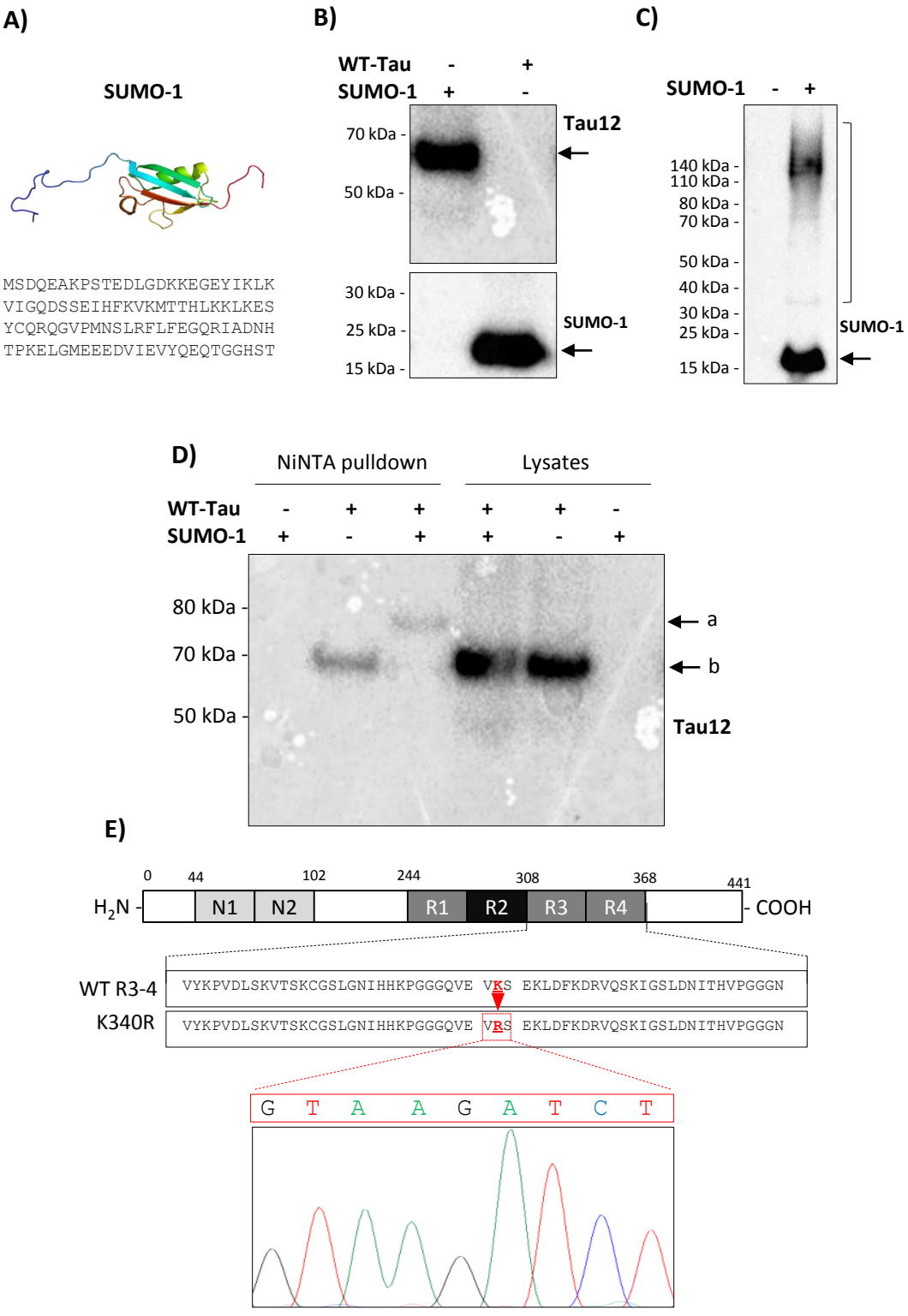

Figure 4.21 Analysis of Tau SUMOylation in HEK293 cells and generation of K340R-Tau mutant. A) SUMO-1 ribbon structure and primary amino acid sequence. **B)** Western blot analysis of HEK293 cells transiently transfected with WT-2N4R-Tau or SUMO-1-His (20 µg / lane). **C)** SUMO-1 western blotting of NiNTA pulldowns from HEK293 cells transiently expressing WT-2N4R-Tau (left lane) and SUMO-1-His (right lane). Arrow and bracket indicate SUMO-1 immunoreactivity consistent with SUMO-1-His monomer and SUMOylated proteins, respectively. **D)** Western blotting analysis of NiNTA pulldown from HEK293 lysates with transient WT-2N4R-Tau and SUMO-1-His expression. Upper and lower arrows indicate SUMOylated and and non-SUMOylated Tau12 cross-reactive bands, respectively. **E)** Schematic representation of 2N4R-Tau with lysine (K)340 in red. Sequence following mutagenesis of K340>R is shown beneath, with chromatogram confirming correct sequence of cDNA. The mutated form of the protein was termed 'K340R' Tau.

There was no difference in the levels of the 67 kDa Tau12 cross-reactive band detected from lysates of HEK293 cells (co)-transfected with WT-2N4R-Tau or K340R-2N4R-Tau (and SUMO-1-His) (**figure 4.22 B** and **D**). Moreover, a SUMO-1 cross reactive band consistent with the SUMO-1-His monomer was detected from both sets of cells (**figure 4.22 B**). This demonstrated the expression of the SUMO-1-His and 2N4R-Tau proteins in respectively transfected cells (**figure 4.22 B**).

NiNTA purification of SUMO-1 – WT-2N4R-Tau / K340R-2N4R-Tau co-transfected HEK293 cell lysates demonstrated SUMO-1 cross reactivity in SDS-PAGE, with the detection of protein bands consistent with SUMO-1-His monomer (15 kDa) and SUMOylated protein (>15 kDa). The pattern of SUMO-1 cross reactivity was similar between both sets of cells (**figure 4.22 Ci**).

Tau12 immunoblotting of the NiNTA pulldown revealed a cross reactive band migrating at 80 kDa, consistent with SUMO-1-His-2N4R-Tau from the lysates of HEK293 cells co-transfected with WT-2N4R-Tau and SUMO-1-His. A co-migrating Tau12 cross reactive band was also detected in the NiNTA pulldown from HEK293 cells co-transfected with K340R-2N4R-Tau and SUMO-1-His (**figure 4.22 Cii**). However, the intensity of this 80 kDa Tau12 cross reactive band (SUMO-Tau) was significantly reduced in HEK293 cells co-transfected with K340R-2N4R-Tau and SUMO-1-His, confirming that the level of SUMOylation of K340R-2N4R-Tau was reduced relative to that of WT-2N4R-Tau (28.7±11%, mean ± SEM, n=3, p=0.0034, **figure 4.22 E).**

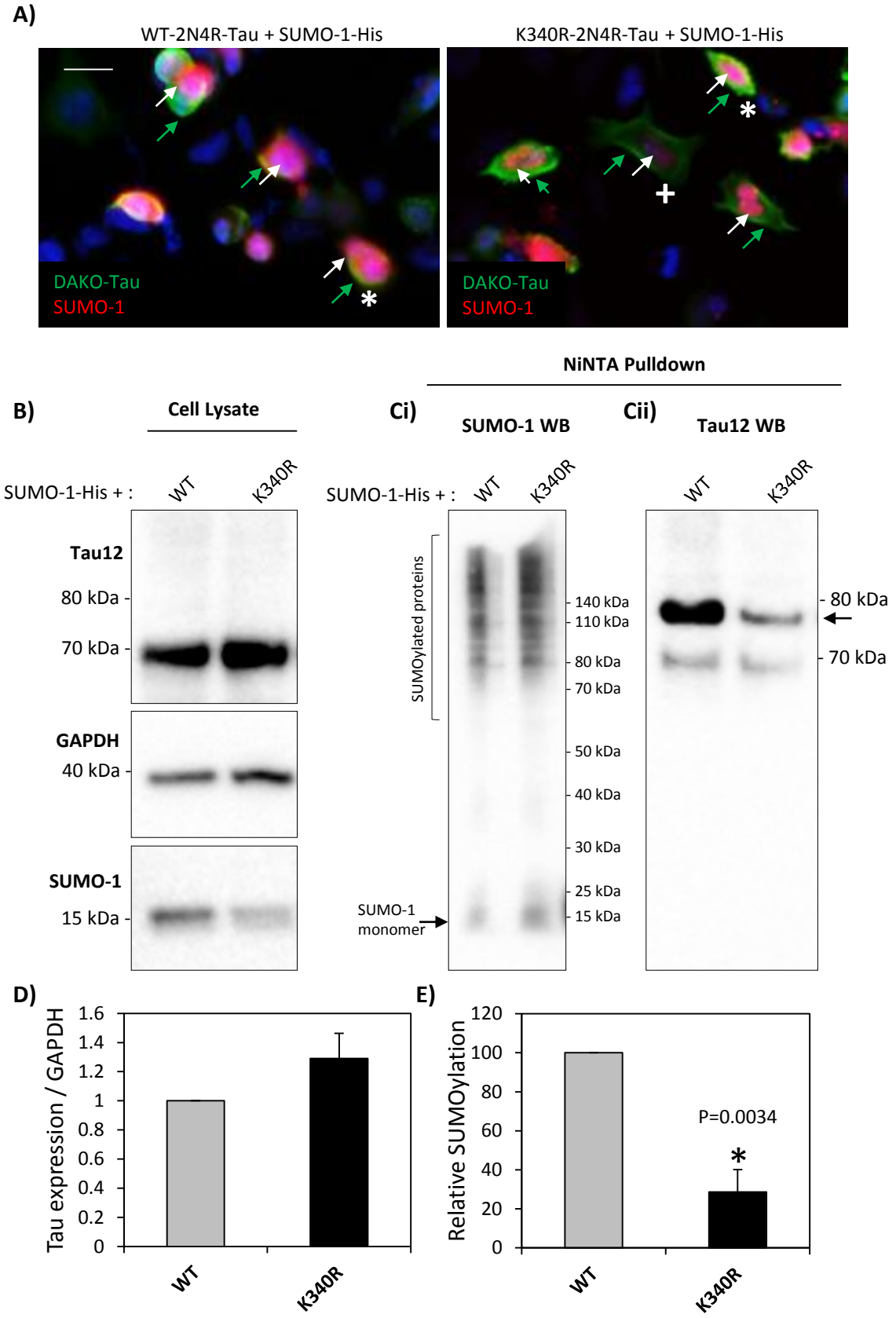

Figure 4.22 Analysis of SUMOylation of K340R-Tau protein in HEK293 Cells. A) DAKO-Tau and SUMO-1 co-immunostaining analysis of HEK293 cells transiently co-transfected with WT / K340R-2N4R-Tau and SUMO-1-His (48 hours, reagent mediated transfection). Green arrows indicate cytoplasmic Tau staining and white arrows indicate nuclear SUMO-1 staining. Scale bar 10 µm. **B)** Western blot analysis of HEK293 cell lysates transiently expressing WT / K340R-2N4R-Tau and SUMO-1-His. **C)** NiNTA pulldown from lysates of HEK293 transiently co-expressing WT / K340R-2N4R-Tau and SUMO-1-His (48 hours, reagent mediated transfection). NiNTA pulldowns analysed by Western blotting with **Ci)** SUMO-1 and **Cii)** Tau12 antibodies. Arrow indicates an 80 kDa Tau12 reactive band from NiNTA pulldowns, corresponding in size to SUMOylated 2N4R-Tau. **D)** Quantification of WT / K304R-2N4R-Tau expression levels in transiently transfected HEK293 cells, values are expressed relative to GAPDH and normalised to WT levels (mean ± SEM, n=3). **E)** Quantification of SUMOylated WT and K304R-2N4R-Tau when transiently expressed in HEK293 cells. Values are expressed relative to intracellular Tau expression levels and normalised to WT SUMOylation levels (mean ± SEM, n=3, Student's T-test).

4.6.3 Characterisation of SH-SY5Y clones with stable expression of K340R-2N4R-Tau

SH-SY5Y clones with stable expression of K340R-2N4R-Tau were generated by transfection and selection of G418 resistant colonies.

Tau12 Western blotting of two independent K340R-2N4R-Tau SH-SY5Y clones (c106 and c205) revealed minor and major Tau12 cross reactive bands migrating at 67 kDa and 50 kDa, respectively (**figure 4.23 A**). The minor band accounted for ~10% of the total intensity of Tau12 cross reactive bands from WT-2N4R-Tau and K340R-2N4R-Tau SH-SY5Y cells. Expressed relative to GAPDH, levels of the major 67 kDa Tau12 reactive band did not differ between K340R-2N4R-Tau and WT-2N4R-Tau SH-SY5Y clones suggesting similar levels of ectopic Tau expression (**figure 4.23 B**).

DAKO-Tau immunostaining demonstrated strong immunoreactivity in the cytoplasm and neurites of the K340R-2N4R-Tau SH-SY5Y clones. K340R-2N4R-Tau SH-SY5Y clones had DAKO-Tau immunostaining higher than that in normal SH-SY5Y cells in 72% and 69% cells for c106 and c205, respectively (**figure 4.23 C**).

4.6.4 Analysis of Tau phosphorylation in K340R-2N4R-Tau SH-SY5Y clones

WT-2N4R-Tau and K340R-2N4R-Tau SH-SY5Y cell pellets (two clones of each) were extracted (1% Tx100) in the presence of phosphatase inhibitors and subjected to immunoblotting with antibodies against three phosphorylated Tau residues: pS356, pT205 and pT181.

A single pS356, pT205 and pT181 cross reactive band was detected in the lysates from WT-2N4R-Tau and K340R-2N4R-Tau SH-SY5Y cells. The band from each antibody was detected migrating at 67 kDa, consistent with ectopically expressed Tau (**figure 4.24 A**).

Levels of immunoreactivity from the phospho-antibodies were expressed relative to total Tau levels (detected with Tau12) for each of the clones. Cross reactivity at pS356 and pT205

detected from K340R-2N4R-Tau SH-SY5Y cell lysate was reduced to 0.43±0.09 (n=3) and 0.3±0.04 (n=2) times that of levels detected from WT-2N4R-Tau SH-SY5Y cell lysates (**figure 4.24 B**,) whereas cross reactivity of pT181 was increased 1.4±0.04 times relative to WT (n=2, **figure 4.24 B**). Combining the data from pS356 and pT205 revealed a significant decrease in phosphorylation of Tau at these residues in K340R-2N4R-Tau SH-SY5Y cells relative to WT-2N4R-Tau SH-SY5Y cells (0.38±0.06 times relative to WT, K340R n=5, WT n=6, *p*=0.0001, **figure 4.24 C**).

Overall these data suggested that Tau phosphorylation in K340R-2N4R-Tau SH-SY5Y cells was de-regulated relative to that in WT-2N4R-Tau SH-SY5Y cells.

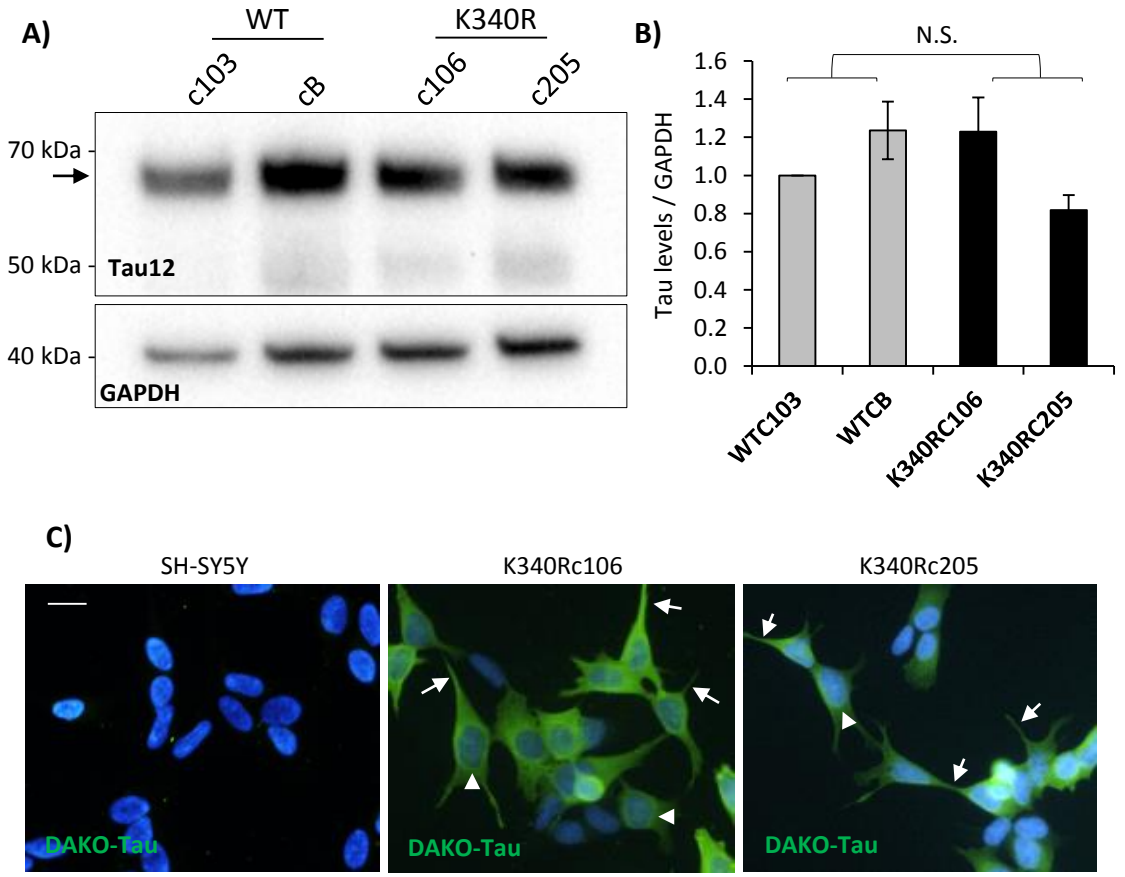

Figure 4.23 Characterisation of SH-SY5Y cells stably expressing K340R-2N4R-Tau. A) Western blot analysis of SH-SY5Y clones stably expressing WT-2N4R-Tau and K340R-2N4R-Tau (20 µg / lane, arrow indicates major Tau12 reactive band). **B)** Quantification of Tau expression levels in WT and K340R-2N4R-Tau SH-SY5Y cells. Levels are expressed relative to GAPDH and normalised to WTc103 (mean ± SEM, n=4). Student's T-test performed between combined values for WT and K340R (no significant differences found – n.s.). **C)** DAKO-Tau immunocytochemical analysis of SH-SY5Y clones stably expressing WT-2N4R-Tau and K340R-2N4R-Tau.

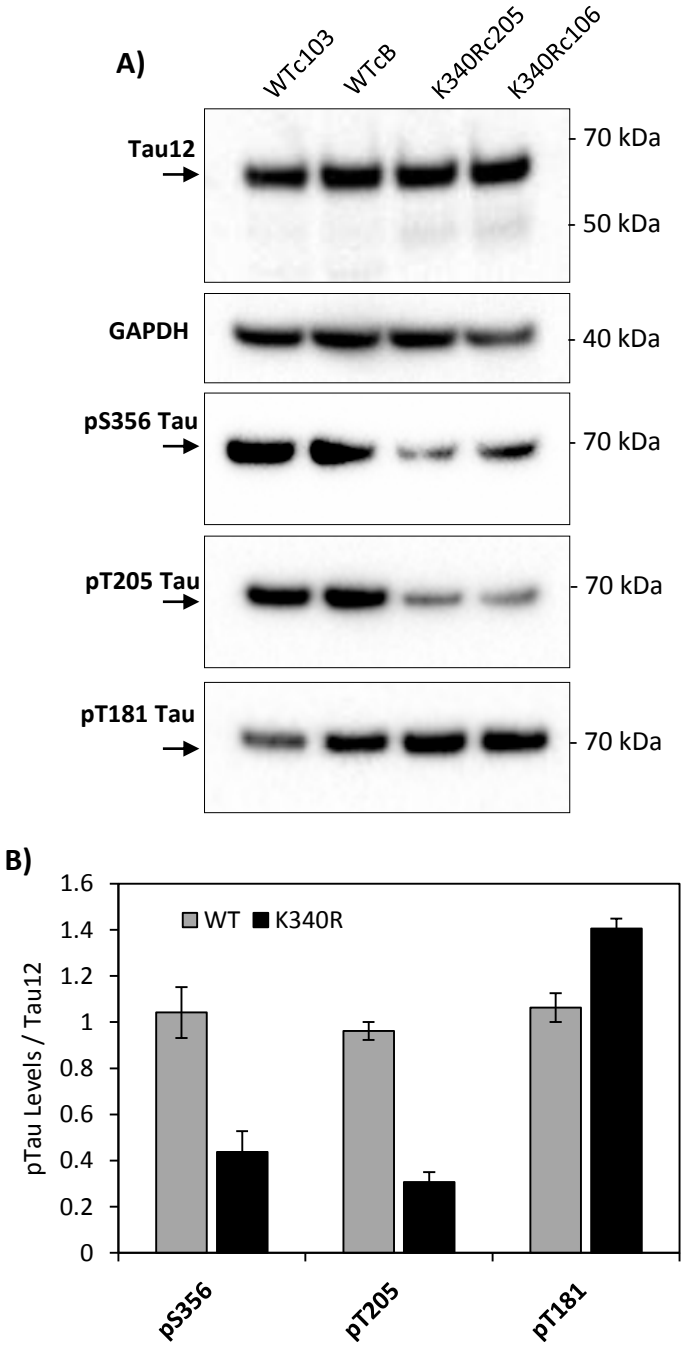

Figure 4.24 Analysis of steady state Tau phosphorylation levels in K340R-2N4R-Tau SH-SY5Y cells. A) Western blotting analysis of total (Tau12) and phosphorylated Tau (pS356, pT205, pT181) levels in WT-2N4R-Tau and K340R-2N4R-Tau SH-SY5Y cells (20 µg protein was loaded / lane). **B**) Quantification of phosphorylation levels of WT-2N4R-Tau and K340R-2N4R-Tau (at T205, S356 and T181; values are expressed relative to total Tau –Tau12 – levels; mean ± SEM, pS356 n=4, pT205 n=2, pT181 n=2). N.b. one anomalous data point was omitted from this analysis, corresponding to pS356 of K340R-Tau).

4.6.5 Tau – Tubulin co-immunostaining analysis of K340R-2N4R-Tau SH-SY5Y clones

To investigate the effects of K340R-2N4R-Tau expression on the microtubule network, Tau and Tubulin double immunostaining of WT-2N4R-Tau and K340R-2N4R-Tau SH-SY5Ycells was performed.

K340R-2N4R-Tau SH-SY5Y clones had distinct morphological features from WT-2N4R-Tau SH-SY5Y cells. Visual analysis suggested that K340R-2N4R-Tau clones had more neurites than WT-2N4R-Tau SH-SY5Y clones, furthermore, these neurites were positively stained with Tubulin antibody (**arrows**, **figure 4.25 A**). Quantification revealed that WT clones displayed one Tubulin positive neurite every 8±1.5 cells, whereas K340R-2N4R-Tau clones had tubulin positive neurites every 2±0.3 cells (n=4, *p*=0.003, **figure 4.25 B**).

Moreover, co-localisation analysis (Image J plugin) revealed increased co-localisation of DAKO-Tau staining with Tubulin immunostaining in K340R-2N4R-Tau SH-SY5Y cells compared to that in WT-2N4R-Tau SH-SY5Y cells (r^2=0.8±0.02 vs r^2=0.74±0.01; Pearson's correlation coefficient, n=2, **figure 4.25 C**) suggesting an increased association of K340R-2N4R-Tau and microtubules in SH-SY5Y cells.

These findings demonstrated that K340R-2N4R-Tau SH-SY5Y and WT-2N4R-Tau SH-SY5Y cells were distinguished on the basis of their morphologies and sub-cellular character – the former having increased neurite processes and Tau – Tubulin co-localisation.

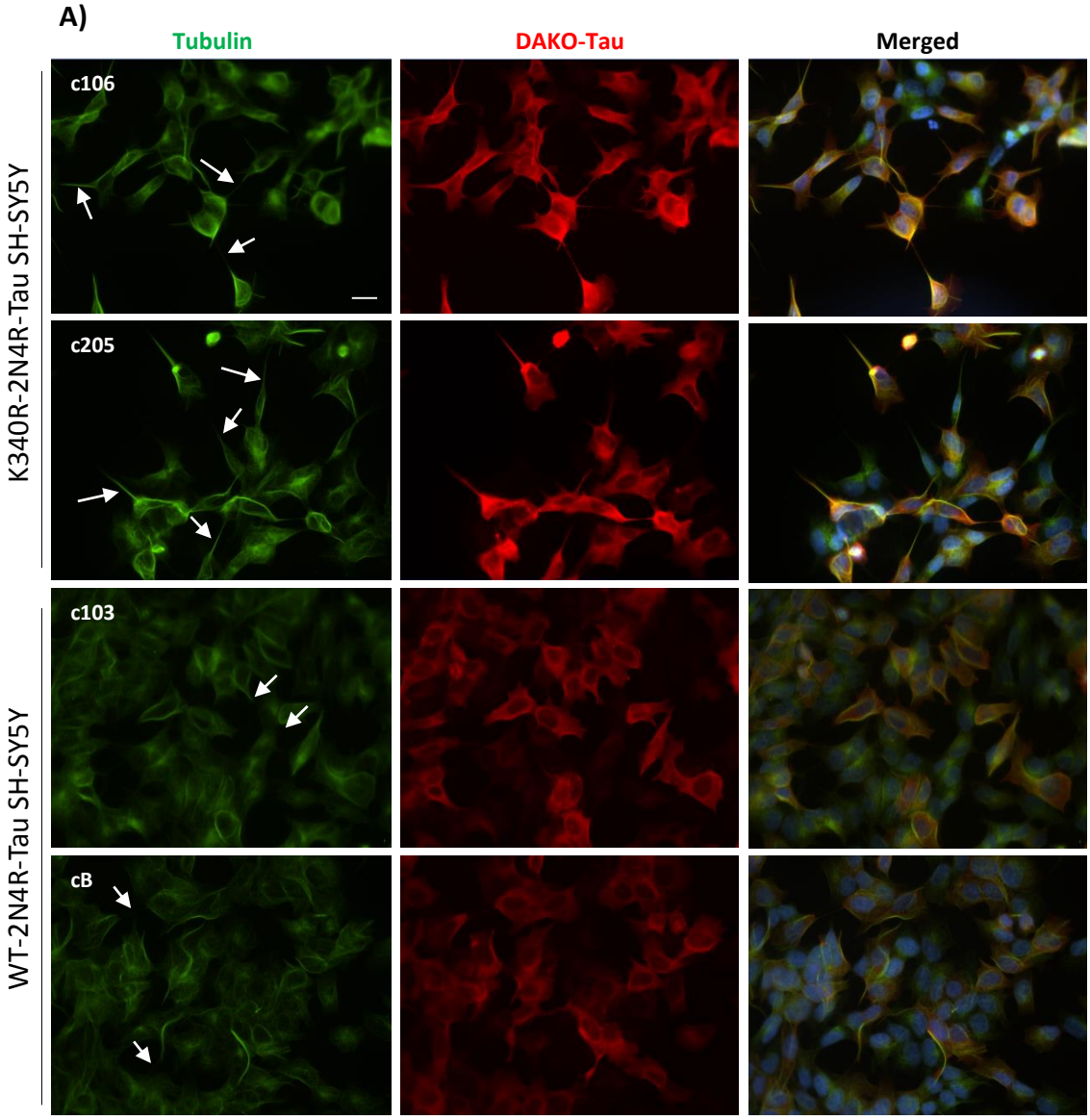

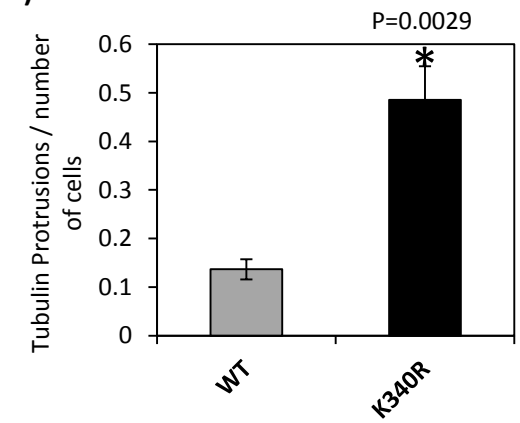

C)

Pearson's Correlation (r^2)

Clone	Field 1	Field 2
WTcB	0.77	0.74
WTc103	0.71	0.77
K340Rc106	0.83	0.83
K340Rc205	0.82	0.75

Figure 4.25 Tau – Tubulin co-immunostaining analysis of K340R-2N4R-Tau SH-SY5Y clones. A) DAKO-Tau and tubulin co-immunostaining of cultured SH-SY5Y cells with stable expression of WT-2N4R-Tau and K340R-2N4R-Tau. White arrows indicate tubulin positive protrusions which are quantified in **B)** (values are normalised to number of cells, mean ± SEM, n=4, two clones of each construct analysed on two separate occasions, Student's T-test)**. C)** Results of co-localisation analysis (ImageJ plugin) between Tubulin and DAKO-Tau immunostaining in WT and K340R-2N4R-Tau SH-SY5Y cells. Values refer to Pearson's correlation coefficient calculated when correlating the intensity of staining and Tubulin staining in each pixel.

4.6.6 Total and exosomal release of Tau from K340R-2N4R-Tau SH-SY5Y cells

Total extracellular Tau from K340R-2N4R-Tau SH-SY5Y cells was analysed by Tau12 dot-blot of 24 hour conditioned optiMEM. Tau12 immunoreactivity was detected in the conditioned medium of two K340R-2N4R-Tau SH-SY5Y clones and two WT-2N4R-Tau SH-SY5Y clones (**figure 4.26 A)**. No significant differences were observed in the levels of extracellular Tau from SH-SY5Y cells expressing the respective proteins, although there was a trend toward decreased levels from K340R-2N4R-Tau SH-SY5Y cells (0.5±0.1 times relative to WT, mean ± SEM, K340R n=6, **figure 4.26 B**).

Exosomes were isolated from the 24 hour conditioned optiMEM from two WT-2N4R-Tau clones and three K340R-2N4R-Tau clones (addition of K340Rc102, 5 x 10 cm / isolation). Tau12 cross reactive bands were detected in the exosomes from all clones analysed, migrating as a major band of 62 kDa (**arrow**, **figure 4.26 C**)

Levels of the major Tau12 cross reactive band (relative to Alix) were reduced in the exosomes isolated from K340R-2N4R-Tau SH-SY5Y conditioned optiMEM relative to those isolated from WT-2N4R-Tau SH-SY5Y clones (K340Rc102, 0.4±0.065, n=2; K340Rc106, 0.1±0.08, n=2; K340Rc205, 0.5±0.25, n=3, **figure 4.26 Di**). When values from each of the clones were combined a significant reduction in exosomal Tau release from K340R-2N4R-Tau SH-SY5Y cells was observed, a reduction to 0.4±0.1 times that of WT levels when expressed relative to Alix (mean ± SEM, n=7, p=0.002, **figure 4.26 Dii**).

Next, the exosomes were isolated from the conditioned prespun medium of two WT-2N4R-Tau and two K340R-2N4R-Tau SH-SY5Y clones (5 x 10 cm plates / clone). A Tau12 cross reactive band migrating at 62 kDa was detected in the exosomes from each clone (**arrow, figure 4.27 A**). Levels of this band were significantly reduced in the exosomes isolated from K340R-2N4R-Tau SH-SY5Y cells relative to those from WT-2N4R-Tau SH-SY5Y cells. When expressed relative to cellular protein levels were reduced to 0.1±0.08 times (relative to WT,

mean ± SEM, n=3, *p*=0.029) and when expressed relative to exosomal Alix, levels were reduced to 0.2±0.1 times (relative to WT, mean ± SEM, n=3, *p*=0.006; figure **4.27 B** and **C**).

Overall these findings suggested that exosomal release of K340R-2N4R-Tau from SH-SY5Y cells was reduced relative to the exosomal release of WT-2N4R-Tau, thereby implicating the process of Tau SUMOylation in its exosomal release.

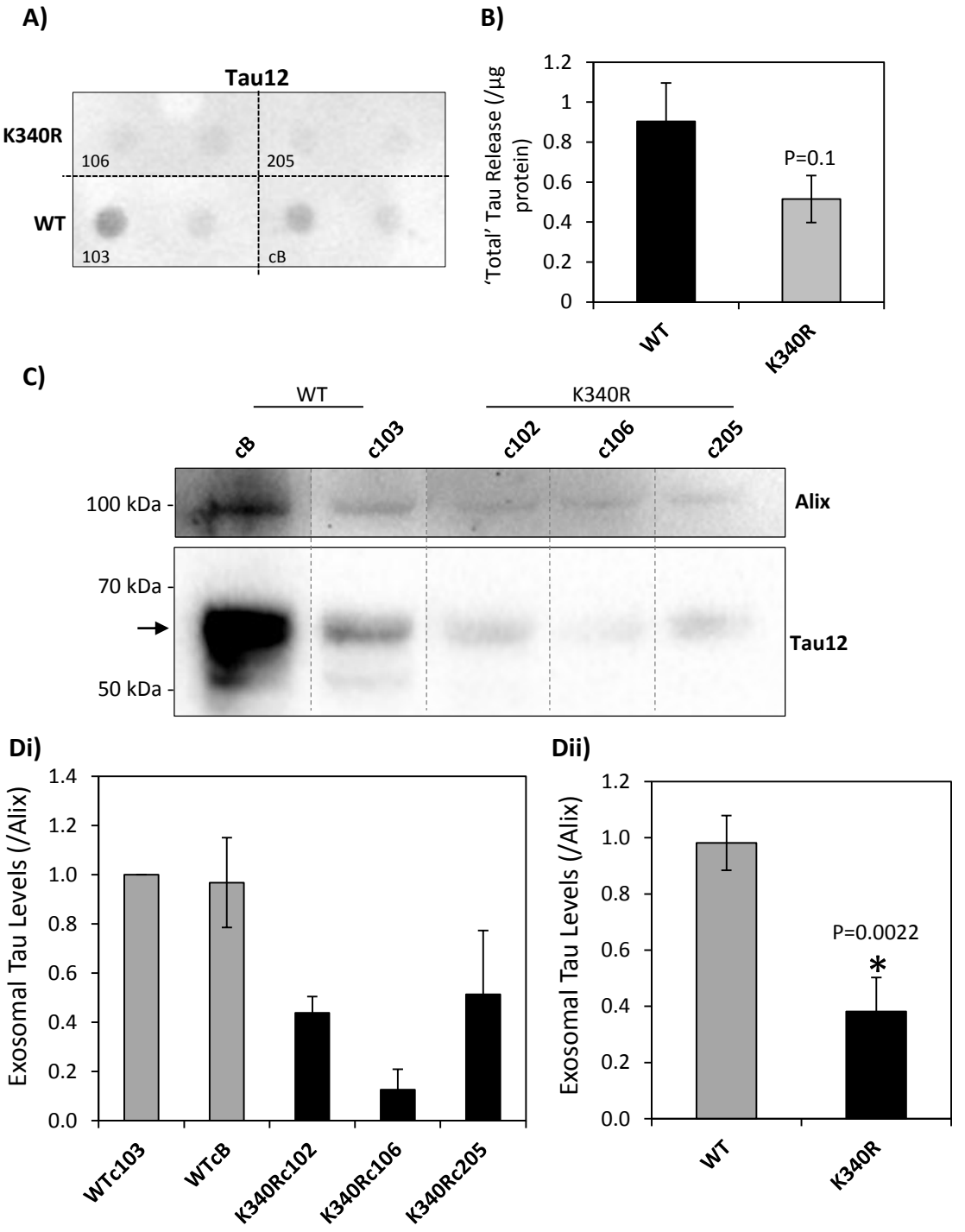

Figure 4.26 Analysis of total and exosomal Tau release from 24 hour conditioned optiMEM of K340R-2N4R-Tau SH-SY5Y cells. A) Dot-blot analysis of 24 hour conditioned optiMEM from WT and K340R-2N4R-Tau SH-SY5Y cells (200 µl ≈ 1/10th of conditioned medium from one well of a 6 well plate loaded / dot). **B)** Quantification of total Tau in the 24 hour conditioned optiMEM from WT-2N4R-Tau and K340R-2N4R-Tau SH-SY5Y cells (exosomes from the CM of 5 x 10 cm / lane). Levels are expressed relative to µg of cellular protein and normalised to WT-2N4R-c103 release levels (mean ± SEM, WT n=4, K304R n=6, Student's T-test). **C)** Western blot analysis of exosomes isolated from WT-2N4R-Tau and K340R-2N4R-Tau expressing SH-SY5Y cells. **Di)** Quantification of exosomal Tau levels from WT-2N4R-Tau and K340R-2N4R-Tau SH-SY5Y clones (left graph). Values are expressed relative to exosomal Alix levels and normalised to WTc103 (mean ± SEM, WTcB n=3, K340Rc102 n=2, K340Rc106 n=2, K340Rc205 n=3) and **Dii)** statistical analysis of combined values (right graph), expressed relative to exosomal Alix and normalised to WT mean (n=7, Student's T-test).

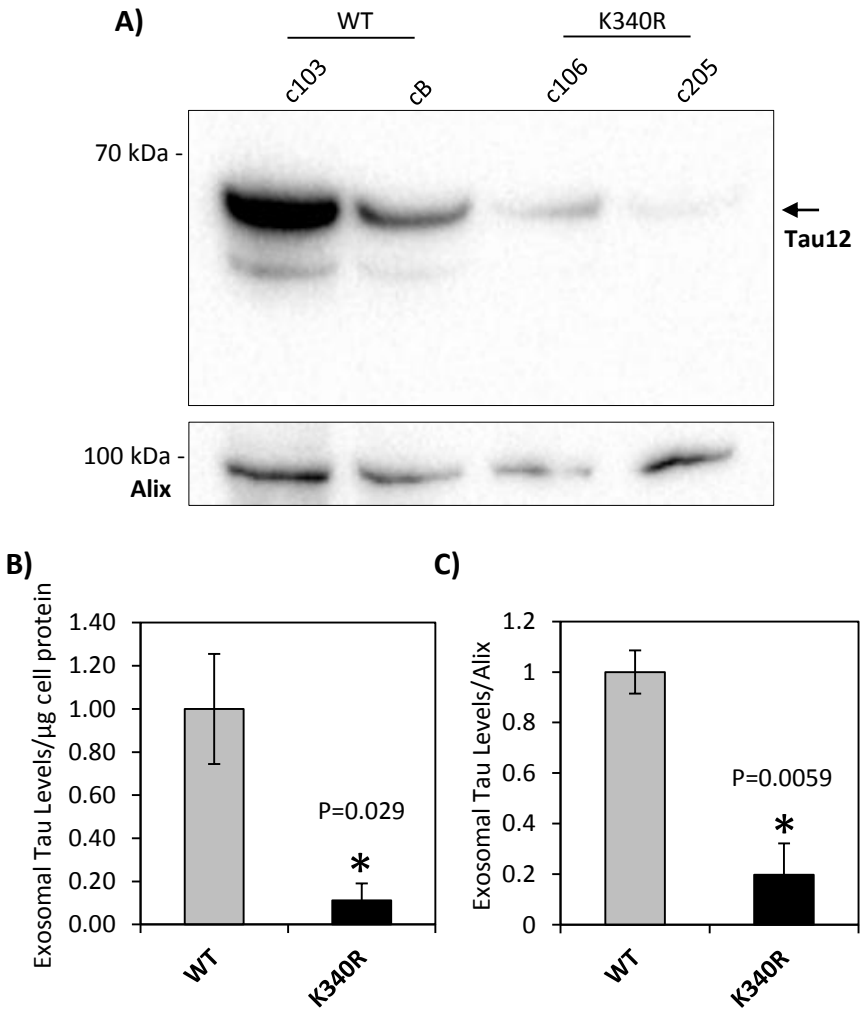

Figure 4.27 Analysis of exosomal Tau release in 24 hour conditioned prespun medium from K340R-2N4R-Tau SH-SY5Y cells. A) Western blot analysis of exosomes isolated from the prespun conditioned medium of K340R-2N4R-Tau and WT-2N4R-Tau SH-SY5Y clones (exosomes from CM from 5 x 10 cm / lane; arrow indicates major Tau12 reactive band). **B)** Quantification of exosomal Tau levels from WT-2N4R-Tau and K340R-2N4R-Tau SH-SY5Y clones. Values are expressed relative to exosomal Alix levels and normalised to WT mean (mean ± SEM, n=3, Student's T-test). **D)** Exosomal Tau levels expressed relative to cellular protein levels (mean ± SEM, n=3, Student's T-test).

5 Results 3: Analysis of the cellular uptake and trans-cellular transmission of Tau protein

5.1 Introduction and aims

The study of the transcellular spread of Tau protein is confounded by a number of factors. The spreading of Tau between cells can be conceptually dissociated into the processes of release (of which exosomal release is a subset; studied in **chapters 3 & 4**) and uptake. When both of these processes occur between cells in a physiologically embedded system, the process is referred to as spreading or trans-cellular transmission. We therefore aimed to identify the key variables constraining the study of Tau uptake and trans-cellular Tau transmission.

When studying the uptake of Tau by recipient cells, the source of extracellular Tau used is a key variable; a number of studies have investigated the direct uptake of recombinant Tau from the extracellular medium (Wu et al. 2012; Davis et al. 2018), whilst other studies have used Tau derived from the brains of rTg4510 (P301L-Tau) mice to study uptake (Takeda et al. 2015). These studies indicated that aggregated Tau was readily internalised by primary neurons in culture. The repeat domain of Tau ('RD-Tau') is a pro-aggregating Tau construct composed of just the microtubule binding regions (see methods **figure 2.1** for constructs). In order to optimise parameters for studying Tau transmission, we aimed to assess the uptake of RD-Tau with C-terminal GFP / dsRed tags ('RDeGFP-Tau' / 'RD-dsRed-Tau') recovered from stably expressing donor SH-SY5Y cells and incubated with naïve recipient SH-SY5Y cells.

Other sources of extracellular Tau include Tau protein secreted into the medium by cells, and exosomes isolated from the conditioned medium of Tau expressing cells. These sources of extracellular Tau represent more physiological forms of Tau as opposed to

recombinant derived material and we aimed to assess the uptake of these forms of Tau by recipient cells.

The recipient cell population is another key variable to consider when studying Tau uptake and spreading. Different cell types including primary neurons, iPSC derived neurons and dividing cells have been used by previous studies (Wu et al. 2012; Davis et al. 2018; Karch et al. 2012).

We aimed to assess if SH-SY5Y cells represented a good recipient cell system for the uptake and transmission of Tau protein, and we also used primary neurons as a recipient cell system. Using SH-SY5Y cells as a recipient cell system is confounded by the endogenous expression of human Tau in these cells, thus ruling out the possibility of using Tau antibodies to directly study uptake by ICC. Therefore the source of exogenous Tau used to study uptake by SH-SY5Y cells must be tagged, in this chapter we have used Tau constructs with GFP, dsRed and HA tags to enable detection distinct from endogenous Tau in SH-SY5Y cells.

The uptake of Tau by recipient cells must be detected by a suitably sensitive methodology. ICC and immunoprecipitation of co-cultured cells / treated recipient cells represent potentially complementary methods for studying different patterns of Tau uptake. ICC more easily reveals focal transmission whereas immunoprecipitation is able to effectively concentrate the Tau taken up by a large population of recipient cells.

Other confounding variables include experimentally defined parameters such as amount of material added to recipient cells and time of incubation before analysis. Some studies demonstrated internalisation of Tau over short time periods (30 minutes to 4 hours) whereas other studies analysed recipient cells after 6 days (Davis et al. 2018; Wu et al. 2016).

The transmission of Tau protein between cells can be studied by co-culturing two populations of cells each expressing a differently tagged form of Tau (or one naïve

population and one population expressing Tau). The presence of both forms of tagged Tau in one cell represents transmission of Tau from one cell to another. Cells may be co-cultured either directly in the well such that they form physical connections, or in transwell inserts that keep the distinct populations physically separated whilst allowing them to share medium, including the Tau released into it. Co-culture has advantages over the addition of exogenously derived extracellular Tau to recipient cells as in this system the process of release is occurring continuously. The dynamics of co-culture therefore more closely approximate that occurring in living tissues, than with the single 'pulse' addition of exogenous material. In this chapter we aimed to analyse the transmission of Tau protein between SH-SY5Y cells in co-culture.

Finally, bafilomycin can be used to treat donor cells, recipient cells and cells in co-culture to potentiate processes relating to transmission of Tau. Bafilomycin is hypothesised to increase the chances of observing transmission because lysosomal dysfunction increases Tau release (Mohamed et al. 2014) and decreases Tau degradation (Hamano et al. 2008).

Overall the aims for this chapter were:

1) Study the uptake of aggregating RD-Tau, that had been recovered from stably expressing SH-SY5Y cells, by recipient naïve SH-SY5Y cells
2) Study the uptake of extracellular Tau that had been released by donor cells
3) Investigate the transmission of Tau protein between cells in direct co-culture

5.2 Analysis of the uptake of Tau protein by recipient cells

5.2.1 Characterisation of RDeGFP-Tau SH-SY5Y Cells

SH-SY5Y cells with stable ectopic expression of RD-eGFP-Tau (with the ΔK280 mutation, see methods **figure 2.1** for construct) were generated by transfection followed by selection with G418. ICC analysis with GFP antibody demonstrated clear immunoreactivity in the cytoplasm and neurites of 6 independent clones (c1, c4, c5, c8, c10 and c202; **figure 5.1 A**). RD-Tau has previously been demonstrated to aggregate into insoluble forms when expressed in cell culture models (Wang et al. 2007), we therefore assessed the aggregation state of RDeGFP-Tau stably expressed in SH-SY5Y cells by sequential extraction in 1% (w/v) Tx100 and 1% (w/v) SDS. DAKO-Tau immunoblot of Tx100 extracts demonstrated the same profile of cross-reactive bands from all RDeGFP clones (**figure 5.1 B** – '**Soluble**') which consisted of three bands migrating at 50 kDa, 40 kDa and 25 kDa (arrows, **figure 5.1 B**). The 50 kDa band was consistent with the full-length RDeGFP-Tau (RD kDa = 23 kDa, GFP kDa = 27 kDa), whilst the lower bands were consistent with cleavage products. The 25 kDa band was consistent with RD-Tau with the C-terminal GFP tag cleaved off (predicted kDa = 23 kDa). No DAKO-Tau cross reactive bands were detected in the Tx100 insoluble fraction from normal SH-SY5Y cells, which suggested that endogenous Tau in SH-SY5Y cells did not aggregate to an appreciable extent. Consistent with our earlier work (**figure 3.1**), <1% of ectopic 2N4R-Tau was Tx100 insoluble (**figure 5.1 B**). The level of Tx100 insoluble DAKO-Tau 50 kDa cross-reactive bands from RDeGFP-Tau SH-SY5Y cells was increased relative to that detected from WT-2N4R-Tau SH-SY5Y cells by 17 – 113 times (c202 and c1, respectively; **figure 5.1 C**) suggesting that ectopically expressed RDeGFP-Tau had increased aggregation propensity, consistent with previous reports (Wang et al. 2007). Exosomes were isolated from the 24 hour conditioned optiMEM medium of RD-eGFP-Tau c8 SH-SY5Y cells. GFP immunoblotting demonstrated a cross reactive band at 50 kDa co-migrating with the GFP cross reactive band detected in the cell lysate (arrow, **figure 5.1 D**) demonstrating

the exosomal release of ectopically expressed RDeGFP-Tau. A lower molecular weight GFP cross reactive band migrating at 35 kDa was detected in the exosomal fraction, but not in the cells (asterisks, **figure 5.1 D**). The cross reactivity and migration profile of this band suggested it was constituted by GFP (27 kDa) and some C-terminal RD-Tau sequence (≥ 8 kDa).

5.2.2 Extraction of RD-eGFP-Tau from SH-SY5Y cells and stability in cell culture medium

To extract RDeGFP-Tau for incubation with recipient cells, RDeGFP-Tau c8 SH-SY5Y cells were resuspended in growth medium and lysed by nitrogen bombing. The resultant lysate was clarified at 4000 x g and the supernatant ('Input') was added to recipient SH-SY5Ycells in culture for increasing periods of time. GFP immunoblotting of donor RD-eGFP-Tau c8 cells prior to and post extraction detected a single band migrating at 50 kDa, consistent with expression of the RDeGFP-Tau protein (**arrow, figure 5.2 A**). The amount of total RD-eGFP-Tau extracted was 53±4%, whilst recovery of the cytosolic protein, GAPDH was also ~50% (**figure 5.2 A** and **B**). The RD-eGFP-Tau extract was added to recipient SH-SY5Y cells and the medium was sampled over the course of three hours. Levels of the 50 kDa GFP cross reactive band added to the culture medium decreased over the course of the incubation (0.5 – 3 hours), as demonstrated by Western blot analysis of the conditioned medium (**figure 5.2 A**). The 50 kDa GFP cross reactive band in the input material was reduced by 78% after 30 minutes incubation, and remained at this level until three hours (**figure 5.2 C**). Recipient SH-SY5Ycells that were incubated with RD-eGFP-Tau extract were also analysed by GFP immunoblot, however, no specific GFP cross reactive bands were detected. This suggested that RD-eGFP-Tau recovered from RD-eGFP-Tau SH-SY5Y cells was not taken up to a detectable level by recipient SH-SY5Y cells over the time course analysed (**red box, figure 5.2 A**).

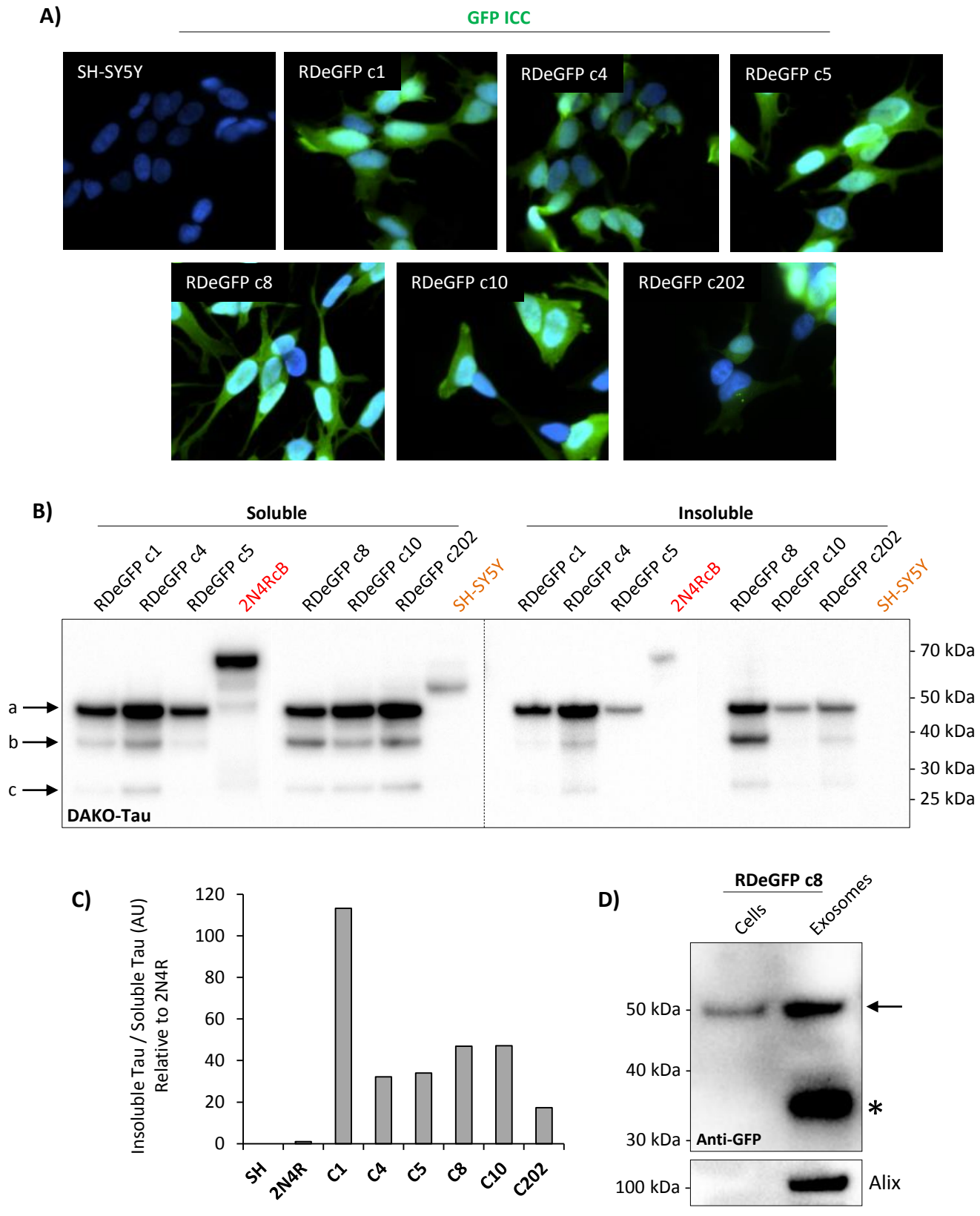

Figure 5.1 Characterisation of SH-SY5Y cells with stable expression of RDeGFP-Tau. A) GFP immunostaining of normal SH-SY5Y and SH-SY5Y clones with stable expression of RDeGFP-Tau. **B)** Solubility analysis of stably expressed RDeGFP-Tau. Normal SH-SY5Y cells, and clones with stable expression of WT-2N4R-Tau or RDeGFP-Tau were extracted sequentially in 1% Tx100 (soluble) and 1% SDS (insoluble) and loaded at 1% and 83%, respectively. **C)** Quantification of insoluble DAKO-Tau cross-reactive bands in the RDeGFP-Tau SH-SY5Y clones. Levels of insoluble Tau were expressed relative to levels of soluble Tau (SH = SH-SY5Y). **D)** Western blot analysis of cell lysates (0.1 µg) and exosomes (5 x 10 cm, 24 hour conditioned optiMEM medium) from RDeGFP-Tau SH-SY5Y c8 cells. Arrow indicates a co-migrating cellular and exosomal GFP immunoreactive band. Asterisks indicates a GFP immunoreactive band present in the exosomes.

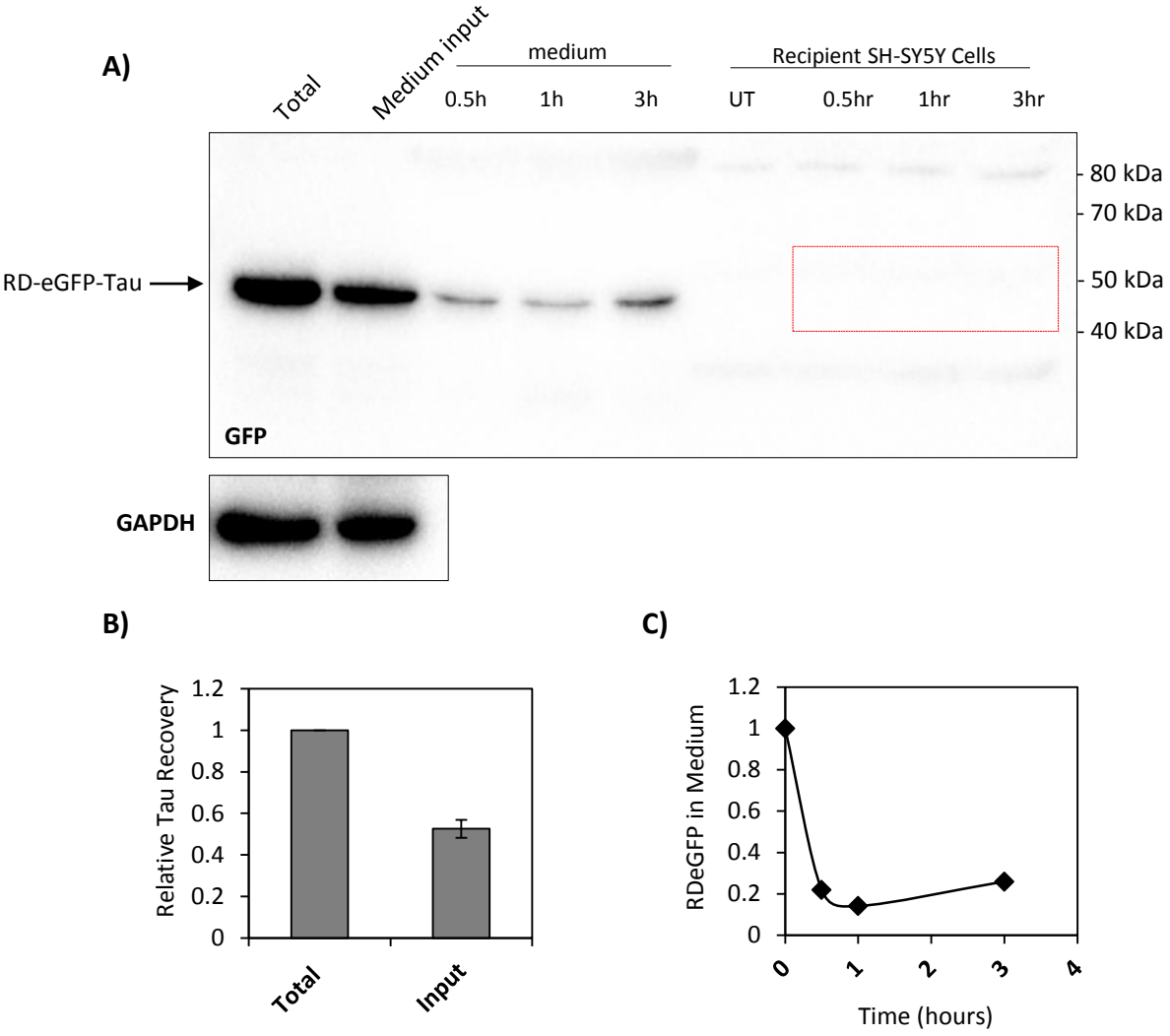

Figure 5.2 Analysis of the recovery of RD-Tau-eGFP from SH-SY5Y cells by nitrogen bombing and stability of recovered RD-eGFP-Tau in cell culture medium. A) Western blot analysis of RD-Tau-eGFP liberated from SH-SY5Y cells by nitrogen bombing. Liberated RD-eGFP-Tau was added to culture medium (equivalent to 1 x 10 cm of RDeGFP SH-SY5Y / 2 ml in 6 well plates) with recipient SH-SY5Y cells. Culture medium and recipient cells (normal SH-SY5Y cells in 6 well plates) analysed at increasing time points for the presence of RD-eGFP-Tau. Equal proportions of 'Total', 'medium input' and 'medium' loaded, and all of the recipient cells (i.e. 1 well of a 6 well plate / lane) were analysed. Arrow indicates major GFP reactive band. **B)** Quantification of the proportion of Tau liberated ('input') by pressure lysis (mean ± SEM, n=3). **C)** Western blot analysis of the proportion of cellular GAPDH liberated by pressure lysis **D)** Quantification of Tau-RD-eGFP remaining in the SH-SY5Y culture medium after increasing periods of time (incubated in the presence of cell monolayer at 37°C, 5% CO_2).

5.2.3 Uptake of RDeGFP-Tau from SH-SY5Y extract by primary cortical neurons

Primary cortical neurons may represent a more suitable cell system than undifferentiated SH-SY5Y cells for studying the uptake of extracellular Tau protein, owing their post-mitotic state. We therefore aimed to assess the uptake of RDeGFP-Tau by primary cortical mouse neurons, we also changed the experimental parameters and analysed recipient cells at 24 hours post treatment, owing to the above observations (**figure 5.2 A**). As above, RD-eGFP-Tau c8 SH-SY5Y cells were lysed by nitrogen bombing and clarified at 4000 x g. The resultant extract from 1 x 10 cm plate was added to primary mouse cortical neurons (1 well of a 6 well plate) for 24 hours which were then analysed by GFP immunostaining. No GFP immunoreactivity was detected associated with primary mouse cortical neurons treated with extract from 1 x 10 cm plate of normal SH-SY5Ycells. However strong GFP immunostaining was observed associated with neurons treated with an equivalent amount of extract from SH-SY5Y cells expressing RD-eGFP-Tau (**figure 5.3 A**). GFP immunostaining was detected in the cell bodies and neurites of the recipient neurons (**white arrowheads** and **arrows**, respectively, **figure 5.3 A,** enlarged sections). Primary mouse cortical neurons treated with increasing concentrations of RDeGFP-Tau SH-SY5Y extract (from 0.4 – 4 x 10 cm plates / 6 well) demonstrated GFP immunostaining which increased with the concentration of lysate added (**figure 5.3 B**). Integrating the fluorescence intensity from several fields for each concentration (normalised to number of nuclei / field) revealed a linear relationship (r^2=0.98) between concentration of lysate added and intensity of GFP immunostaining (**figure 5.3 C**). These observations were consistent with the uptake of RD-eGFP-Tau by recipient primary mouse cortical neurons in culture.

Cortical neurons treated with RD-eGFP-Tau extract were co-stained with CellMask Orange (CMO) to stain the plasma membrane; GFP immunostaining was then performed followed by confocal Z-stack analysis to understand the relationship between the cell boundary and the associated GFP immunoreactivity arising from RD-eGFP-Tau extract. CMO appeared as

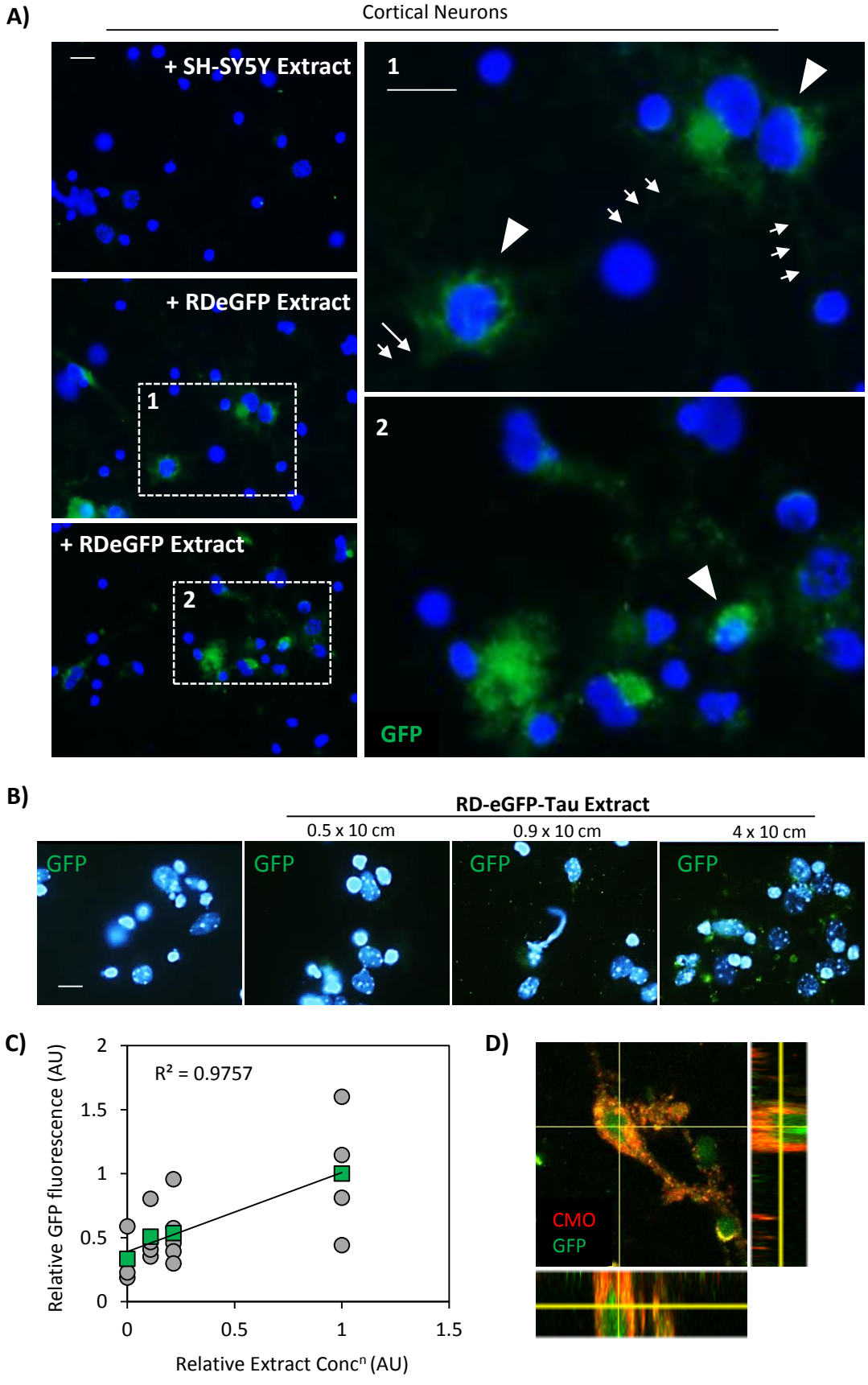

Figure 5.3 Immunocytochemical analysis of the uptake of RDΔK280eGFP by primary mouse cortical neurons in culture. A) GFP immunostaining analysis of primary mouse cortical neurons treated with SH-SY5Y (equivalent to 1 x 10 cm plate) or RDΔK280eGFP SH-SY5Y cell lysate (equivalent to 0.5 – 1 x 10 cm) for 24 hours. **B)** GFP immunostaining of primary mouse cortical neurons treated with increasing concentrations of RDΔK280eGFP SH-SY5Y cell lysate, equivalent to (from left to right) no treatment, 0.4 x 10 cm, 0.9 x 10 cm, 4 x 10 cm plates for 24 hours. **C)** Quantification of GFP fluorescence intensity of GFP immunostained primary neurons treated with increasing concentrations of RDΔK280eGFP SH-SY5Y cell lysate. Line of best fit is fitted to the mean values (green squares) obtained from four fields / concentrations (grey circles, n=1). **D)** Confocal Z-stack analysis of CNs treated with RDeGFP lysate. Cells were stained with cell mask orange (CMO) prior to immunocytochemistry with anti-GFP. Scale bars 10 µm.

a red stain demarking the edges of the neurons (**figure 5.3 D**). GFP immunostaining was detected colocalised with CMO staining, suggesting association with plasma membrane and potentially uptake (orange regions, **figure 5.3 D**). However, large spherical regions of GFP immunostaining were detected superior to the cell bodies, suggesting an association of some of the RD-eGFP-Tau with the exterior of the cells.

5.2.4 Uptake of RD-dsRed-tau by recipient SH-SY5Y cells

Because the levels of free RD-eGFP-Tau added to recipient SH-SY5Y were rapidly reduced (**figure 5.1 A**) we aimed to assess the uptake of RD-*dsRed*-Tau by recipient SH-SY5Y cells. We also extended analysis of the recipient cells to 24 hours.

SH-SY5Y cells with stable expression of RD-dsRed-Tau (with the ΔK280 mutation, see methods **figure 2.1** for construct) were generated by transfection of SH-SY5Y cells and selection in G418. Clones were analysed by Western blotting, solubility analysis and ICC (see appendix **figure 7.1** for full characterisation).

Analysis of one clone, RD-dsRed-Tau c9, by direct fluorescent microscopy demonstrated dsRed puncta in the cytoplasm of expressing cells (arrows, **figure 5.4 A**), suggesting the aggregation of RD-dsRed-Tau in these cells. Moreover, native PAGE analysis of this clone demonstrated higher molecular weight DAKO-Tau cross reactive bands, suggesting oligomerisation of ectopic RD-dsRed-Tau (**figure 4.3**). We therefore opted to use this clone as a source of aggregating Tau for investigating uptake by recipient SH-SY5Y cells.

RD-dsRed-Tau SH-SY5Y cells ± 200 nM bafilomycin A1 48 hr pre-treatment (to increase Tau levels in the cells), were lysed by nitrogen bombing, clarified at 4000 x g and the extract was added to recipient SH-SY5Y cells in culture. RFP immunoblot detected a major band migrating at 40 kDa from the resultant lysate, consistent with expression of RD-dsRed-Tau in the donor cells (arrow, **figure 5.4 B**). The intensity of RD-dsRed-Tau in the culture medium was relatively stable over 24 hours incubation time, in the presence and absence

of recipient cells ; 71±0.02% of RD-dsRed added to recipient SH-SY5Ycells was still present in the culture medium after 24 hours incubation (**figure 5.4 A** and **B**).

Western blotting of recipient cells revealed no specific RFP cross reactive bands from recipient cells treated with RD-dsRed-Tau extract at any time point (1, 3 or 24 hours), or RD-dsRed extract pre-treated with 200 nM bafilomycin for 1 and 3 hours. However, an RFP cross reactive band migrating at 40 kDa was detected associated with the recipient SH-SY5Y cells treated with bafilomycin pre-treated RD-dsRed-Tau lysate for 24 hours, which co-migrated with RD-dsRed-Tau in the donor cells. This suggested internalisation of RD-dsRed-Tau by the recipient cells (**figure 5.4 D**). Of the RD-dsRed-Tau added to recipient SH-SY5Y cells, 0.0065% was detected associated with recipient cells, 73% remained in the culture medium and 26% was unaccounted for (i.e. was neither internalised nor remained in the culture medium; **figure 5.4 D**).

Collectively these results suggested that Tau present in the cellular extracts of RD-Tau expressing SH-SY5Y cells could become associated with recipient cells in culture. Both normal SH-SY5Y cells and primary mouse cortical neurons displayed evidence of Tau uptake.

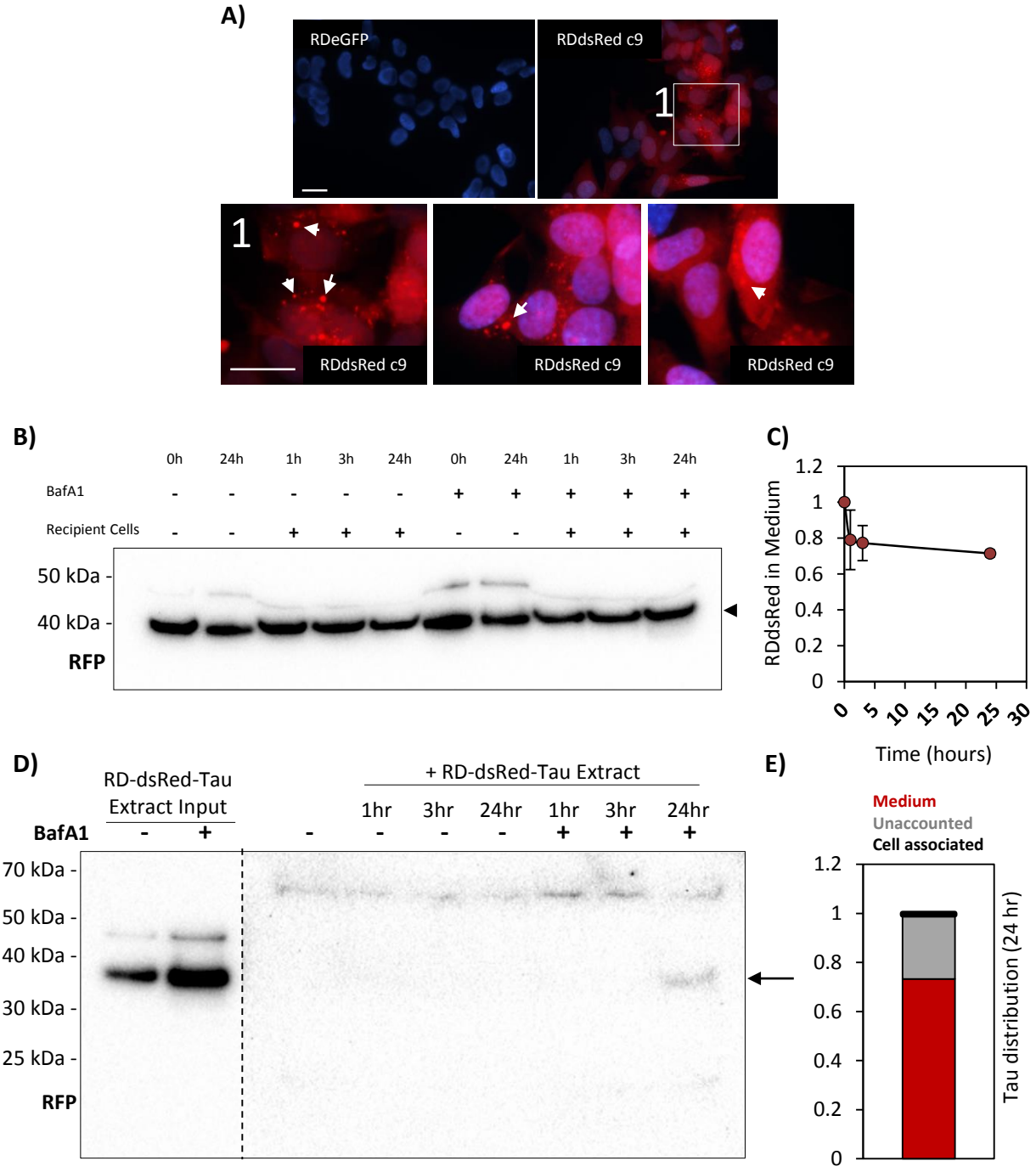

Figure 5.4 Analysis of the uptake of RD-dsRed-Tau by naïve SH-SY5Y cells in culture. A) Direct fluorescent microscopy analysis of fixed RD-dsRed-Tau c9 SH-SY5Y cells. **B)** Western blot analysis of the stability of RD-Tau-dsRED (recovered by nitrogen bombing) in SH-SY5Y cell culture medium for increasing periods of time in the presence / absence of bafilomycin and recipient SH-SY5Y cells (equivalent to 1 x 10 cm of RDdsRed-Tau SH-SY5Y added per well of 6 well plate. E.W. = empty well, same proportions of 'input' and 'medium' were analysed in each lane). **C)** Quantification of the stability of RD-Tau-dsRED in the culture medium over 24 hours (mean ± SEM, n=2, values normalised to 'input' value). **D)** Western blot analysis of recipient SH-SY5Y cells following treatment with liberated RD-Tau-dsRED (equivalent to 1 x 10 cm / 6 well of recipient SH-SY5Y, ± 200 nM bafilomycin A1, pre- and co-treatment). Detection was with anti-RFP. Each lane of recipient cells corresponds the cells from 1 well of a 6 well plate. **E)** Analysis of the distribution (extracellular – red/ unaccounted – grey / internalised – black) of RD-Tau-dsRED after addition to the culture medium of SH-SY5Y cells for 24 hours. Calculated by integration of the relevant band intensities and corrected for loading. Unaccounted Tau was calculated by Input – (extracellular + internalised) and all values were expressed as percentages of input.

5.2.5 Uptake of tau protein released by 2N3R-GFP-Tau by naïve SH-SY5Y cells

Following these findings we aimed to assess if Tau secreted into the extracellular space by donor SH-SY5Y cells (rather than Tau released by cellular lysis) could be taken up by recipient cells.

SH-SY5Y cells expressing 2N3R-GFP-Tau were used as a donor cell system. These cells were selected because they expressed Tau with a GFP tag that could therefore be distinguished from endogenous Tau. The secretion of Tau into the medium and exosomes by 2N3R-GFP SH-SY5Y cells was confirmed using Western blot analysis of 24 hour conditioned optiMEM. An 88 kDa Tau12 cross reactive band, consistent with 2N3R-GFP-Tau was detected in the cells (0.1 µg), medium (0.03 x 10 cm plates) and exosomes (5 x 10 cm plates) of 2N3R-GFP SH-SY5Y cells (**figure 5.5 A**).

The 24 hour conditioned medium (normal medium) of 2N3R-GFP SH-SY5Y cells, ± 200 nM bafilomycin, was harvested and centrifuged at 12k x g. The resulting supernatant, containing free and exosomal released Tau (**figure 5.5 A**), was added to recipient normal SH-SY5Y cells in culture at a ratio of 1:1 (culture vessel volume) for 1, 7 or 24 hours. Recipient cells were then harvested, lysed and immunoprecipitated with DAKO-Tau capture any Tau that had been taken up.

Tau12 immunoblotting of DAKO-Tau immunoprecipitated 2N3R-GFP SH-SY5Y donor cell lysates demonstrated one immunoreactive band migrating at 88 kDa, consistent with 2N3R-GFP-Tau (band '**a**'**, figure 5.5 B**). Donor cells were grown in 60 mm dishes, and 0.01% and 0.002% of the donor cell material was IP'd in two separate reactions, equivalent to roughly 250 and 50 cells, respectively (calculated using the relationship that a confluent 1 x 10 cm plate ≈ 10^6 cells). The 88 kDa Tau12 cross reactive band was detected from both reactions, demonstrating the sensitivity of this technique to detected ectopic 2N3R-GFP-Tau. A band migrating at 50 kDa, consistent with endogenous SH-SY5Y Tau was IP'd from

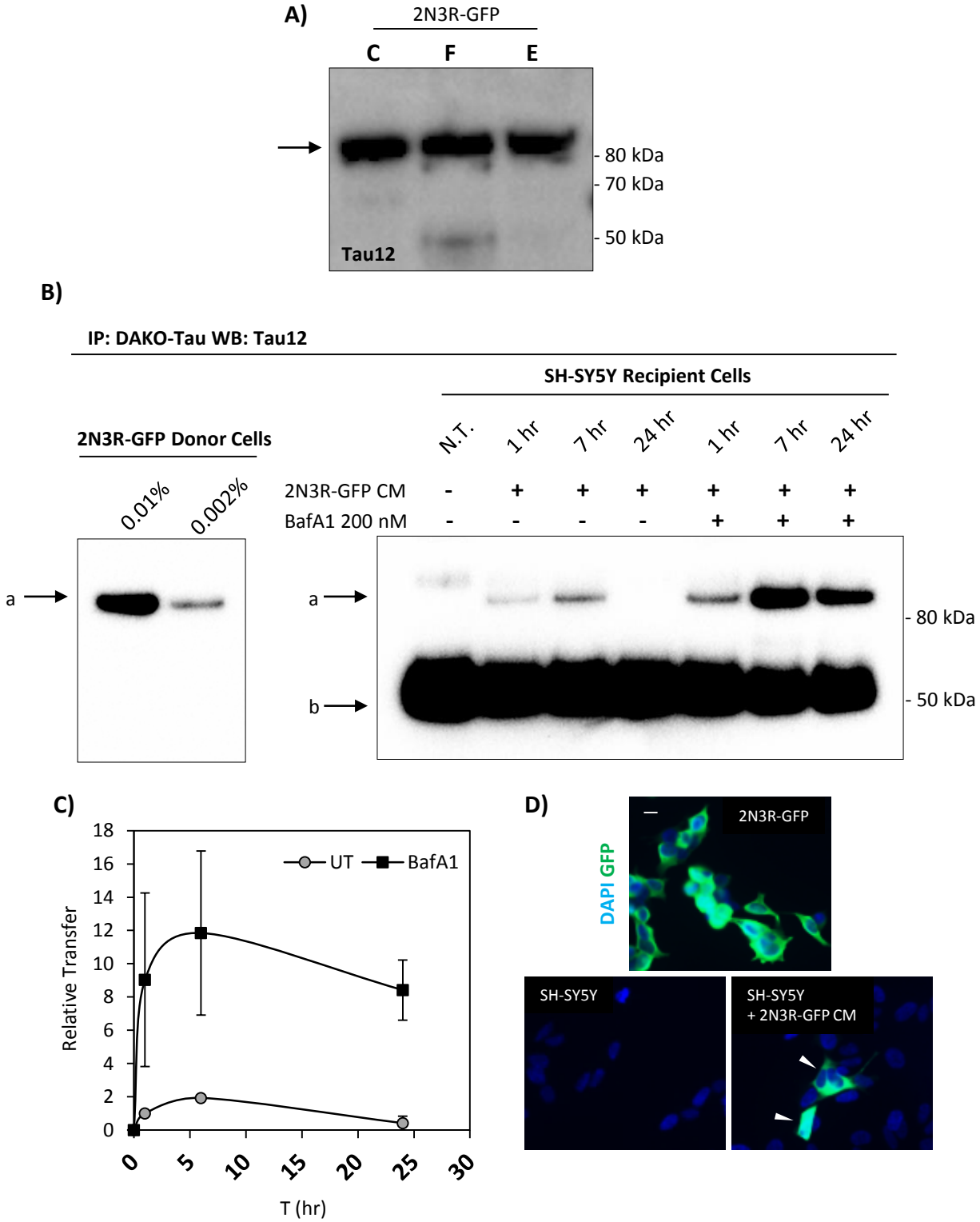

Figure 5.5 Analysis of 2N3R-GFP-Tau uptake by recipient SH-SY5Y cells via conditioned medium transfer. **A)** Western blot analysis of 2N3R-GFP in cellular lysates ('C' – 0.1 µg), medium (free, 'F' – 0.03 x 10 cm; DAKO-Tau IP'd exosome supernatant) and exosomes ('E' – 5 x 10 cm; 24 hour conditioned optiMEM) from 2N3R-GFP SH-SY5Y cells. **B)** IP and western blot analysis of SH-SY5Y cells (on 6 well plates) treated with 24 hour conditioned medium from 2N3R-GFP SH-SY5Y cells (2.5 ml / well). Conditioning and treatment was performed in the presence or absence of 200 nM bafilomycin and treatment was performed for increasing periods of time. IP was performed on all of the recipient cells and all of the eluate was loaded. Upper and lower arrows indicate Tau12 cross reactive bands consistent with 2N3R-GFP and endogenous SH-SY5Y Tau, respectively. **C)** Quantification of Tau12 cross reactivity at 88 kDa in recipient SH-SY5Y cells. Immunoreactivity was integrated and normalised to 1 hour treatment in the absence of bafilomycin (mean ± SEM, n=2). **D)** GFP immunocytochemical analysis of SH-SY5Y cells treated with 24 hour conditioned medium from 2N3R-GFP SH-SY5Y cells (6 hours treatment, 200 nM bafilomycin). White arrowheads indicate strongly GFP positive cells in the recipient population.

all recipient cells (band '**b**'**, figure 5.5 B**). This band was not detectable in the IP of 2N3R-GFP donor cells because 10,000 – 50,000 times less material was used for IP.

The 88 kDa band (band '**a**', **figure 5.5 B**) was not detected in the DAKO-Tau immunoprecipitated untreated recipient SH-SY5Y cells. However, the 88 kDa Tau12 cross reactive band was IP'd from recipient SH-SY5Y cells treated with 2N3R-GFP conditioned medium for 1 and 7 hours. Moreover, the intensity of this band in recipient SH-SY5Y cells was increased by bafilomycin pre- and co-treatment, which also increased the detection window of this band to 24 hours (**figure 5.5 B** and **C**).

GFP immunostaining of recipient SH-SY5Ycells treated with 24 hour conditioned 2N3R-GFP medium revealed the presence of cells positive for GFP immunostaining in the recipient SH-SY5Y population (**white arrowheads, figure 5.5 D**). These positive cells may have represented cells taking-up 2N3R-GFP-Tau from the conditioned medium, or may have been false positives, representing transfer of whole cells from the donor population to the recipient population in the conditioned medium.

5.2.6 Studying trans-cellular Tau transmission with transwell inserts

Transwell inserts represent a co-culturing system that allows the exchange of medium and its components (such as free and exosomal Tau) between two physically separated (non-interchangeable) cell populations (see **figure 5.6 A** for a diagram). We used the transwell insert system to mitigate the chance of false positives arising from the exchange of whole cells in conditioned medium transfer experiments (**figure 5.5 D**) and to prolong the exchange of Tau between donor and recipient cell populations. 2N3R-GFP and normal SH-SY5Y cells were used as donor and recipient cells, respectively, and co-cultured for 24 or 48 hours in the presence or absence of 200 nM bafilomycin. As above, bafilomycin was used to increase Tau release from the donor cells and decrease degradation in the recipient

cells, thereby increasing the chances of observing transmission. Following co-culture recipient cells were harvested, lysed and DAKO-Tau immunoprecipitated.

Tau12 immunoblot of DAKO-Tau IP'd 2N3R-GFP donor cells revealed one cross reactive band migrating at 88 kDa, consistent with 2N3R-GFP expression in recipient cells (band '**a**', **figure 5.6 B**). A 50 kDa Tau12 cross reactive was DAKO-Tau immunoprecipitated from normal SH-SY5Y cells cultured alone, consistent with endogenous SH-SY5Y Tau (band '**b**', figure **5.6 B**). This 50 kDa band was also IP'd from recipient SH-SY5Y cells co-cultured with 2N3R-GFP SH-SY5Y cells in the transwell system for 24 and 48 hours, in the presence and absence of bafilomycin. However, the Tau12 cross reactive 88 kDa band was not detectable in the IP from cells co-cultured under any condition, suggesting that under these conditions, Tau released from 2N3R-GFP SH-SY5Y cells did not associate with recipient SH-SY5Y cells cultured in the lower chamber of the transwell system to detectable levels (**figure 5.6 B**). Again, the Tau12 cross reactive band consistent with 2N3R-GFP-Tau (band '**a**' **figure 5.6 B**) was detected in the DAKO-Tau IP from 50 2N3R-GFP SH-SY5Y cells. Therefore, if transmission had occurred to the extent such that the quantity of Tau taken up by the recipient cells was equal to that expressed in 50 donor cells at the time recipient cells were IP'd, we would have detected it. This demonstrated that transmission, if occurring, was occurring below this level.

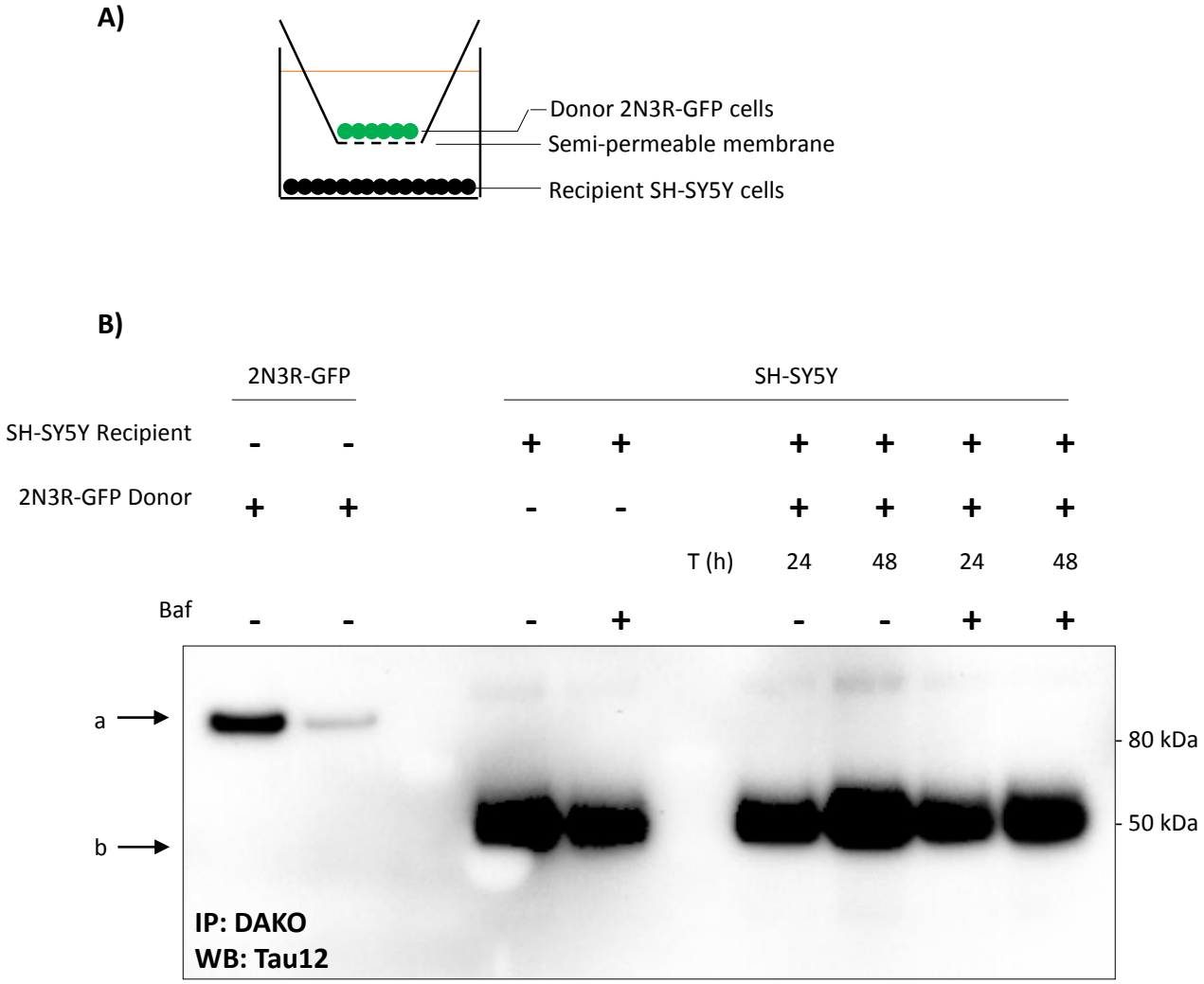

Figure 5.6 Use of transwell co-culturing system to study trans-cellular Tau transmission. A) Diagram of transwell co-culturing system. Donor cells (2N3R-GFP SH-SY5Y) are cultured in the insert which consists of a semi-permeable membrane with 1 µm pores. This allows for exchange of the conditioned medium and its components with the recipient cells cultured below in the 6 well plate (normal SH-SY5Y) without allowing the exchange of cells. **B)** Normal SH-SY5Y and 2N3R-GFP SH-SY5Y were co-cultured in transwell inserts according to the diagram in **A)** for 24 or 48 hours, in the presence or absence of bafilomycin. Recipient cells were then harvested, lysed and immunoprecipitated with DAKO-Tau (1 well of a 6 well plate i.e. all of the recipient cells / IP). Tau12 immunoblot of immunoprecipitated proteins was then performed. Donor cells and recipient cells cultured alone are analysed in the first and second pair of lanes, respectively.

5.2.7 Uptake of exosomal Tau by naïve SH-SY5Y recipient cells

Conditioned medium contains both free and exosomal Tau, with exosomal Tau accounting for ~1% of total extracellular Tau (**figure 3.11 C**). We aimed to study whether Tau released in exosomes was taken up by recipient SH-SY5Y cells in culture.

Exosomes were isolated from the conditioned prespun or optiMEM medium from 2N3R-GFP SH-SY5Y cells (10 x 10 cm plates for each) and resuspended in optiMEM or prespun medium, before being added to naïve SH-SY5Y cells in culture. After 24 hours, recipient cells were harvest, lysed and immunoprecipitated with DAKO-Tau and analysed by Tau12 immunoblot. An 88 kDa Tau12 immunoreactive band was detected from DAKO-Tau IP'd 2N3R-GFP lysates (band '**a**', **figure 5.7 A**), demonstrating the fidelity of immunoprecipitation. Moreover, a 50 kDa Tau12 immunoreactive band was immunoprecipitated from untreated and treated recipient normal SH-SY5Y cells, consistent with endogenous SH-SY5Y Tau (band '**b**' **figure 5.7 A**). However, Tau12 cross reactivity at 88 kDa was not detected in the DAKO-Tau IP'd SH-SY5Y cells treated with 2N3R-GFP SH-SY5Y exosomes, nor were any Tau12 cross reactive bands that differentiated untreated and treated SH-SY5Y recipient cells. This suggested that we were unable to detect Tau transmission under these conditions and with this methodology. The IP methodology was sufficient to detect levels of 2N3R-GFP-Tau equal to that expressed in ~50 2N3R-GFP SH-SY5Y cells (**figure 5.5 B**; **figure 5.6 B**). Our data demonstrated that levels of 2N3R-GFP-Tau in the exosomes from 10 x 10 cm plates was roughly equivalent to that in 0.2 µg cellular lysate (**figure 3.18**; **figure 5.5 A**), representing the levels in ~1200 cells (1 mg ≈ 10^6 cells). Therefore, if ≥4% (1200 / 50) of the exosomal Tau was taken up by the recipient cells at the time of harvest, we would have detected it. This suggested that if Tau uptake from 2N3R-GFP-Tau SH-SY5Y exosomes was occurring, it was occurring below this level.

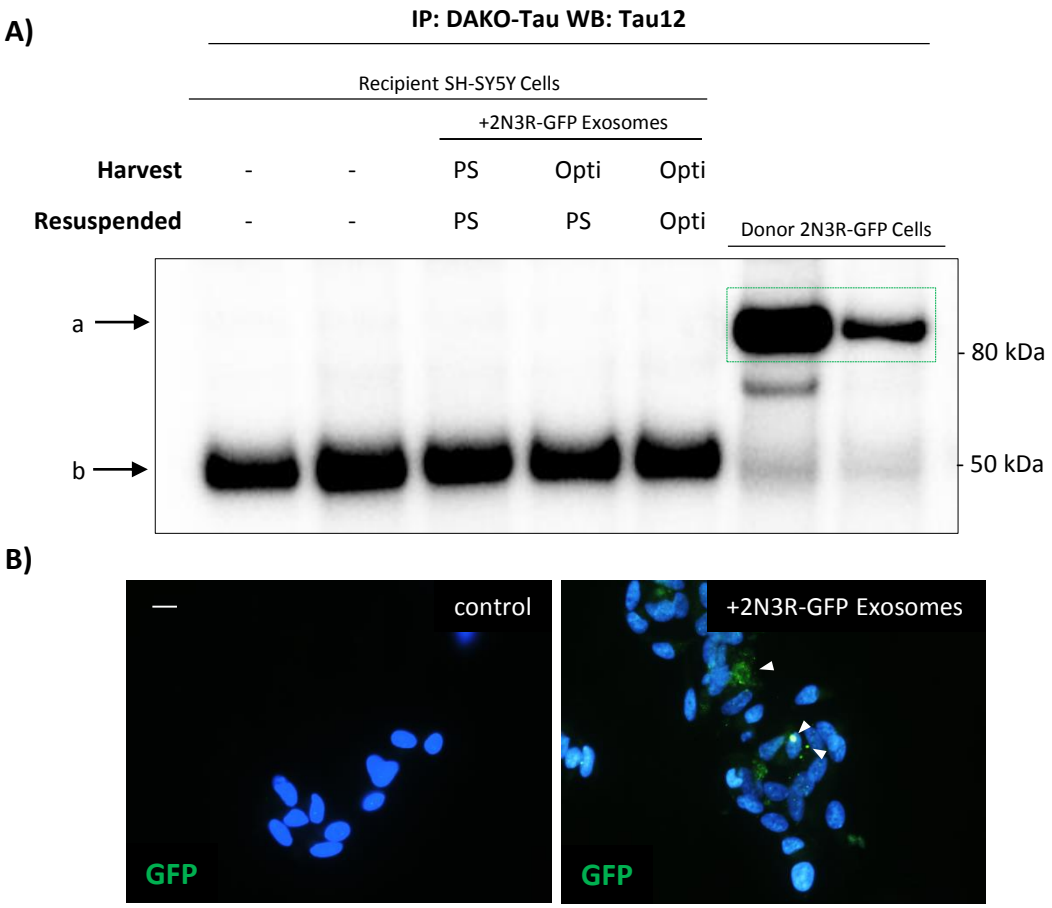

Figure 5.7 Analysis of recipient SH-SY5Y cells following treatment with exosomes from 2N3R-GFP SH-SY5Y conditioned medium. Normal SH-SY5Y cells in culture (in 6 well plates) were treated with exosomes isolated from the conditioned medium of 2N3R-GFP SH-SY5Y cells (10 x 10 cm plates / isolation). Exosomes were harvested from the conditioned prespun (PS) or optiMEM (opti) of donor cells, and resuspended in prespun or optiMEM medium. 24 hours later recipient cells were harvested, lysed and IP'd with DAKO-Tau (1 well 6 well plate / IP i.e. all of the recipient cells) . **A)** Tau12 immunoblotting of the immunoprecipitated lysates was performed. Bands 'a' and 'b' indicateTau12 cross reactive bands consistent with 2N3R-GFP and endogenous SH-SY5Y Tau, respectively. **B)** GFP immunocytochemical analysis of SH-SY5Y cells treated with 2N3R-GFP SH-SY5Y exosomes (10 x 10 cm) for 24 hours. White arrowheads indicate regions of GFP immunoreactivity.

GFP immunostaining of recipient SH-SY5Y cells treated with exosomes isolated from the conditioned medium of 2N3R-GFP SH-SY5Y cells (from 10 x 10 cm plates, isolated in prespun and resuspended in prespun medium) revealed some GFP immunoreactive puncta associated with SH-SY5Y nuclei, whereas no GFP immunostaining was detected in untreated SH-SY5Y cells (**white arrowheads, figure 5.7 B**), suggesting that some exosomal Tau-GFP was associated with the recipient cells. We cannot exclude that these puncta represented cleaved GFP, although no such GFP fragments were detected in the exosomes isolated from the conditioned medium of the 2N3R-GFP SH-SY5Y cells. On the other hand, this GFP immunostaining may have represented a level of transmission below this sensitivity of the IP – WB approach, thus explaining the discrepancies in the data.

5.2.8 Uptake of exosomal HA-P301L-2N4R-Tau by primary cortical neurons

We changed the parameters for studying the uptake of exosomal Tau by neuronal cells. We changed the donor cell system to SH-SY5Y cells expressing HA-P301L-2N4R-Tau. These cells were used as they were expressing a pathological form of Tau that we had confirmed the exosomal release of (**figure 4.4**). Moreover, the N-terminal HA tag represented a sensitive method of detection that would not cross detect endogenous Tau. Furthermore, we changed the recipient cell system to primary cortical neurons on the suggestion that these cells may have represented a more suitable system to detect exosomal Tau uptake.

Primary mouse cortical neurons were treated with exosomes isolated from the 24 hour conditioned optiMEM of HA-P301L-2N4R-Tau SH-SY5Y cells. HA immunostaining demonstrated no immunoreactivity in untreated primary mouse cortical neurons, whereas neurons treated with exosomes from HA-P301L-2N4R-Tau SH-SY5Y cells for 1 and 24 hours demonstrated HA immunoreactivity. At 1 hour immunoreactivity was punctate, and at 24 hours treatment time HA positivity was detected in patterns consistent with the neurites and cell bodies of treated neurons (**white arrowheads, figure 5.8 A**). We did not

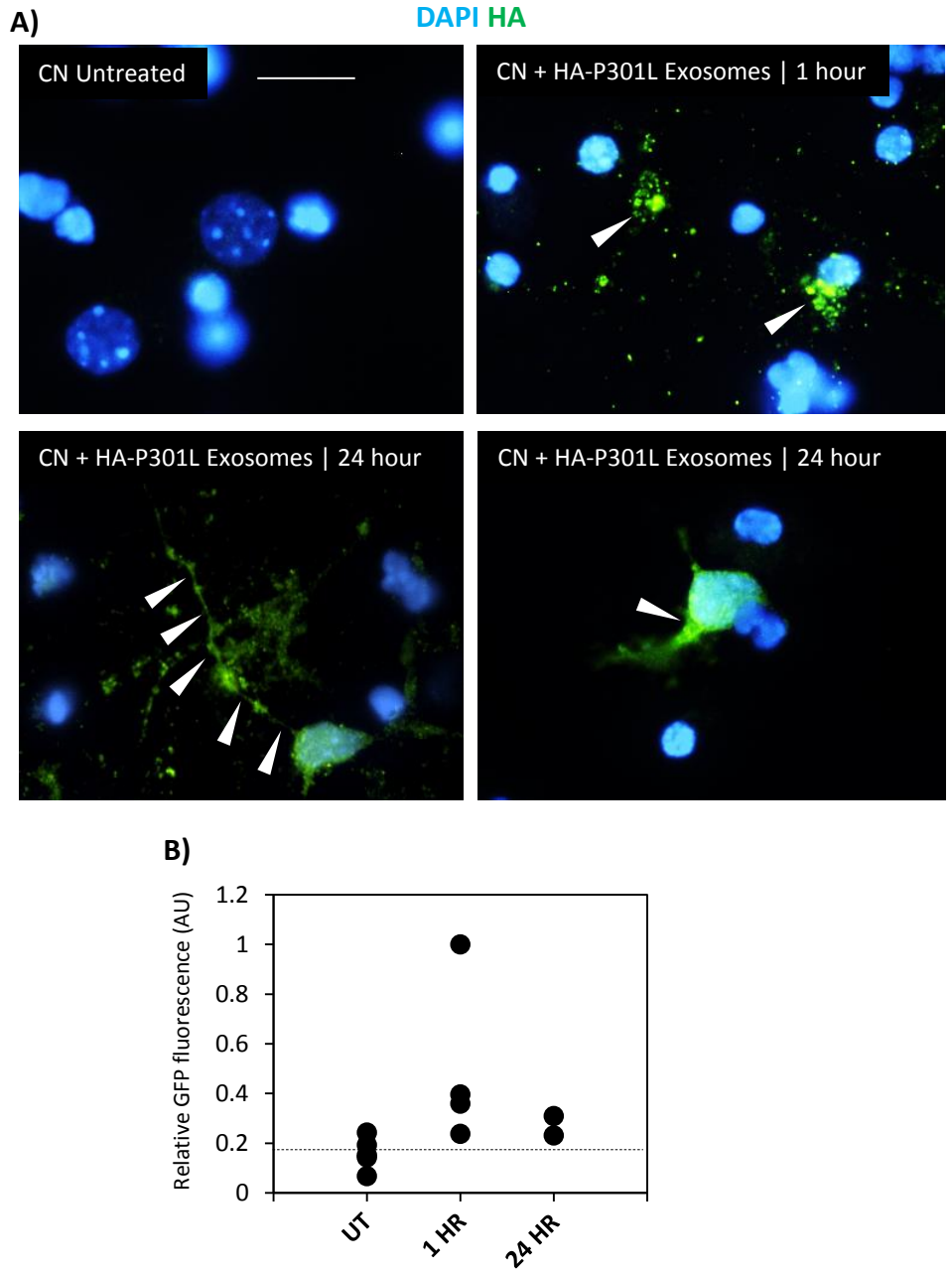

Figure 5.8 Immunocytochemical analysis of primary mouse cortical neurons treated with exosomes isolated from conditioned medium of P301L-2N4R-Tau SH-SY5Y cells. A) HA immunostaining of mouse primary cortical neurons treated with exosomes isolated from the 24 hour conditioned optiMEM from HA-P301L-2N4R SH-SY5Y cells (10 x 10 cm, exosome pellet resuspended in complete NeuorBasal medium). Treatment was conducted for 1 and 24 hours on cortical neurons in 6 well plates). White arrowheads indicate areas of HA immunoreactivity. **B)** Quantification of HA fluorescence in recipient cortical neurons treated with HA-P301L-2N4R exosomes. Fluorescence was integrated over the whole field (40 X magnification) and normalised to the number of nuclei in the field, each black dot represents one field (n=1; 4 – 18 cells / field counted). Black dashed bar indicates mean fluorescence of untreated samples.

counterstain the neurons in this experiment to avoid introducing background fluorescence that may have interfered with the HA-Tau signal.

The HA fluorescence intensity from untreated cortical neurons and cortical neurons treated with exosomes isolated from the conditioned medium of HA-P301L-2N4R-Tau SH-SY5Y cells was integrated (ImageJ) and normalised to the number of cells in the field. Higher intensity signal was detected from cortical neurons treated with exosomes isolated from HA-P301L-2N4R-Tau conditioned medium for 1 and 24 hours, relative to untreated cortical neurons (4 fields analysed / condition, 4 – 18 cells / field, expressed relative to number of cells / field; **figure 5.8 B**).

These observations are consistent with the uptake of exosomally associated HA-P301L-2N4R-Tau by recipient primary mouse cortical neurons in culture.

5.3 Transmission of Tau protein between Cells

5.3.1 Transmission of tau protein between directly co-cultured SH-SY5Ycells

The ability of Tau to move between directly co-cultured cells was investigated. Initially HA-0N3R SH-SY5Y and 2N3R-GFP SH-SY5Y populations were cultured separately and analysed by HA and GFP co-immunostaining. 2N3R-GFP and HA-0N3R SH-SY5Y cells were strongly stained by GFP and HA antibodies, respectively, whilst no staining was observed in the other channel from each cell line (**figure 5.9 A**).

Next, 2N3R-GFP and HA-0N3R SH-SY5Y cells were co-cultured for 48 hours in the presence of 200 nM bafilomycin A1. Bafilomycin treatment was adopted to increase Tau release and decrease its degradation, thereby increasing the chance of observing transmission. HA / GFP co-immunostaining analysis of the co-cultured cells demonstrated the association of HA immunoreactive puncta with GFP positive cells. GFP immunoreactivity was dispersed throughout the cytoplasm, consistent with ectopic expression of 2N3R-GFP, whilst HA

immunoreactivity localised in puncta within these cells (**figure 5.9 B** upper and lower panels).

2N3R-GFP cells co-cultured with HA-0N3R SH-SY5Y cells in the absence of bafilomycin did not demonstrate associated HA immunoreactivity at rates above background levels, which demonstrated that this process was potentiated by lysosomal compromise (**figure 5.10 A**). Furthermore, there was a linear correlation between the seeding density of co-cultured cells and percentage of 2N3R-GFP SH-SY5Y cells demonstrating HA immunoreactivity (r^2 = 0.67, **figure 5.10 B**) and percentage of 2N3R-GFP SH-SY5Y cells with HA immunoreactivity only exceeded baseline levels (i.e. in the absence of bafilomycin) when cells were cultured at high seeding densities (i.e. 100,000 – 500,000 cells / 6 well). At high cell densities, HA immunoreactivity was detected in 11±2% of 2N3R-GFP SH-SY5Y cells (**figure 5.10 C**). These observations suggested that cell – cell contact was important for HA spread to 2N3R-GFP SH-SY5Y cells. Confocal Z-stack analysis demonstrated that HA immunoreactivity associated with 2N3R-GFP SH-SY5Y cells was located inside of the cells and, furthermore, appeared to be located inside vacuolar spaces which were not co-positive for GFP (**figure 5.10 D**).

The intensities of DAPI, GFP and HA immunostaining across line segments drawn through regions of HA immunoreactivity in 2N3R-GFP cells were plotted. This analysis confirmed the presence of HA immunoreactivity in 2N3R-GFP SH-SY5Y cells (red peaks, **figure 5.10 E**). Moreover, HA immunoreactivity was detected in regions of cells where GFP intensity was locally reduced (**arrows, figure 5.10 E**) and in juxta-nuclear regions (**asterisk, figure 5.10 E**).

Collectively these observations suggested that HA-0N3R-Tau from HA-0N3R SH-SY5Y cells was transmitted to 2N3R-GFP SH-SY5Y cells when these cells were directly co-cultured.

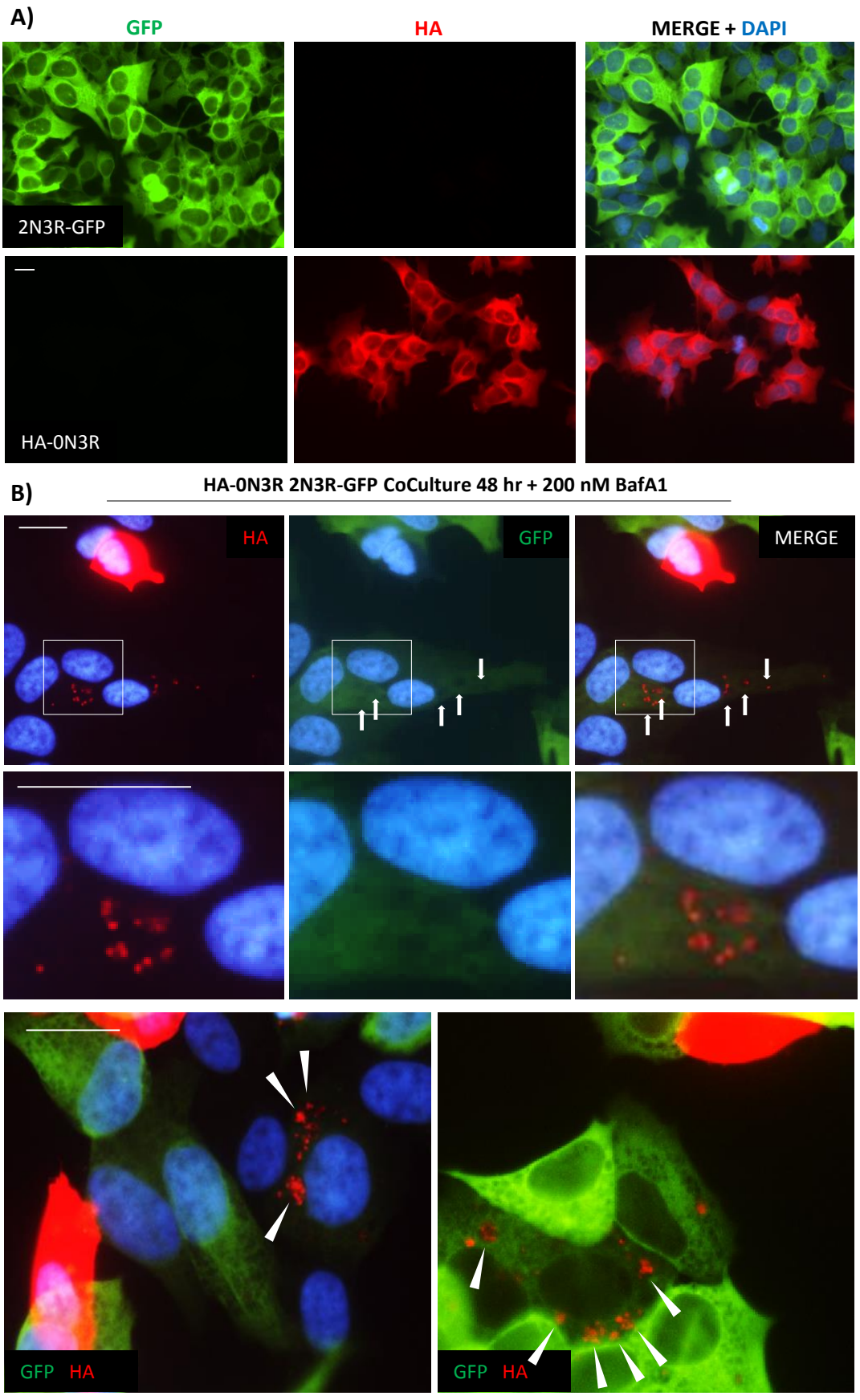

Figure 5.9 Immunocytochemical analysis of co-cultured 2N3R-GFP and HA-0N3R-Tau SH-SY5Y cells. A) Individually cultured 2N3R-GFP and HA-0N3R SH-SY5Y cells co-immunostained with GFP and HA antibodies. **B)** HA / GFP co-immunostaining of 2N3R-GFP and HA-0N3R SH-SY5Y cells co-cultured for 48 hours in the presence of 200 nM bafilomycin A1. white arrows in upper panel indicate vacuolar regions in the 2N3R-GFP cells, occupied by HA immunoreactivity. White arrowheads in the lower panel indicate HA immunoreactivity observed in association with 2N3R-GFP SH-SY5Y cells.

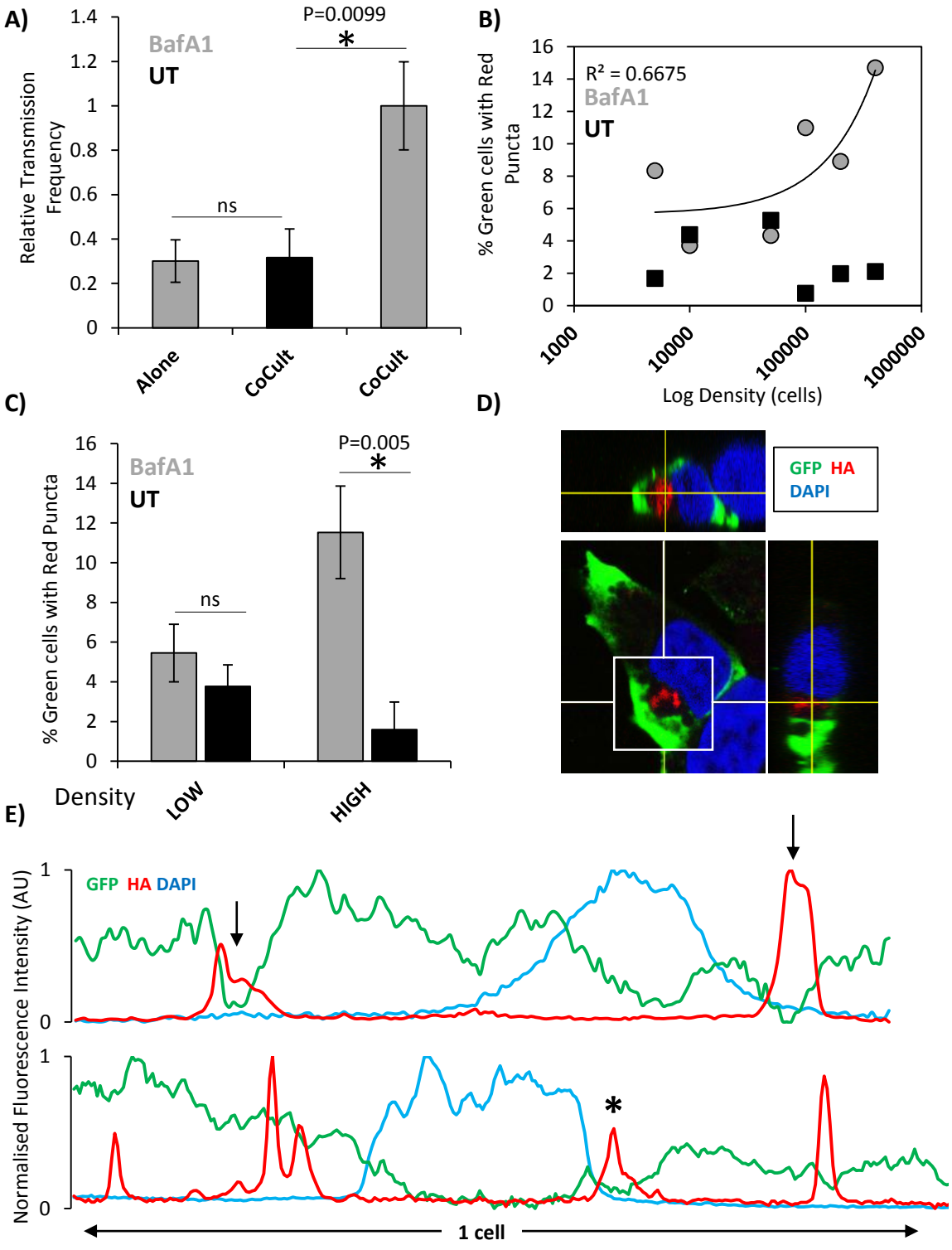

Figure 5.10 Characterisation of Tau transmission between directly co-cultured SH-SY5Y cells. HA-0N3R-Tau and 2N3R-GFP-Tau SH-SY5Y cells were co-cultured at increasing densities in 6 well plates and analysed by HA / GFP co-immunostaining. **A)** Quantitative analysis of HA immunoreactivity detected in 2N3R-GFP SH-SY5Y cells following co-culture with HA-0N3R SH-SY5Y cells in the presence and absence of 200 nM bafilomycin (48 hours). 2N3R-GFP cells with HA immunoreactive were counted as positive and expressed as a percentage of total cell count. Values from non bafilomycin treated co-cultured cells and 2N3R-GFP SH-SY5Y cultured alone were expressed relative to co-culture values in the presence of bafilomycin (mean ± SEM, n=6, Student's T-test vs. 'alone', ns = not significant). **B)** Correlation analysis of percentage of HA positive 2N3R-GFP cells with cell seeding density, following 48 hour co-culture with HA-0N3R SH-SY5Y cells (A, black squares = untreated, grey circles = 200 nM bafilomycin A1). **C)** Analysis of percentage of 2N3R-GFP exhibiting HA immunoreactivity after co-culture with HA-0N3R SH-SY5Y at low (5-50k cells / 6 well) and high (100-400k cells / well) densities in the absence (black bars; UT) and presence (grey bars) of 200 nM bafilomycin for 48 hours (mean ± SEM. n=6, Student's T-test vs. 'UT', ns = not significant). **D)** Confocal Z-stack analysis of an HA positive 2N3R-GFP SH-SY5Y cell, following co-culture with HA-0N3R SH-SY5Y cells (48 hours, 200 nM bafilomycin A1). **E)** Analysis of integrated fluorescence intensity of DAPI, GFP and HA staining across line segments 2N3R-GFP SH-SY5Y cells displaying peaks of HA immunoreactivity after co-culture with HA-0N3R SH-SY5Y cells.

5.3.2 Trans-cellular movement of HA-P301L-2N4R-Tau from SH-SY5Ycells to cortical neurons in direct co-culture

We analysed Tau transmission from HA-P301L-2N4R-Tau SH-SY5Y cells to primary mouse cortical neurons using a direct co-culture system. Primary mouse cortical neurons cultured alone did not demonstrate any Tau12 immunostaining, consistent with the epitope of Tau12 being specific for human Tau (**figure 5.11 A**). Cortical neurons were positively stained with βiii Tubulin antibody labelling neurites of these cells (**figure 5.11 A**).

Tau12 – βiii Tubulin co-immunostaining of co-cultured HA-P301L-2N4R-Tau SH-SY5Y and primary cortical neurons demonstrated intense Tau12 staining of SH-SY5Y cells. Moreover, Tau12 immunoreactivity was detected in the βiii Tubulin positive neurites emanating from primary mouse cortical neurons (**white arrows**, **figure 5.11 B**). HA immunoreactivity was punctate, as demonstrated by the plot of HA fluorescence intensity along a line segment through the staining. This also demonstrated the co-localisation between HA and Tubulin (**figure 5.11 C**). As Tubulin was also staining SH-SY5Y cells, we cannot exclude that this represented a neurite from an HA-P301L-2N4R-Tau SH-SY5Y cell. When co-cultured, however, HA-P301L-2N4R-Tau SH-SY5Y cells and primary mouse cortical neuron neurites came into close proximity, and diffuse Tau12 immunoreactivity was detected along this boundary (**arrows**, merged image, **figure 5.11 B**). These findings suggested that Tau12 immunoreactive species expressed in HA-P301L-2N4R-Tau SH-SY5Y cells were potentially transmitting to primary mouse cortical neurons when these cells were co-cultured.

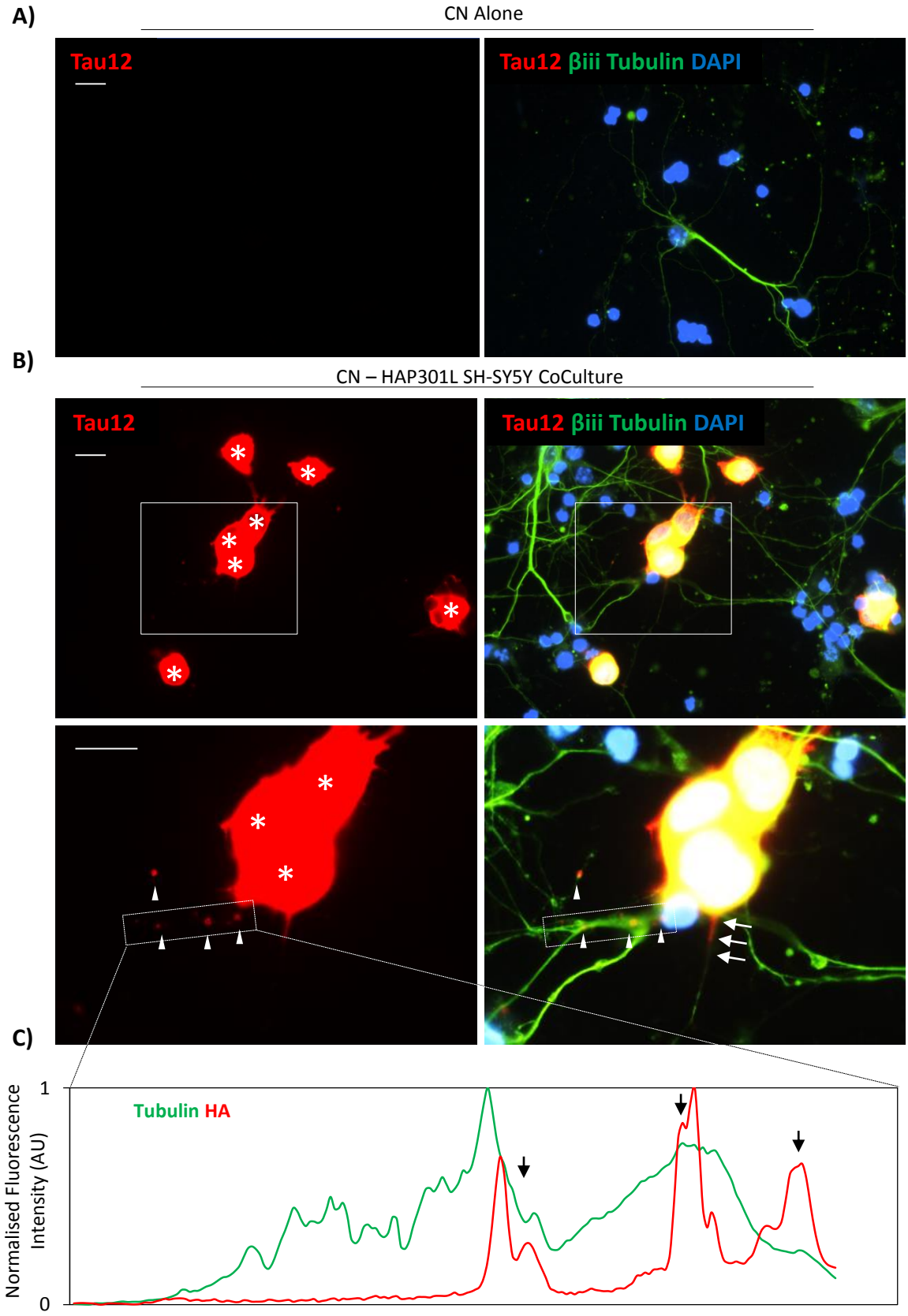

Figure 5.11 Immunocytochemical analysis of co-cultured primary mouse cortical neurons with P301L-2N4R-Tau SH-SY5Y cells. A) Immunocytochemical analysis of primary mouse cortical neurons (cultured alone) with Tau12 and Tubulin. Tau12 does not detect Mouse Tau. **B)** Tau12 and Tubulin immunocytochemical analysis of primary mouse cortical neurons co-cultured with HA-P301L-2N4R SH-SY5Y cells (24 hours). HA-P301L-2N4R-Tau SH-SY5Y cells are indicated by the white asterisks. White boxed regions in upper panel designate enlarged regions in lower panel. White arrowheads in lower panel indicate regions of colocalisation between Tau12 and Tubulin immunoreactivity and the white dashed box region indicates the region used for **C)** plot of fluorescent intensity profiles of Tubulin and HA immunostaining through line segment of the ICC image. Arrows indicate HA immunoreactive puncta and correspond to the arrowheads in **B)**. (CN = cortical neurons).

5.4 Analysis of the toxicity of HA-P301L-2N4R-Tau SH-SY5Y exosomes to primary cortical neurons

Exosomes were isolated from the 24 hour conditioned optiMEM of HA-P301L-2N4R-Tau and normal SH-SY5Y cells by differential ultracentrifugation, resuspended in NeuroBasal medium, serially diluted and added to primary mouse cortical neurons in culture (96 well plates). 24 hours later, MTT assay of the primary mouse cortical neurons was used to assess viability of the neuronal cells.

Exosomes isolated from the conditioned medium of normal SH-SY5Y cells reduced MTT activity in primary cortical neurons in a dose dependent manner; lower concentrations (equal to the exosomes from 0.03 – 0.1 x 10 cm plates) had no effect on cell viability, whereas higher concentrations (equal to the exosomes from 0.12 – 0.5 x 10 cm plates) significantly reduced cell viability of primary mouse cortical neurons (**figure 5.12 A and B**). On the other hand exosomes isolated from the conditioned medium of HA-P301L-2N4R SH-SY5Y cells significantly reduced the viability of primary mouse cortical neurons at all concentrations (exosomes from 0.03 – 0.5 x 10 cm plates; a stoichiometry surface area of 7.4 to 25 times) (**figure 5.12 A** and **B**).

A sample of the exosomes used to treat primary cortical neurons were analysed by Western blotting. Tau12 immunoreactivity at 65 kDa was detected in the exosomes isolated from HA-P301L-2N4R-Tau SH-SY5Y cells. There was no difference in the levels of Alix immunoreactivity (at 100 kDa) between the exosomes isolated from normal and HA-P301L-2N4R-Tau SH-SY5Y cells (**figure 5.12 C** and **D**) suggesting that primary mouse cortical neurons were treated with comparable quantities of exosomes from each cell line.

These findings suggested that exosomes isolated from the conditioned medium of HA-P301L-2N4R-Tau SH-SY5Y cells were selectively toxic to primary mouse cortical neurons as assessed by MTT assay.

A)

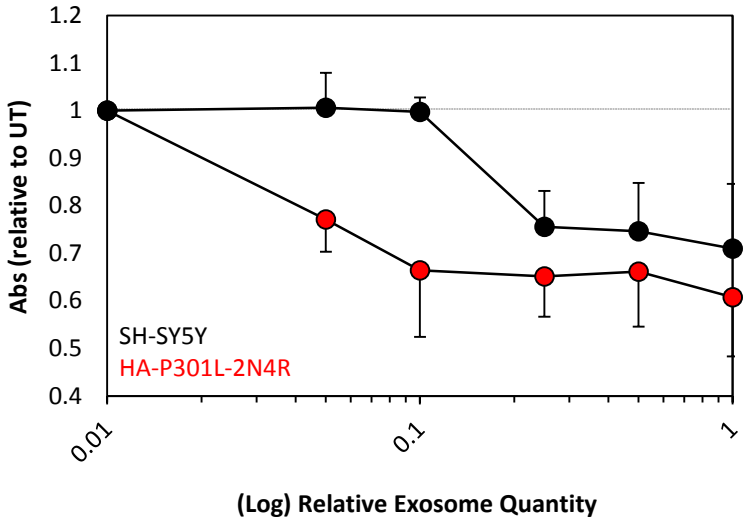

B)

T-TEST *P*-VALUES (vs UT)

Relative Exosome Quantity

	0.05	0.1	0.25	0.5	1
SH-SY5Y	0.937	0.937	0.018	0.047	0.077
HAP301L	0.031	0.021	0.001	0.002	0.011

C)

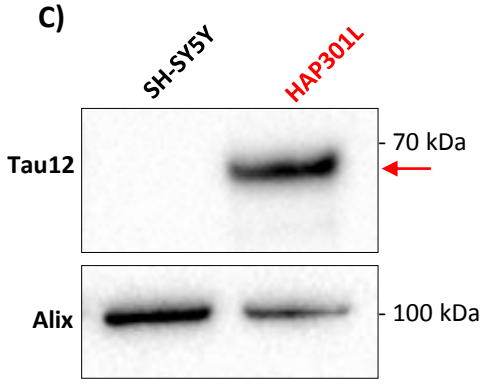

D)

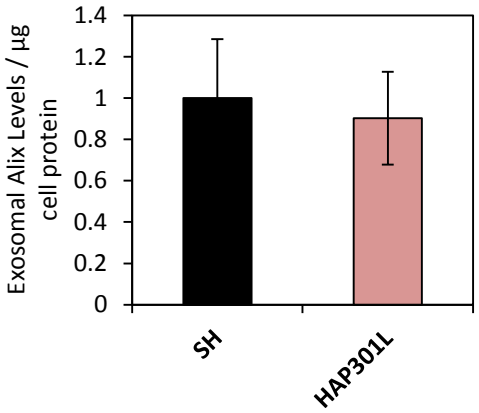

Figure 5.12 MTT analysis of primary mouse cortical neurons treated with P301L-2N4R-Tau exosomes. A) MTT analysis of cortical neurons treated with increasing amount of exosomes (from 0.03 – 0.5 x 10 cm, 24 hour conditioned optiMEM, resupsended in Neurobasal medium) from normal (black circles) and HA-P301L-2N4R-Tau expressing (red circles) SH-SY5Y cells. Treatment was for 24 hours. Each bar represents the mean ± SEM from four independent experiments (each independent experiment representing the mean of four technical replicates). **B)** Statistical analysis of MTT absorbance values from cortical neurons treated with exosomes from SH-SY5Y and HA-P301L-2N4R SH-SY5Y cells. *P*-values were obtained by performing a non-paired Students T-test between the untreated sample (UT) and the respective treated samples. **C)** Western blot analysis of Alix and Tau levels in the exosomal samples with which cortical neurons were treated (exosomes from 24 hour conditioned optiMEM corresponding to 5 x 10 cm plates was loaded). **D)** Quantification of Alix levels in the samples used to treat primary cortical neurons (mean ± SEM, n=3, no significant difference observed).

6 Discussion

6.1 Tau expression in SH-SY5Y cells

6.1.1 Endogenous Tau expression in SH-SY5Y cells

Endogenous Tau in undifferentiated SH-SY5Y cells was detected by Tau12 immunoblotting as two species, one major and one minor band. The major band migrated consistently with 0N3R-Tau (~50 kDa) and the minor band migrated consistently with 1N3R / 0N4R-Tau. Because the Tau ladder was not separated into 6 distinct bands in our gel system, we were unable to identify if the minor band represented 1N3R or 0N4R-Tau.

PCR of mRNA isolated from undifferentiated SH-SY5Y cells did not amplify any 4R Tau mRNA species (Uberti et al. 1997) therefore suggesting that the minor band detected in our analysis represented 1N3R-Tau. And other studies have suggested that endogenous Tau in undifferentiated SH-SY5Y cells is characterised as foetal, consistent with expression of 3R-Tau (Tanka et al. 1995).

6.1.2 Ectopic Tau expression in SH-SY5Y cells

In order to investigate the exosomal release of Tau we ectopically expressed distinct Tau isoforms in SH-SY5Y cells.

Our findings suggested that ectopic expression of 2N4R-Tau in SH-SY5Y gave rise to the full length protein as evidenced by its cross reactivity with N-terminal (Tau12) and C-terminal (Tau46) antibodies. Ectopic 2N4R-Tau protein migrated anomalously in SDS-PAGE, appearing as 17 kDa larger than predicted by its AA sequence, a migration pattern which is consistent with previous reports (Goedert & Jakes 1990). The migration of ectopically expressed 2N3R-Tau was also anomalous, migrating at an apparent molecular weight of 57 kDa, 14 kDa larger than its predicted size (2R = 3 kDa). These observations demonstrate that the 2nd microtubule binding repeat did not account for the anomalous migration of

2N4R-Tau. Moreover, migration of the Tau repeat domain (AA244 – 372) migrates at 14 kDa in SDS-PAGE, precisely as predicted from its amino acid composition (Yao et al. 2003) further demonstrating that the anomalous migration of Tau cannot be localised to this region of the protein. Indeed, limited digestion of tubulin bound 2N4R-Tau liberated the N-terminal projection domain which, when analysed by SDS-PAGE, ran anomalously slowly thus accounting for the apparent molecular weight of full-length Tau (Steiner et al. 1990).

Anomalous migration in SDS-PAGE can be accounted for by alterations in SDS binding ratio of specific proteins (Rath et al. 2009), or may be contributed to by the structural rigidity conferred by proline rich regions (Kirkland et al. 1998). Since Tau protein contains a proline rich region (25% proline) in the N-terminal projection domain – the same domain that confers decreased electrophoretic mobility, (Friedhoff et al. 2000), it is likely that that this explains the behaviour of Tau in SDS-PAGE. Our findings also demonstrated that ectopically expressed Tau was phosphorylated (at S356, T181 and T205) which accounted for a small proportion (~2 kDa) of its decreased migration in SDS-PAGE.

Ectopically expressed 2N4R-Tau exceeded levels of endogenous Tau expression by 20 times. However, levels of ectopically expressed Tau did not exceed that observed in human hippocampi when expressed relative to the neuron specific marker beta-three Tubulin (Menezes and Luskin, 1994). SH-SY5Y cells have previously been reported to express low levels of Tau relative to human brain (Zhong et al. 1999; Agholme et al. 2010), ectopically expressing 2N4R-Tau in SH-SY5Y cells therefore brought Tau levels in these cells closer to that observed in human brain.

6.1.3 Microtubule binding of endogenous and ectopically expressed Tau

We used a previously published ultracentrifugation approach to investigate the association of endogenously and ectopically expressed Tau with the microtubule network (Derisbourg

et al. 2015; Dou et al. 2003; Fath et al. 2002.; Hamdane et al. 2003; Krishnamurthy & Johnson 2004; Nagiec et al. 2001; Wagner et al. 1996).

Using this approach we observed that a large percentage (80%) of endogenous SH-SY5Y Tau was not associated with microtubules, consistent with previous reports that demonstrate Tau extracted from SH-SY5Y cell lysates does not bind efficiently to microtubules (Tanaka et al. 1995). This may have been due to the fact that endogenous SH-SY5Y Tau is highly phosphorylated, including at epitopes reminiscent of PHF-Tau, rendering it unable to stimulate the formation of microtubules (Tanaka et al. 1995; Zhong, Iqbal and Grundke-Iqbal, 1999). SH-SY5Y cells have a low Tau : HMW MAP ratio, suggesting that under normal conditions HMW MAPS (such as MAP2) co-ordinate microtubule dynamics in these cells (Zhong et al. 1999).

A slightly larger proportion (~30%) of ectopically expressed 2N4R-Tau was associated with microtubules. Although this proportional increase was not statistically significant, in absolute levels this translated into 20 times more ectopic Tau being associated with microtubules than endogenous Tau demonstrating that ectopically expressed 2N4R-Tau readily associates with the microtubule network at levels far exceeding that of endogenous Tau. This may have been explained by its higher affinity for microtubules, or an effect of increased concentration.

When expressed in NIH 3T3 cells, disease associated mutants of Tau (P301L, R406W, V337M) co-localise with microtubules. However, co-expression of WT-Tau displaces these Tau mutants to the cytoplasm, demonstrating that the binding of Tau to microtubules is a competitive process (Lu and Kosik, 2001). We did not assess the effects of ectopic Tau expression on the association of endogenous Tau with microtubules, although it is possible that ectopically expressed 2N4R-Tau may have displaced endogenous Tau from the microtubules.

6.2 Enrichment of exosomes from the conditioned medium of SH-SY5Y cells

6.2.1 Size of exosomes

We used a differential ultracentrifugation methodology to enrich exosomes from the conditioned medium of SH-SY5Y cells, adapting a published method (Quah & Neill 2005). Differential ultracentrifugation is considered the gold standard preparative methodology for enrichment of exosomes from extracellular fluids since exosomes were first identified in 1983 (Pan and Johnstone, 1983; Momen-Heravi et al. 2013). We analysed our exosome population in terms of its size distribution and expression of protein markers specific to exosomes. NTA, which detects Brownian motion of particles using light scattering thereby inferring particle size, has been widely adopted to analyse PSDs of biofluid derived vesicles (Dragovic et al. 2011; Willms et al. 2016). Using NTA we obtained a mode size of 83 nm for the diameter of our exosomal population, which is consistent with previous studies which have obtained peak modal diameters of between 80 and 100 nm of exosomes isolated from the culture medium of SH-SY5Y cells (Alvarez-Erviti et al. 2011; Marimpietri et al. 2013; Tannetta et al. 2013.; Li et al. 2015).

We also used tuneable resistive pulse sensing (TRPS), a technology which utilises the magnitude of resistance of nanoparticles to an electrical current to compute their size on a particle by particle basis, to size the particles in our exosome population. TRPS has also been used to gauge the PSD of extracellular vesicles (Anderson et al. 2015.; Polanco et al. 2016). With TRPS analysis we obtained a larger peak modal size than that obtained with NTA, of 117-128 nm. Whilst this is still consistent with exosome vesicles (Anderson et al. 2015.; Polanco et al. 2016) divergences in the data obtained with these two sizing technologies has previously been reported (van der Pol et al. 2014). Such divergences have been ascribed to differences in the lower limit of detection between the two technologies.

Because NTA can detect particles <100 nm in size and the lower detection limit for TRPS is 100 nm, TRPS will overestimate the modal size of a heterogeneous particle population if it contains many vesicles <100 nm, as our population did. Alternative characterisation techniques such as transmission electron microscopy may represent an even lower detection limit as well as providing morphological information.

6.2.2 Expression of exosomal markers

We also analysed the expression of specific protein markers in our exosome population, namely Alix, TSG101, Hsc70, Flotilin-1 and CD-81, all of which were detected in our exosome population.

These proteins are widely discussed as 'specific' to exosomes and all were positively detected in our vesicle population. Alix protein is involved in endomembrane sorting (Hurley and Odorizzi, 2012) as is TSG101, whereas Hsc70 is a chaperone protein potentially involved in the formation of exosomes and targeting of substrates (Géminard et al. 2001, 2004). CD-81 is a tetrapsanin with roles in extracellular vesicle formation (Andreu and Yáñez-Mó, 2014) whilst flotilin-1 is localised to lipid-raft microdomains and has roles in endocytosis and trafficking (Meister and Tikkanen, 2014). The functional differentiation of these markers suggests they may in fact be distinguishing different sub-populations of exosomes. A view which is reinforced by their differential equilibrium distribution following sucrose gradient ultracentrifugation (Baietti et al. 2012; Frühbeis et al. 2013). In fact, it has been shown that distinct sub-populations of exosomes with distinct densities and cargo are released by cultured cells (Willms et al. 2016) and this may be reflective of different biogenesis pathways (e.g. ESCRT dependent and independent pathways).

Furthermore, microvesicles, which shed directly from the plasma membrane, may share some of the same protein markers as exosomes including Alix (van Niel & Raposo 2018). Microvesicles are formed by direct shedding of the plasma membrane and their size range

overlaps with that of exosomes (Tricarico et al. 2017). Knockdown of Rab27a, which inhibits the formation of endosomally derived vesicles, decreased levels of Hsc70, Tsg101 and Alix in the 100,000 x g pellet, suggesting thse markers are derived endosomally and therefore constitute exosome specific markers, thus validating their use to distinguish exosomes in the present study. However, the levels of some 'exosomal' markers (CD9, Mfge8) were unaffected by Rab27a knockdown, and vesicles of 30 – 100 nm were still isolated under these conditions (Angelique Bobrie et al. 2012). These findings argue that differential ultracentrifugation co-sediments vesicles derived from different cellular sources.

These findings further compound the interpretation of the identity of the extracellular vesicles studied here. Because our exosomes were isolated by size and analysed by a bulk approach, it is likely that we were analysing different sub-populations of exosomes. It would be informative to adopt immune-affinity and refined physical (i.e. density gradient) approaches to isolate sub-populations of exosomes from the conditioned medium of SH-SY5Y cells and probe the distribution of Tau protein therein.

6.3 The release of tau protein in exosomes from SH-SYY cells

In the present work we demonstrated that Tau protein is released in exosomes from SH-SY5Y cells. Studies investigating exosomal Tau release have been steadily increasing since the first descriptions in 2012 (Saman et al. 2012; Simón et al. 2012).

The early observations of exosomal Tau release from cell cultures adopted transient / induced expression of Tau protein and were met with critiques about the validity of such models to accurately reflect proteostasis (Pooler et al. 2013; Dujardin et al. 2014). In fact, Simón et al. (2012) suggested that exosomal release of Tau was precisely the result of its ectopic overexpression, a sentiment reflected by the very title of their publication (Tau Overexpression Results in its Secretion via Membrane Vesicles; Simon et al. 2012). Pooler et al. (2013) and Dujardin et al. (2014) attempted to detect Tau protein in the exosomes

isolated from the conditioned medium of primary rat cortical neurons, and both declared its detection as essentially ambiguous. However, using the same cell system (primary rat cortical neurons) and detection methodology (Western blotting), Wang et al. (2017) unambiguously demonstrated the presence of exosomal Tau, potentially because these authors isolated exosomes from a large volume of conditioned medium (from 10-16 x 150 mm plates).

Following this, other recent work has taken advantage of the increased sensitivity of ELISA and Simoa technology to demonstrate the facticity of exosomal Tau release. Tau was detected in the exosomes from N2a, iHCN, and primary rat hippocampal neuronal cultures (Kanmert et al. 2015) and iPSC derived neurons (Guix et al. 2018).

We established, in accordance with earlier and contemporaneous studies, the exosomal release of ectopically expressed Tau from neuroblastoma cells. Moreover, we demonstrated the exosomal release of endogenous SH-SY5Y Tau. The detection of endogenous SH-SY5Y Tau in exosomes demonstrates that release of Tau in exosomes is a constitutive and physiological process.

Ectopic 2N4R-Tau was expressed at levels 20 times higher than that of endogenous SH-SY5Y Tau. Levels of ectopic Tau in the exosomes were also 20 times higher than that of endogenous Tau. Therefore the proportional levels of cellular and exosomal Tau were similar between endogenous and ectopic Tau. This suggests that the ectopic expression of Tau did not induce its release in exosomes from SH-SY5Y cells, but merely increased the levels of this pathway in proportion to the levels of Tau expression.

Our observations and those mentioned above therefore serve to reinforce the status of Tau protein as a bona-fide exosomal cargo, and suggest earlier failures to detect exosomal Tau may have been due to limitations in sensitivity.

Table 6.1 summarises the recent work focussed on the study of exosomal Tau release from cell culture models.

Table 6.1 Summary of published reports investigating exosomal Tau release

Study	Cell model(s)	Exosome isolation	Tau detected?	Detection method(s)	Form(s) of exosomal Tau / comments
Saman et al. 2012 Saman et al. 2014	M1C with 0N4R induced	Differential UC	Yes	WB - Tau12, DAKO-Tau Mass-spec ELISA	AT180, AT100, AT270, AT8, PHF-1
	AD CSF	Sucrose gradient differential UC	Yes	WB ELISA	AT270 (35, 52, 68 kDa - multimers)
Simon et al. 2012	HEK with 3R-Tau	Differential UC	Yes	WB Immunogold EM	
Karch et al. 2012	SH-SY5Y cells - endogenous	Differential UC	No	WB – Tau7	
Santa Maria et al. 2012	SH-SY5Y cells with GFP-Tau	Differential UC	No	WB - RD3, RD4	
Pooler et al. 2013	Primary rat cortical neurons	Differential UC	Ambiguous	WB - DAKO-Tau	
Dujardin et al. 2014	Primary rat cortical neurons	Differential UC	Yes – EM No – WB	WB – N/C-term ELISA Immunogold EM	
	Primary rat neurons infected with 1N4R	Differential UC	Yes	WB – N-term	FL (?)
	Rat brain ISF	Differential UC	Yes	Immunogold EM – C/N-term	
Kanmert et al. 2015	N2a	Differential UC	Yes	ELISA: Tau5-BT2	Mid-region – not further characterised
	iHCN	Sucrose gradient differential UC	Yes	ELISA: Tau5-BT2	
	Primary rat hippocampal neurons	Sucrose gradient differential UC	Yes	ELISA: Tau5-BT2	
Asai et al. 2015	Primary microglia	Differential UC	Yes	WB – Tau46	Oligomeric released by microglia
	PS19 mouse brain			WB – T22 Immunogold EM	
Polanco et al. 2016	WT and rTg4510 mouse brain	Differential UC	Yes	WB – Tau5, AT8, AT100. AT180, AT270, pS262, pS422	
Reilly et al. 2017	iN transduced with RD-LM	ExoQuik-TC	Yes	WB – DAKO-Tau	
Wang et al. 2017	Primary rat cortical neurons	(Sucrose gradient) differential UC	Yes	WB - DAKO-Tau, Tau N-term, Tau C-term	FL dephosphorylated
	N2a with Tau-GFP	(Sucrose gradient) differential UC	Yes	WB - DAKO-Tau	FL
	CSF	Differential UC	Yes (?)	WB - DAKO-Tau, 12E8, PHF-1	FL (?)
Guix et al. 2018	iPSC derived neurons	Differential UC	Yes	ELISA FL:Tau12, Tau46 Mid-region: Tau5-BT2	FL (80%) and mid-region
	CSF	Differential UC	Yes	ELISA Simoa	FL (6-12%) and mid-region
	Plasma	ExoQuik precipitation then L1CAM IP	Yes	ELISA Simoa	FL (2%) Mid-region pT181
Stern et al. 2016	Plasma (control and CTE)	SEC	Yes	Fluorescent NTA. Clone D-8 Tau antibody with quantum dot secondary antibody	Tau increased in CTE exosomes

6.3.1 Effects of growth conditions on release of exosomes and exosomal release of tau

Exosomes isolated from the conditioned medium of SH-SY5Y cells grown in optiMEM reduced serum medium had higher Alix levels per μg of cellular protein than when cells were grown in prespun serum containing medium. This suggests that growth conditions had a specific impact upon the quality and / or quantity of exosomes released from SH-SY5Y cells.

Li et al. (2015) demonstrated that growth in optiMEM was associated with an increase in the number of extracellular vesicles released by cells compared to growth in prespun serum containing medium. Proteomic and gene ontology analyses also demonstrated that exosomes released from cells cultured in optiMEM contained higher levels of proteins involved in EV biogenesis such as ARF6 and small GTPase / Ras related proteins (Li et al. 2015). This suggests that growth in optiMEM promotes exosome release from neuroblastoma cells.

We observed that when SH-SY5Y cells were grown in prespun serum containing medium, exosomal Tau release was increased. Given the above, this suggests that the exosomes released from SH-SY5Y cells grown in prespun serum medium contained more Tau per exosome. There are however, alternative hypotheses consistent with this observation such as Tau enrichment in exosomal sub-populations when cells are grown in prespun containing medium.

6.3.2 Location and quantity of exosomal Tau

Using protease K digestion, we determined that a pool of exosomal associated Tau was located within the exosomal lumen. Tau protein associated with extracellular vesicles isolated from normal and rTg4510 mouse brain was also demonstrated to be intraluminal (Polanco et al. 2016). Furthermore, using high salt dissociation and protease K digestion studies, Wang et al. (2017) also characterised exosomal Tau as intraluminal.

Our data also suggest that there may have been a pool of extra-luminal exosome associated Tau which was more susceptible to protease K digestion; this susceptible pool may have been trans-membranous with an extracellular facing N-terminus (because we used Tau12 for detection) cleaved by protease K. Tau protein can insert into lipid membranes which impacts is structure (Jones et al. 2012) and membranes can provide a surface for the aggregation of Tau (Elbaum-Garfinkle, Ramlall and Rhoades, 2010). These observations suggest that the microenvironment of exosomes may be a privileged locality for protein aggregation.

In our study, 1.2% of extracellular Tau was co-pelleted with exosome vesicles. This is consistent with Wang et al. (2017) and Dujardin et al. (2014) who demonstrated that 2 – 3% of extracellular Tau from rat cortical neurons was exosomal. However, Kanmert et al. (2015) report that exosomal Tau from N2a cells represents 0.2% of all extracellular Tau, an order of magnitude lower. An even smaller proportion of extracellular Tau from induced human cortical neurons and rat primary hippocampal neurons was observed to be exosomal at 0.01% (Kanmert et al. 2015). The discrepancy between these findings and our own may originate in the different cell types used, or in the technical use of ELISA vs Western blotting.

6.3.3 Quantification of extracellular Tau

There are a number of factors to consider when quantifying extracellular Tau levels, especially when using clones with variable Tau expression levels. Some authors (Yamada et al. 2011; Simon et al. 2012; Dujardin et al. 2014) have demonstrated a positive correlation between intracellular Tau expression levels and extracellular Tau levels. Thus expressing extracellular Tau levels relative to total Tau levels (intracellular + extracellular) reveals effects on release of the Tau construct being studied, independently of its expression level

in the cell. This approach was used by Croft et al. (2017) to demonstrate that Tau release was increased from 3xTg AD slice cultures.

In the present study, however, when intracellular Tau levels were correlated with exosomal Tau release from a number of clonal SH-SY5Y cells expressing various Tau constructs, no relationship was observed between these two parameters (**figure 4.9 D**). However, utilising an inducible α-Synuclein expressing HEK293 system, we demonstrated a relationship between intracellular expression levels and exosomal release of the expressed protein in a pattern that was consistent with a 'threshold'. Such considerations indicate that expressing the levels of released Tau protein relative to total Tau expression levels may be a useful way of teasing out differences in the release of different Tau constructs.

In the present study, when studying changes in the levels of exosomal Tau release under various conditions, exosomal Tau levels were expressed relative to an exosomal marker protein, such as Alix or to the quantity of cells from which the exosomes were isolated (as determined by BCA). These two quantification methods generated broadly similar results (data not shown). However, our results also demonstrated that exosomal Alix levels were affected by growth conditions and may have been subjected to regulation by DNAjC5 expression. These findings highlight the importance of quantifying total exosome number and expressing Tau levels relative to this – a technical approach that was beyond the capacity of the present work. Ultimately, the release of Tau in distinct sub-populations of vesicles, perhaps reflective of specific targeting mechanisms, may further obscure such analytical measures and highlights important future work.

6.3.4 Isoforms of Tau released in exosomes

Our findings demonstrated that different isoforms of Tau were released in exosomes from SH-SY5Y cells. Both 2N4R-Tau and 2N3R-Tau were detected in the exosomes isolated from SH-SY5Y clones expressing the respective proteins. These forms of Tau were released in

exosomes at similar levels, indicating that the alternatively spliced second microtubule binding region in Tau did not affect its exosomal release. Moreover, 0N3R-Tau was also released in exosomes. One clone expressing 0N3R-Tau had increased levels of exosomal Tau compared to 2N4R-Tau, but this was not duplicated by an independent clone. Regardless, this finding demonstrates that exosomal Tau release did not depend upon the alternatively spliced regions of Tau per se.

Karch et al. (2012) suggested that the secretion of Tau into the extracellular space is isoform specific. 2N3R-Tau was shown to exhibit the highest rates of release. Our findings suggest that this is not matched by isoform selectivity in exosomal release.

Using custom designed ELISAs and Simoa detection methods, exosomes from human CSF were determined to contain full-length and mid-region Tau species (Guix et al. 2018). This demonstrates that exosomal Tau may be co-constituted by multiple species. Mid-region Tau species were immuno-captured with the Tau5 and BT2 antibodies, the epitopes for which both lie outside of the alternatively spliced regions of Tau. Thus mid-region Tau may have derived from multiple Tau isoforms. In the human brain all six Tau isoforms are expressed and their ratios may change in disease states (Boutajangout et al. 2004; Majounie et al. 2013).

In the current work we studied the exosomal release of Tau when single isoforms were separately expressed in SH-SY5Y cells. It is possible that competitive mechanisms for the exosomal release of selective isoforms and species exist. For example When co-expressed in N2a cells, mutant Huntingtin is secreted at higher levels than WT Huntingtin, despite similar intracellular expression levels (Trajkovic et al. 2017).

It would therefore be informative to investigate how the co-expression of different Tau isoforms and / or Tau mutants affects their release in exosomes, a methodology which may unmask differences which are shielded when isoforms are investigated individually.

6.3.5 Cleavage of Exosomal Tau

We observed that exosomal Tau released from 2N4R-Tau SH-SY5Y cells was smaller than cellular Tau on SDS-PAGE. This finding suggests a specific modification of exosomal Tau. As such, exosomal Tau was cross reactive with N-terminal (Tau12) but not C-terminal (Tau46) antibodies, strongly suggestive of C-terminal cleavage as accounting for the increased migration of exosomal Tau in SDS-PAGE.

The release pattern of ectopically expressed 1N4R-Tau from primary rat neurons yielded a very similar pattern to that presented here, including increased mobility of exosomal Tau which was detected by N but not C-terminal antibodies (Dujardin et al. 2014).

On the other hand, whilst they observed exosomal Tau to be smaller than cellular Tau, Wang et al. (2017) demonstrated exosomal Tau to be full-length as evidenced by cross reactivity with Tau12 and Tau46. When exosomes were dephosphorylated with phosphatase, the migration of exosomal Tau was unaffected, suggesting that exosomal Tau was already dephosphorylated and this accounted for its decreased size on SDS-PAGE.

Extracellular Tau has been demonstrated as dephosphorylated in a number of studies (Plouffe et al. 2012; Mohamed et al. 2015; Croft et al. 2017). Although de-phosphorylation may have contributed to the increased migration of exosomal Tau in our study, our data suggested it could not account for the complete magnitude of the change. This is because dephosphorylation of cellular lysates increased Tau migration to a lesser extent than the increased migration of exosomal Tau vs. cellular Tau. However, we did not directly study the phosphorylation of exosomal Tau in the current study, but our findings and those in literature indicate it as a key part of future work.

We observed that when expressed in SH-SY5Y cells, 0N3R-GFP, 0N4R-GFP, 2N3R-GFP and 2N4R-GFP-Tau proteins were released in exosomes primarily as full length species including the GFP-Tag. This indicates that C-terminal cleavage, as discussed for untagged exosomal

2N4R-Tau, is not a necessary process for the exosomal release of Tau. However, intracellular Tau-GFP constructs did not cross react with Tau46, suggesting a steric hindrance of the C-terminal of Tau by the GFP tag. This is precisely the region we hypothesised cleavage of exosomal Tau to be occurring at, which suggests that C-terminally GFP-tagged Tau constructs may not have represented the ideal system for studying cleavage patterns of Tau.

We did however note that minor Tau species corresponding to cleaved Tau-GFP products were detected in the exosomes from 2N4R-GFP SH-SY5Y cells. One of these minor species was not detected intracellularly and, moreover, co-migrated with the major exosomal Tau species from 2N4R-Tau SH-SY5Y cells. This finding substantiated our interpretation that the exosomal Tau species secreted by 2N4R-Tau SH-SY5Y cells was generated by a cleavage event. Furthermore, this species was detected exclusively in the extracellular fraction which suggests its formation to be an irreversible step in the pathway to release, or potentially as a process occurring downstream of release.

Caspase cleavage of Tau at aspartate 421 is upstream of pathological changes in Tau commensurate with Alzheimer's disease (Rissman et al. 2004). Furthermore, secretion of Tau mimicking D421 cleavage is increased from HEK293 cells (Plouffe et al. 2012). Cleavage at D421 decreases Tau size by ~5 kDa, and abolishes cross reactivity with Tau46. The exosomal Tau species detected in our study is therefore consistent with cleavage at D421, a hypothesis that could be directly tested using antibodies selectively detecting this cleaved form of Tau.

6.4 Lysosomal inhibition increased exosomal Tau release

We observed that lysosomal compromise induced by bafilomycin treatment significantly increased the exosomal release of both WT-2N4R-Tau and 2N3R-GFP-Tau from SH-SY5Y cells. Tau protein has been shown to use endosomal microautophagy as a degradative

pathway (Caballero et al. 2018), a pathway which utilises late endosomes and MVBs. Inhibition of lysosomal function shifts the balance of MVB from degradative to secretory fates (Eitan et al. 2016) consistent with increased exosomal release of lysosomal substrates upon compromise of this system.

Consistent with these findings, lysosomal dysfunction promotes the exosomal secretion of alpha synuclein (Alvarez-Erviti et al. 2011) and inhibiting autophagy increases the exosomal release of TDP-43 in an aggregated form (Iguchi et al. 2016). Generally, lysosomal compromise favours the exosomal secretion of non-degraded lysosomal substrates, including amyloid precursor protein C-terminal fragments (Miranda et al. 2018). Lysosomal compromise moreover increases the free secretion of dephosphorylated Tau protein from primary neurons (Mohamed et al. 2014).

This suggests that lysosomal dysfunction in Alzheimer's disease and other Tauopathies, including CBD and PSP, may promote exosomal Tau release (Piras et al. 2016). Such an effect may be a homeostatic response to failing intracellular disposal mechanisms and points to exosomal secretion of toxic proteins as an alternative mechanism of disposal under conditions of lysosomal compromise. Inhibiting exosomal secretion may therefore promote aggregation of disease associated proteins, as is observed for intracellular aggregation of TDP-43 (Iguchi et al. 2016).

6.5 Increased exosomal release of P301L-Tau from SH-SY5Y cells

We generated SH-SY5Y clones with stable expression of P301L-2N4R-Tau. The P301L mutation in Tau causes frontotemporal dementias (Hutton et al. 1998) and expression of P301L-Tau in mice results in motor disturbances and the appearance of Tau pathology (Lewis et al. 2000). We therefore adopted expression of P301L-2N4R-Tau as a model of a more aggressive Tauopathy-like phenotype.

Native-PAGE analysis demonstrated that P301L-Tau SH-SY5Y cells demonstrated increased higher molecular weight Tau species than WT-Tau SH-SY5Y cells, consistent with increased oligomerisation of P301L-Tau. Furthermore, P301L SH-SY5Y cells were more immunoreactive with the Tau oligomer antibody T22 than was WT Tau SH-SY5Y cells, an effect strongly potentiated with bafilomycin A1 treatment (Lasagna-Reeves et al. 2012). These findings reinforce the use of P301L-Tau expression as a model of Tau misprocessing. It will be informative map to phosphorylation status of P301L-Tau in this model system, specifically at disease associated phosphoepitopes such as PHF-1 and AT8.

Exosomal Tau release from P301L SH-SY5Y cells was significantly increased compared to that from WT Tau SH-SY5Y cells. This finding links pathological intracellular behaviour of Tau to increased exosomal release and suggests that a form of Tau with increased oligomerisation propensity was preferentially released in exosomes.

This observation is consistent with Wang et al. (2017), who demonstrated that insoluble repeat domain Tau was enriched in exosomes relative to cells. Moreover Saman et al. (2012) noted the presence of multimeric and pathologically conformed (AT270) Tau in the CSF exosomes from AD patients. In the present study we were unable to directly observe exosomal oligomeric Tau from P301L SH-SY5Y cells, despite repeated attempts to do so by Native-PAGE analysis. It will be important to determine the true extent of oligomerisation of exosomal Tau and if oligomeric Tau is enriched in exosomes. This analysis may require more sensitive techniques such as ELISA, potentially with the oligomer specific Tau antibodies such as T22 and TOMA (Castillo-Carranza et al. 2014).

In chaperone mediated autophagy client proteins are targeted for lysosomal degradation via Hsc70 interaction. According to recent work, P301L-Tau is not degraded by chaperone mediated autophagy to the same degree as WT-Tau (Caballaro et al. 2018). However, as indicated by our results, P301L-Tau interacted with Hsc70 (see below, **6.6**). In chaperone

mediated autophagy, client proteins must be unfolded for transportation into the lysosomal lumen via LAMP2A. Hsc70 dependent targeting of client proteins to multivesicular bodies in endosomal micro-autophagy, a process which may result in the exosomal release of client proteins, however, does not require proteins to be unfolded (Sahu et al. 2011). Our findings indicated that P301L-Tau was more oligomeric than WT-Tau, the folding state of P301L-Tau may therefore have shifted its fate away from degradation via CMA and towards secretion through targeting to MVBs. This hypothesis requires more research and implicates interaction with Hsc70 in the exosomal targeting of Tau protein.

6.6 Interaction of Tau and Hsc70

Consistent with previous reports (Sarkar, Kuret and Lee, 2008; Wang et al. 2009; Jinwal et al. 2010) we demonstrated interaction between WT-Tau and Hsc70 in living cells using a co-immunoprecipitation approach. The two sets of residues in Tau : ^{336}**QV**EVK^{340} and ^{347}KDR**VQ**^{351} form putative CMA motifs, hypothesised to mediate interaction with Hsc70 (Chiang et al. 1989). We demonstrated that neutralisation of the sequence identity and charge of these motifs by mutation to ^{336}**AA**EVK^{340} and ^{347}KDRV**AA**^{351} significantly impaired interaction of Tau with Hsc70. Previous reports demonstrate that disruption of these motifs in TDP-43 (Huang et al. 2014) and Huntingtin (Qi et al. 2012) prevented interaction of these proteins with Hsc70.

Mutation of these residues in RD-Tau also impaired interaction with Hsc70 in N2a cells (Wang et al. 2009); our results are therefore consistent with, and extend these findings to full-length 2N4R-Tau.

On the other hand, Sarkar et al. (2008) identified two sets of hydrophobic motifs that mediated the interaction of 2N4R-Tau with Hsc70, namely ^{277}II^{278} and ^{308}IV^{309}. Both of these

sets of residues are located within ΦQΦΦ motifs, where Φ represents a strongly hydrophobic amino acid.

What these findings suggest is that interaction with Hsc70 is mediated by different sets of residues in WT-Tau. In fact, the interaction sites of Tau and chaperones (such as Hsc70 and Hsp90) appears to be distributed throughout the microtubule binding region, and local protein environment (including mutations) may influence the interaction of Tau and chaperone proteins (Karagöz et al. 2014; Mok et al. 2018).

In this respect, we demonstrated that deletion of the hydrophobic residues from P301L-2N4R-Tau (^{277}II^{278} and ^{308}IV^{309}) significantly impaired interaction with Hsc70 in SH-SY5Y cells, consistent with Sarkar et al. (2008). On the other hand, disruption of the CMA motifs (^{336}QVEVK^{340} and ^{347}KDRVQ^{351}) in P301L-2N4R-Tau did not affect Hsc70 interaction, although this data (regarding CMA-P301L – Hsc70 interaction) is caveated because it was performed only once.

These findings are interesting because the residues through which P301L-Tau was shown to interact with Hsc70 are located within motifs that drive Tau aggregation in the transition to beta-sheet structure (hexapeptide motifs; von Bergen et al. 2005; Li & Lee 2006). P301L-2N4R-Tau had a greater level of oligomerisation than WT-2N4R-Tau in SH-SY5Y cells, consistent with a structural change in P301L-Tau. It is tempting to speculate that this structural change exposed the hydrophobic motifs making them available to Hsc70 interaction whilst burying the CMA motifs within the molecule, preventing their interaction with Hsc70.

Interpreting these findings with those presented in the literature overall suggests that Tau – Hsc70 interaction may occur at a number of distinct sites in Tau, including the CMA and hydrophobic motifs. In fact, the first CMA motif in Tau shares similar amino acid composition to the hydrophobic motifs identified by Sarkar et al. (2008). There is general consensus that Hsc70 and other chaperones bind to Tau in its microtubule binding domain

(Mok et al. 2018), a process which may be important for engaging Tau species that have become detached from microtubules (Jinwal et al. 2010).

6.6.1 Functional consequences of disrupting Tau – Hsc70 interaction

6.6.1.1 Steady state levels of CMA3-Tau in SH-SY5Y cells

Steady state levels of stably expressed CMA3-2N4R-Tau were significantly higher than WT-2N4R-Tau, confirmed by western blotting and immunocytochemical analyses of three independent SH-SY5Y clones for expressing each construct.

Steady state levels of endogenous SH-SY5Y Tau and ectopic WT-2N4R-Tau were increased by lysosomal compromise with bafilomycin treatment, consistent with earlier reports implicating the lysosomal compartment in Tau degradation (Hamano et al. 2008; Krüger et al. 2012; Caballero et al. 2018). On the other hand, CMA3-Tau levels were not significantly affected lysosomal inhibition. This suggests that the equilibrium levels of CMA3-2N4R-Tau relied less on lysosomal function than WT forms of Tau, which may have contributed to its increased steady state levels. Repeat domains constructs of Tau with mutations in the CMA motifs were not effectively degraded by lysosomal preparations (Wang et al. 2009) which supports the notion that steady state levels of CMA3-2N4R-Tau were increased due to reduced lysosomal processing. The effect of these mutations to disrupt Hsc70 interaction, and the identified role of these motifs suggest that this is due to reduced chaperone mediated autophagy of CMA3-Tau. Specific genetic interference would allow us to localise the site of this effect, whether to CMA (LAMP2A siRNA), autophagy (Atg7 siRNA) or endosomal microautophagy (Vps4 siRNA).

6.6.1.2 Exosomal release of CMA3 Tau and DD Tau

Our findings demonstrated that disruption of Tau – Hsc70 interaction via mutation of the CMA motifs did not affect the exosomal release of Tau. We also investigated exosomal Tau

release from SH-SY5Y cells expressing DD-P301L-Tau, which also had reduced Hsc70 interaction, and again observed no differences.

These findings suggested that under normal, steady state conditions, Hsc70 interaction was not a key determinant of targeting Tau to exosomes in SH-SY5Y cells.

We did however observe that exosomal Tau release from CMA3-Tau cells was differentially regulated than release from WT-Tau cells. Whereas the exosomal release of WT-Tau was increased by growth in prespun serum containing medium vs reduced serum optiMEM, the exosomal release of CMA3-Tau was reduced under these conditions. The composition of exosomes released by cells differs between these two conditions and implicates different biogenesis machinery (see above **6.3.1**). Although these two growth conditions did not affect the exosomal levels of Hsc70 (Li et al. 2015), serum stimulation increases intracellular Hsc70 expression in astrocytic cells (Zeise et al. 1998). It is tempting to speculate that under conditions of growth in prespun serum containing medium there is a shift in the processes targeting proteins to exosomes that favour Hsc70 dependent mechanisms, thus increasing the exosomal release of WT-Tau but not CMA3-Tau.

It is possible that disrupting Tau – Hsc70 favours its interactions with other chaperones, arguably compensating for Hsc70 functionality in the targeting Tau to exosomes. Tau binds to many chaperones (Mok et al. 2018) and it is therefore the position of Tau within a network of interacting partners, chaperones and co-chaperones that will dictate its sub-cellular localisations.

6.7 Role of DNAjC5 in release of Tau from SH-SY5Y cells

We studied the effects of DNAjC5 on Tau homeostasis and secretion by transient transfection of SH-SY5Y cells with stable Tau expression. Ectopic DNAjC5 was detected migrating as one major and one minor band at 30 kDa and 60 kDa, consistent with monomeric and dimeric DNAjC5, respectively. DNAjC5 is known to form SDS resistant

oligomers, a phenomenon dependent upon the cysteine string region of the protein (Braun and Scheller, 1995; Swayne et al. 2003).

In contrast to recent reports, we observed that DNAjC5 expression did not affect global steady state Tau levels (Fontaine et al. 2016). However, in that study transient co-transfection of HEK293 cells with Tau and DNAjC5 was used whereas we were studying stable expression of Tau in SH-SY5Y cells. HEK293 cells do not endogenous express Tau (Ren et al. 2007) therefore ectopic Tau expression in these cells may have been representative of a non-physiological state and the effects of DNAjC5 expression therein also related to this departure from physiological status. However, we did observe by ICC that SH-SY5Y cells with expression of DNAjC5 had lower levels of Tau staining. This suggests that DNAjC5 expression reduced Tau levels on a local level. Bulk analysis of the SH-SY5Y cell population may have obscured this effect, which may have been too small to resolve by immunoblot analysis.

We observed that transient DNAjC5 expression increased release of Tau protein into the medium without increasing LDH release. This indicated that DNAjC5 expression promoted Tau release without inducing cell death, suggesting a specific mechanism of Tau secretion. This is consistent with previous reports demonstrating that DNAjC5 expression promoted the secretion of transiently expressed Tau from HEK293 cells and endogenous Tau from M1C cells and mice organotypic slice cultures. Moreover, Tau secretion from DNAjC5 knockout organotypic slice cultures was reduced (Fontaine et al. 2016). DNAjC5 potentiation of Tau secretion has recently been positioned as downstream of the ER associated deubiquitinase USP19. USP19 engages misfolded proteins (including Tau, TDP-43 and α-Synuclein) for secretion in a process termed misfolded associated protein secretion (MAPS) which is a mechanism of unconventional protein secretion (Xu et al. 2018).

The MAPS pathway of protein secretion releases proteins in a non-vesicular bound 'naked' form, although it does utilise late endosome vesicles as an intermediate in this process (Lee et al. 2016). Late endosomes containing intraluminal vesicles can have secretory fates and are also an intermediate in exosome release (Sahu et al. 2011) which suggests some overlap between MAPS and exosomal secretion of proteins. Consistent with this hypothesis we observed that DNAjC5 was released in exosomes following transient transfection in SH-SY5Y cells in line with recent reports (Deng et al. 2017).

Following this we also observed that transient expression of DNAjC5 promoted exosomal Tau release from SH-SY5Y cells with stable Tau expression. Interestingly, our findings demonstrated that DNAjC5 expression increased total Tau secretion (i.e. 99% free) 1.5 times, whereas it increased exosomal Tau secretion 2 fold. This finding suggests that, relatively, DNAjC5 expression increased the rate of exosomal Tau release greater than it increased the rate of free Tau release, despite the latter contributing to a proportionally larger quantity of total secreted Tau.

In the DNAjC5 experiments we quantified exosomal Tau release relative to cellular protein levels, as DNAjC5 expression also moderately increased exosomal Alix levels. This finding implicates DNAjC5 as involved in promoting exosomal release in general. A hypothesis that is consistent with recent work demonstrating that DNAjC5 promotes the exosomal release of other neurodegenerative proteins Huntingtin and SOD-1 (Deng et al. 2017).

Tau, Hsc70 and DNAjC5 have been demonstrated to participate in a heterotrimeric protein complex (Fontaine et al. 2016). Our findings demonstrate that DNAjC5 is both released in exosomes and that its expression increases the exosomal release of Tau. We also observed that endogenous and ectopic Hsc70 was released in exosomes (appendix **figure 7.2**). The synthesis of these observations is the model that DNAjC5 expression recruits Hsc70 bound Tau protein and targets it for release in exosomal vesicles. Contrary to this hypothesis, we

observed that DNAjC5 promoted the exosomal release of CMA3-2N4R-Tau, a form of Tau demonstrated to have a significantly reduced Hsc70 interaction. However, as discussed above, Tau – Hsc70 interaction may occur at a number of sites in Tau. Following this, we observed that DNAjC5 expression did not affect the exosomal release of DD-P301L-Tau, whilst potentiating the exosomal release of P301L-Tau. These findings serve to implicate Tau – Hsc70 interaction, via Tau's hydrophobic motifs, in the pathway of DNAjC5 potentiation of exosomal Tau release. Therefore, despite having minimal effects on exosomal release under basal conditions, Hsc70 – Tau interaction (at the hydrophobic sites) may be functionally relevant insofar as it is involved in DNAjC5 mediated triaging of Tau to exosomes.

6.8 SUMOylation of Tau and its role in exosomal Tau release

6.8.1 Reduced SUMOylation of K304R-Tau

We demonstrated the SUMOylation of 2N4R-Tau by detection of an 80 kDa Tau12 cross reactive species in the NiNTA precipitates of HEK293 cells co-transfected with 2N4R-Tau and SUMO-1-His. The migration of this species was consistent with the addition of one SUMO molecule (15 kDa) to the 2N4R-Tau molecule (67 kDa). This finding is consistent with previous reports of the SUMOylation of Tau protein in HEK293 cells (Dorval & Fraser, 2006; Luo et al. 2014).

Following this, we observed that mutagenesis of lysine^{340} to arginine significantly reduced the SUMOylation of Tau protein. Consensus SUMOylation motifs are of the form: ΨKX(E/D), where Ψ is a hydrophobic amino acid, K is the lysine to which SUMO is conjugated, X is any amino acid and the motif ends in a glutamate or aspartate (E/D) (Sampson et al. 2001). Tau has two such motifs; VK^{340}SE and AK^{385}TD. Our results demonstrate that ablation of the first motif significantly reduces SUMOylation levels consistent with both Dorval & Fraser (2006) and Luo et al. (2014). However we also detected residual SUMOylated Tau after mutation

of K^{340} to arginine, which suggests SUMOylation of Tau at a distinct site, potentially K^{385}. Because we detected only one SUMOylated Tau band, this suggests that SUMOylation of Tau at the second site only occurs after ablation of the first, a hypothesis we could directly investigate using combinatorial mutagenesis of the two lysine residues.

6.8.2 Phosphorylation status of K340R-Tau

SUMO deficient K340R-Tau had lower levels of steady state phosphorylation at T205 and S356 than did WT-Tau when stably expressed in SH-SY5Y cells. It is possible that these reductions in phosphorylation were a lateral effect stemming from cross-talk between SUMOylation and phosphorylation. This observation is consistent with Luo et al. (2014) who demonstrated that SUMOylation of Tau potentiated Tau phosphorylation (including at pT205) an effect was abolished by the K340R mutation. These observations are also consistent with Dorval & Fraser (2006) who demonstrated that phosphorylation of Tau induced by okadaic acid increased its SUMOylation, arguing for a reciprocal cross-talk between these post-translational modification networks.

Phosphorylation of ser356 has previously been shown to inhibit the ability of Tau to stimulate microtubule assembly, and thr205 is within a region of Tau where phosphorylation also prevents microtubule assembly (Liu et al. 2007). Additionally both of these residues exists as components of phosphoepitopes defining pathological Tau conformers which contribute to intraneuronal neurofibrillary tangles (12E8: pS262/**pS356** and AT8: pS199/pS202/**pT205**) (Augustinack et al. 2002). Moreover, dissociation of Tau from microtubules by colchicine treatment increased the SUMOylation of Tau (Dorval & Fraser. 2006). Consistent with these observations we demonstrated that stably expressed K340R Tau was more highly colocalised with Tubulin than WT-Tau when expressed in SH-SY5Y cells. Moreover, K340R-Tau SH-SY5Y cells extended more Tubulin positive neurites than WT-Tau SH-SY5Y cells in two independent stably expressing clones. It will be

important to utilise microtubule binding assays to fully evaluate the association of K340R-Tau with the microtubule network. Collectively, these observations indicate that Tau SUMOylation may regulate the association of Tau with the microtubule network, an effect that may be mediated via lateral effects on phosphorylation of specific Tau residues.

6.8.3 Reduced exosomal release of K340R-Tau

Exosomal release of K340R-2N4R-Tau was significantly reduced compared WT-2N4R-Tau. This observation was confirmed using independent SH-SY5Y clones with stable expression of WT-Tau or K340R-Tau. Given the reduced SUMOylation of K340R-Tau, these observations suggest that SUMOylation of Tau is in involved in its exosomal targeting.

SUMOylation of alpha-synuclein, a protein involved in the pathogenesis of Parkinson's disease, regulates its exosomal targeting (Kunadt et al. 2015). Similar to our findings, these authors reported that mutation of residues to which SUMO is covalently attached decreased the exosomal release of alpha-synuclein. SUMO mediated exosomal targeting was ESCRT dependent and mediated through interaction of SUMO with phosphoinositols. However in that work SUMO-2 conjugation was studied as a sorting determinant of alpha-synuclein, whereas SUMO-1 was the focus of the present work.

The precise interrelationship between SUMOylation and exosomal targeting is, however, obscure. Whilst it was reported that the SUMOylated form of hnRNPA2B1 was directly detected in exosomes (Villarroya-Beltri et al. 2013) neither SUMOylated alpha-synuclein (Kunadt et al. 2015) nor SUMOylated Tau (present work) was directly detected in exosomes (inferred from their mobility on SDS-PAGE). These findings therefore suggest that SUMOylation of target proteins may be involved in the pathway of their targeting to exosomes, but once there the proteins become deSUMOylated.

Our work suggested that blocking SUMOylation promoted Tau – Tubulin interactions, perhaps through negative regulation of phosphorylation. This subcellular localisation is

consistent with reduced exosomal targeting of Tau as Tau sequestered on the microtubules will not be accessible for translocation to intraluminal vesicles. Our preliminary work also suggested that P301L-Tau was more efficiently SUMOylated than WT-Tau (data not shown). Given the increased exosomal release of P301L-Tau this evidence further implicates SUMOylation in the exosomal targeting of Tau protein. Furthermore, SUMO-1 co-localises with AT8 immunoreactivity in AD brains, linking increased Tau SUMOylation with Tau pathobiology (Luo et al. 2014), taken with our findings this suggests exosomal Tau release may be promoted in disease states.

6.9 Tau uptake by recipient cells and transmission between cells

6.9.1 Uptake of Tau lysate by recipient cells

In the current work, we investigated the uptake of Tau protein by recipient cells in culture. We used Tau protein liberated from SH-SY5Y cells with ectopic expression of pro-aggregating Tau (RD-Tau) as a source of extracellular Tau. RD-Tau was internalised by SH-SY5Y cells and primary cortical neurons as demonstrated by Western blotting and immunocytochemical analyses.

Our analysis revealed that <0.01% of liberated RD-Tau was internalised by SH-SY5Y cells over 24 hours, despite the presence of a large reservoir of extracellular Tau. Uptake of RD-Tau by primary cortical neurons followed a linear relationship with concentration of Tau added to the cells. These observations suggest that uptake mechanisms were not saturated and are therefore consistent with the preferential internalisation of a specific Tau species that was relatively under-represented in our sample.

It was recently demonstrated that primary mouse neurons preferentially internalise higher molecular weight forms of Tau, and that phosphorylation of Tau at pathological epitopes potentiated its internalisation (Takeda et al. 2015). This finding was corroborated by Tau

uptake in N2a cells (Wauters et al. 2016). In these studies the authors observed efficient internalisation of Tau by recipient neurons which was capable of transmitting between fluidically isolated cells. However, in their study, Takeda et al. (2015) used 11-13 month old rTg4510 mouse brain lysates as the source of extracellular Tau. As such, Tau in this system had ample time to undergo extensive aggregation and phosphorylation, thus potentially rendering it more susceptible to internalisation by neuronal cells. Whilst the form of Tau used by Wauters et al. (2016) was generated by recombinant expression, and its phosphorylation was induced by co-expression of GSK-3β in the host cell system.

The source of extracellular Tau used to study uptake in the present study was expressed in a mitotic environment and thus potentially less susceptible to such modifications. As we were extracting Tau from donor cells by pressurised lysis followed by clarification, we achieved a recovery of <100% and some Tau remaining in the post-centrifugation pellet. The Tau contained in this pellet may have represented Tau from unbroken cells, or alternatively, it may have represented species of Tau which were highly aggregated or associated with other structures and thereby co-pelleted at this speed. This pelleted Tau material may therefore have been more efficiently taken up by recipient cells.

Other studies have also demonstrated efficient internalisation of Tau by neuronal cells (Wu et al. 2013; Evans et al. 2018). However these studies used Tau derived from recombinant sources which may help to explain the differences between our work and theirs.

Moreover, we observed that internalisation of RD-Tau by SH-SY5Y cells only occurred when donor and recipient cells were pre- and co-treated with bafilomycin. Bafilomycin treatment was shown to promote oligomerisation of Tau (present work) and lysosomal dysfunction promotes Tau aggregation in cell cultures (Hamano et al. 2008). Additionally, internalised Tau was shown to colocalise with lysosomes (Evans et al. 2018) which suggests that once internalised, Tau protein enters degradative mechanisms. The potentiating effect of

bafilomycin on Tau uptake may therefore be localised to effects in the donor and recipient cells.

6.9.2 Uptake of released tau by recipient cells

Although Takeda et al. (2015) demonstrated that phosphorylated Tau is most efficiently internalised by recipient neurons, the weight of available evidence suggests that Tau released by cells is actually dephosphorylated (Wang et al. 2017; Plouffe et al. 2014). This finding therefore demonstrates that these phosphorylated forms of Tau *may* be taken up by donor cells, but the question is whether these forms of Tau are actually released in an *in vivo* setting and therefore able to promote Tau pathology spread. Tau released by cells directly into the medium and encapsulated in exosomes represents a potential source of Tau for uptake by recipient cells in such a setting. As such, these forms of Tau are more physiologically representative when studying Tau transmission.

Full-length 2N3R-GFP Tau is released freely and exosomally into the medium 2N3R-GFP SH-SY5Y cells. We noted that naïve SH-SY5Y cells treated with the conditioned medium of 2N3R-GFP cells produced the appearance of a cross reactive band consistent with 2N3R-GFP in the recipient cells. However, immunocytochemical analysis of the recipient cell population revealed GFP positivity consistent with over-expressing cells. We were therefore unable to confirm whether the positivity in these experiments represented Tau uptake by recipient cells, or was a technical artefact produced by the carry-over of donor cells to the recipient population. When the same donor and recipient cells were co-cultured in transwell inserts which do not allow the movement of cells between donor and recipient populations, we did not detect ectopic 2N3R-GFP-Tau in the recipient cells, suggesting that our earlier results may have reflected false positives.

Transmission of Tau to recipient cells from conditioned medium has been demonstrated using human iPSC neurons as the donor cells and primary mouse neurons as the recipients

(Wu et al. 2016). iPSC neuronal cell models undergo culture for up to 100 days, therefore allowing the formation of Tau proteins potentially more efficiently internalised by recipient cells. Furthermore, in this experiment recipient cells were treated with conditioned medium for 6 days, a treatment time forbidden in undifferentiated SH-SY5Y cells.

Tau protein present in the ISF of rTg4510 (P301L-Tau) mice can also be internalised by recipient neurons at exquisitely low concentrations (10 ng/ml). Again, the form of Tau present in the ISF may represent species of Tau formed only after long periods of time (Takeda et al. 2015).

6.9.3 Ability of exosomes to transmit Tau pathology

When naïve SH-SY5Y cells were treated with exosomes isolated from the conditioned medium of 2N3R-GFP SH-SY5Y cells and analysed by IP followed by western blotting we did not detect ectopic Tau in the recipient cell population. However it is conceivable that this methodology was not sensitive enough to detect Tau transmission occurring at low levels. Regarding this, immunocytochemical analysis of SH-SY5Y cells treated with 2N3R-GFP exosomes demonstrated some GFP positivity associated with the recipient cells. Furthermore, when primary cortical neurons were treated with exosomes from HA-P301L-2N4R SH-SY5Y cells, we observed increased HA immunoreactivity associated with recipient neurons, a finding that warrants further investigation.

Wang et al. (2017) demonstrated relatively sensitive Tau uptake by recipient neurons treated with exosomes containing Tau-GFP. Moreover, internalised Tau was observed to transfer to second order neurons in microfluidic chambers. The increased level of Tau uptake in their work compared to ours may rest on a number of factors. Wang et al. (2017) used N2a cells as the source of exosomes for their study, and, moreover, those cells were transiently transfected with Tau-GFP. Our data indicate that transient transfection promotes the release of Tau in exosomes, and therefore the exosomes used in that study

may have been more densely loaded with Tau molecules. Furthermore, the authors cultured recipient neurons in microfluidic chambers, devices which often culture neurons in very small wells. Thus the stoichiometry of exosomes: neurons was likely increased in their study relative to ours, in which we cultured neurons in six well plates. This suggests that if we had used fewer neurons as recipients and more exosomes for treatment, we would have increased the chances of (detecting) transmission. Exosomes are well characterised as being taken up by recipient cells (Mulcahy et al. 2014), therefore the question is not whether exosomal Tau may be taken up by recipient neurons *per se*, but the efficiency with which this process occurs relative to the uptake of other forms of extracellular Tau. In the disease state Tau pathology propagates between interconnected neuronal circuits over a period of years, the key is to decipher which transmission processes figure as the rate limiting steps in this transmission.

Two recent studies have demonstrated a role for exosomes in the transmission of Tau between cells with concomitant induction of Tau pathology in the recipient cells. Asai et al. (2015) identified that microglia were able phagocytose recombinant human Tau and secrete it in exosomes. These exosomes were then able to transmit Tau pathology to primary neurons and mouse brain. Polanco et al. (2016) demonstrated that exosomes isolated from the brains of rTg4510 mice were able to seed the aggregation of Tau in the HEK biosensor line.

Evidence suggests that minute quantities of seed competent Tau species induce Tau aggregation in a cyclical manner (Meyer et al. 2014), and Tau oligomers may serve as seed competent forms of Tau (Lasagna-Reeves et al. 2012b). Which forms of extracellular Tau (exosomal vs. free) are seed competent and able to induce aggregation in recipient cells is therefore a central question. These considerations further highlight the importance of fully characterising the oligomeric state of exosomal Tau detected in the current study.

6.9.4 Transmission tau between co-cultured cells

When cells expressing differently tagged forms of Tau were co-cultured we observed robust trans-cellular transmission of Tau protein; our results indicated that Tau from HA-0N3R SH-SY5Y cells spread to neighbouring 2N3R-GFP SH-SY5Y cells.

In another study it was observed that direct contact mediated at synaptic contacts between co-cultured neurons potentiated the transmission of aggregating Tau between cells (Calafate et al. 2015). In our system, transmission correlated with cell-density, thereby implicating a role for direct cell-cell contact in the spread of Tau between cells. We also studied the co-culture of SH-SY5Y cells with ectopic P301L Tau expression and primary mouse cortical neurons in order to model transmission of Tau. These experiments also suggested the spread of P301L-Tau from SH-SY5Y cells to primary neurons. Recent reports have demonstrated robust trans-cellular movement of P301L-Tau between directly co-cultured cells (Wu et al. 2016). However, in this report both the donor and recipient cells were primary neurons, which are more likely to make functional connections than SH-SY5Y cells with primary neurons, the site at which transmission may be hypothesised to occur. Moreover, primary neuronal cultures can be grown for extended periods of time (indeed, Wu et al. (2016) observed transmission after two weeks co-culture), whereas with SH-SY5Y cells the time limit is set by the growth rate of the cells.

Transmission of Tau between co-cultured cells was only observed when lysosomal function was compromised with bafilomycin treatment. As discussed above, bafilomycin increases the exosomal release of Tau, and prevents its intracellular degradation. Lysosomal compromise also increases the total release of Tau (Karch et al. 2012; Mohamed et al. 2015). It is likely that these effects potentiated transmission thereby allowing us to detect it. Indeed, lysosomal inhibition promoted the exosomal transfer of alpha-synuclein (Alvarez-Erviti et al. 2011) and Tau internalised by recipient cells enters the

endosomal/lysosomal network (Evans et al. 2018), both of which support this interpretation.

The role of exosomes in the transmission of Tau between co-cultured cells could be investigated in a number of ways. The NSmase II inhibitor GW4869 inhibits the formation of ceramide and decreases exosome release (Willms et al. 2016; Iguchi et al. 2016). In the present work GW4869 treatment did not decrease levels of exosome markers (data not shown) which may be reflective of alternative exosome biosynthesis pathways. Utilising siRNAs targeted against ESCRT components may provide an alternative way to knockdown exosome release.

Another mechanism for cell-cell transmission of proteins in direct co-culture is via small cytoplasmic bridges termed 'tunnelling nanotubes'. Tunnelling nanotubes have been implicated in the transmission of infective prion proteins (Gousset et al. 2009), mutant Huntington (Costanzo et al. 2013), alpha-synuclein (Abounit et al. 2016) and Tau (Tardivel et al. 2016). However one concern with studies regarding TNTs is that they have predominantly focussed on CAD cells as the model system (murine catacholaminergic neuronal tumour cell line) which raises questions about the generalisability of these findings. We did not directly investigate TNTs in the current work, but they may have represented a component of Tau transmission in our model.

6.10 Toxicity of exosomes from P301L-Tau cells on cortical neurons

Neurons treated with exosomes derived from Tau expressing SH-SY5Y cells were toxic to primary mouse neurons at all concentrations tested, whereas exosomes isolated from normal SH-SY5Y cells were toxic to primary cortical neurons only at higher doses. This demonstrates that P301L-Tau exosomes were selectively toxic to primary cortical neurons. These findings establish the bioactivity of exosomes derived from SH-SY5Y cells upon neuronal cell models, and moreover, pin this bioactivity to Tau protein expression. The

toxic effect may have derived directly from the exosomal Tau, or potentially from other factors in the exosomes that expression of mutant P301L-Tau potentiated. Saman et al. (2014) used proteomic analyses to demonstrate that 0N4R-Tau expression in M1C cells significantly affected the proteome composition of the exosomes derived from these cells. Specifically, Tau expression induced enrichment of proteins with the GO KEGG term of 'Alzheimer' in the exosomes, including amyloid beta precursor protein. Amyloid beta protein has been demonstrated to increase Tau toxicity (Pooler et al. 2015) which suggests that exosomes derived from cells expressing pathological Tau contain a cocktail of toxic mediators, which may underlie the results observed here. Our data demonstrate that the exosomes isolated from cells expressing oligomeric P301L-Tau protein may promote downstream pathological effects in recipient cells. The role of exosomes in the pathogenesis of Tauopathies may therefore extend beyond the direct induction of Tau aggregation to direct toxic effects on neuronal cells.

6.11 Conclusions and future directions

There is growing consensus that the spread of Tau between neurons is important in the progression of Tau pathology in human diseases. This view is reinforced by animal models which demonstrate that pathological Tau can seed the aggregation of monomeric Tau and spread between neighbouring neuronal cells. In this project we have attempted to address the hypothesis that Tau released from cells in exosomes may serve as one vehicle for the spreading of Tau between cells.

Our findings clearly demonstrate that Tau is released from cells in exosomes and that this process is potentiated by pathological changes in Tau (i.e. P301L-Tau). Our work also provides evidence that chaperones can regulate the exosomal release of Tau. Furthermore, we identified that SUMOylation of Tau may be important for its exosomal release. These findings thus highlight potential cellular pathways that regulate exosomal Tau release

which therefore represent targets for interfering with this pathway. Future work should attempt to more clearly define the pathways regulating exosomal Tau release and aim to understand their interrelationship with free Tau release. For example, DNAjC5 has been found to promote both free and exosomal Tau secretion.

This work indicates a more detailed analysis of the precise species of Tau which are released in exosomes. Questions regarding the oligomeric status of exosomal Tau remain unanswered. Analysing Tau species released in exosomes from different cell (e.g. iPSC) and animal models will help to determine whether exosomal Tau represents a seed competent form of Tau and therefore may promote downstream Tau aggregation.

The ability of exosomes to transmit Tau to recipient cells was also investigated; however we were unable to provide clear evidence for the role of exosomes in the uptake of Tau by recipient cells. SH-SY5Y generally internalised Tau at low levels, suggesting they may not have represented the ideal cell system for studying Tau uptake.

Transmission of Tau between cells may occur via exosome dependent and independent pathways. For instance, a recent study suggests that Tau freely released from cells by direct translocation over the plasma membrane is able to transmit to recipient cells (Katsinelos et al. 2018). Future work should focus on dissecting out the relative contributions of each of these release mechanisms to the spread of Tau between cells. One potential system for studying the relative contributions of exosome dependent and independent mechanisms is through the use of K340R-Tau, which was identified in the present work to reduce the release of Tau in exosomes.

Ultimately this work has been focused on investigating one component of a wider hypothesis; that Tau pathology in neurodegenerative diseases progresses via a transmission and seeding mechanism. The role of exosomes in this process is yet to be fully established but the work presented here indicates it as an important area for future work.

7 Appendix

7.1 Alignment of 2N4R-Tau cDNA with translated amino acid sequence

```
atggctgagccccgccaggagttcgaagtgatggaagatcacgctgggacgtacgggttg
 M  A  E  P  R  Q  E  F  E  V  M  E  D  H  A  G  T  Y  G  L  20
ggggacaggaaagatcaggggggctacaccatgcaccaagaccaagagggtgacacggac
 G  D  R  K  D  Q  G  G  Y  T  M  H  Q  D  Q  E  G  D  T  D  40
gctggcctgaaagaatctcccctgcagacccccactgaggacggatctgaggaaccgggc
 A  G  L  K  E  S  P  L  Q  T  P  T  E  D  G  S  E  E  P  G  60
tctgaaacctctgatgctaagagcactccaacagcggaagatgtgacagcacccttagtg
 S  E  T  S  D  A  K  S  T  P  T  A  E  D  V  T  A  P  L  V  80
gatgagggagctcccggcaagcaggctgccgcgcagccccacacggagatcccagaagga
 D  E  G  A  P  G  K  Q  A  A  A  Q  P  H  T  E  I  P  E  G  100
accacagctgaagaagcaggcattggagacacccccagcctggaagacgaagctgctggt
 T  T  A  E  E  A  G  I  G  D  T  P  S  L  E  D  E  A  A  G  120
cacgtgacccaagctcgcatggtcagtaaaagcaaagacgggactggaagcgatgacaaa
 H  V  T  Q  A  R  M  V  S  K  S  K  D  G  T  G  S  D  D  K  140
aaagccaaggggggctgatggtaaaacgaagatcgccacaccgcggggagcagcccctcca
 K  A  K  G  A  D  G  K  T  K  I  A  T  P  R  G  A  A  P  P  160
ggccagaagggccaggccaacgccaccaggattccagcaaaaaccccgcccgctccaaag
 G  Q  K  G  Q  A  N  A  T  R  I  P  A  K  T  P  P  A  P  K  180
acaccacccagctctggtgaacctccaaaatcaggggatcgcagcggctacagcagcccc
 T  P  P  S  S  G  E  P  P  K  S  G  D  R  S  G  Y  S  S  P  200
ggctccccaggcactcccggcagccgctcccgcaccccgtcccttccaaccccacccacc
 G  S  P  G  T  P  G  S  R  S  R  T  P  S  L  P  T  P  P  T  220
cgggagcccaagaaggtggcagtggtccgtactccacccaagtcgccgtcttccgccaag
 R  E  P  K  K  V  A  V  V  R  T  P  P  K  S  P  S  S  A  K  240
agccgcctgcagacagcccccgtgcccatgccagacctgaagaatgtcaagtccaagatc
 S  R  L  Q  T  A  P  V  P  M  P  D  L  K  N  V  K  S  K  I  260
ggctccactgagaacctgaagcaccagccgggaggcgggaaggtgcagataattaataag
 G  S  T  E  N  L  K  H  Q  P  G  G  G  K  V  Q  I  I  N  K  280
aagctggatcttagcaacgtccagtccaagtgtggctcaaaggataatatcaaacacgtc
 K  L  D  L  S  N  V  Q  S  K  C  G  S  K  D  N  I  K  H  V  300
ccgggaggcggcagtgtgcaaatagtctacaaaccagttgacctgagcaaggtgacctcc
 P  G  G  G  S  V  Q  I  V  Y  K  P  V  D  L  S  K  V  T  S  320
aagtgtggctcattaggcaacatccatcataaaccaggaggtggccaggtggaagtaaaa
 K  C  G  S  L  G  N  I  H  H  K  P  G  G  G  Q  V  E  V  K  340
tctgagaagcttgacttcaaggacagagtccagtcgaagattgggtccctggacaatatc
 S  E  K  L  D  F  K  D  R  V  Q  S  K  I  G  S  L  D  N  I  360
acccacgtccctggcggaggaaataaaaagattgaaacccacaagctgaccttccgcgag
 T  H  V  P  G  G  G  N  K  K  I  E  T  H  K  L  T  F  R  E  380
aacgccaaagccaagacagaccacggggcggagatcgtgtacaagtcgccagtggtgtct
 N  A  K  A  K  T  D  H  G  A  E  I  V  Y  K  S  P  V  V  S  400
ggggacacgtctccacggcatctcagcaatgtctcctccaccggcagcatcgacatggta
 G  D  T  S  P  R  H  L  S  N  V  S  S  T  G  S  I  D  M  V  420
gactcgccccagctcgccacgctagctgacgaggtgtctgcctccctggccaagcagggt
 D  S  P  Q  L  A  T  L  A  D  E  V  S  A  S  L  A  K  Q  G  440
ttgtag
 L  -
```

7.2 Sequences of 2N4R-Tau

7.2.1 WT-2N4R-Tau Plasmid cDNA:

ATG GCT GAG CCC CGC CAG GAG TTC GAA GTG ATG GAA GAT CAC GCT
GGG ACG TAC GGG TTG GGG GAC AGG AAA GAT CAG GGG GGC TAC ACC
ATG CAC CAA GAC CAA GAG GGT GAC ACG GAC GCT GGC CTG AAA GAA
TCT CCC CTG CAG ACC CCC ACT GAG GAC GGA TCT GAG GAA CCG GGC
TCT GAA ACC TCT GAT GCT AAG AGC ACT CCA ACA GCG GAA GAT GTG
ACA GCA CCC TTA GTG GAT GAG GGA GCT CCC GGC AAG CAG GCT GCC
GCG CAG CCC CAC ACG GAG ATC CCA GAA GGA ACC ACA GCT GAA GAA
GCA GGC ATT GGA GAC ACC CCC AGC CTG GAA GAC GAA GCT GCT GGT
CAC GTG ACC CAA GCT CGC ATG GTC AGT AAA AGC AAA GAC GGG ACT
GGA AGC GAT GAC AAA AAA GCC AAG GGG GCT GAT GGT AAA ACG AAG
ATC GCC ACA CCG CGG GGA GCA GCC CCT CCA GGC CAG AAG GGC CAG
GCC AAC GCC ACC AGG ATT CCA GCA AAA ACC CCG CCC GCT CCA AAG
ACA CCA CCC AGC TCT GGT GAA CCT CCA AAA TCA GGG GAT CGC AGC
GGC TAC AGC AGC CCC GGC TCC CCA GGC ACT CCC GGC AGC CGC TCC
CGC ACC CCG TCC CTT CCA ACC CCA CCC ACC CGG GAG CCC AAG AAG
GTG GCA GTG GTC CGT ACT CCA CCC AAG TCG CCG TCT TCC GCC AAG
AGC CGC CTG CAG ACA GCC CCC GTG CCC ATG CCA GAC CTG AAG AAT
GTC AAG TCC AAG ATC GGC TCC ACT GAG AAC CTG AAG CAC CAG CCG
GGA GGC GGG AAG GTG CAG ATA ATT AAT AAG AAG CTG GAT CTT AGC
AAC GTC CAG TCC AAG TGT GGC TCA AAG GAT AAT ATC AAA CAC GTC
CCG GGA GGC GGC AGT GTG CAA ATA GTC TAC AAA CCA GTT GAC CTG
AGC AAG GTG ACC TCC AAG TGT GGC TCA TTA GGC AAC ATC CAT CAT
AAA CCA GGA GGT GGC CAG GTG GAA GTA AAA TCT GAG AAG CTT GAC
TTC AAG GAC AGA GTC CAG TCG AAG ATT GGG TCC CTG GAC AAT ATC
ACC CAC GTC CCT GGC GGA GGA AAT AAA AAG ATT GAA ACC CAC AAG
CTG ACC TTC CGC GAG AAC GCC AAA GCC AAG ACA GAC CAC GGG GCG
GAG ATC GTG TAC AAG TCG CCA GTG GTG TCT GGG GAC ACG TCT CCA
CGG CAT CTC AGC AAT GTC TCC TCC ACC GGC AGC ATC GAC ATG GTA
GAC TCG CCC CAG CTC GCC ACG CTA GCT GAC GAG GTG TCT GCC TCC
CTG GCC AAG CAG GGT TTG T**AG**

7.2.2 2N4Rc103 Tau cDNA:

ATG GCT GAG CCC CGC CAG GAG TTC GAA GTG ATG GAA GAT CAC GCT
GGG ACG TAC GGG TTG GGG GAC AGG AAA GAT CAG GGG GGC TAC ACC
ATG CAC CAA GAC CAA GAG GGT GAC ACG GAC GCT GGC CTG AAA GAA
TCT CCC CTG CAG ACC CCC ACT GAG GAC GGA TCT GAG GAA CCG GGC
TCT GAA ACC TCT GAT GCT AAG AGC ACT CCA ACA GCG GAA GAT GTG
ACA GCA CCC TTA GTG GAT GAG GGA GCT CCC GGC AAG CAG GCT GCC
GCG CAG CCC CAC ACG GAG ATC CCA GAA GGA ACC ACA GCT GAA GAA
GCA GGC ATT GGA GAC ACC CCC AGC CTG GAA GAC GAA GCT GCT GGT
CAC GTG ACC CAA GCT CGC ATG GTC AGT AAA AGC AAA GAC GGG ACT
GGA AGC GAT GAC AAA AAA GCC AAG GGG GCT GAT GGT AAA ACG AAG
ATC GCC ACA CCG CGG GGA GCA GCC CCT CCA GGC CAG AAG GGC CAG
GCC AAC GCC ACC AGG ATT CCA GCA AAA ACC CCG CCC GCT CCA AAG
ACA CCA CCC AGC TCT GGT GAA CCT CCA AAA TCA GGG GAT CGC AGC
GGC TAC AGC AGC CCC GGC TCC CCA GGC ACT CCC GGC AGC CGC TCC
CGC ACC CCG TCC CTT CCA ACC CCA CCC ACC CGG GAG CCC AAG AAG
GTG GCA GTG GTC CGT ACT CCA CCC AAG TCG CCG TCT TCC GCC AAG
AGC CGC CTG CAG ACA GCC CCC GTG CCC ATG CCA GAC CTG AAG AAT
GTC AAG TCC AAG ATC GGC TCC ACT GAG AAC CTG AAG CAC CAG CCG
GGA GGC GGG AAG GTG CAG ATA ATT AAT AAG AAG CTG GAT CTT AGC
AAC GTC CAG TCC AAG TGT GGC TCA AAG GAT AAT ATC AAA CAC GTC
CCG GGA GGC GGC AGT GTG CAA ATA GTC TAC AAA CCA GTT GAC CTG
AGC AAG GTG ACC TCC AAG TGT GGC TCA TTA GGC AAC ATC CAT CAT
AAA CCA GGA GGT GGC CAG GTG GAA GTA AAA TCT GAG AAG CTT GAC
TTC AAG GAC AGA GTC CAG TCG AAG ATT GGG TCC CTG GAC AAT ATC
ACC CAC GTC CCT GGC GGA GGA AAT AAA AAG ATT GAA ACC CAC AAG
CTG ACC TTC CGC GAG AAC GCC AAA GCC AAG ACA GAC CAC GGG GCG
GAG ATC GTG TAC AAG TCG CCA GTG GTG TCT GGG GAC ACG TCT CCA
CGG CAT CTC AGC AAT GTC TCC TCC ACC GGC AGC ATC GAC ATG GTA
GAC TCG CCC CAG CTC GCC ACG CTA GCT GAC GAG GTG TCT GCC TCC
CTG GCC AAG CAG GGT TTG T**AG**

7.2.3 Alignment:

100.0% identity in 1326 residues overlap; Gap frequency: 0.0%. Performed using Expasy align online software

```
Plasmid        1 ATGGCTGAGCCCCGCCAGGAGTTCGAAGTGATGGAAGATCACGCTGGGACGTACGGGTTG
cDNA           1 ATGGCTGAGCCCCGCCAGGAGTTCGAAGTGATGGAAGATCACGCTGGGACGTACGGGTTG
                 ************************************************************

Plasmid       61 GGGGACAGGAAAGATCAGGGGGGCTACACCATGCACCAAGACCAAGAGGGTGACACGGAC
cDNA          61 GGGGACAGGAAAGATCAGGGGGGCTACACCATGCACCAAGACCAAGAGGGTGACACGGAC
                 ************************************************************

Plasmid      121 GCTGGCCTGAAAGAATCTCCCCTGCAGACCCCCACTGAGGACGGATCTGAGGAACCGGGC
cDNA         121 GCTGGCCTGAAAGAATCTCCCCTGCAGACCCCCACTGAGGACGGATCTGAGGAACCGGGC
                 ************************************************************

Plasmid      181 TCTGAAACCTCTGATGCTAAGAGCACTCCAACAGCGGAAGATGTGACAGCACCCTTAGTG
cDNA         181 TCTGAAACCTCTGATGCTAAGAGCACTCCAACAGCGGAAGATGTGACAGCACCCTTAGTG
                 ************************************************************

Plasmid      241 GATGAGGGAGCTCCCGGCAAGCAGGCTGCCGCGCAGCCCCACACGGAGATCCCAGAAGGA
cDNA         241 GATGAGGGAGCTCCCGGCAAGCAGGCTGCCGCGCAGCCCCACACGGAGATCCCAGAAGGA
                 ************************************************************

Plasmid      301 ACCACAGCTGAAGAAGCAGGCATTGGAGACACCCCCAGCCTGGAAGACGAAGCTGCTGGT
cDNA         301 ACCACAGCTGAAGAAGCAGGCATTGGAGACACCCCCAGCCTGGAAGACGAAGCTGCTGGT
                 ************************************************************

Plasmid      361 CACGTGACCCAAGCTCGCATGGTCAGTAAAAGCAAAGACGGGACTGGAAGCGATGACAAA
cDNA         361 CACGTGACCCAAGCTCGCATGGTCAGTAAAAGCAAAGACGGGACTGGAAGCGATGACAAA
                 ************************************************************

Plasmid      421 AAAGCCAAGGGGGCTGATGGTAAAACGAAGATCGCCACACCGCGGGGAGCAGCCCCTCCA
cDNA         421 AAAGCCAAGGGGGCTGATGGTAAAACGAAGATCGCCACACCGCGGGGAGCAGCCCCTCCA
                 ************************************************************

Plasmid      481 GGCCAGAAGGGCCAGGCCAACGCCACCAGGATTCCAGCAAAAACCCCGCCCGCTCCAAAG
cDNA         481 GGCCAGAAGGGCCAGGCCAACGCCACCAGGATTCCAGCAAAAACCCCGCCCGCTCCAAAG
                 ************************************************************

Plasmid      541 ACACCACCCAGCTCTGGTGAACCTCCAAAATCAGGGGATCGCAGCGGCTACAGCAGCCCC
cDNA         541 ACACCACCCAGCTCTGGTGAACCTCCAAAATCAGGGGATCGCAGCGGCTACAGCAGCCCC
                 ************************************************************

Plasmid      601 GGCTCCCCAGGCACTCCCGGCAGCCGCTCCCGCACCCCGTCCCTTCCAACCCCACCCACC
cDNA         601 GGCTCCCCAGGCACTCCCGGCAGCCGCTCCCGCACCCCGTCCCTTCCAACCCCACCCACC
                 ************************************************************

Plasmid      661 CGGGAGCCCAAGAAGGTGGCAGTGGTCCGTACTCCACCCAAGTCGCCGTCTTCCGCCAAG
cDNA         661 CGGGAGCCCAAGAAGGTGGCAGTGGTCCGTACTCCACCCAAGTCGCCGTCTTCCGCCAAG
                 ************************************************************

Plasmid      721 AGCCGCCTGCAGACAGCCCCCGTGCCCATGCCAGACCTGAAGAATGTCAAGTCCAAGATC
cDNA         721 AGCCGCCTGCAGACAGCCCCCGTGCCCATGCCAGACCTGAAGAATGTCAAGTCCAAGATC
                 ************************************************************

Plasmid      781 GGCTCCACTGAGAACCTGAAGCACCAGCCGGGAGGCGGGAAGGTGCAGATAATTAATAAG
cDNA         781 GGCTCCACTGAGAACCTGAAGCACCAGCCGGGAGGCGGGAAGGTGCAGATAATTAATAAG
                 ************************************************************

Plasmid      841 AAGCTGGATCTTAGCAACGTCCAGTCCAAGTGTGGCTCAAAGGATAATATCAAACACGTC
cDNA         841 AAGCTGGATCTTAGCAACGTCCAGTCCAAGTGTGGCTCAAAGGATAATATCAAACACGTC
                 ************************************************************

Plasmid      901 CCGGGAGGCGGCAGTGTGCAAATAGTCTACAAACCAGTTGACCTGAGCAAGGTGACCTCC
cDNA         901 CCGGGAGGCGGCAGTGTGCAAATAGTCTACAAACCAGTTGACCTGAGCAAGGTGACCTCC
                 ************************************************************

Plasmid      961 AAGTGTGGCTCATTAGGCAACATCCATCATAAACCAGGAGGTGGCCAGGTGGAAGTAAAA
cDNA         961 AAGTGTGGCTCATTAGGCAACATCCATCATAAACCAGGAGGTGGCCAGGTGGAAGTAAAA
                 ************************************************************
```

```
Plasmid     1021 TCTGAGAAGCTTGACTTCAAGGACAGAGTCCAGTCGAAGATTGGGTCCCTGGACAATATC
cDNA        1021 TCTGAGAAGCTTGACTTCAAGGACAGAGTCCAGTCGAAGATTGGGTCCCTGGACAATATC
                 ************************************************************

Plasmid     1081 ACCCACGTCCCTGGCGGAGGAAATAAAAAGATTGAAACCCACAAGCTGACCTTCCGCGAG
cDNA        1081 ACCCACGTCCCTGGCGGAGGAAATAAAAAGATTGAAACCCACAAGCTGACCTTCCGCGAG
                 ************************************************************

Plasmid     1141 AACGCCAAAGCCAAGACAGACCACGGGGCGGAGATCGTGTACAAGTCGCCAGTGGTGTCT
cDNA        1141 AACGCCAAAGCCAAGACAGACCACGGGGCGGAGATCGTGTACAAGTCGCCAGTGGTGTCT
                 ************************************************************

Plasmid     1201 GGGGACACGTCTCCACGGCATCTCAGCAATGTCTCCTCCACCGGCAGCATCGACATGGTA
cDNA        1201 GGGGACACGTCTCCACGGCATCTCAGCAATGTCTCCTCCACCGGCAGCATCGACATGGTA
                 ************************************************************

Plasmid     1261 GACTCGCCCCAGCTCGCCACGCTAGCTGACGAGGTGTCTGCCTCCCTGGCCAAGCAGGGT
cDNA        1261 GACTCGCCCCAGCTCGCCACGCTAGCTGACGAGGTGTCTGCCTCCCTGGCCAAGCAGGGT
                 ************************************************************

Plasmid     1321 TTGTAG
cDNA        1321 TTGTAG
                 ******
```

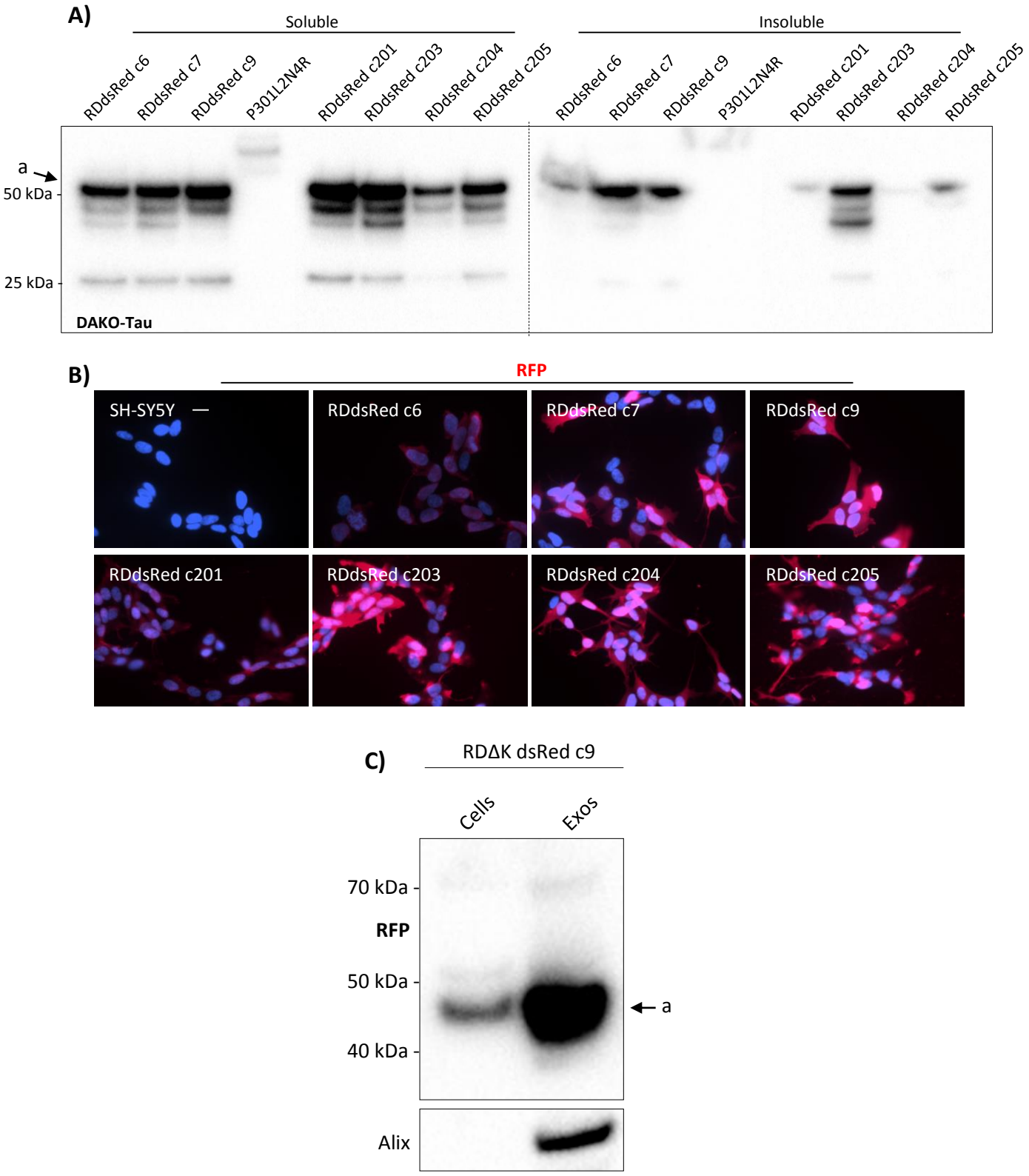

Figure 7.1 Characterisation of SH-SY5Y cells with stable expression of RDdsRed Tau. A) Solubility analysis of SH-SY5Y cells with stable expression of RD-dsRed-Tau. Cells were sequentially extracted in 1% Tx100 and 1% SDS and loaded on the gel in a 1 : 10 ratio. Different exposures have been selected for the 'soluble' and 'insoluble' sides. Band 'a' indicates full-length RD-dsRed-Tau. **B)** RFP ICC analysis of RDdsRed SH-SY5Y clones. Scale bar 10 µm. **C)** Western blot analysis of cell lysates (0.1 µg) and exosomes (isolated from the 24 hour conditioned optiMEM of 5 x 10 cm plates) of RD-dsRed-Tau c9 SH-SY5Y cells. Band 'a' indicates full length RDdsRed-Tau.

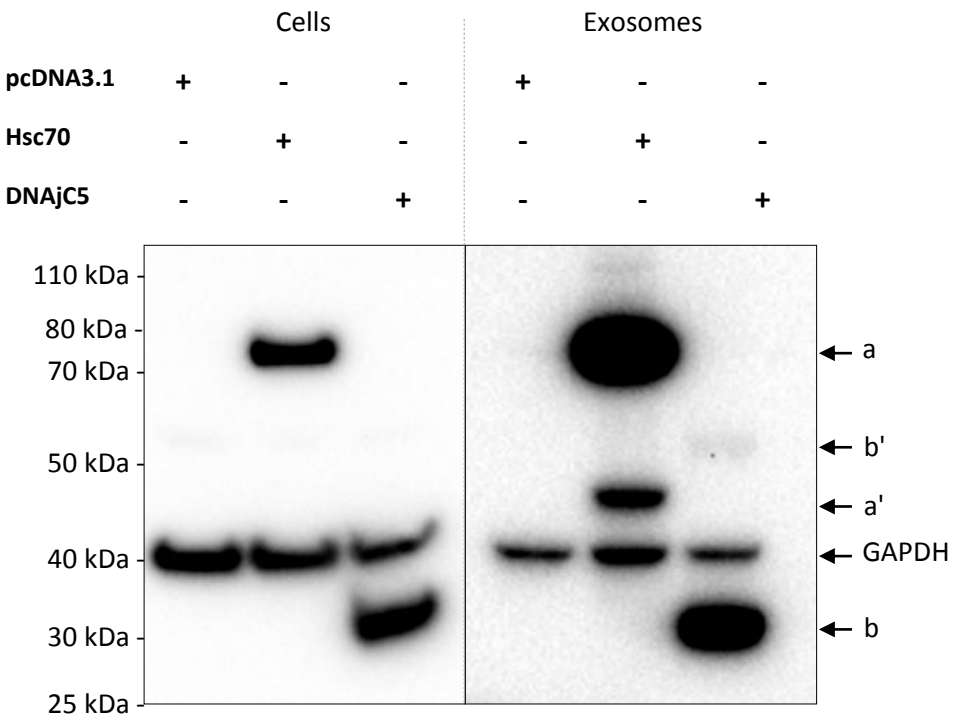

Figure 7.2 Analysis of the exosomal release of DNAjC5 and Hsc70. SH-SY5Y cells were transfected with DNAjC5-FLAG or Hsc70-V5 and grown for 48 hours. During the last 24 hours of expression the cells were grown in optiMEM medium. Exosomes were isolated from the 24 hour conditioned optiMEM medium by differential ultracentrifugation and analysed by Western blotting with FLAG and C5 antibodies. V5 and FLAG cross reactive bands, consistent with monomeric Hsc70 and DNAjC5, respectively, were detected in the respectively transfected cells, as indicated by bands 'a' and 'b', respectively. A 45 kDa V5 cross reactive band consistent with an Hsc70 C-terminal fragment was detected in the exosomes isolated from SH-SY5Y cells transfected with Hsc70-V5 (band 'a'') and a 60 kDa FLAG cross reactive band, consistent with dimeric DNAjC5, was detected in the exosomes isolated from the conditioned medium of SH-SY5Y cells transfected with DNAjC5-FLAG (band 'b'').

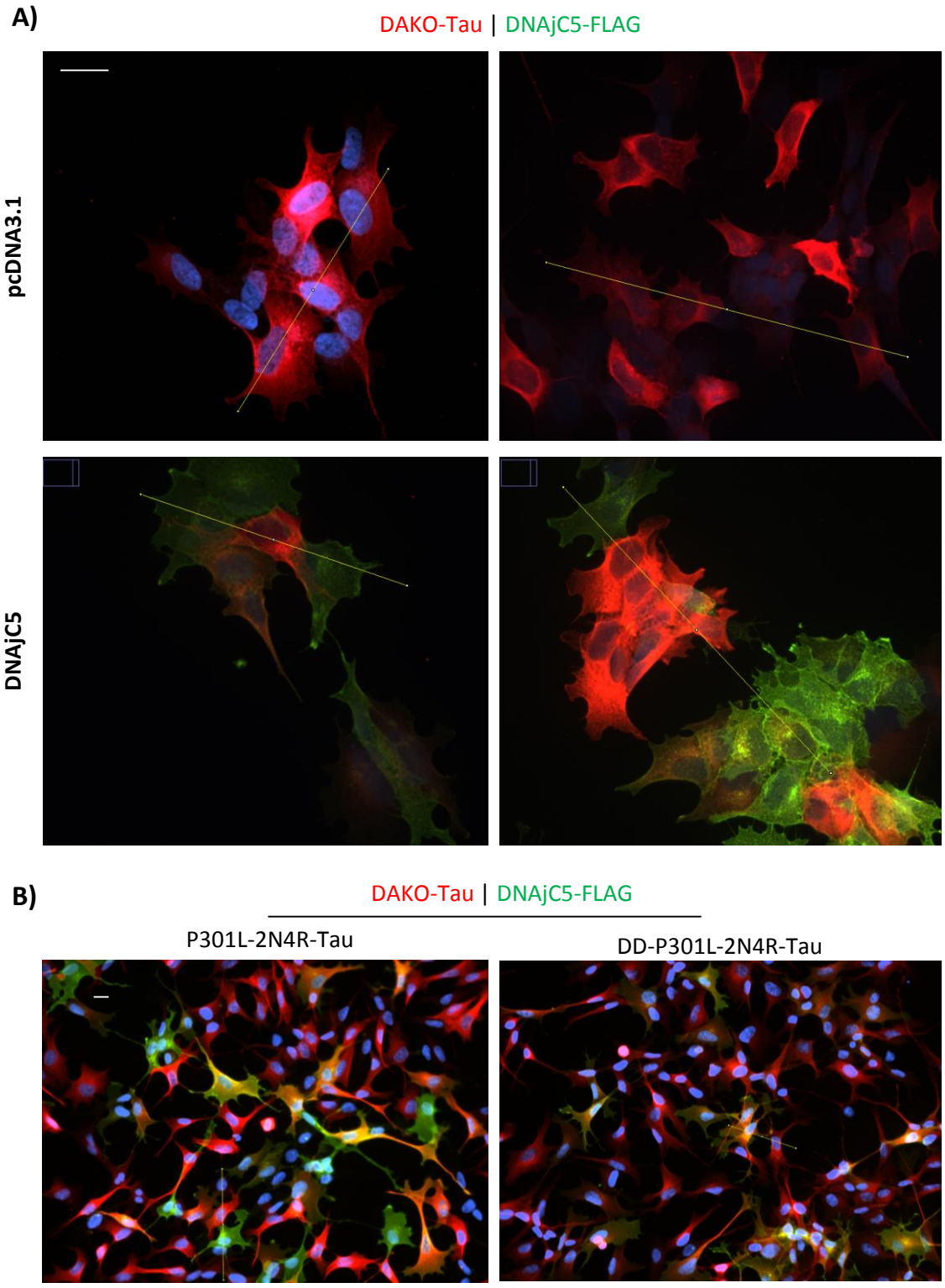

Figure 7.3 ICC images used for Tau and DNAjC5 intensity analysis. A) DAKO-Tau and FLAG co-immunostaining analysis of WT-2N4R-c103 SH-SY5Y cells transfected with DNAjC5-flag.W Yellow lines indicate regions along which the fluorescence intensities of DAPI, DAKO-Tau (red channel) and FLAG (FITC channel) staining were plotted in **figure 4.15**. **B)** Whole field ICC images of DD-P301L / P301L-2N4R-Tau SH-SY5Y cells transiently expressing DNAjC5 co-immunostained with DAKO-Tau and FLAG antibodies. Relates to figure **4.18**. Scale bars 10 µm.

7.6 Summary of Papers Investigating Tau Secretion from Cell Models

Author, year	Model system / biofluid	Source of tau	Type of tau release (free vs. Vesicle)	Detection method	Detection antibody / epitope / type of tau released	Interpretation of release / modulating factors Comments
Croft et al. 2017	Organotypic slice cultures	3xTg-AD mice, (P301L-Tau)	Free release	ELISA	BT2-DAKO	Tau from 3xTg-AD released at increased rate, but not increased by KCl. Dephosphorylated Tau accumulates at membranes with KCl treatment.
			Membrane Tau	WB	Tau (total) Tau-1 (pTau)	
Bright et al. 2014	AD patient derived iPSC cortical neurons (PSEN1 mutation)	Endogenous	Free release into CM	WB, IP, Mass spec	IPN002 (IP), HT7 (IP). 4 species released, not containing MTBR (MS)	Free release of N-terminal fragments. Full length tau not detected in CM, and CM tau not IPed by Tau46
Mohamed et al. 2014	Mouse cortical neurons, 7 days post plating	Endogenous	Free release into CM	IP and WB	52 kDa band detected by Dako Tau	Release stimulated by lysosomal inhibition and starvation
Tang et al. 2014	SH-SY5Y cells with and without a variety of mTOR overexpression	Endogenous	Free release into CM,	Dot blot	PHF-1 , pTau S214, Tau1 All antibodies giving positive signal with and without mTOR overexpression	mTOR overexpression increased free tau (pTau and npTau) detected in CM, but did not affect exosomal tau levels
			Exosome associated release,		PHF-1 , pTau S214, Tau1 All antibodies giving positive signal with and without mTOR overexpression	
Asai et al. 2015	Primary microglia, neurons, astrocytes	Cells incubated with rTau (2N4R) oligomer – aggregate	Exosomes	WB IP-WB	WB Tau46 IP Tsg101 WB Tau46	Phagocytosed Tau exosomally released from microglia but not from neurons or astrocytes. LPS and ATP induced release. P301S Tau released in exosomes, released decreased by microglial depletion
	Mouse brain PS19 mouse	1N4R P301S Tau	Exosomes	EM immuno-gold	PHF-1 HT7	
				Immuno-blot	T22	
Dujardin et al. 2014	Rat primary cortical neurons	Endogenous / infected with h1N4R	Exosomes and 'ectosomes' (20,000 x g pellet)	EM immuno-gold WB	N-term Tau C-term Tau	Tau primarily detected in 'ectosomal' fraction from primary neurons. Found in exosomes when neurons infected with h1N4R C-terminally truncated Tau in exosomes from cell lines
	N1E-115 cells	H1N4R over-expression				

Kim et al. 2010	M1C cells	0N4R inducible expression	Free release in medium	IP- Tau12	Tau46 negative K9JA positive Tau12 positive	E2 negative (ON) isoforms secreted at a higher rate than E2 positive (1N) isoforms, detected with tau12 and K9JA after tau12 IP. Direct WB of concentrated medium tau also performed, E2 positive isoforms secreted less than E2 negative isoforms. Overall, exon 2 was suggested to selectively inhibit the secretion of stably and transiently overexpressed tau.
		1N4R, 1N3R inducible expression			Tau46 negative K9JA positive Tau12 positive	
	NB2a/d1 cells	0N tau (to AA 255) 2N tau (to AA 255) Transient expression			Tau12 WB, 0N tau released, 2N tau not released	
Plouffe et al. 2012	HeLa cells	Different GFP Tau constructs (4R), transiently expressed	Free release. Exosomal release 'checked' but not thoroughly and data not presented here.	IP HT7 WB Various	Tau12 positive 75 kDa (FL), bands at 37 to 50 kDa HT7 Polyclonal tau Secreted tau migrated faster than FL intracellular tau, suggested to be cleaved at the C-terminal as it was not detected by Tau46	Temperature dependent, suggested to be independent of cell death and an active mechanism Brefaldin A insensitive
		Tau Δ421 (C-terminal cleavage construct) transient expression Tau Δ412			Tau Δ421 secreted > tau Δ413 = FL	Preferential secretion of cleavage product at 421
Pooler et al. 2013	Rat primary cortical neurons	Endogenous Tau	Free release	ELISA (post 12,000 x g)		Increased release with KCl and glutamate and AMPA. Inhibited with tetanus toxin Dependent upon synaptic mechanisms Increased release with AMPA normal, physiological process, dependent upon synaptic activity
				WB	Total tau, Tau-1, PHF-1 (negative), TP007, TP70,	

			Exosomes	WB	Total tau, not detected	Apparently not detected in this system
Kanmert et al. 2015	N2a cells	Endogenous	Free release	ELISA (capture 194-241)	Tau with intact middle region. Signal NOT depleted by MC1, fully depleted by BT2 Not depleted by 100,000 x g centrifugation	Time dependent increase in release Un-aggregated
			Exosomes, 200 ml culture medium + / - Tx100 to lyse vesicles and see differences in tau ELISA.	ELISA for tau mid region,	tau ELISA detected exosomal tau	Small amount of exosomal tau (<1%)
	iHCN 45 days differentiated (into cortical neurons).		Free release	ELISA for tau mid region	Tau levels fully depleted by BT2 IP, unaffected by MC1 IP, unaffected by high speed centrifugation	Majority of tau was free floating and un-aggregated
			Exosomes, 100,000 x g pellet	Mid region tau ELISA	Signal detected equal to 0.01% of CM tau levels.	A small percentage of tau is detectable in exosomes
	Primary rat neurons DIV 21		Free release	Tau ELISA mid region	Signal depleted by BT2 but not NC1 or high speed centrifugation	Majority of tau was free floating and un-aggregated
				FL Tau ELISA C-terminal tau ELISA (K9JA + Tau46) C-terminal tau ELISA (K9JA alone) Mid region tau ELISA	Mid region tau ELISA > C-terminal > FL	Majority of tau released under physiological settings was truncated at the C-terminal
Saman et al. 2012	M1C cells	0N4R inducible tau expression	Exosomes	WB, K9JA, Tau12	Reacted with both K9JA and Tau12, potentially C-terminally truncated	Overexpressed 0N4R tau is secreted from M1C cells as exosomally associated, and exosomal tau may be enriched in phospho-epitopes specific for AD.
				Mass spectrometry	Enrichment of phospho-epitopes AT270, AT8, AT100 and AT180	
	AD CSF	Endogenous	Exosomes	WB, ELISA	AT270 enrichment in exosomes,	Increased in early AD

Chai et al. 2012	HEK293 cells	Inducible over-expression of 2N4R tau	Free release (not detected in exosomes by ELISA)	ELISA	HT7 capture CP27 capture	Tau detectable, levels increased in a time dependent manner Brefeldin A and monensin insensitive release (HEK cells only tested) Temperature dependent; release abolished at 25°C.
	iCELL neurons	Endogenous 3R tau expression	Fee release			
Simon et al. 2012	COS-7 cells	Transient over-expression, increasing amounts 2N4R (?)	Free release	WB	7.51 tau antibody, recognising total tau was used. Looked to be FL in medium	Secretion was only observed when expression level was increased. Secretion was independent of cell death
			Exosomes		Migrated similarly to FL IC tau	IC tau colocalised with LAMP2A and cofractionated with TSG101 hsp70, and flotilin-1
	HEK293 cells	Stable expression of 3R tau			Migrated similarly to FL IC tau, but when cultured for 1 week, degraded tau found migrating between 25 and ~ 15 kDa, 7.51 antibody corresponding to AA 315 – 376 used	Tau is present in exosomes isolated from cells transiently and stably overexpressing tau. These exosomes did not induce the death of cortical neurons. Exosomes not characterised
				EM immuno-gold	Polyclonal tau antibody	
Karch et al. 2012	Primary neuronal cultures (mouse) DIV 14	Endogenous tau	Free release	Total tau ELISA,	Total tau detected	Predominantly full length and also phosphorylated at T181 is released from primary neuronal cultures
				IP and WB, IP Tau-1, HJ9.3, Tau7, WB total tau WB pTau181	Migrated similarly to FL IC tau and was detected by all antibodies trialled. Likely full length pTau181 positive	
	SH-SY5Y cells		Free release	Total tau ELISA	Total tau detected	Induced by H_2O_2 cell death in concentration dependent manner. Release increased by BAPTA-AM, thapsigargin, ionomycin, and chloroquine (and heat shock), and insensitive to brefeldin A.

				Radiolabelled proteins, IP tau12 and autoradiogram	Tau detectable in media 6 hours after chase, different bands present inside and outside the cells, identity unknown	Suggested active mechanisms of secretion, differential sorting and secretion of tau species.
			Exosomes	WB Tau7	Not detected	10 x 10 cm plates, 48 hour culture in exosome free media
		Transiently overexpressed 0N3R, 2N3R, 0N4R, 2N4R And FTD tau P301L and 4406W	Free release	ELISA total tau	All isoforms detected in the medium	2N3R claimed to be secreted at increased levels, 2N4R at lowest levels, and 0N3R and 0N4R at similar levels, with similar IC levels of expression and basal toxicity. FTD associated mutant tau was secreted at lower levels than WT type. Transiently transfected 2N4R secreted tau was transmitted to HEK293 cells detected by WB and ICC. It was not stated that medium was centrifuged prior to transfer.
Kim et al. (2102b)	N2a cells	Transient overexpression of FL tau, N-terminal tau and C-terminal tau	Free release	WB concentrated medium	Tau12, detected a fragment migrating faster than full length, that was therefore C-terminally cleaved	

References

Abounit, S. et al., 2016. Tunneling nanotubes spread fibrillar α-synuclein by intercellular trafficking of lysosomes. The EMBO Journal, 35(19), pp.2120–2138.

Adams, S.J. et al., 2010. Three Repeat Isoforms of Tau Inhibit Assembly of Four Repeat Tau Filaments S. T. Ferreira, ed. PLoS ONE, 5(5), p.e10810.

Agholme, L. et al., 2010. An In Vitro Model for Neuroscience: Differentiation of SH-SY5Y Cells into Cells with Morphological and Biochemical Characteristics of Mature Neurons. Journal of Alzheimer's Disease, 20, pp.1069–1082.

Ahmed, Z. et al., 2014. A novel in vivo model of tau propagation with rapid and progressive neurofibrillary tangle pathology: the pattern of spread is determined by connectivity, not proximity. Acta neuropathologica, 127(5), pp.667–83.

Alvarez-Erviti, L., Seow, Y., Schapira, A.H., et al., 2011. Lysosomal dysfunction increases exosome-mediated alpha-synuclein release and transmission. Neurobiology of disease, 42(3), pp.360–7.

Anderson, W. et al., 2015, Observations of Tunable Resistive Pulse Sensing for Exosome Analysis: Improving System Sensitivity and Stability. Langmuir 16;31 (23), pp.6577 – 6587.

Andreadis, A., 2005. Tau gene alternative splicing: expression patterns, regulation and modulation of function in normal brain and neurodegenerative diseases. Biochimica et biophysica acta, 1739(2–3), pp.91–103.

Andreu, Z. & Yáñez-Mó, M., 2014. Tetraspanins in extracellular vesicle formation and function. Frontiers in immunology, 5, p.442.

Angelique Bobrie, A. et al., 2012. Diverse subpopulations of vesicles secreted by different intracellular mechanisms are present in exosome preparations obtained by differential ultracentrifugation. Journal of Extracellular Vesicles, 16(1).

Arnold, S.E. et al., 1991. The Topographical and Neuroanatomical Distribution of Neurofibrillary Tangles and Neuritic Plaques in the Cerebral Cortex of Patients with Alzheimer's Disease. Cerebral Cortex, 1(1), pp.103–116.

Arrasate, M., Pérez, M. & Avila, J., 2000. Tau Dephosphorylation at Tau-1 Site Correlates with its Association to Cell Membrane*. Neurochemical Research, 25(1), pp.43–50.

Asai, H. et al., 2015. Depletion of microglia and inhibition of exosome synthesis halt tau propagation. Nature Neuroscience, 18(11), pp.1584–1593.

Ashman, J.B. et al., 1992. Tau, the Neuronal Heat-Stable Microtubule-Associated Protein, Is Also Present in the Cross-Linked Microtubule Network of the Testicular Spermatid Manchette. BIOLOGY OF REPRODUCTION, 46, pp.120–129.

Augustinack, J.C. et al., 2002. Specific tau phosphorylation sites correlate with severity of neuronal cytopathology in Alzheimer's disease. Acta neuropathologica, 103(1), pp.26–35.

Avila, J. et al., 2016. Tau Structures. Frontiers in aging neuroscience, 8, p.262.

Baas, P.W., Pienkowski, T.P. & Kosik, K.S., 1991. Processes induced by tau expression in Sf9 cells have an axon-like microtubule organization. The Journal of cell biology, 115(5), pp.1333–44.

Baietti, M.F. et al., 2012. Syndecan–syntenin–ALIX regulates the biogenesis of exosomes. Nature Cell Biology, 14(7), pp.677–685.

Baixauli, F., López-Otín, C. & Mittelbrunn, M., 2014. Exosomes and autophagy: coordinated mechanisms for the maintenance of cellular fitness. Frontiers in immunology, 5, p.403.

Bierer, L.M. et al., 1995. Neocortical neurofibrillary tangles correlate with dementia severity in Alzheimer's disease. Archives of neurology, 52(1), pp.81–8.

Biernat, J. et al., 1993. Phosphorylation of Ser262 strongly reduces binding of tau to microtubules: distinction between PHF-like immunoreactivity and microtubule binding. Neuron, 11(1), pp.153–63.

Biundo, F. et al., 2018. A role for tau in learning, memory and synaptic plasticity. Scientific Reports, 8(1), p.3184.

Boluda, S. et al., 2015. Differential induction and spread of tau pathology in young PS19 tau transgenic mice following intracerebral injections of pathological tau from Alzheimer's disease or corticobasal degeneration brains. Acta neuropathologica, 129(2), pp.221–37.

Boutajangout, A. et al., 2004. Expression of tau mRNA and soluble tau isoforms in affected and non-affected brain areas in Alzheimer's disease. FEBS letters, 576(1–2), pp.183–9.

Braak, H. & Braak, E., 1991. Neuropathological stageing of Alzheimer-related changes. Acta Neuropathologica, 82(4), pp.239–259.

Brandt, R., Léger, J. & Lee, G., 1995. Interaction of tau with the neural plasma membrane mediated by tau's amino-terminal projection domain. The Journal of cell biology, 131(5), pp.1327–40.

Braun, J.E.A. & Scheller, R.H., 1995. Cysteine String Protein, a DnaJ Family Member, is Present on Diverse Secretory Vesicles. Neuropharmacology, 34(95), pp.1361–1369.

Bright, J. et al., 2015. Human secreted tau increases amyloid-beta production. Neurobiology of Aging, 36(2), pp.693–709.

Bronner, I.F. et al., 2005. Hereditary Pick's disease with the G272V tau mutation shows predominant three-repeat tau pathology. Brain, 128(11), pp.2645–2653.

Bugiani, O. et al., 1999. Frontotemporal dementia and corticobasal degeneration in a family with a P301S mutation in tau. Journal of neuropathology and experimental neurology, 58(6), pp.667–77.

Bukar Maina, M., Al-Hilaly, Y.K. & Serpell, L.C., 2016. Nuclear Tau and Its Potential Role in Alzheimer's Disease. Biomolecules, 6(1), p.9.

Caballero, B. et al., 2018. Interplay of pathogenic forms of human tau with different autophagic pathways. Aging Cell, 17(1), p.e12692.

Cabrales Fontela, Y. et al., 2017. Multivalent cross-linking of actin filaments and microtubules through the microtubule-associated protein Tau. Nature Communications, 8(1), p.1981.

Caceres, A. & Kosik, K.S., 1990. Inhibition of neurite polarity by tau antisense oligonucleotides in primary cerebellar neurons. Nature, 343(6257), pp.461–3.

Calafate, S. et al., 2015. Synaptic Contacts Enhance Cell-to-Cell Tau Pathology Propagation. Cell reports, 11(8), pp.1176–83.

Carmel, G. et al., 1996. The Structural Basis of Monoclonal Antibody Alz50's Selectivity for Alzheimer's Disease Pathology. Journal of Biological Chemistry, 271(51), pp.32789–32795.

Castillo-Carranza, D.L. et al., 2014. Passive immunization with Tau oligomer monoclonal antibody reverses tauopathy phenotypes without affecting hyperphosphorylated neurofibrillary tangles. The Journal of neuroscience : the official journal of the Society for Neuroscience, 34(12), pp.4260–72.

Chai, X., Dage, J.L. & Citron, M., 2012. Constitutive secretion of tau protein by an unconventional mechanism. Neurobiology of Disease, 48(3), pp.356–366.

Chen, J. et al., 1992. Projection domains of MAP2 and tau determine spacings between microtubules in dendrites and axons. Nature, 360(6405), pp.674–677.

Chiang, H.L. et al., 1989. A role for a 70-kilodalton heat shock protein in lysosomal degradation of intracellular proteins. Science (New York, N.Y.), 246(4928), pp.382–5.

Chiotis, K. et al., 2017. Longitudinal changes of tau PET imaging in relation to hypometabolism in prodromal and Alzheimer's disease dementia. Molecular Psychiatry. 16.

Cho, J.-H. & Johnson, G.V.W., 2004. Primed phosphorylation of tau at Thr231 by glycogen synthase kinase 3beta (GSK3beta) plays a critical role in regulating tau's ability to bind and stabilize microtubules. Journal of neurochemistry, 88(2), pp.349–58.

Clavaguera, F. et al., 2009. Transmission and spreading of tauopathy in transgenic mouse brain. Nature Cell Biology, 11(7) pp.909-913.

Clavaguera, F. et al., 2013. Brain homogenates from human tauopathies induce tau inclusions in mouse brain. Proceedings of the National Academy of Sciences, 110(23), pp.9535–9540.

Cohen, T.J. et al., 2011. The acetylation of tau inhibits its function and promotes pathological tau aggregation. Nature communications, 2, p.252.

Cope, T.E. et al., 2018. Tau burden and the functional connectome in Alzheimer's disease and progressive supranuclear palsy. Brain, 141(2), pp.550–567.

Correas, I., Díaz-Nido, J. & Avila, J., 1992. Microtubule-associated protein tau is phosphorylated by protein kinase C on its tubulin binding domain. The Journal of biological chemistry, 267(22), pp.15721–8.

Costanzo, M. et al., 2013. Transfer of polyglutamine aggregates in neuronal cells occurs in tunneling nanotubes. Journal of cell science, 126(Pt 16), pp.3678–85.

Croft, C.L. et al., 2017. Membrane association and release of wild-type and pathological tau from organotypic brain slice cultures. Nature Publishing Group. 8(3).

D'Souza, I. et al., 1999. Missense and silent tau gene mutations cause frontotemporal dementia with parkinsonism-chromosome 17 type, by affecting multiple alternative RNA splicing regulatory elements. Proceedings of the National Academy of Sciences of the United States of America, 96(10), pp.5598–603.

Danzer, K.M. et al., 2012. Exosomal cell-to-cell transmission of alpha synuclein oligomers. Molecular Neurodegeneration, 7(1), p.42.

Day, R.J. et al., 2015. Caspase-Cleaved Tau Co-Localizes with Early Tangle Markers in the Human Vascular Dementia Brain. PloS one, 10(7), p.e0132637.

Dayanandan, R. et al., 1999. Mutations in tau reduce its microtubule binding properties in intact cells and affect its phosphorylation. FEBS Letters, 446(2–3), pp.228–232.

de Calignon, A. et al., 2010. Caspase activation precedes and leads to tangles. Nature, 464(7292), pp.1201–1204.

de Calignon, A. et al., 2012. Propagation of Tau Pathology in a Model of Early Alzheimer's Disease. Neuron, 73(4), pp.685–697.

Derisbourg, M. et al., 2015. Role of the Tau N-terminal region in microtubule stabilization revealed by new endogenous truncated forms. Scientific Reports, 5(1), p.9659.

DeVos, S.L. et al., 2018. Synaptic Tau Seeding Precedes Tau Pathology in Human Alzheimer's Disease Brain. Frontiers in Neuroscience, 12, p.267.

Díaz-Hernández, M. et al., 2010. Tissue-nonspecific Alkaline Phosphatase Promotes the Neurotoxicity Effect of Extracellular Tau. Journal of Biological Chemistry, 285(42), pp.32539–32548.

Dice, J.F., 1990. Peptide sequences that target cytosolic proteins for lysosomal proteolysis. Trends in biochemical sciences, 15(8), pp.305–9.

Dickson, D.W., 1999. Neuropathologic differentiation of progressive supranuclear palsy and corticobasal degeneration. Journal of Neurology, 246(S2), pp.II6-II15.

Dolan, P.J. & Johnson, G.V.W., 2010. A caspase cleaved form of tau is preferentially degraded through the autophagy pathway. The Journal of biological chemistry, 285(29), pp.21978–87.

Dorval, V. & Fraser, P.E., 2006. Small ubiquitin-like modifier (SUMO) modification of natively unfolded proteins tau and alpha-synuclein. The Journal of biological chemistry, 281(15), pp.9919–24.

Dou, F. et al., 2003. Chaperones increase association of tau protein with microtubules. Proceedings of the National Academy of Sciences, 100(2), pp.721–726.

Dragovic, R.A. et al., 2011. Sizing and phenotyping of cellular vesicles using Nanoparticle Tracking Analysis. Nanomedicine: Nanotechnology, Biology, and Medicine, 7, pp.780–788.

Dujardin, S. et al., 2014. Ectosomes: A New Mechanism for Non-Exosomal Secretion of Tau Protein. PLoS One, 9(6).

Eidenmu, J. et al., 2001. Phosphorylation-mimicking glutamate clusters in the proline-rich region are sufficient to simulate the functional deficiencies of hyperphosphorylated tau protein. Biochem. J, 357, pp.759–767.

Eitan, E. et al., 2016. Impact of lysosome status on extracellular vesicle content and release. Ageing research reviews, 32, pp.65–74.

Elbaum-Garfinkle, S., Ramlall, T. & Rhoades, E., 2010. The role of the lipid bilayer in tau aggregation. Biophysical journal, 98(11), pp.2722–30.

Elie, A. et al., 2015. Tau co-organizes dynamic microtubule and actin networks. Scientific Reports, 5(1), p.9964.

Elliott, E., Tsvetkov, P. & Ginzburg, I., 2007. BAG-1 associates with Hsc70.Tau complex and regulates the proteasomal degradation of Tau protein. The Journal of biological chemistry, 282(51), pp.37276–84.

Elliott, E., Tsvetkov, P. & Ginzburg, I., 2007. BAG-1 associates with Hsc70.Tau complex and regulates the proteasomal degradation of Tau protein. The Journal of biological chemistry, 282(51), pp.37276–84.

Evans, L.D. et al., 2018. Extracellular Monomeric and Aggregated Tau Efficiently Enter Human Neurons through Overlapping but Distinct Pathways. Cell reports, 22(13), pp.3612–3624.

Falcon et al., 2018. Structures of filaments from Pick's disease reveal a novel tau protein fold, Nature, 561, pp.137-140.

Fath, T., Eidenmü, J. & Brandt, R., 2002. Tau-Mediated Cytotoxicity in a Pseudohyperphosphorylation Model of Alzheimer's Disease. Journal of Neuroscience, 22(22) pp.9733-9741.

Fauré, J. et al., 2006. Exosomes are released by cultured cortical neurones. Molecular and cellular neurosciences, 31(4), pp.642–8.

Feinstein, S.C. & Wilson, L., 2005. Inability of tau to properly regulate neuronal microtubule dynamics: a loss-of-function mechanism by which tau might mediate neuronal cell death. Biochimica et biophysica acta, 1739(2–3), pp.268–79.

Ferrer, I. et al., 2014. Glial and Neuronal Tau Pathology in Tauopathies. Journal of Neuropathology & Experimental Neurology, 73(1), pp.81–97.

Fevrier, B. et al., Cells release prions in association with exosomes. Proceedings of the National Academy of Sciences of the United States of America, 101(26), pp.9683-9688.

Finger, E.C., 2016. Frontotemporal Dementias. Continuum (Minneapolis, Minn.), 22(2 Dementia), pp.464–89.

Fischer, D. et al., 2007. Structural and Microtubule Binding Properties of Tau Mutants of Frontotemporal Dementias. Biochemistry, 46(10), pp.2574–2582.

Fitzpatrick, A.W.P. et al., 2017. Cryo-EM structures of tau filaments from Alzheimer's disease. Nature, 547(7662), pp.185–190.

Fontaine, S.N. et al., 2015. The active Hsc70/tau complex can be exploited to enhance tau turnover without damaging microtubule dynamics. Human molecular genetics, 24(14), pp.3971–81.

Fontaine, S.N. et al., 2016. DnaJ/Hsc70 chaperone complexes control the extracellular release of neurodegenerative- associated proteins. The EMBO Journal, 35, pp.1537–1549.

Forrest, S.L. et al., 2018. Retiring the term FTDP-17 as MAPT mutations are genetic forms of sporadic frontotemporal tauopathies. Brain, 141(2), pp.521–534.

Friedhoff, P. et al., 2000. Structure of tau protein and assembly into paired helical filaments. Biochimica et Biophysica Acta (BBA) - Molecular Basis of Disease, 1502(1), pp.122–132.

Frost, B., Jacks, R.L. & Diamond, M.I., 2009. Propagation of tau misfolding from the outside to the inside of a cell. The Journal of biological chemistry, 284(19), pp.12845–52.

Frühbeis, C. et al., 2013. Neurotransmitter-Triggered Transfer of Exosomes Mediates Oligodendrocyte–Neuron Communication B. A. Barres, ed. PLoS Biology, 11(7), p.e1001604.

Fulga, T.A. et al., 2007. Abnormal bundling and accumulation of F-actin mediates tau-induced neuronal degeneration in vivo. Nature Cell Biology, 9(2), pp.139–148.

Géminard, C. et al., 2001. Characteristics of the interaction between Hsc70 and the transferrin receptor in exosomes released during reticulocyte maturation. The Journal of biological chemistry, 276(13), pp.9910–6.

Géminard, C. et al., 2004. Degradation of AP2 During Reticulocyte Maturation Enhances Binding of Hsc70 and Alix to a Common Site on TfR for Sorting into Exosomes. Traffic, 5(3), pp.181–193.

Goedert, M. & Jakes, R., Expression of separate isoforms of human tau protein: correlation with the tau pattern in brain and effects on tubulin polymerization. The EMBO Journal, 9(13), pp.4225–4230.

Goedert, M., Spillantini, M.G. & Crowther, R.A., 1992a. Cloning of a big tau microtubule-associated protein characteristic of the peripheral nervous system (sensory ganglia/sympathetic ganglia/central nervous system/alternative mRNA splicing). Neurobiology, 89, pp.1983–1987.

Goedert, M., Spillantini, M.G., Cairns, N.J., et al., 1992. Tau Proteins of Alzheimer Paired Helical Filaments: Abnormal Phosphorylation of All Six Brain lsoforms. Neuron, 8, pp.159–168.

Gómez-Isla, T. et al., 1997. Neuronal loss correlates with but exceeds neurofibrillary tangles in Alzheimer's disease. Annals of Neurology, 41(1), pp.17–24.

Gómez-Ramos, A. et al., 2008. Extracellular tau promotes intracellular calcium increase through M1 and M3 muscarinic receptors in neuronal cells. Molecular and Cellular Neuroscience, 37(4), pp.673–681.

Gousset, K. et al., 2009. Prions hijack tunnelling nanotubes for intercellular spread. Nature Cell Biology, 11(3), pp.328–336.

Grad, L.I. et al., 2014. Intercellular propagated misfolding of wild-type Cu/Zn superoxide dismutase occurs via exosome-dependent and -independent mechanisms. Proceedings of the National Academy of Sciences of the United States of America, 111(9), pp.3620-3625.

Grüning, C.S.R. et al., 2014. Alternative conformations of the Tau repeat domain in complex with an engineered binding protein. The Journal of biological chemistry, 289(33), pp.23209–18.

Guix, F.X. et al., 2018. Detection of Aggregation-Competent Tau in Neuron-Derived Extracellular Vesicles. International journal of molecular sciences, 19(3).

Guo et al., 2016. Unique pathological tau conformers from Alzheimer's brains transmit tau pathology in nontransgenic mice, Journal of Experimental Medicine, 213(12), pp.2635-2654.

Guo, T., Noble, W. & Hanger, D.P., 2017. Roles of tau protein in health and disease. Acta neuropathologica, 133(5), pp.665–704.

Hamano, T. et al., 2008. Autophagic-lysosomal perturbation enhances tau aggregation in transfectants with induced wild-type tau expression. European Journal of Neuroscience, 27(5), pp.1119–1130.

Hamdane, M. et al., 2003. Mitotic-like tau phosphorylation by p25-Cdk5 kinase complex. The Journal of biological chemistry, 278(36), pp.34026–34.

Hanger, D.P., Anderton, B.H. & Noble, W., 2009. Tau phosphorylation: the therapeutic challenge for neurodegenerative disease. Trends in Molecular Medicine, 15(3), pp.112–119.

Hasegawa, M. et al., 1992. Protein sequence and mass spectrometric analyses of tau in the Alzheimer's disease brain. The Journal of biological chemistry, 267(24), pp.17047–54.

Hefti, M.M. et al., 2018. High-resolution temporal and regional mapping of MAPT expression and splicing in human brain development. PloS one, 13(4), p.e0195771.

Hesse, C. et al., 2000. Cerebrospinal fluid markers for Alzheimer's disease evaluated after acute ischemic stroke. Journal of Alzheimer's disease : JAD, 2(3–4), pp.199–206.

Hogg, M. et al., 2003. The L266V tau mutation is associated with frontotemporal dementia and Pick-like 3R and 4R tauopathy. Acta Neuropathologica, 106(4), pp.323–336.

Holmes, B.B. et al., 2013. Heparan sulfate proteoglycans mediate internalization and propagation of specific proteopathic seeds. Proceedings of the National Academy of Sciences of the United States of America, 110(33), pp.E3138-47.

Holmes, B.B. et al., 2014. Proteopathic tau seeding predicts tauopathy in vivo. Proceedings of the National Academy of Sciences, 111(41), pp.E4376–E4385.

Hong, M. et al., 1998. Mutation-specific functional impairments in distinct tau isoforms of hereditary FTDP-17. Science (New York, N.Y.), 282(5395), pp.1914–7.

Hoover, B.R. et al., 2010. Tau Mislocalization to Dendritic Spines Mediates Synaptic Dysfunction Independently of Neurodegeneration. Neuron, 68(6), pp.1067–1081.

Horiguchi, T. et al., 2003. Nitration of tau protein is linked to neurodegeneration in tauopathies. The American journal of pathology, 163(3), pp.1021–31.

Huang, C.-C. et al., 2014. Metabolism and mis-metabolism of the neuropathological signature protein TDP-43. Journal of cell science, 127(Pt 14), pp.3024–38.

Hurley, J.H. & Odorizzi, G., 2012. Get on the exosome bus with ALIX. Nature Cell Biology, 14(7), pp.654–655.

Hutton, M. et al., 1998. Association of missense and 5'-splice-site mutations in tau with the inherited dementia FTDP-17. Nature, 393(6686), pp.702–5.

Iguchi, Y. et al., 2016. Exosome secretion is a key pathway for clearance of pathological TDP-43. Brain. 139(12), pp.3187-3201

Irwin, D.J. et al., 2016. Deep clinical and neuropathological phenotyping of Pick disease. Annals of neurology, 79(2), pp.272–87.

Jeganathan, S. et al., 2006. Global hairpin folding of tau in solution. Biochemistry, 45(7), pp.2283–93.

Jinwal, U.K. et al., 2010. Hsc70 Rapidly Engages Tau after Microtubule Destabilization. Journal of Biological Chemistry, 285(22), pp.16798–16805.

Jones, E.M. et al., 2012. Interaction of Tau Protein with Model Lipid Membranes Induces Tau Structural Compaction and Membrane Disruption. Biochemistry, 51(12), pp.2539–2550.

Josephs, K.A., 2015. Key emerging issues in progressive supranuclear palsy and corticobasal degeneration. Journal of neurology, 262(3), pp.783–8.

Josephs, K.A., 2017. Current Understanding of Neurodegenerative Diseases Associated With the Protein Tau. Mayo Clinic proceedings, 92(8), pp.1291–1303.

Kahlert, C. & Kalluri, R., Exosomes in tumor microenvironment influence cancer progression and metastasis. Journal of Molecular Medicine (Berlin, Germany), 91(4), pp.431-437.

Kanemaru, K. et al., 1992. Fetal-type phosphorylation of the tau in paired helical filaments. Journal of neurochemistry, 58(5), pp.1667–75.

Kanmert, D. et al., 2015. C-Terminally Truncated Forms of Tau, But Not Full-Length Tau or Its C-Terminal Fragments, Are Released from Neurons Independently of Cell Death. The

Journal of neuroscience : the official journal of the Society for Neuroscience, 35(30), pp.10851–65.

Karagöz, G.E. et al., 2014. Hsp90-Tau Complex Reveals Molecular Basis for Specificity in Chaperone Action. Cell, 156(5), pp.963–974.

Karch, C.M., Jeng, A.T. & Goate, A.M., 2012. Extracellular Tau levels are influenced by variability in Tau that is associated with tauopathies. The Journal of biological chemistry, 287(51), pp.42751–62.

Katsinelos, T. et al., 2018. Unconventional Secretion Mediates the Trans-cellular Spreading of Tau. Cell Reports, 23(7), pp.2039–2055.

Kaufman, S.K. et al., 2018. Tau seeding activity begins in the transentorhinal/entorhinal regions and anticipates phospho‑tau pathology in Alzheimer's disease and PART. Acta Neuropathologica, 136(136), pp.57–67.

Ke, Y.D. et al., 2012. Lessons from Tau-Deficient Mice. International Journal of Alzheimer's Disease, 2012, pp.1–8.

Kfoury, N. et al., 2012. Trans-cellular propagation of Tau aggregation by fibrillar species. The Journal of biological chemistry, 287(23), pp.19440–51.

Kim, W. et al., 2010b. Interneuronal transfer of human tau between Lamprey central neurons in situ. Journal of Alzheimer's disease : JAD, 19(2), pp.647–64.

Kim, W., Lee, S. & Hall, G.F., 2010a. Secretion of human tau fragments resembling CSF-tau in Alzheimer's disease is modulated by the presence of the exon 2 insert. FEBS letters, 584(14), pp.3085–8.

Kirkland, T.N. et al., 1998. Evaluation of the proline-rich antigen of Coccidioides immitis as a vaccine candidate in mice. Infection and immunity, 66(8), pp.3519–22.

Knops, J. et al., 1991. Overexpression of tau in a nonneuronal cell induces long cellular processes. The Journal of Cell Biology, 114(4), pp.725-733.

Kolarova, M. et al., 2012. Structure and Pathology of Tau Protein in Alzheimer Disease. International Journal of Alzheimer's Disease, 2012, pp.1–13.

Köpke, E. et al., 1993. Microtubule-associated protein tau. Abnormal phosphorylation of a non-paired helical filament pool in Alzheimer disease. The Journal of biological chemistry, 268(32), pp.24374–84.

Kosik et al., 1989. Developmentally regulated expression of specific tau sequences. Neuron, 2(4), pp.1389-1397.

Krishnamurthy, P.K. & Johnson, G.V.W., 2004. Mutant (R406W) human tau is hyperphosphorylated and does not efficiently bind microtubules in a neuronal cortical cell model. The Journal of biological chemistry, 279(9), pp.7893–900.

Krüger, U. et al., 2012. Autophagic degradation of tau in primary neurons and its enhancement by trehalose. Neurobiology of Aging, 33(10), pp.2291–2305.

Krumova, P. & Weishaupt, J.H., 2013. Sumoylation in neurodegenerative diseases. Cellular and Molecular Life Sciences, 70(12), pp.2123–2138.

Kunadt, M. et al., 2015. Extracellular vesicle sorting of α-Synuclein is regulated by sumoylation. Acta neuropathologica, 129(5), pp.695–713.

Lachenal, G. et al., 2011. Release of exosomes from differentiated neurons and its regulation by synaptic glutamatergic activity. Molecular and Cellular Neuroscience, 46(2), pp.409–418.

Lasagna-Reeves, C.A. et al., 2012. Identification of oligomers at early stages of tau aggregation in Alzheimer's disease. FASEB journal : official publication of the Federation of American Societies for Experimental Biology, 26(5), pp.1946–59.

Lasagna-Reeves, C.A. et al., 2012b. Alzheimer brain-derived tau oligomers propagate pathology from endogenous tau. Scientific Reports, 2(1), p.700.

Lathuilière, A. et al., 2017. Motifs in the tau protein that control binding to microtubules and aggregation determine pathological effects. Scientific Reports, 7(1), p.13556.

Lau, D.H.W. et al., 2016. Critical residues involved in tau binding to fyn: implications for tau phosphorylation in Alzheimer's disease. Acta neuropathologica communications, 4(1), p.49.

Lee, G., 1990. Views and Reviews Tau Protein: An Update on Structure and Function. Cell Motility and the Cytoskeleton, 15, pp.199-203.

Lee, J.G. et al., 2016; Unconventional secretion of misfolded proteins promotes adaptation to proteasome dysfunction in mammalian cells. Nature Cell Biology, 18(7), pp.767 – 776.

Lee, V.M.-Y., Goedert, M. & Trojanowski, J.Q., 2001. Neurodegenerative Tauopathies. Annual Review of Neuroscience, 24(1), pp.1121–1159.

Lewis, J. et al., 2000. Neurofibrillary tangles, amyotrophy and progressive motor disturbance in mice expressing mutant (P301L) tau protein. Nature Genetics, 25(4), pp.402–405.

Li, J. et al., 2015. Serum-free culture alters the quantity and protein composition of neuroblastoma-derived extracellular vesicles. Journal of Extracellular Vesicles, 4(0).

Li, W. & Lee, V.M.-Y., 2006. Characterization of two VQIXXK motifs for tau fibrillization in vitro. Biochemistry, 45(51), pp.15692–701.

Ling, H. et al., 2016. Astrogliopathy predominates the earliest stage of corticobasal degeneration pathology. *Brain*, 139(12), pp.3237–3252.

Liu, F. & Gong, C.-X., 2008. Tau exon 10 alternative splicing and tauopathies. Molecular neurodegeneration, 3, p.8.

Liu, F. et al., 2002. Involvement of aberrant glycosylation in phosphorylation of tau by cdk5 and GSK-3beta. FEBS letters, 530(1–3), pp.209–14.

Liu, F. et al., 2007. Site-specific effects of tau phosphorylation on its microtubule assembly activity and self-aggregation. The European journal of neuroscience, 26(12), pp.3429–36.

Liu, L. et al., 2012. Trans-Synaptic Spread of Tau Pathology In Vivo. PLoS ONE, 7(2), p.e31302.

Lopresti, P. et al., 1995. Functional implications for the microtubule-associated protein tau: Localization in oligodendrocytes. Neurobiology, 92, pp.10369–10373.

Lu, M. & Kosik, K.S., 2001. Competition for microtubule-binding with dual expression of tau missense and splice isoforms. Molecular biology of the cell, 12(1), pp.171–84.

Luna-Muñoz, J. et al., 2007. Earliest Stages of Tau Conformational Changes are Related to the Appearance of a Sequence of Specific Phospho-Dependent Tau Epitopes in Alzheimer's Disease. Journal of Alzheimer's Disease, 12(4), pp.365–375.

Luo, H.-B. et al., 2014. SUMOylation at K340 inhibits tau degradation through deregulating its phosphorylation and ubiquitination. Proceedings of the National Academy of Sciences of the United States of America, 111(46), pp.16586–91.

Mackenzie, I.R.A. & Neumann, M., 2016. Molecular neuropathology of frontotemporal dementia: insights into disease mechanisms from postmortem studies. Journal of Neurochemistry, 138, pp.54–70.

Majounie, E. et al., 2013. Variation in tau isoform expression in different brain regions and disease states. Neurobiology of aging, 34(7), p.1922.e7-1922.e12.

Malia, T.J. et al., 2016. Epitope mapping and structural basis for the recognition of phosphorylated tau by the anti-tau antibody AT8. Proteins: Structure, Function, and Bioinformatics, 84(4), pp.427–434.

Mandelkow, E.-M. & Mandelkow, E., 2012. Biochemistry and cell biology of tau protein in neurofibrillary degeneration. Cold Spring Harbor perspectives in medicine, 2(7), p.a006247.

Marciniak, E. et al., 2017. Tau deletion promotes brain insulin resistance. The Journal of experimental medicine, 214(8), pp.2257–2269.

Marimpietri, D. et al., 2013. Proteome profiling of neuroblastoma-derived exosomes reveal the expression of proteins potentially involved in tumor progression. PloS one, 8(9), p.e75054.

McKee, A.C. et al., 2013. The spectrum of disease in chronic traumatic encephalopathy. Brain, 136(1), pp.43–64.

McKee, A.C. et al., 2015. The neuropathology of chronic traumatic encephalopathy. Brain pathology (Zurich, Switzerland), 25(3), pp.350–64.

Meister, M. & Tikkanen, R., 2014. Endocytic trafficking of membrane-bound cargo: a flotillin point of view. Membranes, 4(3), pp.356–71.

Menezes, J.R. & Luskin, M.B., 1994. Expression of neuron-specific tubulin defines a novel population in the proliferative layers of the developing telencephalon. The Journal of neuroscience : the official journal of the Society for Neuroscience, 14(9), pp.5399–416.

Meyer, V. et al., 2014. Amplification of Tau fibrils from minute quantities of seeds. Biochemistry, 53(36), pp.5804–9.

Miranda, A.M. et al., 2018. Neuronal lysosomal dysfunction releases exosomes harboring APP C-terminal fragments and unique lipid signatures. Nature Communications, 9(1), p.291.

Mocanu, M.-M. et al., 2008. The Potential for -Structure in the Repeat Domain of Tau Protein Determines Aggregation, Synaptic Decay, Neuronal Loss, and Coassembly with Endogenous Tau in Inducible Mouse Models of Tauopathy. Journal of Neuroscience, 28(3), pp.737–748.

Mohamed, N.-V. et al., 2015. Starvation and inhibition of lysosomal function increased tau secretion by primary cortical neurons. Scientific Reports, 4(1), p.5715.

Mok, S.-A. et al., 2018. Mapping interactions with the chaperone network reveals factors that protect against tau aggregation. Nature Structural & Molecular Biology, 25(5), pp.384–393.

Momen-Heravi, F. et al., 2013. Current methods for the isolation of extracellular vesicles. Biol. Chem, 394(10), pp.1253–1262.

Mukrasch, M.D. et al., 2009. Structural Polymorphism of 441-Residue Tau at Single Residue Resolution G. A. Petsko, ed. PLoS Biology, 7(2), p.e1000034.

Mulcahy, L.A., Pink, R.C. & Carter, D.R.F., 2014. Routes and mechanisms of extracellular vesicle uptake. Journal of extracellular vesicles, 3.

Münz, C., 2011. Antigen processing by macroautophagy for MHC presentation. Frontiers in Immunology, 2, p.42.

Murphy, M.P., LeVine, H. & III, 2010. Alzheimer's disease and the amyloid-beta peptide. Journal of Alzheimer's disease : JAD, 19(1), pp.311–23.

Nagiec, E.E., Sampson, K.E. & Abraham, I., 2001. Mutated tau binds less avidly to microtubules than wildtype tau in living cells. Journal of Neuroscience Research, 63(3), pp.268–275.

Narasimhan, S. et al., 2017. Pathological Tau Strains from Human Brains Recapitulate the Diversity of Tauopathies in Nontransgenic Mouse Brain. The Journal of neuroscience : the official journal of the Society for Neuroscience, 37(47), pp.11406–11423.

Pan, B.-T. & Johnstone, R.M., 1983. Fate of the Transferrin Receptor during Maturation of Sheep Reticulocytes In Vitro: Selective Externalization of the Receptor. Cell Copyright Q, 33, pp.967–977.

Panda, D. et al., 2003. Differential regulation of microtubule dynamics by three- and four-repeat tau: Implications for the onset of neurodegenerative disease. Proceedings of the National Academy of Sciences, 100(16), pp.9548–9553.

Papkovskaia, T.D. et al., 2012. G2019S leucine-rich repeat kinase 2 causes uncoupling protein-mediated mitochondrial depolarization. *Human Molecular Genetics*, 21(19), pp.4201–4213.

Piras, A. et al., 2016. Autophagic and lysosomal defects in human tauopathies: analysis of post-mortem brain from patients with familial Alzheimer disease, corticobasal degeneration and progressive supranuclear palsy. Acta Neuropathologica Communications, 4(1), p.22.

Pittman, A.M., Fung, H.-C. & de Silva, R., 2006. Untangling the tau gene association with neurodegenerative disorders. Human molecular genetics, (suppl 2), pp.R188-95.

Plouffe, V. et al., 2012. Hyperphosphorylation and Cleavage at D421 Enhance Tau Secretion M. R. Cookson, ed. PLoS ONE, 7(5), p.e36873.

Polanco, J.C. et al., 2016. Extracellular Vesicles Isolated from the Brains of rTg4510 Mice Seed Tau Protein Aggregation in a Threshold-dependent Manner. The Journal of biological chemistry, 291(24), pp.12445–66.

Pooler, A.M. et al., 2013. Physiological release of endogenous tau is stimulated by neuronal activity. EMBO reports, 14(4), pp.389–94.

Pooler, A.M. et al., 2015. Amyloid accelerates tau propagation and toxicity in a model of early Alzheimer's disease. Acta neuropathologica communications, 3, p.14.

Poorkaj, P. et al., 2002. An R5L mutation in a subject with a progressive supranuclear palsy phenotype. Annals of Neurology, 52(4), pp.511–516.

Qi, L. et al., 2012. The Role of Chaperone-Mediated Autophagy in Huntingtin Degradation. PLoS ONE, 7(10), p.46834.

Qiang et al., 2018. Tau Does Not Stabilize Axonal Microtubules but Rather Enables Them to Have Long Labile Domains. Current Biology, 28(13), pp.2182-2189.e4.

Quah, B.J.C. & O'Neill, H.C., The immunogenicity of dendritic cell-derived exosomes. Blood cells, molecules & diseases, 35(2), pp.94–110.

Rath, A. et al., 2009. Detergent binding explains anomalous SDS-PAGE migration of membrane proteins. Proceedings of the National Academy of Sciences of the United States of America, 106(6), pp.1760–5.

Ren et al., 2007. Effects of tau phosphorylation on proteasome activity. FEBS Letters, 581 (7), pp.1521 - 1528

Rissman, R.A., Poon, W.W., Blurton-Jones, M., Oddo, S., Torp, R., et al., 2004. Caspase-cleavage of tau is an early event in Alzheimer disease tangle pathology. The Journal of clinical investigation, 114(1), pp.121–30.

Rodríguez-Martín, T. et al., 2013. Tau phosphorylation affects its axonal transport and degradation. Neurobiology of aging, 34(9), pp.2146–57.

Rosenberg, K.J. et al., 2008. Complementary dimerization of microtubule-associated tau protein: Implications for microtubule bundling and tau-mediated pathogenesis. Proceedings of the National Academy of Sciences of the United States of America, 105(21), pp.7445–50.

Sahu, R. et al., 2011. Microautophagy of cytosolic proteins by late endosomes. Developmental cell, 20(1), pp.131–9.

Saint-Aubert, L. et al., 2017. Tau PET imaging: present and future directions. Molecular Neurodegeneration, 12(1).

Saman, S. et al., 2012. Exosome-associated tau is secreted in tauopathy models and is selectively phosphorylated in cerebrospinal fluid in early Alzheimer disease. The Journal of biological chemistry, 287(6), pp.3842–9.

Sampson, D.A., Wang, M. & Matunis, M.J., 2001. The Small Ubiquitin-like Modifier-1 (SUMO-1) Consensus Sequence Mediates Ubc9 Binding and Is Essential for SUMO-1 Modification. Journal of Biological Chemistry, 276(24), pp.21664-21669

Sanders, D.W. et al., 2014. Distinct tau prion strains propagate in cells and mice and define different tauopathies. Neuron, 82(6), pp.1271–88.

SantaCruz, K. et al., 2005. Tau Suppression in a Neurodegenerative Mouse Model Improves Memory Function. Science, 309(5733), pp.476–481.

Sarkar, M., Kuret, J. & Lee, G., 2008. Two motifs within the tau microtubule-binding domain mediate its association with the hsc70 molecular chaperone. Journal of neuroscience research, 86(12), pp.2763–73.

Scaravilli, T., Tolosa, E. & Ferrer, I., 2005. Progressive supranuclear palsy and corticobasal degeneration: Lumping versus splitting. Movement Disorders, 20(S12), pp.S21–S28.

Schneider, A. & Simons, M., 2013. Exosomes: vesicular carriers for intercellular communication in neurodegenerative disorders. Cell and tissue research, 352(1), pp.33–47.

Sengupta, A. et al., 1998. Phosphorylation of Tau at Both Thr 231 and Ser 262 Is Required for Maximal Inhibition of Its Binding to Microtubules. Archives of Biochemistry and Biophysics, 357(2), pp.299–309.

Serrano-Pozo, A. et al., 2011. Neuropathological alterations in Alzheimer disease. Cold Spring Harbor perspectives in medicine, 1(1), p.a006189.

Shimura, H. et al., 2003. CHIP-Hsc70 Complex Ubiquitinates Phosphorylated Tau and Enhances Cell Survival. Journal of Biological Chemistry, 279(6), pp.4869–4876.

Simón, D. et al., 2012. Proteostasis of tau. Tau overexpression results in its secretion via membrane vesicles. FEBS Letters, 586(1), pp.47–54.

Sokolow, S. et al., 2015. Pre-synaptic C-terminal truncated tau is released from cortical synapses in Alzheimer's disease. Journal of neurochemistry, 133(3), pp.368–79.

Sotiropoulos, I. et al., 2017. Atypical, non-standard functions of the microtubule associated Tau protein. Acta neuropathologica communications, 5(1), p.91.

Spillantini, M.G. & Goedert, M., 2013. Tau pathology and neurodegeneration. The Lancet Neurology, 12(6), pp.609–622.

Stein, T.D., Alvarez, V.E. & Mckee, A.C., Chronic traumatic encephalopathy: a spectrum of neuropathological changes following repetitive brain trauma in athletes and military personnel. Alzheimer's Research & Therapy, 6(1).

Steiner, B. et al., 1990. Phosphorylation of microtubule-associated protein tau: identification of the site for Ca2(+)-calmodulin dependent kinase and relationship with tau phosphorylation in Alzheimer tangles. The EMBO journal, 9(11), pp.3539–44.

Stuffers, S. et al., 2009. Multivesicular Endosome Biogenesis in the Absence of ESCRTs. Traffic, 10(7), pp.925–937.

Sündermann, F., Fernandez, M.-P. & Morgan, R.O., 2016. An evolutionary roadmap to the microtubule-associated protein MAP Tau. BMC Genomics, 17(1), p.264.

Swayne, L.A. et al., 2003. Oilgomerization characteristics of cysteine string protein. Biochemical and Biophysical Research Communications, 300(4), pp.921–926.

Takeda, S. et al., 2015. Neuronal uptake and propagation of a rare phosphorylated high-molecular-weight tau derived from Alzheimer's disease brain. Nature communications, 6, p.8490.

Takeuchi, T. et al., 2015. Intercellular chaperone transmission via exosomes contributes to maintenance of protein homeostasis at the organismal level. Proceedings of the National Academy of Sciences of the United States of America, 112(19), pp.E2497-506.

Tanaka, T. et al., 1995. Abnormally phosphorylated tau in SY5Y human neuroblastoma cells. FEBS Letters, 360, pp.5–9.

Tannetta, D.S. et al., Characterisation of Syncytiotrophoblast Vesicles in Normal Pregnancy and Pre-Eclampsia: Expression of Flt-1 and Endoglin. PLoS One 8(2) p.e56754

Tardivel, M. et al., 2016. Tunneling nanotube (TNT)-mediated neuron-to neuron transfer of pathological Tau protein assemblies. Acta neuropathologica communications, 4(1), p.117.

Théry, C., Zitvogel, L. & Amigorena, S., 2002. Exosomes: composition, biogenesis and function. Nature Reviews Immunology, 2(8), pp.569-579

Trajkovic, K. et al., 2008. Ceramide Triggers Budding of Exosome Vesicles into Multivesicular Endosomes. Science, 319(5867), pp.1244–1247.

Trajkovic, K., Jeong, H. & Krainc, D., 2017. Mutant Huntingtin Is Secreted via a Late Endosomal/Lysosomal Unconventional Secretory Pathway. The Journal of neuroscience : the official journal of the Society for Neuroscience, 37(37), pp.9000–9012.

Tricarico, C., Clancy, J. & D'Souza-Schorey, C., 2017. Biology and biogenesis of shed microvesicles. Small GTPases, 8(4), pp.220–232.

Tuerde et al., 2018. Isoform-independent and -dependent phosphorylation of microtubule-associated protein tau in mouse brain during postnatal development, Journal of Biological Chemistry, 293(5), pp.1781-1793.

Uberti, D. et al., 1997. Characterization of tau proteins in human neuroblastoma SH-SY5Y cell line. Neuroscience Letters, 235(3), pp.149–153.

van der Pol, E. et al., 2014. Particle size distribution of exosomes and microvesicles determined by transmission electron microscopy, flow cytometry, nanoparticle tracking analysis, and resistive pulse sensing. Journal of Thrombosis and Haemostasis, 12(7), pp.1182–1192.

van Niel, G. & Raposo, G., 2018. Shedding light on the cell biology of extracellular vesicles. Nature Reviews Molecular Cell Biology, 19(4), pp.213-228

Vandermeeren, M. et al., 1993. Detection of tau proteins in normal and Alzheimer's disease cerebrospinal fluid with a sensitive sandwich enzyme-linked immunosorbent assay. Journal of neurochemistry, 61(5), pp.1828–34.

Villarroya-Beltri, C. et al., 2013. Sumoylated hnRNPA2B1 controls the sorting of miRNAs into exosomes through binding to specific motifs. Nature communications, 4, p.2980.

von Bergen, M. et al., 2000. Assembly of tau protein into Alzheimer paired helical filaments depends on a local sequence motif ((306)VQIVYK(311)) forming beta structure. Proceedings of the National Academy of Sciences of the United States of America, 97(10), pp.5129–34.

von Bergen, M. et al., 2005. Tau aggregation is driven by a transition from random coil to beta sheet structure. Biochimica et Biophysica Acta (BBA) - Molecular Basis of Disease, 1739(2–3), pp.158–166.

Wagner, U. et al., 1996. Cellular phosphorylation of tau by GSK-3 beta influences tau binding to microtubules and microtubule organisation. Journal of cell science, 109 (Pt 6), pp.1537–43.

Wang, Y. & Mandelkow, E., 2012. Degradation of tau protein by autophagy and proteasomal pathways. Biochemical Society Transactions, 40(4), pp.644-652

Wang, Y. & Mandelkow, E., 2016. Tau in physiology and pathology. Nature reviews. Neuroscience, 17(1), pp.5–21.

Wang, Y. et al., 2009. Tau fragmentation, aggregation and clearance: the dual role of lysosomal processing. Human molecular genetics, 18(21), pp.4153–70.

Wang, Y. et al., 2017. The release and trans-synaptic transmission of Tau via exosomes. Molecular neurodegeneration, 12(1), p.5.

Wang, Y.P. et al., 2007. Stepwise proteolysis liberates tau fragments that nucleate the Alzheimer-like aggregation of full-length tau in a neuronal cell model. Proceedings of the National Academy of Sciences of the United States of America, 104(24), pp.10252–7.

Wauters, M., Wattiez, R. & Ris, L., 2016. Internalization of the Extracellular Full-Length Tau Inside Neuro2A and Cortical Cells Is Enhanced by Phosphorylation. Biomolecules, 6(3).

Wenning, G.K. et al., 1998. Natural history and survival of 14 patients with corticobasal degeneration confirmed at postmortem examination. J Neurol Neurosurg Psychiatry, 64, pp.184–189.

Willms, E. et al., 2016. Cells release subpopulations of exosomes with distinct molecular and biological properties. Scientific Reports, 6(1), p.22519.

Wolfe, M.S., 2009. Tau mutations in neurodegenerative diseases. The Journal of biological chemistry, 284(10), pp.6021–5.

Wollert, T. & Hurley, J.H., 2010. Molecular mechanism of multivesicular body biogenesis by ESCRT complexes. Nature, 464(7290), pp.864–869.

Wolozin, B. & Davies, P., 1987. Alzheimer-related neuronal protein A68: specificity and distribution. Annals of neurology, 22(4), pp.521–6. A

Wu, J.W. et al., 2013. Small misfolded Tau species are internalized via bulk endocytosis and anterogradely and retrogradely transported in neurons. The Journal of biological chemistry, 288(3), pp.1856–70.

Wu, J.W. et al., 2016. Neuronal activity enhances tau propagation and tau pathology in vivo. Nature Neuroscience, 19(8), pp.1085–1092.

Xu, Y. et al., 2018. DNAJC5 facilitates USP19-dependent unconventional secretion of misfolded cytosolic proteins. Cell Discovery, 4(1), p.11.

Yamada et al., 2011. In Vivo Microdialysis Reveals Age-Dependent Decrease of Brain Interstitial Fluid Tau Levels in P301S Human Tau Transgenic Mice. Journal of Neuroscience, 31(37), pp.13110-13117.

Yamada, K. et al., 2014. Neuronal activity regulates extracellular tau in vivo. The Journal of Experimental Medicine, 211(3), pp.387–393.

Yao, T.-M. et al., 2003. Aggregation Analysis of the Microtubule Binding Domain in Tau Protein by Spectroscopic Methods. J. Biochem, 134, pp.91–99.

Young, J.J. et al., 2018. Frontotemporal dementia: latest evidence and clinical implications. Therapeutic advances in psychopharmacology, 8(1), pp.33–48.

Yuzwa, S.A. et al., 2012. Increasing O-GlcNAc slows neurodegeneration and stabilizes tau against aggregation. Nature Chemical Biology, 8(4), pp.393–399.

Zeise, E. et al., 1998. Nuclear translocation of stress protein Hsc70 during S phase in rat C6 glioma cells. Cell stress & chaperones, 3(2), pp.94–9.

Zempel, H. & Mandelkow, E., 2014. Lost after translation: missorting of Tau protein and consequences for Alzheimer disease. Trends in Neurosciences, 37, pp.721–732.

Zhong, J., Iqbal, K. & Grundke-Iqbal, I., 1999. Hyperphosphorylated tau in SY5Y cells: similarities and dissimilarities to abnormally hyperphosphorylated tau from Alzheimer disease brain. FEBS Letters, 453(1–2), pp.224–228.

Zhukareva, V. et al., 2002. Sporadic Pick's Disease: A Tauopathy Characterized by a Spectrum of Pathological Tau Isoforms in Gray and White Matter. Ann Neurol, 51, pp.730–739.

Zimmerman, B. et al., 2016. Crystal Structure of a Full-Length Human Tetraspanin Reveals a Cholesterol-Binding Pocket. Cell, 167(4), p.1041–1051.e11.